UNIVERSITY OF SOUTHAMPTON

# Quantifying the Effect of Two Root Traits on Phosphorus Uptake

by

Daniel M. McKay Fletcher

A thesis for the

degree of Doctor of Philosophy

in the

Faculty of Engineering and Physical Sciences

Department of Mechanical Engineering

Bioengineering Sciences Research Group

July 2020

UNIVERSITY OF SOUTHAMPTON

# ABSTRACT

FACULTY OF ENGINEERING AND PHYSICAL SCIENCES

DEPARTMENT OF MECHANICAL ENGINEERING

Doctor of Philosophy

by Daniel M. McKay Fletcher

Organic acid exudation and the ability of plants to respond to heterogeneous nutrient supplies in the soil are two traits that are important for phosphorus acquisition. The ability of plants to react to heterogeneous nutrient supplies is an instance of pheneotypic plasticity, known as root plasticity. This trait is evolutionary beneficial as plants can identify regions of soil that have high phosphorus content and proliferate in those regions, ultimately resulting in lower photosynthate expenditure on acquiring phosphorus. Organic acid exudation is the release of weak acids from the root into the soil. These acids are thought to improve phosphorus acquisition by increasing the solubility of phosphorus in soil. However, quantifying the benefit of these two traits experimentally remains a difficult problem due to challenges in controlling root growth, exudation and root surface area.

In this thesis we used mathematical modelling to assess the relative benefits of these two traits. Special attention was paid to the *real* root geometries and phosphorus movement in the models; both were characterised by complimentary experiments. In particular, we used 3D X-ray computed tomography images of plant roots grown in soil as the geometry in our models. Furthermore, two approaches for measuring soil phosphorus were used to verify the results obtained from the models. One approach was elemental mapping (Scanning Electron Microscopy with Electron Dispersive X-ray Spectroscopy) of thin-sections of soil samples. From these maps, elemental concentrations of phosphorus was determined, which were then compared to model predictions. Another experimental technique was the use of microdialysis probes to sample soil solution and evaluate soil phosphorus concentrations at a range of different times. Microdialysis probes can also exude solutes as they sample soil solution. This functionality is exploited to verify models of organic acids solubilising soil sorbed phosphorus.

The verified models were then used to investigate the benefit in terms of phosphorus uptake due to root plasticity and organic acid exudation under realistic soil conditions. Using the root system of a plant that had responded to a fertiliser pellet and a plant that had not as geometries in a phosphorus uptake model determined that the responding plant absorbed more phosphorus from the pellet. Fitting models to the phosphorus uptake/organic acid exudation of microdialysis probes yielded the rate at which organic acids solubilise soil adsorbed phosphorus. This rate was used in a model of a single root exuding organic acids and absorbing phosphorus. We found that for this single root, organic acid exudation did not contribute to phosphorus uptake. This model was then extended to whole root structure geometries extracted from X-ray computed tomography images. We found that roots could collectively exude enough organic acids into the soil to gain a noticeable increase in phosphorus uptake. Moreover, we identified some features of whole root systems which enhance the phosphorus uptake benefits that derive from organic acid exudation.

# Contents

# List of Figures

# List of Tables

# List of Publications

1. **Fletcher, D.M.M.**, Keyes, S.D., Daly, K.R., Van Veelen, A. & Roose, T. (2019), 'A multi-image-based approach for modelling plant-fertiliser interaction', *Rhizosphere* p. 100152. (Fletcher, Keyes, Daly, Van Veelen & Roose (2019)).

2. **Fletcher, D.M.M.,** R. Shaw, Sánchez-Rodrìguez, A.R., Daly, K.R., van Veelen, A., Jones, D.L. & Roose, T. (2019), 'Quantifying citrate-enhanced phosphate root uptake using microdialysis', *Plant and Soil*. (Fletcher, Shaw, Sánchez-Rodríguez, Daly, van Veelen, Jones & Roose (2019)).

3. **Fletcher, D.M.M.**, Ruiz, S.A., Dias, T., Petroselli, C. & Roose, T. (2020), 'Linking root structure to functionality: The impact of root system architecture on citrate enhanced phosphate uptake', *New Phytologist.* (Fletcher et al. (2020))

4. Ruiz, S.A.*, **Fletcher, D.M.M.***, Boghi, A., Chadwick, D., Jones, D.L. & Roose, T. (2020), 'Image-based quantification of soil microbial dead zones induced by nitrogen fertilization', *Science of The Total Environment (2020).* * denotes equal contribution by authors. (Ruiz et al. (2020)).

5. Van Veelen, A., Koebernick, N., Scotson, C. S., **Fletcher, D.M.M.**, Huthwelker, T., Borca, C. N., Mosselmans, J. F. W. & Roose, T. (2019), 'Root induced soil deformation influences Fe, S and P: Rhizosphere chemistry investigated using synchrotron XRF and XAS', *New Phytologist.* (Van Veelen et al. (2019)).

6. Ruiz, S. A., Koebernick, N., Duncan, S., **Fletcher, D.M.M.**, Scotson, C., Boghi, A., Marin, M., Bengough, A. G., George, T., Brown, L. et al. (2019), 'Significance of root hairs at the field scale – modelling root water and phosphorus uptake under different field conditions', *Plant and Soil.* (Ruiz et al. (2019)).

7. Duncan, S.J., Daly, K.R., **Fletcher, D.M.M.**, Ruiz, S., Sweeney, P. & Roose, T. (2019), 'Multiple scale homogenisation of nutrient movement and crop growth in partially saturated soil', *Bulletin of Mathematical Biology* **81**(10), 3778–3802. (Duncan et al. (2019)).

8. Keyes, S., Cooper, L., Duncan, S., Koebernick, N., **Fletcher, D.M.M.**, Scotson, C., Van Veelen, A., Sinclair, I. & Roose, T. (2017), 'Measurement of micro-scale soil deformation around roots using four-dimensional synchrotron tomography and image correlation', *Journal of The Royal Society Interface* **14**(136), 20170560. (Keyes et al. (2017)).

# Declaration of Authorship

I, **Daniel McKay Fletcher**, declare that this thesis titled **Quantifying the Effect of Two Root Traits on Phosphorus Uptake** and the work presented in it is my own and has been generated by me as the result of my own original research. I confirm that:

- This work was done wholly or mainly while in candidature for a research degree at this University;
- Where any part of this thesis has previously been submitted for a degree or any other qualification at this University or any other institution, this has been clearly stated;
- Where I have consulted the published work of others, this is always clearly attributed;
- Where I have quoted from the work of others, the source is always given. With the exception of such quotations, this thesis is entirely my own work;
- I have acknowledged all main sources of help;
- Where the thesis is based on work done by myself jointly with others, I have made clear exactly what was done by others and what I have contributed myself;
- Parts of this work have been published as: Fletcher, Keyes, Daly, Van Veelen & Roose (2019), Fletcher, Shaw, Sánchez-Rodríguez, Daly, van Veelen, Jones & Roose (2019) and Fletcher et al. (2020):

Signed: Date:

# Acknowledgements

I would like to thank my supervisors Tiina Roose and Keith Daly for their invaluable support throughout my PhD. Tiina guided me in a shift from a mathematician to a scientist and helped navigate me through many of the problems in this thesis. Keith provided patient guidance through many of the technical aspects of this work and helped as a supervisor and as a friend. Samuel Keyes and Nico Koebernick guided me through the basics of image-processing. Simon Duncan answered my numerous Comsol and maths questions and is a great fishing companion. Siul Ruiz has been a brilliant research partner over the last year and a half of my PhD. We have worked together in an engaging and productive manner through this time. The pore-scale nitrogen manuscript is testament to this. Callum Scotson and Katy Williams have provided great biological knowledge and were always there to answer my questions. Arjen Van Veelen and Chiara Petroselli have provided guidance on the chemistry aspects of this PhD. I would like to thank all the above people for reading parts of my thesis and offering reassurance in the final months. Davey Jones, Rory Shaw and Antonio Sánchez-Rodríguez contributed by performing the microdialysis experiments at the University of Bangor, much of the the work in this thesis would have been impossible without them. For the last two years of my PhD I have had dyslexia study skills support from Sadhbh O'Dwyer. Her guidance and encouragement has improved my writing to a publishable level. Without her help, this thesis would be much harder to read. Many of the people mentioned above are not just supervisors or colleagues, but are also friends. Much of the following applies to these people as well.

I would like to thank my parents James Fletcher and Angela McKay, my twin brother Jack and my little brother Samuel for their support throughout the PhD. I count myself lucky to have such a a loving family. My friends in Southampton outside of the university have always been there for support and revelry, particularly Robert Milner. I would like to mention my girlfriend Eleanor Thomason for her love and kindness over the last year and a half. You have calmed my stress and anxiety numerous times, I am thankful to have you in my life. Finally, I would like to thank the gastroenterologist team, and the doctors and nurses at Southampton General Hospital for treating and caring for me during my diagnosis of Crohns disease. The two weeks spent in hospital was the most difficult time of my life, your care and expertise brought me back to health, for which I am forever thankful.

# Chapter 1

# Introduction

## 1.1 Overview

The primary focus of this thesis is the nutrient uptake from soil by plants, specifically the uptake of phosphorus (P). P is a vital nutrient for plant growth and health as it is a component in many important plant biochemical reactions including photosynthesis, respiration, seed and fruit production, root growth and storing energy. As such, P is a fundamental component of most fertilisers used in agriculture. Worryingly, the traditional P resources for fertilisers, mined rock phosphate, is quickly dwindling as the population increases and the mines are depleted (Cordell et al. (2009)). Additionally, climate change is reducing the amount of arable land. All this contributes to difficulties in producing enough food to feed the growing population. Unless these trends are addressed the difficulties will only increase in the following years. One approach to tackle this problem is a more sustainable agricultural use of P. This can be achieved through a greater understanding of the interactions between plants and soil. In particular, P fertilisation practices and crop breeding programmes could benefit from a greater understanding of the processes involved in P uptake.

We focus on two root traits that are thought to play an important role in P acquisition, these are: root plasticity and organic acid exudation by roots. Root plasticity refers to the ability of plants to alter root growth in response to environmental factors. In particular, plants can respond to local high P regions in the soil with local root proliferation, increasing P absorption in that

region. Organic acid exudation is the release of weak acids from roots into the soil. These acids are thought to improve P acquisition by increasing P solubility in soil. In this thesis we use a mathematical modelling approach to quantify the increase in P uptake due to these two traits. Mathematical modelling allows us to control the variables that previous experimental methods cannot achieve, thereby allowing the contribution of each component of P uptake to be quantified. However, to ensure the predictability of a model, care has to be taken to accurately parameterise and verify it using experimental data. In this thesis we propose two novel approaches for parameterising models of P uptake. We go on to use the verified models to investigate the P uptake benefit due to organic acid exudation and root plasticity.

The work in this thesis is presented as three scientific research articles:

- Chapter 2 corresponds to the article Fletcher, D.M.M., Keyes, S.D., Daly, K.R., Van Veelen, A. & Roose, T. (2019), 'A multi-image-based approach for modelling plant-fertiliser interaction', *Rhizosphere* p. 100152.
- Chapter 3 corresponds to the article Fletcher, D.M.M., Shaw, R., Sánchez-Rodrìguez, A.R., Daly, K.R., van Veelen, A., Jones, D.L. & Roose, T. (2019), 'Quantifying citrate enhanced phosphate root uptake using microdialysis', *Plant and Soil*.
- Chapter 4 corresponds to the article Fletcher, D.M.M., Ruiz, S.A., Dias, T., Petroselli, C. & Roose, T. (2020), 'Linking root structure to functionality: The impact of root system architecture on citrate enhanced phosphate uptake', *New Phytologist.*

The introduction to the thesis is divided into six sections. In section 1.2 we introduce the role of P in plant nutrition and agriculture. In section 1.3 we review the literature regarding two root traits, namely root plasticity and organic acid exudation. In section 1.4 we introduce techniques for modelling plant P uptake from soil. In section 1.5 we introduce experimental approaches for parameterising models of P uptake. In section 1.6 we summarise the main points of the introduction. Finally, in section 1.7 we present the structure of the rest of the thesis and the declaration of work.

## 1.2 Plant Nutrition and Fertilisation

All plants require at least twelve essential nutrients to complete their life cycle; deficiencies in these nutrients leads to limited growth, reduced grain yields and incomplete life cycles (Barber (1995)). One of these essential nutrients is phosphorus. Along with nitrogen and potassium P is required in relatively high amounts, and is thus classified as a primary macro-nutrient. P makes up between 0.02 and 0.5% of soil, and it is often the limiting factor in achieving optimal crop yields. A characteristic feature of P is its low mobility in soil compared to other nutrients. This is due to slow diffusion, fast binding rates to soil particles and slow desorption rates (Barber (1995)). Compared to the other primary macro nutrients, nitrogen and potassium, the concentration of P available to plants (*i.e* dissolved in soil water) in soil is low. Inorganic P in solution is usually in the form of hydrogen phosphate or dihydrogen phosphate depending on the pH of the soil solution. Phosphates in solution react quickly with soil minearal surfaces, reducing the amount available to plants. Furthermore, the majority of P in soil is either in mineral forms (with very low water solubility), a component in an organic material such as dead plant matter or bound to the surface of soil constituents such as aluminium or iron oxide (Barber (1995)).

Plants can react to poor soil conditions in an effort to mitigate nutrient deficiency in one of two ways. The first is through local changes to the soil environment by altering the chemical, structural and biological conditions. This altered region of soil is known as the *rhizosphere* and is hypothesised to increase the uptake nutrients via a number of processes. For example, roots can exude organic acids which solubilise soil-sorbed P previously unavailable to the plants (Gerke, Beißner & Römer (2000)). In addition, roots also exude chemicals that promote bacterial growth, these bacteria then play a beneficial role in soil nutrient cycling (Osorio Vega (2007)). Secondly, plants change their structural development to improve acquisition of nutrients. For example, deficiencies of nitrogen and P result in increased root to shoot ratio in order to acquire more of the nutrients limiting growth (Hermans et al. (2006)); P scarcity can trigger early root growth in rice in an effort to overcome the deficiency (Gamuyao et al. (2012)) and plants can react to locally high nutrient concentrations and promote root growth in that region (Drew & Saker (1978)).

Before the industrial revolution, most soil P replenishment came from manure and human waste. To keep up with food demand for the rapidly growing population, guano (bird or bat excreta, rich in nitrogen and phosphate) and rock phosphate were used as P rich fertiliser in crop production. Towards the end of the 19th century guano supplies had started running out, throughout the 20th century the use of mined rock phosphate grew rapidly and was applied in large quantities to replenish depleted soils (Cordell et al. (2009)). Mined rock phosphate is now the primary source of P for fertiliser. However, some estimations predict it to run out in the next 50-100 years (Cordell et al. (2009)). Furthermore, Sattari et al. (2016) predicted that P input (both organic and mineral) to global grasslands will have to be more than four times that of the input of 2005 to keep up with milk and meat demands in 2050. Combining this with the predicted P requirements for crop lands, it is estimated that total mineral P use must double by 2050. This paints a pessimistic future as scarcity of resources tends to result in rising prices of fertilisers and, hence, food. Some soils in Europe and North America are now said to have reached a level where only small amounts of P need to be applied in order to replace what is lost to the crops. Developing agricultural practices that utilise 'legacy' P supplies in well fertilised fields will help reduce P usage in the nutrient rich soils of Europe and America (Stutter et al. (2012)). The same cannot be said about soils in Asia and Africa where P stocks are low (Cordell et al. (2009)). Therefore, demand for phosphate rock in these countries has grown with their population rise. In Sub-Saharan Africa, the new emerging economies, 75% of the soils are said to be 'nutrient deficient'. The demand for P fertilisers in this region is likely to increase and the UN has already called for increased access to fertilisers in this region without an obvious means to supply this essential nutrient (Cordell et al. (2009)). Rock phosphate is not a renewable resource. Most reserves are in either Morocco, China or the USA. In the USA, rock phosphate reserves are said to have approximately 25 years left. To protect their food production, China has imposed a 135% export tariff on rock phosphate. Morocco is in control of approximately one third of what is left of the world's rock phosphate supply. However, the political situation here is sensitive. Morocco occupies Western Sahara to control rock phosphate reserves and the extraction and trading of rock phosphate with state owned company is condemned by the UN (Cordell et al. (2009)). Alternate P fertilisation strategies need be developed to address this global issue.

Dwindling and expensive rock phosphate is not the only cause for concern, salinisation of soil, desertification, increased temperatures and water scarcity due to climate change will all affect

global food production (Fedoroff et al. (2010)). Current yield growth due to traditional breeding programmes is not sufficient to meet projected demands for the major grains (Furbank & Tester (2011)). Fertilisation itself is not a trivial problem, plants need different nutrients at different points in their life cycle and excess of one nutrient can inhibit the acquisition of another (Rennenberg (1984)). The current soil nutrient status, soil organic matter and acidity affect how some fertilisers impact on the plant and soil (Vaz et al. (1993)). Additionally, over fertilised fields can cause problems as water soluble chemicals can move through the ground water and over the soil surface, subsequently polluting rivers (Breeuwsma & Silva (1992)). Spreading current advances in agricultural practices globally (Baulcombe et al. (2009)) and innovations in agricultural science will be required to produce high yields in *sub-optimal* nutrient, soil, water and climate conditions to keep up with the growing populations in an altering climate. One approach is to harness the innate traits (some of which are mentioned above) of plants to survive in poor conditions via selective breeding or genetic modification (Topp et al. (2016), Fedoroff et al. (2010), Baulcombe et al. (2009), Den Herder et al. (2010), Koevoets et al. (2016)). Previous research has identified a rice gene, PSTOL1, which has been shown to increase grain yield in P deficient conditions (Gamuyao et al. (2012)). Expression of this gene also enhances early root growth which could explain the plants tolerance to low P (Gamuyao et al. (2012)). Interestingly, this gene is missing from modern rice varieties, suggesting these varieties would not be suitable for P deficent soils. Researchers have identified further cases where generations of breeding crops based on aboveground performance (*e.g.* grain mass) have negatively impacted belowground traits (Wissuwa et al. (2009), Den Herder et al. (2010)). Furthermore, a modelling study found that changes in root system architecture could directly account for historic yield trends in maize while above ground changes had little direct effect on increases in biomass (Hammer et al. (2009)), suggesting previously unmeasured changes in belowground traits could partly account for historic yield increases.

Improving plant belowground phenotyping tools, particularly image-based methods, has been identified as a new avenue for utilising the genetic wealth of plants for agricultural improvement (Topp et al. (2016), Furbank & Tester (2011)). When analysing the phenotype of genetic modifications, the conclusion 'no visible phenotype' occurs throughout the literature (Furbank & Tester (2011)). This is in part due to a lack of appropriate tools to measure the subtle phenotype differences in roots (Furbank & Tester (2011)). With this in mind, we propose a complimentary

approach: assessing the functionality of root traits and phenotypes to determine their serviceability using modelling. This could serve two purposes, firstly, the functionality of a phenotype may not be immediately clear from visual inspection and further investigation may be required to determine if the phenotype could be useful in an agricultural setting. Secondly, previously undetectable phenotypical differences amongst genotypes may manifest themselves under investigation of functionality. In the following, we describe two root traits, namely root plasticity and organic acid exudation, and we review the literature to evaluate their role in P acquisition.

## 1.3 Root traits

Two root traits are studied throughout this work; the root response to heterogeneous nutrient distribution and the exudation of organic acid to solubilise previously unavailable P. These traits are thought to be important under P deficiency, however, we also discuss how they could be utilised to improve fertiliser use efficiency. We highlight that these two traits are inherently linked using the example of cluster roots, and uncoupling the two to determine quantitative P gains for each trait individually is difficult.

### 1.3.1 Root plasticity

Root System Architecture (RSA) refers to the spatial arrangement of roots within the soil (Lynch (1995)). The RSA of a plant is formed by altering morphogenetic features such as the root growth rate, formation of lateral roots and angles of root growth (Rogers & Benfey (2015)). RSA is known to be governed by genetic and environmental factors, the latter is what we refer to as root plasticity or more generally as 'phenotypic plasticity' (it is worth noting that the RSA response to environmental factors is ultimately governed by genetics (Niu et al. (2012))). RSA plasticity is of evolutionarily benefit due to the intrinsic heterogeneous distribution of water and nutrients within the soil combined with the complex mechanical properties that inhibit/direct plant growth (Grossman & Rice (2012), Rogers & Benfey (2015), Rich & Watt (2013), Lynch (1995)). However, root plasticity comes at the nutrient and carbon expense of forming the roots and may not always be beneficial (Rajaniemi (2007)). Some authors suggest that root activity in search of nutrients is so important that plants spend half of their available photosynthate on

it (Fogel (1985)). RSA carbon cost under P stress may be a significant factor in reduced plant productivity. Therefore, it is important to take into account the carbon expenditure (both root biomass and exudation) per unit of nutrient absorbed when considering the nutrient benefits of root plasticity, this is referred to as 'uptake efficiency' (Lynch (1995), Nielsen et al. (1994)). Despite the significance of root plasticity on the ability to acquire nutrients and water, agricultural breeding programmes typically select plants based on performance in homogeneous growth media (Grossman & Rice (2012)) and hence overlook root plasticity.

The RSA of plants respond to both nitrogen and P scarcity/heterogeneity (Rogers & Benfey (2015)). Responses to low nitrogen are species dependent, but in general low nitrogen causes the roots to grow deeper with fewer roots near the soil surface. Low P typically causes a reduction in primary root growth, increases lateral and root hair formation and cluster root formation (Rogers & Benfey (2015), Niu et al. (2012)). We refer the reader to Niu et al. (2012) for a thorough review of RSA responses to low P availability. Local exposure of high nitrogen and P to primary roots promotes local lateral formation and extension in barley (Drew (1975)). Figure 1.1 shows the dramatic localised response when barley is grown in heterogeneous nutrient solution. When soil was enriched with phosphate patches, P uptake rates increase but not N uptake rates (Jackson & Caldwell (1991)). However, the authors reason that, as there was no sign of greater root density in the patches, increased P uptake was due to root proliferation due to P stress prior to the introduction of the P rich patches. Other experiments have suggested that RSA is important for immobile nutrients like P but not mobile nutrients like nitrogen when plants are in competition (Fitter et al. (2002)). Additionally, models have determined that increased root length density is one of the most important factors for P uptake (Silberbush & Barber (1983)). The RSA response to nutrient heterogeneity is a trait which could potentially be utilised in fertilisation, particularly P pellet based fertilisation. Talboys et al. (2016) suggest that the P mineral struvite (known to be only slightly water soluble, with solubility increasing in the presence of root exudates) shows promise for efficient P fertilisation. The pellet releases more P in the presence of roots which can then be absorbed by the plant rather than immobilised by the soil (Talboys et al. (2016)). They do not mention, however, the potential added benefit of local root proliferation near the pellet due to root plasticity, increasing P uptake efficiency both in terms of carbon cost and the ratio of absorbed to immobilised P. This omission may be because the region of high P concentration due to the pellet (radius in the order of mm) is smaller than the regions of soil considered in

previous studies ($\sim$ 25 cm Jackson & Caldwell (1989), $\sim$ 5 cm Zhang & Forde (1998), $\sim$ 5 cm Drew (1975), $\sim$ 1.5 cm Gross et al. (1993)) and that the size of regions are often not well controlled in these previous experiments.

Quantifying the direct P uptake benefit of RSA responses to P heterogeneity is difficult experimentally. In order to induce RSA responses, additional P needs to be added to the soil and thus the plant will absorb more P than a control by virtue of there being more available in the soil. Often, equal quantities of P are distributed in contrasting patterns. Yano & Kume (2005) compared P uptake in soil columns with additional P distributed in half-half (half the soil column was treated with P) arrangements or as many small patches. They found plants in the half-half distribution absorbed more P but the authors did not consider uptake efficiency. In a similar study Kume et al. (2006) found uniformly distributed P performed the best in terms of P uptake per plant but patchy distributed P performed better in terms of P uptake per unit root length. However, root plasticity is beneficial because it allows the plant to adapt and make the most of the quantity and distribution of the available P. Hence, these types of experiments do not capture the entire benefit of root plasticity for P acquisition in natural conditions as each condition has the same quantity of available P.

Experiments which compare P uptake in varieties/mutants which are less plastic may have scope to quantify the benefit of plasticity (Fitter et al. (2002)). However, the current lack of understanding of the genes which control root phenotypes, as well as the lack of phenotyping in soil, makes it hard to identify such varieties and mutants (Topp et al. (2016)). Typically, RSA measurements are limited to root length/mass when assessing the plastic response of RSA to nutrient distribution (Kume et al. (2006), Flavel et al. (2012), Fitter et al. (2002)). 3D techniques are now being used in phenotyping to determine the genetics of RSA traits (Topp et al. (2013)). These include geometrical and topological measurements of RSAs such as solidity, convex hull volume and 'bushiness' which could be important factors in a plant's ability to acquire nutrients (Topp et al. (2013)). However, variations in root surface area will likely dominate P uptake response and may overwhelm any possible benefits that could be attributed to other root plastic responses (Raghothama & Karthikeyan (2005)). Mathematical modelling allows more control when investigating P benefits from root plasticity. In a modelling study, root P uptake in patchy P distributions was evaluated for both a model root system that had proliferated in response to

P and one that had not. It was found that model plants with root plasticity absorbed 28% more P from the P patches but the authors did no consider uptake efficiency (Jackson & Caldwell (1996)). However, there are difficulties associated with representing the RSA within a model due to its geometric complexity and the low throughput of imaging RSA *in situ*. Clearly there are numerous questions to be answered in terms of how to assess P uptake, how to capture RSA within a model and the relationship between RSA and P uptake. We will return to these questions throughout this thesis.

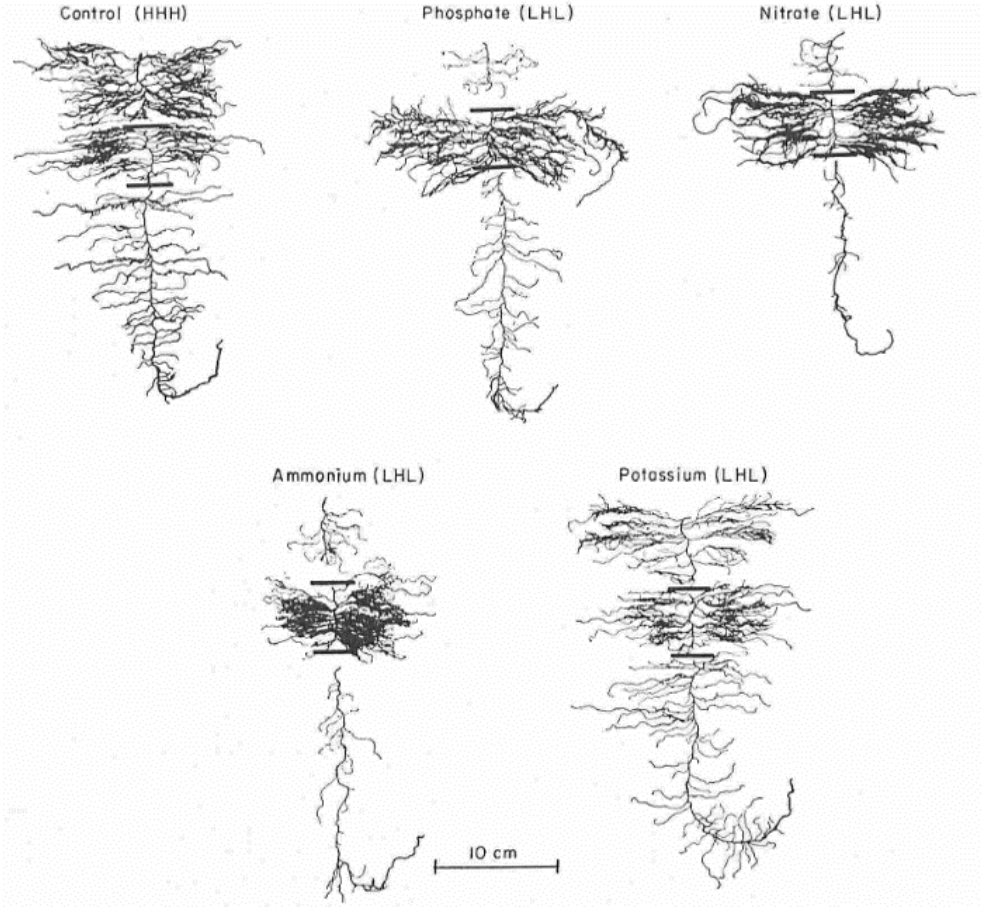


FIGURE 1.1: RSA response of barley (*Horedeum vulgare*) to varying nutrient distributions when grown in nutrient solutions. LHL refers to strips of low, high and low layers of nutrients starting from the top. Layers of high nutrient solution have 100 times more nutrients than low. The lines demonstrate where each layer starts. HHH have complete nutrient solution in all layers. Taken from the seminal work of Drew (1975).

### 1.3.2 Organic Acid Exudation

Organic acids exuded by roots, such as citrate, malate and oxalate are thought to serve a number of purposes, including metal-tolerance (particularly aluminium) and the promotion of microbial

proliferation in the rhizosphere which in itself serves a number of beneficial purposes (Jones (1998), Pellet et al. (1995)). Of importance for this work, is that organic acids can solubilize P and other nutrients adsorbed to the soil surfaces (Gerke, Beißner & Römer (2000), Oburger, Jones & Wenzel (2011)). Roots contain a wide range of organic acids internally, some are known to be intermediate compounds in energy cycles, for example citrate and malate in the tricarboxylic cycle. Typically, the quantity of organic acids within roots is between one and four percent of total dry weight (Jones (1998)). Equilibrating the cation-anion (*i.e* positive-negative) imbalance within the roots caused by root absorption of positively charged nutrients is known to partly govern organic acid concentration within roots (Jones (1998), Chang & Roberts (1991), Marschner (1995)). This feature of organic acids contributes to metal-tolerance through the organic acid (both exuded into the soil and within the root) reacting with the positively charged metal ions rendering them benign (Jones (1998)). Similarly, lack of phosphate ions within the roots would lead to an accumulation of organic acid anions, therefore exudation of these ions would amend the positive-negative in balance within the root.

The large organic acid concentration gradient between the root ($0.5 - 10$ mM) and the adjacent soil and the electric-charge gradient across the root membrane are proposed to be passive mechanisms of organic acid release (Jones (1998)). Roots can alter organic exudation rates based on their developmental stage and in response to biotic and abiotic stresses, such as nutrient deficiency and metal toxicity (Adeleke et al. (2017)), suggesting there are active mechanisms for exudation. The opening of channels within the root lipid bilayer is one such mechanism (Jones (1998)). An understanding of organic acid exudation (exudation in general) patterns remains elusive due to the difficulty in measuring the spatiotemporal dynamics of exudates *in situ*. Organic acids can immediately react with the soil or are removed by microbes. Furthermore, measurements of organic acids in soil depend heavily on the choice of sampling technique. Hydroponic systems eliminate some of these problems, however, this approach fails to capture many important processes that are prominent in soil, including microbial degradation, soil sorption, variable pore sizes and heterogeneously distributed water (Oburger & Jones (2018)).

Although organic acids are known to solubilise soil-adsorbed P, the contribution of these acids to P uptake remains unclear. A number of experiments have been carried out to investigate the concentration of organic acid added to the soil solution versus the concentration of P in soil

solution, determining at least 1 mM of organic acid is required to solubilise significant amounts of P (Gerke, Beißner & Römer (2000), Jones & Darrah (1994), Khademi et al. (2010), Mench & Martin (1991)). Concentrations of citrate in the soil are often reported between 1 and 50 μM which significantly less than the required concentration for P solubilisation (Khademi et al. (2010)). However, as mentioned, sampling root exudates in soil is difficult. Measurements of soil solution are often bulk-scale and may average-out small regions of high citrate concentration immediately adjacent to the root (Khademi et al. (2010)). Furthermore, organic acid exudation and subsequent soil adsorption, P solubilisation and root P uptake are dynamic processes; singular bulk scale measurements of organic acid concentrations may not be representative of the process (Jones (1998)). More details on the mechanisms of organic acid P solubilisation are introduced in chapter 3.

Researchers have used mutants/varieties of high or low organic acid exuding plants to quantify the benefits of citrate exudation in terms of additional P absorbed. Lopez-Bucio et al. (2000) created transgenic tobacco plants that had increased synthesis and exudation of citrate (one line two-times, another four-times the amount of citrate exuded by the control plant). They found the mutants could complete their life-cycle in low P alkaline soil while the controls could not. Furthermore, when grown in the same soil which was supplemented with all nutrients at optimal conditions except for P there was no difference in dry shoot mass after 30 days, but the mutants had between 23 and 35% more fruit dry weight. To confirm that the increased vigour in the mutants was due to citrate exudation, 1 mM of citrate was added to the soil. In this situation no difference in biomass could be detected between the control and mutants. However, the concentration of citrate added in this case is much more than that exuded by plants and thus this verification is not conclusive. Furthermore, there was no consideration of variations in root length between the control and mutants. This may be an important factor as later experiments have failed to confirm the results of Lopez-Bucio et al. (2000). Delhaize et al. (2001) tried to replicate the mutants of Lopez-Bucio et al. (2000) and found they exuded similar quantities of citrate as the control. No difference in shoot biomass could be detected between low and high citrate exuding near-isogenic wheat varieties (Ryan et al. (2014)). In the work of Ryan et al. (2014), shoot weight in poor P conditions were normalised by shoot weight in optimal nutrient conditions to account for the inherent vigour of the high-exuding plants relative to the low. Above ground vigour suggests there could also be a difference in RSA between the two varieties

which could account for the P-tolerance of the high-exuding wheat rather than (or along with) citrate exudation. In another study by Güsewell & Schroth (2017), the benefit of citrate exudation could not be detected; high and low exuding subgenera had similar growth responses to varying soil P conditions. High exuding mutants of rapeseed had higher P accumulation in their shoots compared to the wild type in both low and high P conditions (Wang, Xu, Kou, Shi, Zhang & Xu (2013)). However, these authors did not normalise the low P results by the high P results to account for any natural vigour of the mutant (as in Ryan et al. (2014)). Relative vigour may well explain this result: percentage difference of shoot P content between the wild type and the high exuding mutant was three times higher in the high P conditions than the low P conditions. This is particularly notable as organic acid exudation is known to be important when plants are under P stress as opposed to optimal P conditions. Furthermore, there was no consideration of variations in RSA nor was root P content measured. Similarly, Koyama et al. (2000) found high exuding *Arabidopsis thaliana* mutants had higher P content in their leaves than the wild type. However, they also reported that the root elongation rate in most of the mutants was more than 20% higher than the wild type. Interestingly, the high exuding mutant which had similar elongation rates to the wild type had similar leaf P content to the wild type. A high malate exuding tobacco plant absorbed more P than the wild type when P was supplied as aluminium phosphate, iron phosphate and calcium phosphate but not potassium phosphate. However, root length in the mutant was greater than the wild type in all P treatments except in the potassium phosphate treatment (Lü et al. (2012)). These studies have demonstrated that determining the P gains from organic acid exudation is difficult experimentally. Root length/surface area needs to be quantified due its large contribution to P uptake (Silberbush & Barber (1983)). When a high exuding plant absorbs more P than a low exuding plant but also has more roots, it is unclear whether the high exuding plant absorbed more P because of its increased root surface area, or because organic acids provided a P boost which supplied the nutrients for root proliferation.

Similar to root plasticity, many researchers use modelling approaches to gain more control when assessing the benefits due to organic acid exudation in P uptake. When modelling a single sugar beet root Gerke, Römer & Beißner (2000) found that oxalate exudation could increase P uptake by a factor between 1.5 and 6 when compared to a non-exuding root in P fixing conditions. Similarly, a model root system growing in a rhizotron was found to absorb up to 11% more P due to citrate exudation depending on exudation patterns (Schnepf et al. (2012)). It is important

to consider the entire root system when modelling citrate exudation and P solubilisation as roots in close proximity can collectively create regions of high organic acid concentration in the soil, known as facilitation (De Parseval et al. (2017)). However, modelling approaches for assessing the serviceability of citrate exudation for P uptake are not without their problems. Due to the difficulty in measuring root exudates, accurately determining the rate at which roots exude organic acids is difficult. Organic acids react with the soil constituents and are consumed by microbes which are heterogeneously distributed in the soil. These interactions may have feedback loops (a greater carbon supply for microbes will increase their population) and are likely non-linear (Jones (1998), Oburger, Leitner, Jones, Zygalakis, Schnepf & Roose (2011)). Furthermore, there is a lack of consistent spatiotemporal methods for measuring organic acids and P in soil (Oburger & Jones (2018)). Therefore, determining and parameterising the mechanism which governs solubilisation of P in soil by organic acids (which ultimately determines the effectiveness of organic acids for P uptake) remains challenging. Previous models often estimate these parameters based on intuition (Zygalakis & Roose (2012)), or use bulk-scale experiments (Gerke, Beißner & Römer (2000)). Improving parameterisation methods is vital for reliably determining the effectiveness of organic acids for P uptake via modelling. However, models (without parameterisation) can offer hypothesis and inform future experiments. We discuss approaches for modelling organic acid solubilisation of P from soil in chapter 3.

Root organic acid exudation is a trait that can also be utilised in P fertilisation. Struvite ($NH_4$ Mg $PO_4 \cdot 6H_2O$) is a renewable source of P (and nitrogen), and is a candidate for next-generation sustainable fertilisation (Talboys et al. (2016)). Struvite pellets are only slightly soluble in water (169.2 mg $l^{-1}$ 25°C (Bhuiyan et al. (2007)), but its solubility dramatically increases in the presence of root exudates, *e.g.* citrate, oxalate, malate and acetate (Ahmed et al. (2016), Talboys et al. (2016)). As such, fertiliser dissolution is promoted when roots are near the pellet and the plant will absorb the P rather than the P becoming immobilised by the soil. While this could provide some benefit in fertiliser efficiency, struvite does not supply enough P in the early stages of plant development. Therefore it has been suggested that using a mixed struvite-Monoammonium Phosphate (MAP) fertiliser can overcome this issue due to the solubility of MAP (Talboys et al. (2016)). Subsequent reports explicitly demonstrate plants that were grown with pure granular struvite over 100 days have dry matter yield only increased 4 times in acid-P-deficient soils and 1.6 times in calcareous-P-deficient soil, while MAP pellets increased dry

matter yield 20 and 10 times respectively (Everaert et al. (2017)). However, these measurements did not take into account the carbon cost of the Root System Architecture (RSA) required to achieve these yields, nor the P immobilisation through soil adsorption. Both these qualities have been identified as potential contributors to sustainable P fertilisation (Talboys et al. (2016)).

### 1.3.3 Cluster roots

Cluster roots are a plastic root response to nutrient deficient soil characterised by a large number of branch roots (known as 'rootlets') over a small length of an axial root. The rootlets have a short life cycle but are constantly replaced by growth of the axial root (Shane & Lambers (2005)). The cluster root response occurs in multiple plant families, Proteaceae, Casurinaceae, Fabaceae and Myricaceae for example; and can be found in some crop species *e.g. Lupinus albus* (White Lupin), *Macadamia integrifolia* (Macademia nut) and *Cucurbita pepo* (Field pumpkin) (Shane & Lambers (2005)). The cluster roots of *Hakea prostrata* at a number of stages in their life cycle can be seen in Figure 1.2. P deficiency initiates cluster root formation as does low nitrogen, iron and potassium (Liang & Li (2003), Arahou & Diem (1997)). Cluster roots' strategy for P acquisition in poor soil is two pronged. Firstly, the increased root surface in contact with the soil allows access to more soil P. Secondly, cluster root organic acid exudation is thought to be two orders of magnitude higher than non-cluster root forming species (Shane & Lambers (2005), Jones (1998), Schubert (2005)). The 'P mining' ability of these roots is amplified by the root density causing organic acid facilitation; roots in close proximity exude simultaneously creating high organic acid concentrations in the soil. Cluster-root formation is found in almost all species in the Proteaceae family, it is no coincidence that these species can inhabit the severely nutrient-impoverished soils of South Africa and Australia (Shane & Lambers (2005)). Models have suggested that cluster roots can absorb 35% additional P from citrate exudation due to their dense RSA (Zygalakis & Roose (2012)).

Cluster-root forming species' two pronged approach for survivability in severe nutrient deficiency justifies their expensive carbon cost of their formation and enhanced organic acid exudation (Shane & Lambers (2005)). The function and strategy of cluster roots is not limited to cluster root forming species; we evaluated the two facets of the cluster-root strategy in non-cluster-root forming species in the previous two subsections, we found it was hard to decouple

the P gains of organic acid exudation from RSA changes. These two traits are highly exaggerated in cluster-roots which suggest that organic acid exudation and RSA plasticity are fundamentally interlinked. Although cluster roots are not studied in this thesis, they offer a heuristic as to why RSA and organic acid exudation may need to be considered together.

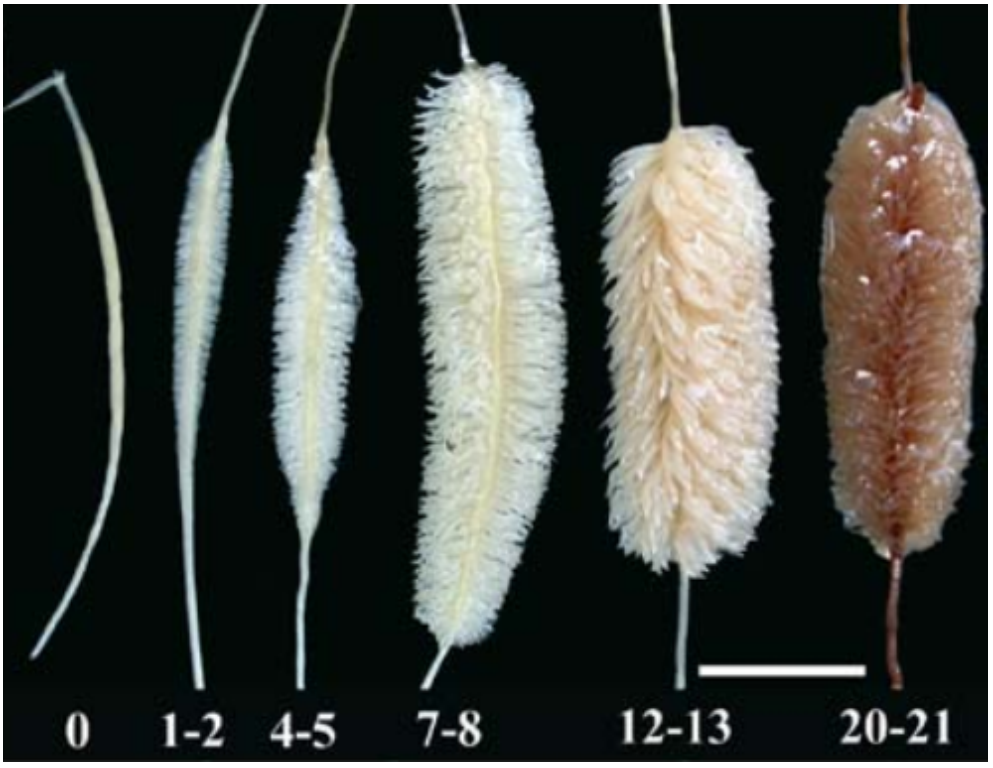


FIGURE 1.2: Six ages of the cluster roots of *H. prostrata* grown in nutrient solution with extremely low P ($\leq$ 1 $\mu$M). The ages of the cluster roots are displayed below. The white scale bar is 10 mm. Taken from Shane & Lambers (2005)

## 1.4 Modelling Plant Phosphorus Uptake

### 1.4.1 Why use modelling?

In the previous section we discussed the difficulties in determining the role of two root traits in P uptake experimentally. When assessing the response of plants to heterogeneous nutrient distribution, additional P had to be introduced to the growth media to induce the plastic response. Hence, it was hard to maintain a like-for-like comparison with a control. Furthermore, we argued that because root surface area dominates P uptake, determining the benefit of other RSA (topological or geometrical) variations would be difficult. Similarly, when assessing the benefit

of organic acid exudation in terms of P uptake, it was difficult to control for variations in RSA, which could also account for increased P uptake. When using mathematical modelling, the equations controlling root traits can be turned on or off to determine their benefit under varying soil conditions. For example, models can achieve the control that the previously cited authors aimed for in the experiments with high/low organic acid exuding mutants. A model can be solved both with and without organic acid exudation using the same RSA and P conditions to quantify the benefit of organic acid for P uptake (Schnepf et al. (2012), Gerke, Römer & Beißner (2000), Zygalakis & Roose (2012)). However, in order to make such confident predictions, the model must first be parameterised and verified through comparison to experiments in order to confirm the models accuracy ((Roose et al. (2016), Vereecken et al. (2016))).

### 1.4.2 Modelling P uptake

#### A single root model

Models describing nutrient movement and the uptake of nutrients by plants have existed since the 1960s (Barber (1995)). The classic Nye-Tinker-Barber model describes the uptake of nutrients by a single root and often forms the basis for many more advanced models which consider an entire plant or field. We briefly introduce the Nye-Tinker-Barber model here, a more detailed explanation is given in the books Barber (1995) and Tinker & Nye (2000). Consider a cylindrical root of radius $r_0$ within a cylinder of soil with infinite radius and volumetric water content $\phi 1$ [$m^3$ of soil solution $m^{-3}$ of soil] which takes values between the residual water content and saturation. The movement of nutrients is assumed to be governed by the advection-diffusion-reaction equation (in cylindrical coordinates)

$$\frac{\partial(\phi c)}{\partial t} = \frac{1}{r}\frac{\partial}{\partial r}(r\phi D\frac{\partial c}{\partial r} + rvc) - d_s, \quad r_0 < r < \infty, \tag{1.1}$$

where $c = c(t,r)$ [mol $m^{-3}$] is the concentration of the nutrient at radius $r > r_0$ and $t > 0$, $D$ [$m^2$ $s^{-1}$] is the diffusion rate of the nutrient in the pore water, $v$ [m $s^{-1}$] is the flow of water, and $d_s$ [mol $m^{-3}$ $s^{-1}$] is the nutrient-soil adsorption-desorption term given by

$$d_s = \frac{\partial c_s}{\partial t} = k_a c - k_d c_s, \quad r_0 < r < \infty, \tag{1.2}$$

where $c_s = c_s(t,r)$ [mol m$^{-3}$] is the concentration of soil adsorped nutrient at $r > r_0$ and $t > 0$, $k_a$ [s$^{-1}$] is the rate at which nutrient adsorbs to soil, and $k_d$ [s$^{-1}$] is the rate at which nutrient desorbs from soil. Often, a simplification is made by assuming adsorption and desorption happen quickly relative to diffusion and advection *i.e.* it is assumed soil reactions are in equilibrium, arriving at

$$c_s \approx \frac{k_a}{k_d} c. \tag{1.3}$$

$k_a/k_d$ is defined as the buffer power, $b$, of the nutrient in the soil, it represents the proportion of soil adsorbed nutrient to nutrient in solution. Substituting the time derivative of equation (1.3) into (1.1) we obtain[1]

$$(\phi + b)\frac{\partial c}{\partial t} = \frac{1}{r}\frac{\partial}{\partial r}(r\phi D\frac{\partial c}{\partial r} + rvc), \quad r_0 < r < \infty, \tag{1.4}$$

To represent the single cylindrical root with radius $r_0$ absorbing nutrients, the Michaelis-Menten equation is used as a boundary condition,

$$\phi D\frac{\partial c}{\partial r} + vc = -\frac{F_m(c - c_{min})}{K_m + (c - c_{min})}, \quad r = r_0, \tag{1.5}$$

where $F_m$ [mol s$^{-1}$ m$^{-2}$] is the maximum nutrient uptake rate, $c_{min}$ [mol m$^{-3}$] is the soil solution nutrient concentration when uptake stops and $K_m$ [mol m$^{-3}$] is the nutrient concentration when uptake is half of $F_m$ (Barber (1995)). Figure 1.3 demonstrates the relationship between the Michaelis-Menten parameters ($F_m$, $K_m$ and $c_{min}$), nutrient concentration and root absorption rate.

An initial uniform concentration of nutrient in the soil is usually assumed. Far from the root it is assumed the root does not affect the nutrient concentration

$$c(t = 0) = c_0, \quad r_0 < r < \infty, \tag{1.6}$$

$$c = c_0, \quad r \to \infty. \tag{1.7}$$

The non-dimensional Péclet number (the non-dimensional ratio of advection to diffusion) is small for P due to its high soil buffering, hence, the advective transport of P is often assumed to be negligible ($v = 0$) (Roose et al. (2001), Jungk & Claassen (1997), Heppell et al. (2015*a*)).

[1] We need two time scales to do this rigorously

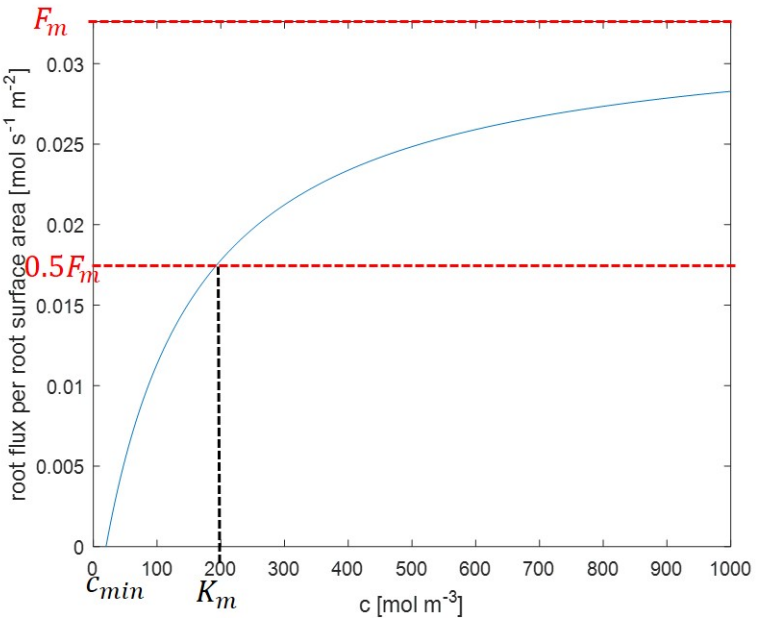


FIGURE 1.3: Michaelis-Menten uptake kinetics. The relationship between nutrient concentration, $c$ [mol m$^{-3}$] at the root surface, $r = r_0$, and root nutrient uptake per root surface area [mol s$^{-1}$ m$^{-2}$] *i.e.* the right hand side of equation (1.5). The parameter values are selected to be representative of phosphorus, $F_m = 3.26 \times 10^{-2}$ mol s$^{-1}$ m$^{-2}$, $K_m = 200$ mol m$^{-3}$ and $c_{min} = 20$ mol m$^{-3}$ Barber (1995). One can see $K_m$ is the nutrient concentration when root uptake is half $F_m$.

This model is suitable for measuring the P absorption by a single root with uniform uptake properties in homogeneous soil. However, when considering the P absorption of an entire plant, the RSA also needs to be considered.

**A root system model**

Roose et al. (2001) extended the Nye-Tinker-Barber model to measure the P uptake of an entire plant, see also Heppell et al. (2015*b*). This was achieved by considering the RSA as parameters and using an approximate analytic solution for P uptake in the single root model. Each root was considered to have radius $a$ and it was assumed that the roots were much farther apart than $a$ so that roots do not interact. An approximate analytic solution for P flux, $F_D(t,a)$, of the single root model (assuming $v = 0$) was found using a perturbation approach by Roose et al. (2001):

$$F_D = \frac{2F_m c_0}{K_m + c_0 + L + (4c_0K_m + (K_m - c_0 + L)^2)^{1/2}}, \tag{1.8}$$

where

$$L = \frac{F_m a}{2\phi D} ln(1 + 4e^{-\gamma} \frac{\phi D}{(\phi + b)a^2} t), \tag{1.9}$$

and $\gamma \approx 0.5772$ is Euler's constant, the other parameters are from the single root model. The root system is assumed to be constructed of roots of different order, distributed evenly throughout the soil. The radius of a root of order $i$ is assumed to be $a_i$. Roots have zones of length $l_a$ and $l_b$, the apical zone and basal zone respectively where they are known not to branch. Between these non-branching zones, $i+1$ order roots develop at intervals of length $l_n$. Hence, a root of length $l$ has $ceil((l - l_a - l_b)/l_n)$ branches. The elongation rate is assumed to decrease with age and is described by

$$\frac{dl_i}{dt} = L_i = r_i(1 - \frac{l_i}{K_i}), \tag{1.10}$$

where $l_i$ is the length of the root, $r_i$ [m s$^{-1}$] is the initial growth rate and $K_i$ is the maximum length of an $i$-th order root. From this, the total length of roots of order $i$ at time $t$ can be calculated as $l_i(t)$ (we refer the reader to Roose et al. (2001) for details of the calculation) and their corresponding total P uptake is

$$F_i(t) = 2\pi a_i L_i F_D(t, a_i). \tag{1.11}$$

The total P uptake at time $t$ is then the sum of all root orders

$$F_{tot}(t) = \sum_i F_i(t) \tag{1.12}$$

This approach serves as a fast approximation of the P uptake of a plant as no computationally expensive numerical schemes are required to solve it. However, assuming roots are sufficiently distant so that the P uptake of one root does not affect that of another fails to capture important interactions. For example, the competition by adjacent roots for the same soil P supply, plastic root responses to heterogeneous P supply and facilitation of root exudation (if exudation was added to the model) would be overlooked using this modelling approach. To incorporate these features into a model, the RSA should be considered in more detail. Root system growth models can be included as local parameters controlling volumetric P uptake in a model (Leitner et al. (2010*a*)). This approach captures the interactions between roots and is discussed further in chapter 4. Before we discuss another approach for including the RSA within models, we first

introduce an approach for imaging RSAs for the purpose of including them directly in models, then a numerical approach for solving differential equations on non-planar, non-cylindrical and non-spherical domains.

### 1.4.3 X-ray Computed Tomography

X-ray computed tomography (XCT) is a non-destructive 3D method for imaging internal structures. A single X-ray radiograph is created by passing X-rays through a sample and measuring their intensity, denser material attenuates more X-rays and can be distinguished from other less dense material. XCT scans take thousands of radiographs of the same sample from thousands of angles in order to obtain 3D information. From each angle we learn the integral of the linear attenuation coefficients (a value which describes the fraction of the X-ray that is attenuated) along each X-ray path. More formally, if $f(x,y,z)$ is the function of density of a sample to be reconstructed and $L(\theta)$ is a plane through the sample defined by angle $\theta$ then one XCT radiograph through the plane $L(\theta)$ yields

$$Rf(L(\theta)) = \int_{L(\theta)} f(x,y,z)dxdydz.$$

This is known as the Radon transform of $f$. The Radon transform has a well known inverse which can be used to obtain $f(x,y,z)$ from $Rf$ provided $Rf$ is known for all angles, $\theta$ (Radon (1917)). In practice, discrete versions of the inverse Radon transform, known as the filtered back projection and iterative techniques, are used to reconstruct the XCT density data into euclidean coordinates (Singh et al. (2010)).

We now briefly introduce XCT and discuss some important concepts for quantification and visualisation of roots using XCT. Reconstructed XCT data is described in terms of voxels (three dimensional pixels) whose 'colour' or greyvalue corresponds to the density of the material at the location of space that the voxel represents. The size of the voxel is defined by the length of its sides, often the voxels are cubic and can be defined by one length. The resolution of an XCT scan can be defined by how close two objects can be together before they are identified as touching in the reconstructed XCT images. The resolution of an XCT scan can be no smaller than the voxel side length. There is a trade-off between field of view and voxel size of an XCT image; as

voxel size decreases the volume of sample that can be scanned decreases. The contrast between the material of interest and the background refers to their difference in greyvalue. In order to identify and quantify which voxels correspond to the material of interest, a process known as image segmentation, there should be high contrast between the material and the background.

XCT has been used to visualise roots in optically opaque growth media such as soil (Keyes et al. (2013), Peth et al. (2008), Tracy et al. (2010), Topp et al. (2013)). Root length measurements obtained using XCT were within 8% of WinRHIZO (Regent Instruments, Canada) a typical destructive method of quantifying roots (Flavel et al. (2012)). However, the accuracy of root quantification using XCT is dependent on the voxel size, resolution, and contrast of the scan. There are a number of difficulties that can arise when scanning roots in soil. The attenuation (greyvalue) of roots is similar to water and organic matter within the soil. Hence poor contrast between the roots and soil is often obtained. Drying the sample before scanning can be used to mitigate this effect but this can alter the root and soil structure (Tracy et al. (2010)). As a result, automatic segmentation of the roots from the soil is hard to achieve and authors often rely on slow throughput manual segmentation approaches to identify, quantify and visualise roots when using XCT (Keyes et al. (2013), Koebernick et al. (2017), Ahmed et al. (2016)). Furthermore, it is difficult to image large RSAs and resolve fine lateral roots and root hairs simultaneously due to the trade off between voxel size and field of view. XCT scans of roots in soil are typically used for visualising and measuring RSAs (Ahmed et al. (2016), Topp et al. (2013), Tracy et al. (2010)) but the segmented roots can also be used to represent the RSA in models (Daly et al. (2018)). This is achieved by meshing the segmented roots and using the mesh as a domain in a finite element approximation to partial differential equations.

### 1.4.4 The Finite Element Method

When solving differential equations numerically, the continuum of space and time need to be reduced to finite sets to be handled by computers. The finite element method is a powerful tool to discretize space in a partial differential equation (PDE). It uses the geometry of the domain to build polynomials of small support that can approximate the solution to a PDE in an appropriate finite linear combination. The following is guided by the lecture notes of Iserles (2007). Before approximating PDEs using the finite element method, we first describe a more general, but

simpler problem which forms the basis of the finite element approach. Consider a Hilbert space $V$, a bilinear form, $a$, on $V$, $f$, a bounded linear functional on V and the problem $P$:

- Find $u \in V$ such that $a(u,v) = f(v)$ for all $v \in V$.

If $V$ is infinite dimensional (*e.g.* the space of $L^2$-integrable functions on $\mathbb{R}^n$) then solving problem $P$ numerically is difficult. Instead, we can approximate a solution of $P$ by considering an $n$-dimensional subspace, $V_n \subset V$, and solving the problem $P_n$:

- Find $u_n \in V_n$ such that $a(u_n, v_n) = f(v_n)$ for all $v_n \in V_n$.

As $V_n$ is a finite dimensional Hilbert space it can be spanned by a finite orthogonal basis, $\{\phi_1, \ldots, \phi_n\}$. Hence, we can write $u_n$ as a linear combination of the basis functions, $u_n = \sum_{i=1}^{n} U_i \phi_i$. Moreover, if $a(u_n, \phi_n) = f(\phi_n)$ for all $i = 1, \ldots, n$, then, $a(u_n, v_n) = f(v_n)$ for all $v_n \in V_n$. After using the linearity of $a$, the problem $P_n$ is equivalent to the problem $P_n^{'}$:

- Find $\{U_1, \ldots, U_n\}$ such that $\sum_{i=1}^{n} U_i a(\phi_i, \phi_j) = f(\phi_j)$ for $j = 1, \ldots, n$.

This is a set of linear equations in $U_i$ and can be written in matrix form:

$$A\mathbf{U} = \mathbf{f}, \tag{1.13}$$

where $\mathbf{U} = (U_1, \ldots U_n)^T$, $\mathbf{f} = (f(\phi_1), \ldots, f(\phi_n))^T$ and $A = \{a_{i,j}\}_{i,j=1}^{n}$ with $a_{i,j} = a(\phi_i, \phi_j)$. In short, we have approximated problem $P$ with a liner algebra problem.

The finite element method re-writes a PDE into the form of problem $P$ and applies the above approach to find an approximate solution. This requires the notion of the weak formulation and solution of a PDE. As an example we consider the Poisson equation in 2D:

$$\begin{aligned} -\Delta u &= f, \ \ \mathbf{x} \in \Omega, \\ u &= 0, \ \ \mathbf{x} \in \partial\Omega, \end{aligned} \tag{1.14}$$

where $\Omega \subset \mathbb{R}^2$ is open and has a piecewise smooth boundary. A solution of PDE (1.14) in the classical sense is a function $u \in C^2(\Omega) \cap C(\bar{\Omega})^2$ which satisfies both equations in (1.14). In

[2] $C^l(\Omega)$ is the space of $l$ times continuously differentiable real valued functions on $\Omega$

real world situations it is often the case that $f$ is discontinuous and PDE 1.14 does not make mathematical sense, as a continuous function, $\Delta u$, is equal to a discontinuous function $f$. We deal with this using the notion of weak solutions. The general idea is to pass the extra derivative onto a 'test' function under an integral using integration by parts. First we introduce two Hilbert spaces of functions, $H^1(\Omega) = \{g \in L^2(\Omega) : \frac{\partial g}{\partial x_i} \in L^2(\Omega),\ i = 1,2\}$[3] *i.e.* $L^2$ integrable functions whose (weak) derivatives are also $L^2$ integrable. This is a Hilbert space with inner product:

$$(u,v)_{H^1(\Omega)} := (u,v)_{L^2(\Omega)} + \int_\Omega \frac{\partial u}{\partial x}\frac{\partial v}{\partial x} + \frac{\partial u}{\partial y}\frac{\partial v}{\partial y}.$$

And $H_0^1(\Omega) = \{g \in H^1(\Omega)\ :\ g = 0 \text{ on } \partial\Omega\}$, notice if $u \in H_0^1(\Omega)$ then it automatically satisfies the boundary conditions of PDE 1.14. Let $u \in H_0^1(\Omega)$, we multiply the Poisson equation by some $v \in H_0^1(\Omega)$ and integrate:

$$\begin{aligned} \int_\Omega -v\nabla\cdot\nabla u &= \int_\Omega fv \\ \Leftrightarrow \int_\Omega \nabla v\cdot\nabla u &= \int_\Omega fv, \end{aligned}$$

the equivalence holds after integrating by parts and using the fact $v = 0$ on the boundary. Notice that $u$ in the last expression only needs to be differentiable.

A weak solution of PDE (1.14) is a function $u \in H_0^1(\Omega)$, which satisfies the weak formulation:

$$\int_\Omega \nabla v\cdot\nabla u = \int_\Omega fv, \quad \forall v \in H_0^1(\Omega). \tag{1.15}$$

If $u$ is a weak solution and also $C^2$ then $u$ is also a classical solution, and, if $u$ is a classical solution it is automatically a weak solution.

When using the finite element method to solve PDE 1.14 we notice that when it is in its weak form, it is in the form of problem $P$. Define $a : H_0^1(\Omega)\times H_0^1(\Omega) \to \mathbb{R}$ as

$$a(u,v) = \int_\Omega \nabla v\cdot\nabla u,$$

[3]The derivatives here are defined in the 'weak' sense. Weak derivatives agree with classical derivatives when classical derivatives exist.

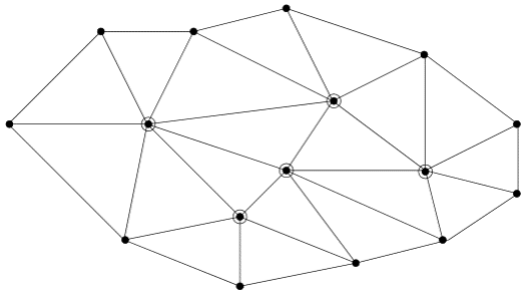

FIGURE 1.4: An example of a triangular mesh, the internal nodes have been circled as they are used to define the basis functions.

$u, v \in H_0^1(\Omega)$, and $l : H_0^1(\Omega) \to \mathbb{R}$ as

$$l(v) = \int_\Omega fv$$

Clearly $a$ is a bilinear form and $l$ is linear on $H_0^1(\Omega)$. Hence, the weak formulation can be written:

- find $u \in H_0^1(\Omega)$ such that $a(u,v) = l(v)$ for all $v \in H_0^1(\Omega)$.

We can now use the approach used on problem $P$ to approximate a weak solution of the Poisson equation. The difficulty is the choice of the finite dimensional subspace of $H_0^1(\Omega)$. Ideally, the subspace is chosen so that the matrix inversions are computationally inexpensive and that the resulting approximation incurs a small error. One way to achieve this is by choosing basis functions with 'small' support (*i.e.* so the basis functions are non-zero on small regions of $\Omega$) so that the matrix $A$ is sparse and regular. The typical way of doing this is subdividing $\Omega$ into 'elements' on which the basis functions are supported. Triangles are often used to create the elements (Figure 1.4) and 'hat functions' are often used as the functions (Figure 1.5). Suppose $\Omega \subset \mathbb{R}^2$ has polygonal boundary so that a triangular mesh fits in it exactly. Moreover, assume in the triangulation any pair of triangles either meets at an apex, a complete edge, or not at all. An example can be seen in Figure 1.4. Figure 1.5 shows an illustration of a hat function supported on 6 triangular elements. If we define basis functions in this way for each node, only neighbouring basis functions will have non-empty support intersections. We now continue with the example of the Poisson equation.

Let $\Omega = (0,1) \times (0,1)$ and mesh the domain as shown in Figure 1.6, this mesh was chosen to be regular to make things easier when defining the basis functions. However, meshes with different

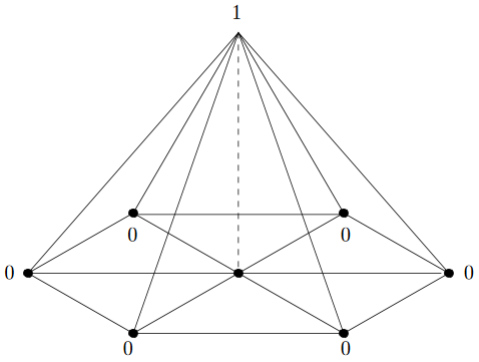


FIGURE 1.5: A pictorial representation of the hat function defined on the central node.

sized elements can also be used. The nodes are labelled $(x_i, y_j)$ and are the points circled in Figure 1.6. We define the basis function centred around node $(x_i, y_j)$ as

$$\phi_{i,j} = \begin{cases} 1 - \frac{x-x_i}{h} - \frac{y-y_j}{h}, & (x,y) \in 1 \\ 1 - \frac{y-y_j}{h}, & (x,y) \in 2 \\ 1 - \frac{x_i-x}{h}, & (x,y) \in 3 \\ 1 - \frac{x_i-x}{h} - \frac{y_j-y}{h}, & (x,y) \in 4 \\ 1 - \frac{y_j-y}{h}, & (x,y) \in 5 \\ 1 - \frac{x-x_i}{h}, & (x,y) \in 6 \\ 0, & \text{otherwise,} \end{cases} \tag{1.16}$$

where $1, \ldots, 6$ represent the 6 triangles surrounding the node $(x_i, y_j)$, shown in Figure 1.7 and $h$ is the triangle side length. This equation defines the function shown in Figure 1.5. These functions have derivatives,

$$\frac{\partial \phi_{i,j}}{\partial x} = \begin{cases} \frac{-1}{h}, & (x,y) \in 1 \cup 6 \\ \frac{1}{h}, & (x,y) \in 3 \cup 4 \\ 0, & \text{otherwise,} \end{cases} \tag{1.17}$$

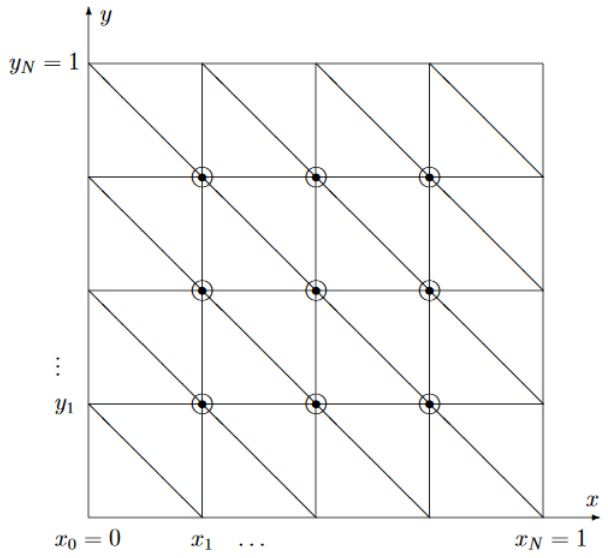


FIGURE 1.6: A regular mesh of a square with uniform side length $h$

and

$$\frac{\partial \phi_{i,j}}{\partial y} = \begin{cases} \frac{-1}{h}, & (x,y) \in 1 \cup 2 \\ \frac{1}{h}, & (x,y) \in 4 \cup 5. \\ 0, & \text{otherwise.} \end{cases} \tag{1.18}$$

Therefore, the equivalent of problem $P_n$ when approximating the Poisson equation using the finite element method is: find $\{U_{i,j}\}_{i,j=1}^{N-1}$ such that $\sum_{i,j=1}^{N-1} U_{i,j} a(\phi_{i,j}, \phi_{k,l}) = f(\phi_{k,l})$ for all $k,l = 1,\ldots,N-1$. For a given $k,l$

$$\begin{aligned} \sum_{i,j=1}^{N-1} U_{i,j} a(\phi_{i,j}, \phi_{k,l}) &= \sum_{i,j=1}^{N-1} U_{i,j} \int_\Omega \frac{\partial \phi_{i,j}}{\partial x}\frac{\partial \phi_{k,l}}{\partial x} + \frac{\partial \phi_{i,j}}{\partial y}\frac{\partial \phi_{k,l}}{\partial y} dxdy \\ &= \frac{1}{h^2}(4U_{k,l} - U_{k-1,l} - U_{k+1,l} - U_{k,l-1} - U_{k,l+1}), \end{aligned}$$

the second equality holds as the only basis functions with overlapping support with $\phi_{k,l}$ are those centred above, below, to the left and to the right of the node $(x_k, y_l)$. Additionally, the finite dimensional approximation to the linear functional is

$$l(\phi_{k,l}) = \int_\Omega f \phi_{k,l} dx.$$

After re-labelling double indices to single indices using the mapping $(k,l) \mapsto (k-1)(N-1)+l$

we see that this is the matrix which would arise from the central difference formula on a regular grid. However, in this case the contribution of the force, **f**, is averaged by the basis functions. The power of the finite element approach is the adaptability of meshes to fit a range of shapes

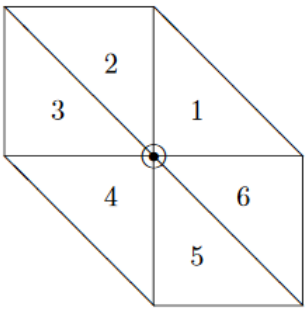


FIGURE 1.7: Mesh labelling system around each internal node.

and sizes. One can see that defining basis functions on an irregular mesh, although notationally difficult, can be achieved and hence more complicated geometries can be considered.

Throughout this report PDEs also contain time-derivatives. However, for any time $t$ we can write

$$a(u(x,t),v) = \int_{\Omega} f(x,t)vdx \tag{1.19}$$

and use the above approach to discretize the spacial variables. To approximate solutions in time, standard time stepping approaches can be used. When using explicit time-steppers, stability conditions become tied to the maximal element side length and time-step size. However using implicit time-steppers, like the backward Euler method, the stability of the entire method is dependent only on the time-step size.

The finite element method can be integrated with XCT data to produce a powerful tool for studying spatially complex problems on real geometries. Such a combination is known as image-based modelling. This approach uses meshes of segmented XCT data as the support of basis functions in a finite element method. As such, the *geometry* of the system is not approximated by parameters or cylinders but as elements within a finite element scheme. A similar model to the single root model (Equations (1.1), (1.2) and (1.5)) in Cartesian coordinates was solved on XCT extracted sections of root and root hairs to quantify P uptake (Keyes et al. (2013)). In

this case, individual soil particles were meshed and soil P sorption was modelled as a boundary condition on the soil surfaces rather than as a volumetric reaction. Whole (young) RSA have also been used as the domain for image-based models. Daly et al. (2018) used wheat RSA in the domain for a water flow and uptake model. Image-based modelling comes at the price of computational expense; while the single root model only had one space variable, image-based models from XCT data require all three space variables. Moreover, to resolve small geometric features like fine lateral roots, root hairs and soil particles, the mesh has to be formed of small elements, increasing the dimension and reducing the sparsity of the matrix, $U$, to be inverted and thus increasing computation time and memory requirements. To ensure the predictability of models, suitable experiments are required to determine their parameterss. We now introduce approaches for measuring soil P for the purpose of modelling.

## 1.5 Measuring Soil Phosphorus and Parameterising Models

P in soil can exist in many forms, the forms are often classified into one of four categories: 1) P dissolved in soil solution; 2) P adsorbed to inorganic soil constituent surfaces; 3) P minerals, usually calcium, aluminium or iron phosphates; 4) P in organic matter such as dead plant material (Barber (1995)). Of interest in this work is P in soil solution, P adsorbed to soil surfaces and the relationship between the two. As discussed in section 1.2, P in soil solution is in a forward/backward chemical reaction with soil-sorbed P; solution P can become adsorbed to soil surfaces, equally sorbed P can desorb into soil solution. P in soil solution is directly available to plants. However, the amount of P available to plants is also dependent on the rates of adsorption/desorption. When P is absorbed by the roots, the amount of P in soil solution decreases, shifting the state of the chemical equilibrium and promoting desorption of P from soil surfaces based on the backward reaction rate (Barber (1995), Abdu (2006)). The term ‘available P’ (or labile P) refers to the amount of soil P which can be absorbed by plants. Traditional methods for evaluating available P typically add water, acids, salts, and/or bases to soil, leave it for a certain amount of time, then the concentration of P in the resulting solution is measured (Abdu (2006)). The reaction rates of P with soil surfaces have been investigated using isotopically labelled $^{33}$P, two equilibration times were detected — an equilibrium appears relatively quickly, usually within one or two days, then a much slower one appears. ‘Available P’ often refers to

the P that reaches equilibrium relatively quickly (Barber (1995)), however, 'available P' in this sense is dependent on how soil P is extracted. The buffer power, which controls the ratio of solution to adsorbed P in uptake models (Equation (1.4) and (1.9)) is often determined using the traditional soil extraction methods mentioned above (Barber (1995), Keyes et al. (2013), Gerke, Beißner & Römer (2000)). However, assuming that the quantity of adsorbed P can be well approximated using solution P using a singular parameter, $b$, is an approximation for two reasons. Firstly, the proportion of adsorbed to solution P varies depending on the concentration of P in the soil solution, known as the adsorption isotherm (which varies dramatically from soil to soil). This assumption is often addressed by adding a range of P concentrations to the soil, leaving it to approach equilibrium, then measuring how much is left in soil solution (Kinniburgh (1986), Barber (1995), Sanchez & Uehara (1980)). This is included in models by replacing the approximation $c_s = bc$ (Equation (1.3)) with a more general function, $c_s = f(c)$ and fitting the parameters in $f$ to the adsorption isotherm experiments (Kinniburgh (1986)). The function $f$ is typically assumed to be either the Langmuir equation

$$f(c) = \frac{aBc}{1+ac} \tag{1.20}$$

where $a$ is a parameter related to bonding energy and $B$ is the adsorption maximum, or the Freundlich adsorption equation, $f(c) = ec^d$, where $e$ and $d$ are empirical parameters (Barber (1995)). Secondly, the derivation of buffer power requires the assumption that the soil reaction rates are 'fast' relative to geometrically-impeded diffusion, *i.e* the assumption made when going from Equations (1.1)+(1.2) to Equation (1.4). The same assumption is made when using the Langmuir equation or Freundlich adsorption equation (Schnepf et al. (2012)). This approximation is less commonly addressed but may be important. The labile-pool of P is often left one or two days to equilibrate when measuring adsorption isotherms, suggesting that these reactions are, in fact, not so fast. Furthermore, plant available P is dependent on the desorption rate of P from soil surfaces (Barber (1995), Abdu (2006)) as well as the equilibrium state. We attribute the scarcity of modelling studies using dynamic P adsorption/desorption reactions to the lack of experiments investigating soil P adsorption/desorption rates, which itself is attributed to the shortage of non-destructive soil solution sampling techniques. Previous studies have estimated soil adsorption/desorption rates based on pseudo-dynamic experiments where multiple

replicates are sampled at a range of times (Zhang et al. (2012), Wang et al. (2005)) (see the supplementary material of Keyes et al. (2013) to see how these experiments can be used to estimate P adsorption rates). Large variation in the data is expected when using this approach due to the heterogeneity between replicates, this is demonstrated by the large error bars in the sorption kinetic experiments of Zhang et al. (2012).

### 1.5.1 Microdialysis Probes

Microdialysis probes offer a non-destructive method for sampling soil solution. As such, they can be used to continuously measure P concentration to assess P adsorption kinetics. Microdialysis probes consist of a semi-permeable membrane with plumbing to allow water to travel around the probe from an inlet to an outlet (Figure 1.8). The 'perfusate' is the solution which is fed into the probe and the 'dialysate' is what is collected. As the perfusate passes through the microdialysis probe, solutes from the external solution can pass across the semi-permeable membrane into the probe, which is then collected. Similarly, solutes in the perfusate can pass from the probe into the external solution. This feature can be utilised so that the probe can simultaneously absorb phosphate and exude organic acids while measuring both quantities (Demand et al. (2017)). The relative recovery (the ratio of the concentration of solute in the dialysate to the external solution) increases when the flow rate decreases as the exchange time along the membrane increases. Furthermore, due to the small size of the probes they can be used to sample small regions of soil. We review some of the uses of microdialysis probes in soil and difficulties that may arise when using them to assess P adsorption kinetics in chapter 3.

## 1.6 Conclusions

The possible benefits to P uptake from organic acid exudation and root plasticity in response to heterogeneous P in the soil were found to be important traits. It was argued that it is difficult to quantify their benefits through experimental means, primarily due to the problems of controlling for root surface area/mass/length. The theory of modelling P uptake was introduced and proposed as a method for assessing the benefits of these root traits. However, models which represented the root system architecture as parameters and assumed roots are 'sufficiently far apart'

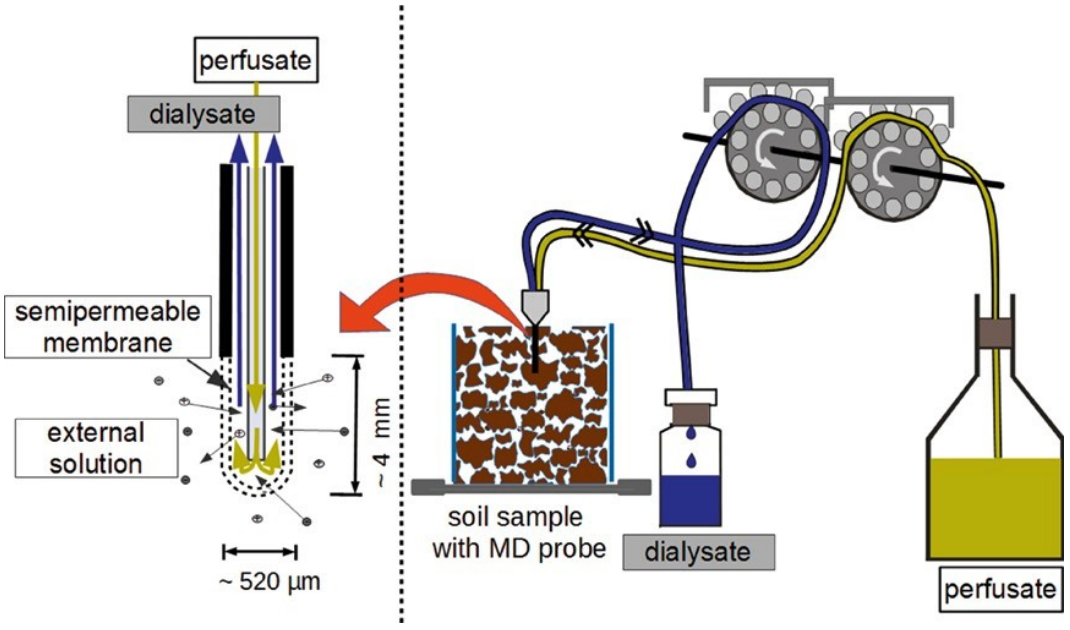


FIGURE 1.8: Diagram explaining microdialysis nomenclature and operation. Figure taken from (Demand et al. (2017)).

were not suitable for investigating P uptake by plants when positive and negative interference play an important role. Instead, using meshes of root system architectures extracted from XCT scans of real roots in soil as the elements in a finite element scheme was proposed as a suitable modelling approach. However, ensuring the model is accurate is an important step before using it to make predictions. It was argued that it is difficult to parameterise P uptake models (particularly ones with dynamic soil reactions) using destructive sampling and microdialysis was proposed as a means of non-destructively sampling soil solution. We now highlight problems and research questions that have been alluded to in the introduction that we hope to investigate in the following chapters:

1. How does root plasticity affect P uptake efficiency from the fertiliser pellet?
2. Can microdialysis probes be used to determine the P uptake benefit due to organic acid exudation?
3. Can microdialysis probes be used as model roots in experiments?
4. Does root system architecture affect the P uptake benefit of citrate exudation? If so, is there any measures of the root system architecture that can predict the P uptake benefit?

## 1.7 Thesis Structure and Declaration of Work

The work in this thesis primarily involves verifying and parameterising root P uptake models and using these models to assess the role of two root traits for P uptake. Throughout, models are parameterised and informed by experiments to ensure accuracy. Each scientific chapter is a published paper (chapter 2 - Fletcher, Keyes, Daly, Van Veelen & Roose (2019), chapter 3 - Fletcher, Shaw, Sánchez-Rodríguez, Daly, van Veelen, Jones & Roose (2019)) and (chapter 4 - Fletcher et al. (2020)).

In chapter 2 we investigated root P uptake from a fertiliser pellet. We proposed elemental mapping as a method for verifying and parameterising image-based models. The 3D XCT data (used as the geometry in the model) was aligned with the 2D elemental maps with an approach borrowed from medical imaging to ensure accurate verification. The parameterised model was then used to quantify the difference in P uptake between a root system that had responded to the presence of a fertiliser pellet and one that had not. It was found that a plant that had reacted to the fertiliser pellet had 12.5% increased P uptake near the fertiliser pellet. The author wrote the manuscript and the author and co-authors edited it. Plant preparation and XCT imaging was carried out by Dr. Samuel Keyes at μ-Vis, University of Southampton. Thin-section preparation and elemental mapping was carried out by the Scanning Electron Microscope Facility at the National Oceanography Centre, Southampton. All other tasks were carried out by the author. We would also like to acknowledge the contribution of the reviewers and editor of Rhizosphere for their helpful comments when the paper was under review for publication. Chapter 2 differs slightly from the publication in *Rhizosphere* (Fletcher, Keyes, Daly, Van Veelen & Roose (2019)), we included the supplementary material into the chapter and extended the introduction to include a more thorough review of 2D-3D image correlation methods.

Chapter 3 involved measuring soil P mobilisation by citrate in soil using microdialysis probes. Microdialysis probes have complex interactions with the soil, hence, these interactions were calibrated using mathematical modelling to aid interpretation of the results. Using modelling and microdialysis probe results, we quantified the rate at which citrate can mobilise P from soil. This rate was then used in a model of a single exuding root to determine the benefit of citrate on P uptake. It was found that a single root exuding citrate at a typical rate did not enhance P

uptake. However, as the exudation rate increased, dramatic gains in P uptake was observed. The author wrote the manuscript and the author and co-authors edited it. Microdialysis experiments were carried out by Dr. A.R. Sánchez-Rodrìguez, Dr. R. Shaw and Prof. D.L. Jones at Bangor University, Wales, all other tasks were completed by the author. We would like to acknowledge the reviewers and editor of *Plant and Soil* for their helpful comments when the manuscript was under review.

In chapter 4, we extended the verified model of chapter 3 to domains obtained from XCT in order to investigate the role of root system architecture in citrate enhanced P uptake. Eleven image-based models of growing root systems absorbing P were solved with and without citrate exudation to determine its benefit for P uptake. Percentage additional P uptake due to citrate exudation was compared to geometrical and topological measurements of the root system architecture to determine important phenotypes for P tolerance. There was large variation in citrate enhanced P uptake (normalised by the quantity of citrate exuded) amongst the eleven root system architectures, suggesting that root structure plays an important role in citrate enhanced P uptake. Number of root tips and average inter root tip distance of the plants were found to play an important role in citrate enhanced P uptake. The author wrote the manuscript and the author and co-authors edited it. All tasks were completed by the author. The time-resolved root system architectures were taken from Daly et al. (2018).

In chapter 5, we draw conclusions from the three scientific chapters and suggest further experiments and models which could be used to further understand the role of root plasticity and citrate exudation in P uptake.

### 1.7.1 Additional PhD Work

The author worked on projects that are not included in this thesis throughout their PhD. We briefly describe the work the author contributed to published and soon-to-be submitted articles. The manuscript 'Image-based quantification of soil microbial dead zones induced by nitrogen fertilization' (Ruiz et al. (2020)) used image-based modelling and microbial respiration experiments to determine microbial activity reduction around a fertiliser pellet induced by high nitrogen concentrations. Pellet, soil and pore structure were extracted from an XCT images to form the basis of a domain to solve a two-phase water-air model upon. The water phase (at multiple

saturations) was then meshed to form the domain of a nitrogen diffusion model. Complimentary experiments determined the concentrations of nitrate and ammonium which inhibit microbial activity. From this data an inhibition map around the fertiliser pellet was created. The author is joint first author on this manuscript and carried out all the image-processing, meshing and modelling (with exception of the two-phase modelling) with Dr. Siul Ruiz. The author also contributed to writing and editing the manuscript.

The article 'Root induced soil deformation influences Fe, S and P: Rhizosphere chemistry investigated using synchrotron XRF and XAS' (Van Veelen et al. (2019)) regards the difference in soil chemistry between bulk and rhizosphere soil. X-ray fluorescence microscopy and X-ray absorption near-edge structure were used to map and characterise P iron and sulfur in soil. Iron and sulfur were shown to accumulate near the root. Furthermore, iron was shown to reduce and more P adsorbed to organic surfaces closer to the root. The author helped with sample preparation, data acquisition and editing.

The article 'Significance of root hairs at the field scale – modelling root water and phosphorus uptake under different field conditions' (Ruiz et al. (2019)) aimed to quantify the significance of root hairs on P uptake at the plant scale using modelling. Root hairs were found to contribute to 50% of P uptake. The author helped with the numerical implementation of the model and edited the manuscript.

The article 'Multiple scale homogenisation of nutrient movement and crop growth in partially saturated soil' (Duncan et al. (2019)) used homogenisation to derive average equations of nutrient movement in soil containing growing tubers. The soil was modelled as a pore elastic material that could deform with tuber growth, which ultimately altered the transport properties of the nutrient through the soil. The homogenised equations were within 2% of the full set of equations but significantly reduced computation time. The author helped with model formulation, averaging and writing. The author designed and implemented the numerical demonstration of convergence of the homogenisation. The author and Dr. Siul Ruiz handled the reviewers comments before publication.

'Measurement of micro-scale soil deformation around roots using four-dimensional synchrotron tomography and image correlation' (Keyes et al. (2017)) used time resolved high resolution XCT to image roots growing in soil. Both wild type and root-cap-less maize plants were imaged. Two

methods were used to track soil displacement by the root, namely digital volume correlation and morphometric particle tracking. The cap-less plants had more soil displacement the wild type plant in dry soil. The author helped with data collection, contributed with the design and implementation of the particle tracking software and edited the manuscript.

# Chapter 2

# A multi image-based approach for modelling plant-fertiliser interaction

**Daniel M. McKay Fletcher**[a], **Samuel D. Keyes**[a], **Keith R. Daly**[a], **Arjen van Veelen**[a], **Tiina Roose**[a]

[a]Bioengineering Sciences Research Group, Department of Mechanical Engineering, School of Engineering Sciences, Faculty of Engineering and Physical Sciences, University of Southampton, Southampton, UK.

## 2.1 Abstract

Phosphorus fertilisation is crucial for crop yields. However, traditional phosphate resources are dwindling, thus a more efficient use of phosphorus fertilisers is required for sustainable farming (Cordell et al. (2009)). This study demonstrates the scope of image-based models parameterised by elemental maps by assessing how a plastic root system architecture may improve phosphorus root uptake from a fertiliser pellet. A multi-image based modelling method was developed by utilising structural imaging coupled with elemental maps. Structural imaging was used to capture barley (*Hordeum vulgare L. cv. Optic*) root, soil and fertiliser pellet configurations as a domain for numerical simulations. Elemental mapping was used to image phosphorus in soil thin-sections of the same samples. These two imaging modes were aligned using an automated

method and image-based models describing the diffusion and root-uptake of phosphorus in soil were parameterised using the elemental maps. Structural imaging showed root length density was increased inside and near the fertiliser pellet, indicating a plastic response by the plant to the fertiliser pellet (Drew (1975)). Averaging elemental data revealed phosphorus gradients from the pellet. Modelling results suggested: the pellet only enhances phosphorus uptake of roots within 2 mm over 30 days, densely packed roots decrease phosphorus uptake efficiency, and a root system that responded to nutrients from a fertiliser have comparatively increased phosphorus uptake efficiency near the pellet. The combination of structural and elemental imaging provides the means to accurately parameterise both the geometric and chemical aspects of models describing phosphorus movement in root-soil-fertiliser systems. This approach may be applicable to other plant-soil systems where structure and elemental quantities are important to the problem.

## 2.2 List of Symbols

| | |
|---|---|
| C | control treatment containing only soil |
| CG | fertiliser treatment containing soil and a crystal green fertiliser pellet |
| PL | plant treatment containing soil and plant |
| PLCG | plant fertiliser treatment containing soil, plant and fertiliser |
| $c_l$ | phosphorus concentration in spherical model [mol $m^{-3}$] |
| $D$ | diffusion coefficient of phosphorus in water [$m^2$ $s^{-1}$] |
| $\phi$ | volumetric water content [$m^3$ $m^{-3}$] |
| $b$ | buffer power of phosphorus [-] |
| $r$ | radius in spherical model [m] |
| $r_f$ | average radius of the fertiliser pellet [m] |
| $r_b$ | distance from centre of the fertiliser pellet to edge of the domain [m] |
| $t$ | time [s] |
| $D_{eff}$ | effective diffusion of phosphorus in bulk soil [$m^2$ $s^{-1}$] |

| | |
|---|---|
| $c_0$ | initial concentration of phosphorus in the soil [mol m$^{-3}$] |
| $c_f$ | concentration of phosphorus immediately adjacent to the fertiliser pellet [mol m$^{-3}$] |
| CGEDS units | relative unit of concentration in the CG elemental map |
| PLCGEDS units | relative unit of concentration in the PLCG elemental map |
| $\mathbf{v}$ | $n$-vector containing averaged elemental data at increasing distance from the fertiliser pellet in CG treatment [CGEDS units] |
| $r_i$ | grid points of $\mathbf{v}$ in radial coordinates [m] |
| $t_*$ | 30 days |
| $\Omega \subset \mathbb{R}^3$ | image-based model domain representing homogeneous soil |
| $\Gamma \subset \mathbb{R}^2$ | the boundary of $\Omega$ |
| $\Gamma_f \subset \Gamma$ | the fertiliser surface |
| $\Gamma_r \subset \Gamma$ | the root surface |
| $\Gamma_b \subset \Gamma$ | the image boundary |
| $P_l$ | concentration of phosphorus in the image-based model [mol m$^{-3}$] |
| $\lambda$ | linear root-uptake rate of phosphorus [m s$^{-1}$] |
| $P_f = c_f$ | concentration of phosphorus immediately adjacent to the fertiliser pellet [mol m$^{-3}$] |
| $\mathbf{n_r}$ | unit normal to root surfaces pointing into the domain [m] |
| $\mathbf{n_f}$ | unit normal to the fertiliser surface pointing into the domain [m] |
| $P_l^0$ | initial concentration of phosphorus in the soil (image-based model) [mol m$^{-3}$] |
| $\mathbf{u}$ | $n$-vector containing averaged elemental data at increasing distance from the fertiliser pellet in CG treatment [PLCGEDS units] |
| $x_i$ | grid points of $\mathbf{v}$ or $\mathbf{u}$ in Cartesian coordinates [m] |

## 2.3 Introduction

Phosphorus (P) is one of the most important nutrients for plant growth and thus P fertilisation is often needed to obtain high crop yields (Barber (1995)). Due to the increasing global population, the demand for P fertilisers is rising (Cordell et al. (2009)). However, only 10-20% of P fertiliser applied to a field is taken up by the crop in a growing season, the rest is immobilised in the soil (Cornish (2009)). The primary source of (inorganic) P is the finite resource rock phosphate, however the supplies are dwindling (Cordell et al. (2009)). To ensure a continued and sustainable use of P, it is necessary to develop more efficient usage of P, find renewable alternatives to rock phosphates and optimise agriculture practices. The carbon cost of the Root System Architecture (RSA) required to access P from the fertiliser and the quantity of P immobilised through soil adsorption have been identified as potential contributors to sustainable P fertilisation (Talboys et al. (2016)).

Roots respond to heterogeneous nutrient distributions in soil with a dynamic RSA (Drew (1975)), a trait which could be exploited to improve the efficiency of pellet-based fertilisers. Experiments have shown that RSA responses are more important for less mobile ions such as phosphate than mobile ions such as nitrate in terms of competition with other plants (Fitter et al. (2002)). Furthermore, models have suggested that an increased root length density is an important factor for enhanced P uptake (Silberbush & Barber (1983)). Roots can increase lateral root length and branching by either a positive response to regions of high nutrient concentrations, or as a means of searching for scarce nutrients. When white lupin (*Lupinus albus*) experiences low P conditions the RSA reacts to the stress by forming cluster roots (Johnson et al. (1996)). The increased root surface area is thought to enable higher P uptake. This is a high-risk, high-reward strategy as the carbon cost of such RSA responses are high, while the amount of P in the region may be small. Barley (*Hordeum vulgare*) roots have been shown to react locally to patches of increased phosphate and nitrate concentration by increasing both branching and extension of lateral roots (Drew (1975)). When 4 cm of seminal barley root is supplied with P and the rest of the RSA is deprived, lateral root growth is greatly enhanced in the P rich regions and subdued in the P deprived regions (Drew & Saker (1978)). In the same study it was shown that total lateral root length in the locally P rich regions was 15 times longer in comparison with those grown in a uniform P region (Drew & Saker (1978)). Similar issues were addressed using X-ray Computed

Tomography (XCT), Flavel et al. (2012) found adding both banded and uniformly distributed P increased total root length compared to a no P control. However, there was no significant difference in total root length between the two P treatments, but local root length changes around the P bands were not quantified.

Despite the significance of the RSA on P uptake efficiency (defined as P absorbed by the plant per carbon spent on the root system) conventional root-soil interaction models typically reduce the RSA to simple parameters related to root length density, root growth rates, and/or root branching rates (Itoh & Barber (1983), Silberbush & Barber (1983), Barber (1995), Wang, Ridoutt, Luo & Probert (2013), Heppell et al. (2015*b*)). To assess the nuance and importance of RSA on P uptake from a fertiliser source in soil using modelling, the RSA should explicitly be considered (Gérard et al. (2017)). Image-based modelling provides a means to simulate P uptake of a RSA by basing the domain of the model from 3D images of roots in soil. A similar approach was taken to study water uptake (Daly et al. (2018)).

Image-based models (models which are solved on domains from imaged samples) have been used in many research topics when geometry plays an important role in the functionality of the system (Tsubota & Adachi (2004), Zhao et al. (2013), Daly et al. (2016), Roose et al. (2016), Cooper et al. (2017), Daly et al. (2018), Koebernick et al. (2017)). Image-based models improve on classical models where roots, or other geometrical structures such as bone or tissues, are represented by parameters and solved in idealised geometries. However, recent reviews have called for models of soil to be verified with experiments to produce more predictive tools (Roose et al. (2016), Vereecken et al. (2016)). In this paper, the 2D elemental mapping technique Scanning Electron Microscopy with Electron Dispersive X-ray Spectroscopy (SEM-EDS) was applied to thin-sections of the imaged samples as a means for verifying and informing image-based models. To demonstrate this multi-image-based approach, an image-based model describing root P uptake from a small fertiliser pellet is fit to P elemental maps. The capabilities of the model are demonstrated by investigating root P uptake efficiency of different RSAs from a fertiliser pellet. The model is used to approximate P uptake from a mixed struvite and monoammonium phosphate (MAP) pellet. It is hypothesised that a plastic RSA can improve P uptake efficiency from fertiliser pellets by decreasing the overall carbon cost while maintaining a high rate of P acquisition. We demonstrate that these models provide the means to investigate such hypothesis.

The barley plants used in this study were grown with and without the addition of a single struvite-MAP pellet. After a 30 day growth period, the samples were 3D imaged using XCT to provide structural information. These images were used both to parameterise finite element modelling and to investigate root length density around the fertiliser pellet. XCT offers a non-destructive method to study root-soil-fertiliser structure in undisturbed samples. With the use of tomographic techniques, soil, root and root hair structures have been examined (Keyes et al. (2013), Peth et al. (2008), Tracy et al. (2010)). In addition, XCT has been used to estimate root length. Flavel et al. (2012) showed that XCT analysis yielded similar root length measurements (8% less) when compared with a destructive washing method using WinRhizo analysis software, the standard method for root length measurement. However, with XCT there is a trade-off between the resolution and the field of view, making it difficult to image full root systems while resolving smaller roots.

To complement the XCT data with chemical information for the purpose of modelling, high spatial resolution chemical measurements are necessary. Several possible techniques are described in the literature such as autoradiographs of radioactively labelled P which produces images showing depletion zones around the roots (Bhat & Nye (1973, 1974), Hattingh et al. (1973), Hübel & Beck (1993)). Kuchenbuch & Jungk (1982) proposed a method where roots are separated from a region of soil with a nylon mesh. The soil is then frozen and sectioned with increasing distance from the mesh and the exchangeable solute is estimated in bulk in the soil sections. This approach is effective for P as demonstrated by Jungk & Claassen (1989) and Gahoonia & Nielsen (1992). More recently Diffusive Gradients in Thin films (DGT) has been used to detect P depletion zones in the rhizosphere. This method produces 50 μm by 333 μm resolution maps with Laser Ablation Inductively Coupled Plasma Mass Spectrometry (Santner et al. (2012)). DGT has also been used to detect P gradients originating from P rich gel into a no-P gel (Ding et al. (2013)). In this contribution 2D elemental mapping using Scanning Electron Microscopy Electron Dispersive X-ray Spectroscopy (SEM-EDS) on resin perfused soil samples is proposed as a means for verifying image-based models. SEM-EDS has proven an effective method for investigating associations of heavy metals with soil chemicals (Yarlagadda et al. (1995)), black carbon morphological and chemical properties in soil (Brodowski et al. (2005)), the effect of apatite as a means of forming insoluble pyromorphite to remediate lead

contaminated soils (Laperche et al. (1997)), organic carbon distribution in soil aggregates (Wan et al. (2007)) and analysing forensic soil from crime scenes (Cengiz et al. (2004)).

To effectively combine XCT and SEM-EDS data, the 2D image slices representing the thin-sections were required to be found within the 3D-XCT data. The thin-sections could lie in any orientation and depth in the XCT stack, as shown in Figure 2.1, hence, locating the correct slice poses a challenging computational problem. P gradients originating from a fertiliser pellet in the soil are expected to be narrow and sharp over 30 days (approximately 4 mm) (Barber (1995)). Disturbances caused by the resin perfusion and thin sectioning process could affect P gradients observed in the SEM-EDS data, although, the SEM-EDS studies mentioned above have assumed disturbances to be negligible. The alignment of the XCT and SEM-EDS data can verify that the resin perfusion and thin sectioning process does not alter the morphology significantly. Furthermore, alignment allows the understanding of the original 3D embedding of the 2D chemical maps. In particular, the 3D distribution of roots around the thin-section can be calculated using the aligned XCT data. Few methods exist for aligning XCT to SEM-EDS, Hapca et al. (2011) offer a statistical approach for aligning the data. Their method uses Pearson Correlation Coefficient (PCC) as a measure of image similarity to compare two 2D images of the same dimensions, the XCT slice (from a selection of orientations) with the highest PCC with the thin-section is chosen as the aligned XCT data. This method is computationally expensive as each slice of each orientation needs to be compared to the thin-section. Furthermore, if the SEM-EDS and XCT slices are not the same size, two further search parameters are introduced for image cropping. Another approach is to manually pair points in the two data sets that represent the same space, then use these points to form a transformation matrix to orientate the XCT data normal to the thin-section (De Boever et al. (2015)). However, to ensure the paired points are correct, the XCT data has to be oriented approximately normal to the thin-section a-priori, which is the majority of the original problem. Methods exist for the more general problem of aligning 2D images to 3D images. One such method is to manually searching through the slices and orientations of the 3D data and finding the slice that looks most similar to the 2D image (Zeller-Plumhoff et al. (2017)). This approach can be time consuming, and both user and sample dependent. An approach similar to Hapca et al. (2011) is taken in Kubias et al. (2008), where the norm of the difference of the flattened images is used as the measure of image similarity instead of PCC. Chicherova et al. (2014) offers a qualitative approach to solve the

problem using 2D computer vision techniques. This computer vision approach can compare images of different dimensions and scales. As a similar approach is taken in this study, a full description of this method is given in the Materials and Methods section and a comparison of this approach with that of Hapca et al. (2011) is given in the Discussion.

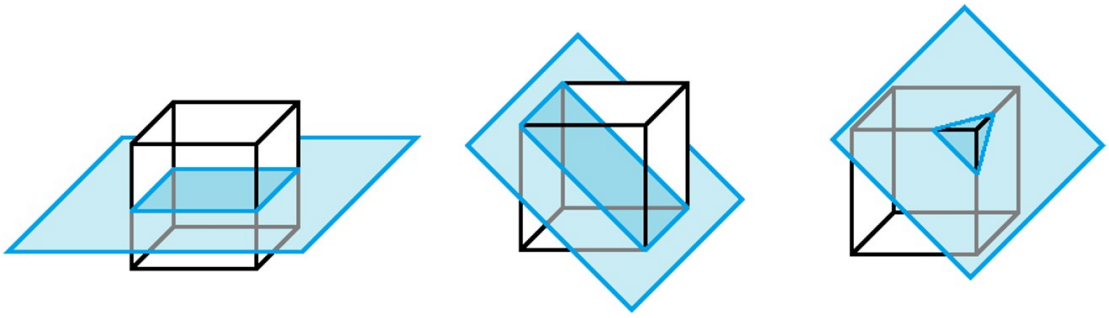

FIGURE 2.1: The 2D-3D alignment problem. In each case the blue slice represents a possible location of the 2D thin-section used for chemical mapping and the cube represents the 3D-XCT stack. The thin-section can lie in any orientation and depth; finding it within the XCT stack poses a difficult problem.

To study P uptake by plants and the importance of RSA in this contribution, elemental maps of the thin-sections were aligned to 3D XCT images using an automated method. The XCT data was used to provide a geometric parameterisation for a model describing the movement of P in soil from a fertiliser pellet and subsequent uptake by roots. The P movement model was parametrised using the gradients detected in aligned SEM-EDS maps. Finally, the parametrised model was used to investigate how changes in RSA affect P uptake from a fertiliser pellet.

## 2.4 Materials and methods

### 2.4.1 Experimental

#### 2.4.1.1 Plant preparation and growth

**Soil preparation**

The soil growth media was a sand-textured Eutric Cambisol collected from the surface Ah horizon of a lightly sheep-grazed plot at Abergwyngregyn, North Wales (53°14'N, 4°01'W). Soil was sieved to $< 5$ mm to remove stones. Sterilisation was required in order to use the shared growth chambers at the University of Southampton, thus, the soil was autoclaved and air dried

at $23 \pm 1$°C for 2 days. The soil was subsequently sieved to sizes between 1680 µm and 1000 µm, producing a well-aggregated, textured growth medium. The soil properties are summarised in Table 2.2.

Samples were prepared in 50 mL falcon tubes to a soil bulk density of $1.508 \pm 0.045$ g cm$^{-3}$. Four treatments were prepared covering all combinations of two variables: plant and no-plant, and pellet and no-pellet. The samples containing no plant are denoted C for control, with plants PL, with fertiliser CG and with both fertiliser and plants PLCG. Three replicates of each treatment representing the four conditions were prepared for imaging after 30 days of growth or incubation in soil.

TABLE 2.2: General properties of the Eutric Cambisol soil used in the experiments. Measurements of crystalline and amorphous Fe and Al, and total Fe, Al and Ca taken from Oburger, Jones & Wenzel (2011) analysis on the same soil. CDB indicates citrate-dithionate-bicarbonate extractable (Jackson et al. (1986)), AAO indicates acid-ammonium-oxalate extractable (Loeppert & Inskeep (1996)). Available phosphate was extracted with 0.5 M acetic acid using a soil-to-solution ratio (SSR) of 1 : 10 (w/v) (Oburger et al. (2009)). Values represent means ± Standard Error of the Mean (SEM). Nutrient data expressed on a dry soil weight basis

| Property | Mean± SEM |
|---|---|
| pH($H_2O$) | $6.12 \pm 0.05$ |
| Electrical conductivity (µS cm$^{-1}$) | $26.5 \pm 0.1$ |
| Water holding capacity (g kg$^{-1}$) | $356 \pm 6$ |
| Total C (g kg$^{-1}$) | $25.35 \pm 1.47$ |
| Total N (g kg$^{-1}$) | $2.95 \pm 0.06$ |
| Clay (%) | 20 |
| Silt (%) | 37 |
| Sand (%) | 43 |
| Crystalline Fe/Al (CBD) | |
| Fe (g kg$^{-1}$) | $1.4 \pm 0.1$ |
| Al (g kg$^{-1}$) | $1.6 \pm 0.0$ |
| Amorphous Fe/Al (AAO) | |
| Fe (g kg$^{-1}$) | $5.0 \pm 0.1$ |
| Al (g kg$^{-1}$) | $1.6 \pm 0.0$ |
| Total (Aqua regia) | |
| Fe (g kg$^{-1}$) | $46 \pm 0.5$ |
| Al (g kg$^{-1}$) | $28 \pm 0.6$ |
| Ca (g kg$^{-1}$) | $1.9 \pm 0.1$ |
| Exchangeable Ca (mg kg$^{-1}$) | $501 \pm 122$ |
| Exchangeable K (mg kg$^{-1}$) | $46.1 \pm 12.6$ |
| Exchangeable Na (mg kg$^{-1}$) | $25.4 \pm 5.1$ |
| Available P (mg kg$^{-1}$) | $22.6 \pm 6.2$ |
| P sorption capacity (mg kg$^{-1}$) | 150 |

**Plant growth**

Barley (*Hordeum vulgare L.*) cv. Optic was selected for study. Seeds were germinated in the dark between sheets of damp Millipore filter paper at $21 \pm 2°C$ for 3 days prior to transplanting to soil growth media in a 50 ml falcon tube. The germinated seeds were placed in a growth cabinet on a $16/8$ hour day/night cycle at constant temperature of 23°C and constant humidity of 60%. The plants were watered by perforating the falcon tubes at the bottom and placing them in a pool of water with a depth of 2 cm.

**Fertiliser additions**

The fertiliser pellets used were 20% struvite and 80% mono-ammonium phosphate (MAP) (Ostara, Vancouver, Canada, http://ostara.com/). This ratio of low water solubility struvite and high water solubility MAP was found to offer the required initial P for plants as well as a sustained source over a growing period (Talboys et al. (2016)). In the phosphorus addition conditions (CG, PLCG) a pellet of 0.3 g $\pm$0.02 g was placed at the centre of the tube at a depth of approximately 10 mm below the seed. A covering of approximately 10 mm soil was added above the seeds.

#### 2.4.1.2 Imaging Studies

**XCT imaging parameters**

Each of the three replicates of the four conditions were imaged with XCT after the 30 day growth/incubation period. XCT data was acquired using the Custom 450/225 kVp Hutch at the μVis Centre for Computed Tomography at the University of Southampton. The detector provided 2000 elements in each axis, the optimal projection number was 3142 over a rotation of 360°. The tube voltage of 160 kV provided acceptable transmission at an exposure time of 134 ms. Two times image averaging was used to suppress ring artefacts, giving a scan time of approximately 15 minutes per sample. Due to the need to capture extensive RSA rather than single roots, the resulting voxel side length of 20 μm was insufficient to image root hairs and the micro-porous structure of soil. Three small glass beads of approximately 500 μm diameter were bonded to the exterior of each tube prior to imaging as fiducial markers. The purpose was twofold: to guide sectioning of the resin-perfused block following XCT (see following section) and aid alignment of each XCT scan to the corresponding planar thin-section.

**XCT reconstruction and segmentation**

Data were reconstructed to 8-bit volumes using a standard filtered back-projection implemented in CTPro 3D (Nikon, Japan). Due to the trade-off between resolution and field of view when using XCT, it is difficult to image entire RSA with sufficient resolution and contrast-to-noise ratio to segment roots (particularly lateral roots) using an automated method. As such, often large amounts of time has to be spent segmenting roots and other small features manually (Flavel et al. (2012), Mooney et al. (2012), Keyes et al. (2013), Ahmed et al. (2016), Koebernick et al. (2017)). Avizo 9 (FEI Company, Oregon, US) was used to manually extract the RSA. To ensure root length measurements were accurate and no bias was given to specific regions of soil, a systematic manual segmentation approach was taken. Visible roots were segmented in one of the three orthogonal cross sectional planes to which they were most perpendicular in order to achieve accurate root length measurements. In each plane ($x-y$, $x-z$, $y-z$), the soil volume was divided into quadrants. One pass of all quadrants was made before moving onto the next, and if no unclassified roots could be seen in a quadrant, the next quadrant/orientation was considered. The manual segmentation process terminated when one full pass of each quadrant and all three orthogonal orientations found no unclassified roots. The root segmentation was time consuming therefore only two of each PL and PLCG replicates was segmented. One replicate of each treatment was segmented in the cuboid region of dimensions $14.4 \times 14.4 \times 3.52$ mm$^3$ centred around the location (or would-be location in the PL case) of the pellet to investigate root length density changes. Another replicate of each treatment was segmented in only a quadrant surrounding the pellet for the purpose of modelling, the location of this region can be seen in Figure 2.4. Soil solids were segmented into two phases: solid primary mineral phase with high X-ray attenuation and the clay-water mixture phase with a lower attenuation and pore size class below the imaging resolution. Primary minerals are defined as dense particles (the highest attenuation) larger than resolution so not to become blurred by partial-volume effects. The clay-water mixture phase is a catch-all definition of regions with density between air and primary mineral and is relative to the scan settings and soil. It includes water, clay, minerals below resolution and organic matter. It is important to note that scan resolution and particle size affects this soil classification. For example, a better resolution would resolve smaller minerals moving them from clay-water-mixture to the mineral phase. Similarly, if particle size was smaller, minerals may not be resolved and classified as clay-water mixture phase. Soil segmentation was achieved

using 3D median filtering and thresholding. It is worth noting that primary mineral particles with radius less than approximately 0.04 mm were classified as clay-water mixture due to the median filter often smoothing these small particles to the clay-water mixture grey value range, this is important when analysing the SEM-EDS images. Furthermore, any non-root organic matter (of which there is little) in the soil was classified as clay-water mixture due to its attenuation being in the same range as the clay-water mixture phase. Partial volume effects caused a one pixel film around the primary mineral phase to be classified as clay-water mixture. This artefact was removed using a 3D erosion. To segment the fertiliser pellet, its approximate convex hull was first segmented manually, holes were then masked out using smoothing and thresholding. The remaining grey levels were classified as air-filled pores. An example of the resulting segmentation can be seen in Figure 2.2b. The individual steps of the segmentation can be seen in Figure 2.3. From this segmentation, the macro-porosity of the soil, $\phi$, can be calculated as the ratio of the volume of the pore space to the entire soil volume (Peyton et al. (1992), Tracy et al. (2010)).

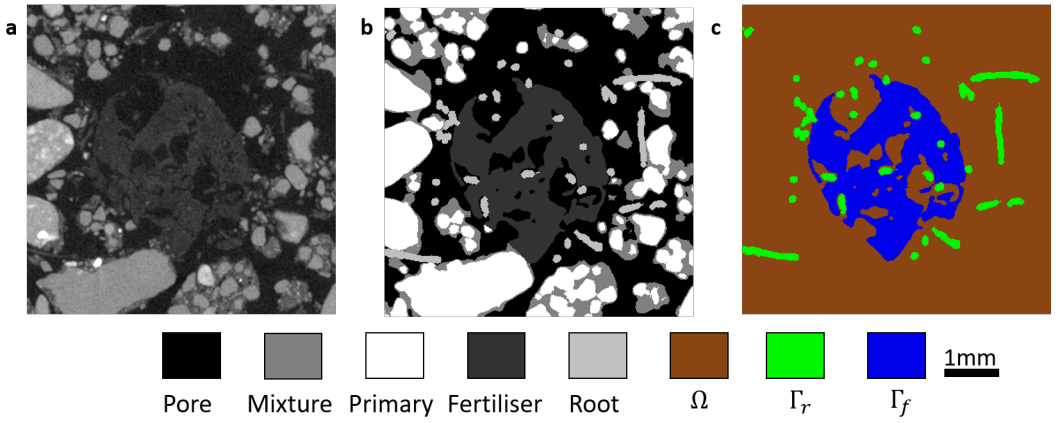


FIGURE 2.2: Example processing of raw XCT data into classified images used for analysis and modelling. a) A raw XCT slice of the plant-fertiliser treatment, b) Segmentation of the raw XCT data into its phases (the result of the segmentation routine described in the XCT section) c) Geometry used for image-based modelling, $\Omega$ is the volume representing homogeneous clay-water mixture, air-filled pore and primary mineral; the outside surface of $\Gamma_r$ represents the root surface boundary; and the outside surface of $\Gamma_f$ represents the fertiliser surface boundary.

### Meshing

For the purposes of modelling, the clay-water mixture, pore and primary mineral phases was assumed homogeneous and meshed as a volume. As the roots and fertiliser are only considered as boundaries in the model, only the surfaces are meshed (Figure 2.2c). The computational mesh suitable for finite element modelling was generated using ScanIP 2016 (Synopsys, California,

USA). Typically, the resulting volume element volume ratio was $2 \times 10^{-6}$ with an average element quality of 0.711. The surface element area ratio was $5 \times 10^{-4}$ with an average element quality of 0.7195.

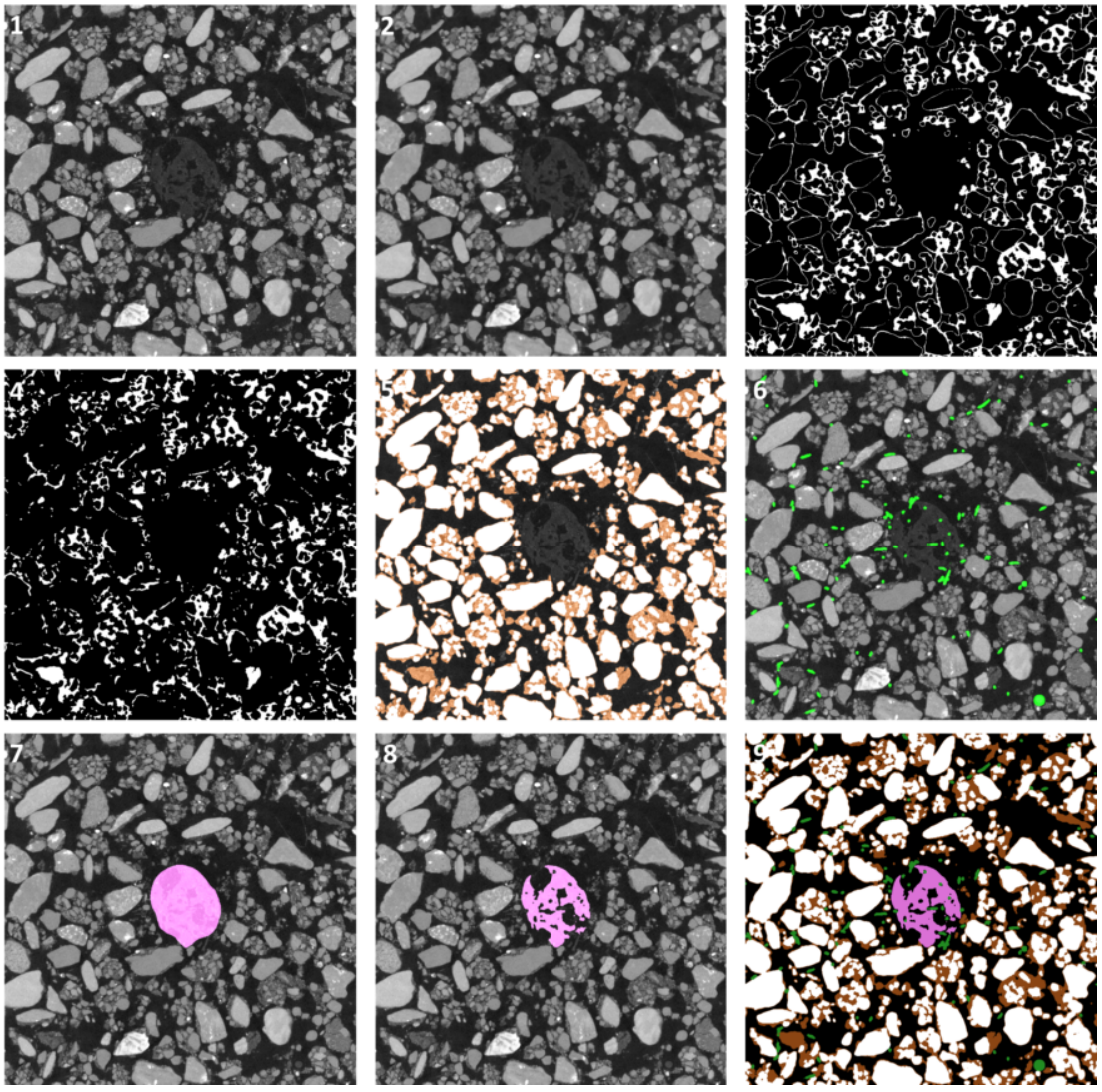


FIGURE 2.3: Visual demonstration of the image segmentation process. 1) A slice from the raw reconstructed data. 2) A 2 pixel 3D median filter applied to the raw data. 3) Threshold of the clay-water mixture phase, showing the layer around primary mineral particles caused by a partial volume effect. 4) The clay-water mixture phase after an opening and closing routine. 5) The final soil segmentation overlaid on the raw data. 6) The manual root segmentation overlaid on the raw data. 7) The approximate convex hull of the fertiliser overlaid on the raw data. 8) Threshold of the fertiliser pellet within the approximate fertiliser region overlaid on the raw data. 9) Final segmentation of each phase.

### Elemental Mapping

Single samples of each of the 4 treatments were prepared and elementally mapped using a LEO

1450VP SEM-EDS system (Zeiss, Oberkochen, Germany). Thin-sections suitable for SEM-EDS mapping were first prepared from the samples. As large soil samples are not rigid enough to be cut into thin-sections *in vivo*, they are embedded in epoxy resin before thin-sectioning. The only tested method for achieving this is drying (air or freeze) the samples before perfusing them with resin (Hapca et al. (2015, 2011), Sayen et al. (2009), Voegelin et al. (2007)). The samples were prepared for elemental mapping at the thin section laboratory at the National Oceanographic Centre, University of Southampton after the 30 day growth/incubation period. Standard fixation comprises of air drying and perfusing a two part epoxy resin thinned with 10% acetone (by mass) into the microcosms at atmospheric pressure then curing at room temperature for two days. Longitudinal polished sections of 250 μm thickness were produced through the seed and pellet location, using the fiducial markers and XCT data to guide the sectioning process. The sections were ground flat using a fixed diamond abrasive and cleaned afterwards in an ultrasonic bath. The samples were then polished with hydrocarbon oil and diamond slurry and cleaned again.

The spot size of the system was between 1 and 3 μm depending on the relative atomic mass. The detection limit of the method is approximately 0.009 wt% (Goldstein et al. (2017)). Shot noise (noise where the Poisson process behind photon emission and detection is apparent in the data) was present in the P signal due to the high spatial resolution (9.6 μm pixel side length) of the method and low P content in the sample (340ppb of labile P as determined by Inductively Coupled Plasma Mass Spectrometry), see column P-EDS in Figure 2.8.

The distribution of P in soil is inherently heterogeneous and the P signal is noisy due to low P content, thus to extract useful information from the data denoising and averaging methods were used. To denoise the data, spatial averages were taken over regions with increasing distance from fertiliser pellets/roots in each EDS map (we refer to this data as averaged EDS data).

Measurements from EDS are only relative to the scan, hence, concentrations cannot be compared between maps without calibration. The fertiliser pellet was used as a calibrator to compare measurements between the CG and PLCG maps. The average intensity of the pellet was calculated in both the PLCG and CG scans to derive a relative calibration between the maps, 1 PLCGEDS unit (the measure of P concentration relative to PLCG SEM-EDS scan) $= 0.725$ CGEDS unit (the measure of P concentration relative to the CG SEM-EDS scan). However, as no standards

were embedded in the samples absolute P concentration cannot be extracted from the EDS data. Using the back scattered electron image (BSEI) obtained from the SEM, the signal in the images could be classified by material phase using the same image segmentation method as that for the XCT data. Due to the resin perfusion process, roots were not visible in the BSEIs and hence could not be segmented directly.

**Alignment**

To be sure the thin-sectioning processes did not disturb the sample, each thin-section was compared to XCT data of the sample before resin perfusion and thin-sectioning. This was achieved by finding the XCT slice which corresponds to the thin-section plane, and measuring similarity using the statistical measure of PCC.

If the same approach as Hapca et al. (2011) was applied to one of the current sets of XCT and EDS data it would take $543,524$ times longer than the computations carried out in Hapca et al. (2011) due to the larger image sizes. Instead, the method of Chicherova et al. (2014) for aligning histology section to XCT data was adapted to align SEM-EDS to XCT. This approach makes use of a 2D object detection and description technique known as the Scale Invariant Feature Transform (SIFT) (Lowe (1999)). The method compares objects in each XCT slice to the Back Scattered Electron image (BSEI) of the thin-section by comparing the descriptors. If two objects are similar enough, the corresponding location in the XCT stack is saved. Once this process has been carried out for an entire stack, the aligned XCT slice is taken to be the best fit plane to the resulting points from each XCT slice. The whole stack is then re-oriented in the direction normal to said plane. The resulting XCT slices were larger than the thin-sections. Thus, to find the location of the thin-section on the matched XCT slice, the XCT slice was cropped to the same dimensions as the BSEI at every possible location and the PCC between the BSEI and cropped XCT slice was calculated. The crop with the maximum PCC was selected as the location of the thin-section on the aligned XCT slice.

### 2.4.2 Modelling

To capture the complexity of the system an image-based model, which considers the geometry of the root-soil-fertiliser system, was implemented. This model requires subsampling of the

XCT data to be computationally viable but large enough to avoid artificial boundary effects. Furthermore, model predictions were required to be optimised to fit the averaged EDS data. To approximate the appropriate size of the subsample and have a good initial guesses for the minimisation, a simpler model which does not consider the geometry was first solved and fit to the averaged EDS data. This was achieved using a spherical equilibrium-reaction diffusion model and minimisation.

#### 2.4.2.1 Spherical equilibrium-reaction diffusion model

An impeded diffusion model similar to that presented in Tinker & Nye (2000) (see chapter 1 for an introduction to this) was used as preliminary model (here we used spherical coordinates due to the approximate radial symmetry of the problem)

$$(\phi + b)\frac{\partial c_l}{\partial t} = \phi \frac{1}{r^2}\frac{\partial}{\partial r}(Dr^2\frac{\partial c_l}{\partial r}), \tag{2.1}$$

$$c_l = c_f, \quad r = r_f, \tag{2.2}$$

$$D\frac{\partial c_l}{\partial r} = 0, \quad r = r_b \tag{2.3}$$

$$c_l = c_0, \quad t = 0, \tag{2.4}$$

where $r_f$ is the radius of the fertiliser pellet, $r_b$ is the distance from the centre of the fertiliser pellet to the edge of the domain, $c_l$ [mol m$^{-3}$] is the concentration of P in soil solution at time $t$ and distance $r$ from the centre of the fertiliser pellet, $D$ [m$^2$ s$^{-1}$] is the diffusion coefficient of P in soil pore water, $b$ is the buffer power of P in soil, $c_f$ is the concentration of P in the fertiliser pellet, $\phi$ is the soil volumetric water content and $c_0$ is the initial P concentration in the soil pore water. In order to calculate the approximate effective diffusion of P in the soil $D_{eff} = \frac{D\phi}{\phi+b}$, solutions of the spherical diffusion model described by Equations (2.1-2.4) were fit to the averaged EDS data, with the fertiliser boundary value, $c_f$, calculated from the EDS data as the P average in the annulus closest to the pellets. The fertiliser radius $r_f$ is calculated from the XCT data and $r_b$ is chosen large enough to eliminate boundary effects. Let $c_l(t,r;D_{eff},c_0)$ be the solution to Equations (2.1-2.4) for a given $D_{eff}$ and $c_0$, and let $\mathbf{v} = (v_1,\ldots,v_n)$ be the averaged EDS data of increasing distance from the fertiliser pellet, the minimisation problem is

then

$$\min_{D_{eff},c_0\geq 0}\sum_i (c_l(t_*,r_i;D_{eff},c_0)-v_i)^2, \tag{2.5}$$

where $r_i$ are the grid points of $\mathbf{v}$ and $t_* = 30$ days. The PDE was solved numerically using MATLAB pdep solver and the minimisation problem was solved with MATLAB fmincon implementation of an interior-point algorithm. As the boundary condition is given in relative EDS intensity, $c_l$ has the same units. The initial condition $c_0$ is a second fitting parameter as it is unknown from the EDS data alone.

#### 2.4.2.2 Image-based model

To investigate how changes of root architecture around a fertiliser pellet affect plant P uptake, image-based models, which account for the root-fertiliser geometry are required. The soil is assumed homogeneous and represented by $\Omega \subset \mathbb{R}^3$. The phases segmented from the XCT data are used to define the geometry of $\Omega$ and its boundary $\Gamma$. Let $\Gamma_r$ represent the root surface, $\Gamma_f$ represent the fertiliser surface and let $\Gamma_b$ represent the image boundary (that is, the edge of the region considered) then $\Gamma = \Gamma_r \cup \Gamma_f \cup \Gamma_b$. Figure 2.2c shows an illustration of the domain and its boundaries on a 2D slice.

Equations governing the dynamics of P were imposed on the geometry. P in homogeneous soil moves by diffusion and advection (Roose et al. (2001)). As only small volumes of soil with negligible hydraulic gradient are considered, the effect of advection can be discounted (Roose & Fowler (2004)). P is known to adsorb to and desorb from soil particles (Barber (1995)). This is assumed to be a linear first order reaction which happens rapidly on the diffusion time scale, thus the amount of adsorbed P can be well approximated by P in solution using the buffer power (Roose et al. (2001)). As the soil is assumed homogeneous these reactions happen in the whole domain, thus the movement of P is governed by the partial differential equation,

$$(\phi + b)\frac{\partial P_l}{\partial t} = \nabla \cdot \phi D \nabla P_l, \quad \mathbf{x} \in \Omega, \tag{2.6}$$

where $P_l(t,x)$ [mol m$^{-3}$] is the P concentration at point $\mathbf{x} \in \Omega$ and $t > 0$, $\phi$ is the macro porosity of the soil, $b$ is the buffer power of P in the soil and $D$ [m$^2$ s$^{-1}$] is the diffusion rate of P in soil pore water.

The uptake rate of P by roots is linear in P at low concentrations (Barber (1995)). As the soil was P deficient we assume linear uptake

$$\phi D \nabla P_l \cdot \mathbf{n_r} = \lambda P_l, \quad \mathbf{x} \in \Gamma_r \tag{2.7}$$

where, $\lambda$ [ms$^{-1}$] is the P uptake rate (Tinker & Nye (2000)) and $\mathbf{n_r}$ is the unit normal to the root surface pointing into $\Omega$. The parameter $\lambda$ is related to the more common Michaelis-Menten uptake parameters with the approximation $\lambda \approx F_{max}/K_m$ where $F_{max}$ [mol s$^{-1}$ m$^{-2}$] is the maximum uptake rate and $K_m$ [mol m$^{-3}$] is the P concentration when uptake rate is half the maximum. It is assumed that the fertiliser pellet has a uniform concentration therefore the following boundary condition is imposed on the fertiliser pellet surface,

$$P_l = P_f, \quad \mathbf{x} \in \Gamma_f, \tag{2.8}$$

where $P_f$ [mol m$^{-3}$] is the concentration of P at the fertiliser surface.

On the image boundary, $\Gamma_b$, a zero-flux boundary condition is imposed,

$$\phi D \nabla P_l \cdot \mathbf{n_b} = 0, \quad \mathbf{x} \in \Gamma_b, \tag{2.9}$$

where $\mathbf{n_b}$ is the unit normal to $\Gamma_b$ pointing into $\Omega$. Uniform initial conditions are assumed

$$P_l = P_l^0, \quad t = 0, \mathbf{x} \in \Omega \tag{2.10}$$

where $P_l^0$ [mol m$^{-3}$] is the initial concentration of P in solution.

#### 2.4.2.3 Selecting the domain

The scanned samples were too large to segment, mesh and solve models on in their entirety, therefore subsamples had to be chosen. The region of the soil columns chosen for segmentation, meshing and image-based modelling is shown in Figure 2.4. This region contains the preliminary diffusion length scale (using the preliminary $D_{eff}$, calculated by minimising Equation (2.5)) from the fertiliser pellet to the edge of the domain along its long edges and a section of

the fertiliser pellet is contained in one corner. Choosing the top right quadrant in the PLCG treatment and bottom right quadrant in the CG treatment maximised the EDS data contained within the sub-region, eliminating any user choices. Further, imposing no-flux boundary conditions on all the internal boundaries except the top boundary is justified due to the radial symmetry of diffusion (modulo soil and root heterogeneity) of P from the pellet in the entire sample. A zero-flux condition on the top boundary is physically unjustified as in reality this is not the top of the soil column. However, the distance from the pellet to the top boundary is the approximate diffusion length scale. Hence, little P from the pellet will reach this boundary over 30 days, minimising this artificial boundary effect.

### 2.4.3 Parametrising the image-based model

The model has unknown parameters, however many of these can be calculated from the XCT and elemental data. The macro porosity of the soil, $\phi$, was calculated directly from the XCT data and the diffusion coefficient of P in water, $D$ is known. The remaining parameters, $P_l^0$, $\lambda$ and $b$ were fit to the averaged EDS data from the CG and PLCG treatments. First, $P_l^0$ and $b$ are fit to the CG averaged EDS data. Let $\mathbf{v} = (v_1, \ldots, v_n)$ be the CG averaged EDS data with increasing distance from the fertiliser pellet and let $P_l(t, \mathbf{x}; b, P_l^0)$ be the solution of the image-based model described by Equations (2.6-2.10) with the geometry extracted from the CG XCT images (in this case there is no root boundary, $\Gamma_r$) for a given $P_l^0$ and $b$. The initial condition, $P_l^0$ and buffer power, $b$ were calculated as the values which minimised the least square distance between the model solution and the averaged EDS data,

$$\min_{P_l^0, b} \sum_i (P_l(t_*, x_i; b, P_l^0) - v_i)^2, \tag{2.11}$$

where $x_i$ are the grid points of $\mathbf{v}$ and $t_* = 30$ days. Once the physical parameters were fit, the root uptake, $\lambda$, was fit to the averaged EDS data from the PLCG treatment. Let $\mathbf{u} = (u_1, \ldots, u_n)$ be the PLCG averaged EDS data and let $P_l(t, x; \lambda)$ be the solution to the image-based model described by Equations (2.6-2.10) with the geometry extracted from the PLCG XCT images for a given $\lambda$. The root-uptake rate, $\lambda$, was calculated as the value which minimised the least square

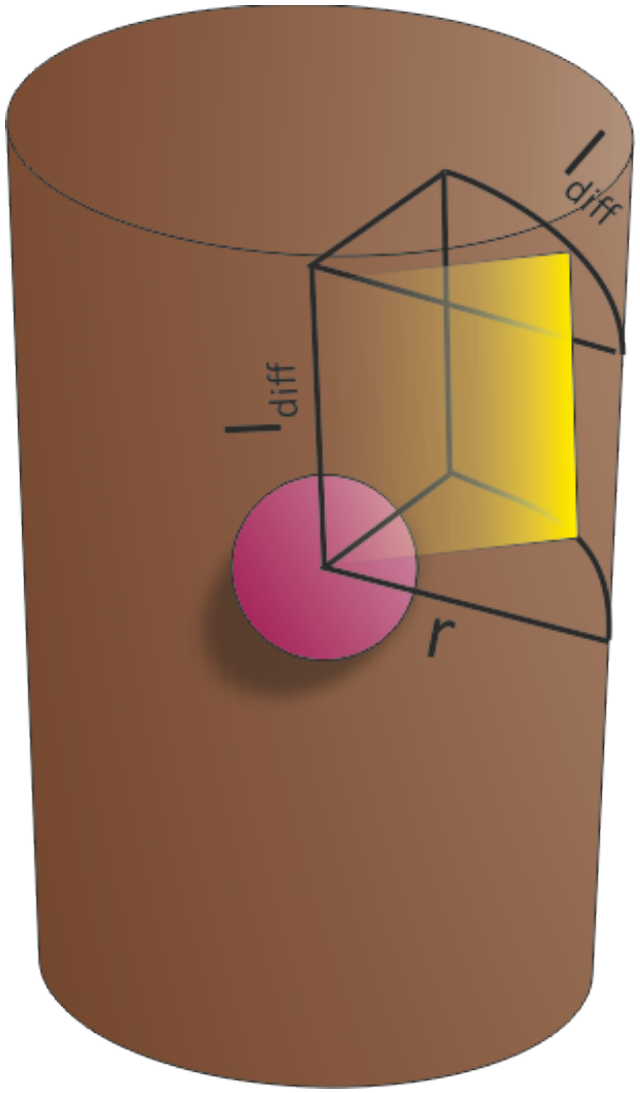


FIGURE 2.4: Subsample chosen for image-based modelling. The outlined black region is the subsample of the XCT images chosen for modelling. The pink sphere represents the fertiliser pellet and the yellow plane represents the location of the thin-section within the sample. $l_{diff} = 15.92$ mm is the diffusion length scale over 30 days (using the preliminary $D_{eff}$, calculated by Equation 2.5), and $r = 12.38$ mm is the distance from the centre of the pellet to the edge of the soil sample calculated from the image data.

distance between the model solution and the averaged EDS data,

$$\min_{\lambda} \sum_{i} (P_l(t_*, x_i; \lambda) - u_i)^2, \tag{2.12}$$

where $x_i$ are the grid points of $\mathbf{u}$.

### 2.4.4 Numerical Experiments

Once the image-based model was parametrised, simulations were run to assess how RSA affects P uptake from the fertiliser pellet. Predicted plant P uptake in the PLCG treatment was compared to that in the PL treatment where an artificial fertiliser pellet was added to the computational mesh in the same location as the PLCG treatment to add an equivalent source of P. In this comparison, the only difference between the models is the RSA; in the PLCG case the RSA has reacted to the fertiliser pellet while the PL RSA has not. The amount of P from the fertiliser pellet that becomes adsorbed to the soil is compared between the two treatments. Furthermore, root P uptake rate per root surface area with distance from the fertiliser pellet is measured to determine the soil region where the fertiliser replenishes P supplies previously diminished by roots.

### 2.4.5 Numerical simulations and minimisation algorithms

A finite element method was implemented in Comsol 5.3 to solve the image-based model. Order one Lagrange polynomials were chosen as the basis functions when running minimisation algorithms for speed, while order two Lagrange polynomials were used for the Numerical Experiments. The resulting system of linear equations was solved using the MUMPS algorithm. Backwards differentiation formulas between orders 1 were 5 are used to step in time. Minimisations were solved using MATLAB fmincon interior point algorithm. The initial point for minimisation problem (2.11) was selected as the solution to the spherical minimisation problem described by Equation (2.5), using $b = \frac{\phi D}{D_{eff}} - \phi$. The initial point for minimisation problem (2.12) was selected as $\lambda = 0$ ms$^{-1}$. Table 2.3 summarises the treatments and their use in modelling and data fitting.

TABLE 2.3: Summary of treatments and the use of their XCT and SEM-EDS data for modelling.

| **Treatment** | **Abbreviation** | **Input** | **Use** |
|---|---|---|---|
| Control | C | N/A | Baseline |
| Fertiliser | CG | N/A | Calculating $b$ and $P_l^0$ (Equation (2.11) |
| Plant Fertiliser | PLCG | $b$ and $P_l^0$ | Calculating $\lambda$ (Equation (2.12)) and numerical experiments |
| Plant | PL | $b$, $P_l^0$ and $\lambda$ | Numerical experiments |

## 2.5 Results

### 2.5.1 Imaging studies

#### 2.5.1.1 XCT

Lateral barley roots are seen to penetrate through the fertiliser pellet in each of the three plant-fertiliser replicates (Figure 2.2 and 2.5). Processed XCT data suggests that within approximately 2 mm of the centre of the fertiliser pellet lateral root length density is over 3 times the bulk measurement (illustrated with red dots in Figure 2.6). To be sure that the observed trait is not an artefact caused by pellet location in the centre of the tube, the PL scan was segmented in the region where the pellet would be placed, and root length density was measured with increasing distance from the centre of the tube (plotted with blue dots in Figure 2.6). The PL root length density stayed relatively constant when compared with the PLCG root length density.

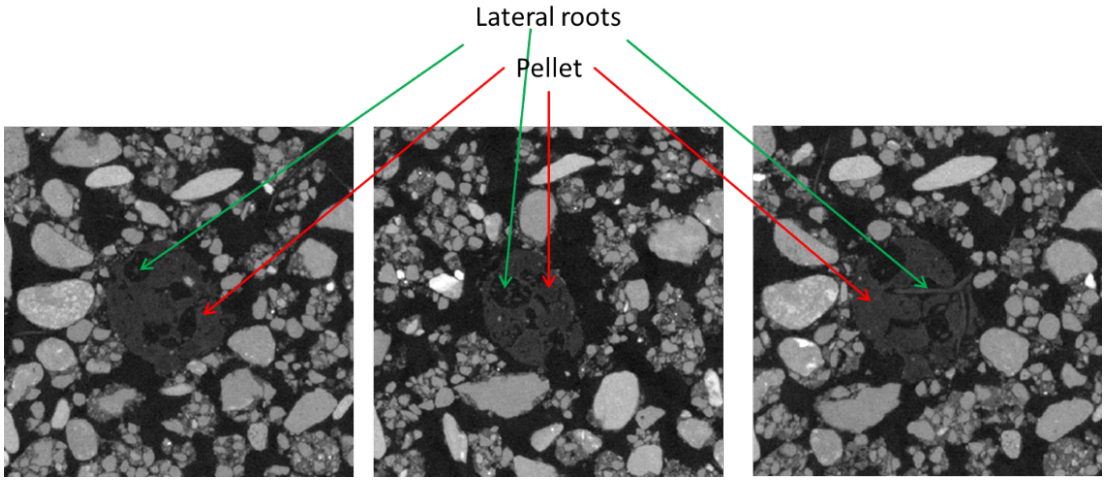


FIGURE 2.5: 2D slices from a XCT scan of a sample containing both plant and fertiliser pellet. The fertiliser pellet can be seen in the centre of each image. Lateral roots can be seen inside the pellet.

#### 2.5.1.2 Elemental Mapping

SEM-EDS reveals that most P heterogeneity in sandy-loam soil originates from mineral particles (Figure 2.7). P in mineral forms, such as apatite, is likely unavailable to plants directly. Further, P was detected in the air-filled pore space. This was caused by fine soil fractions becoming

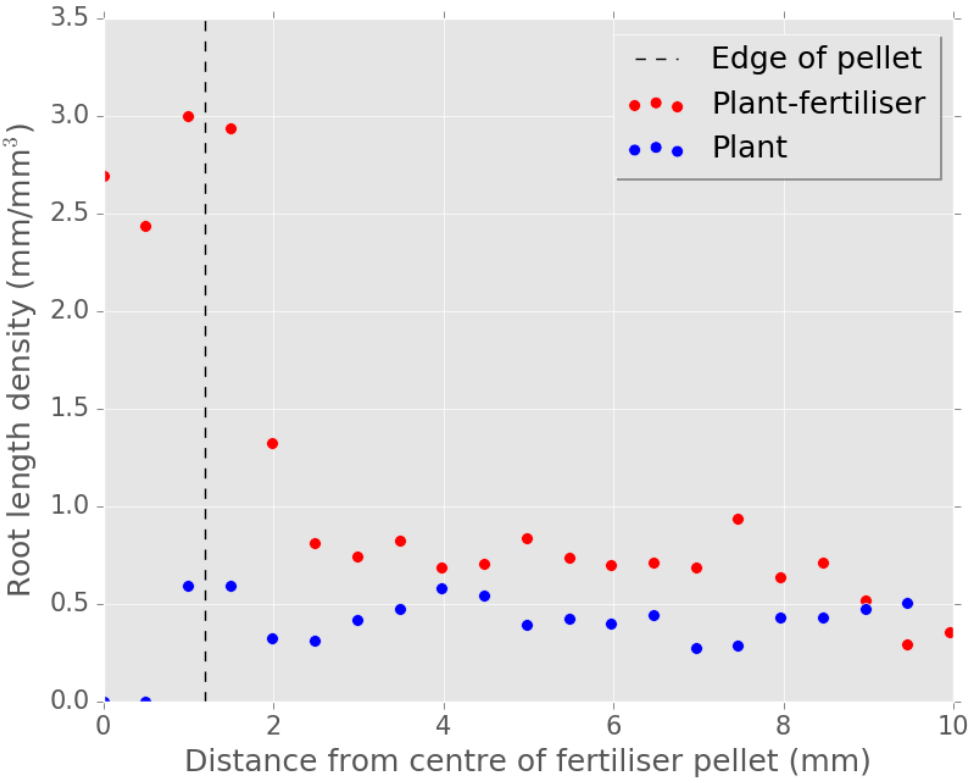


FIGURE 2.6: Root length density with increasing distance from the centre of a fertiliser granule in one plant and one plant-fertiliser treatment. The red dots shows the plant-fertiliser treatment. The blue dots shows the plant only treatment with an artificial ('dummy') fertiliser pellet located in the centre of the tube. The first two data points are zero in this case as there were no roots in the region closest to the centre of the tube. The black dashed line shows the approximate edge of the fertiliser granule.

suspended in the resin during perfusion, see Figure 2.7, an artifact of the process. As such, only P in the clay-water mixture phase is considered from the SEM-EDS data from here onwards. Averaging P concentarion with distance from the edge of the fertiliser pellet in the CG treatment shows a short gradient, Figure 2.12.

#### 2.5.1.3 Alignment

Aligning the SEM-EDS BSEI to XCT data shows that the resin perfusion and thin-sectioning process did not disturb the sample. Table 2.4 shows the PCCs between the BSEI of the thin-sections and the aligned XCT slices. Figure 2.8 shows sub-regions of the aligned XCT slices, along with the corresponding regions in the BSEIs and P maps. Figure 2.9 and 2.10 show a visual comparison of the best and worst matches for the entire images. Any movement of P is

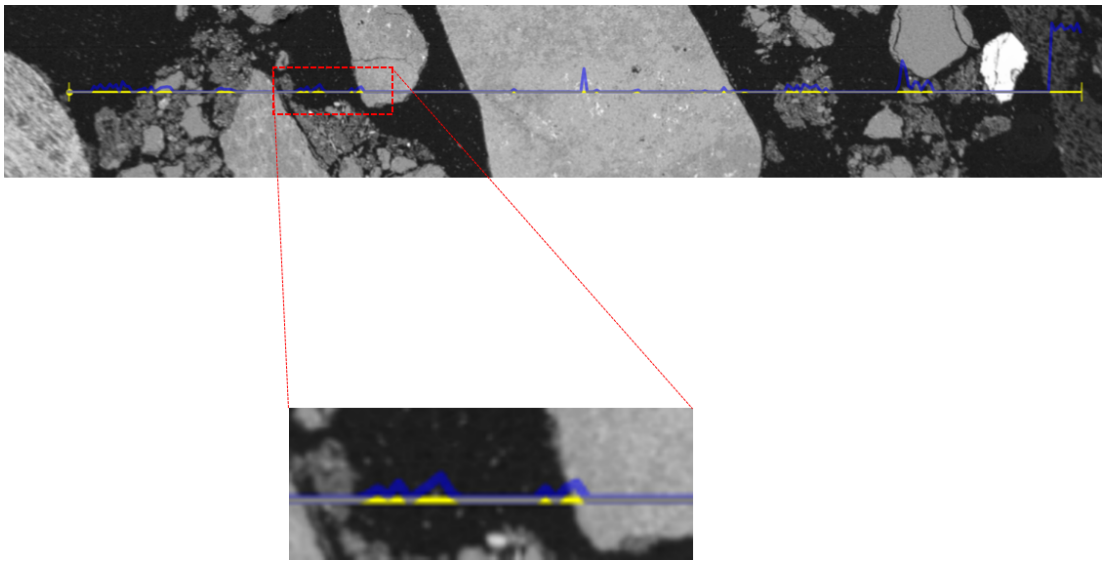

FIGURE 2.7: A high dwell-time SEM-EDS line scan of the fertiliser-soil treatment. The yellow line shows the path taken during the line scan, the blue line shows relative elemental P content. The fertiliser pellet makes up the far right of the image. The zoomed area highlights soil fractions suspended in the resin gives a non-zero P signal.

attributed to natural causes as opposed to an experimental artefact, thus any observed P gradients are characteristic of soil in situ.

TABLE 2.4: PCC (Pearson Correlation Coefficient) between the entire aligned XCT slice and the back scattered electron images of the thin-section.

| **Treatment** | **PCC** |
|---|---|
| C | 0.169 |
| CG | 0.091 |
| PL | 0.329 |
| PLCG | 0.485 |

The XCT scans were orientated in the direction normal to the thin-section, and all roots were segmented in a 0.5 mm region either side of the thin-section. From this segmentation, a 3D distance transform of the roots could be calculated on the thin-section, see Figure 2.11, and average P content with distance from root could then be calculated. However, no P gradient originating from the roots could be detected in both the PL and PLCG treatment. This is due to the sensitivity of the method; the roots do not alter the soil P profile enough to distinguish changes due to roots from noise (unlike the fertiliser, which supplies enough P to detect its effect on the soil profile).

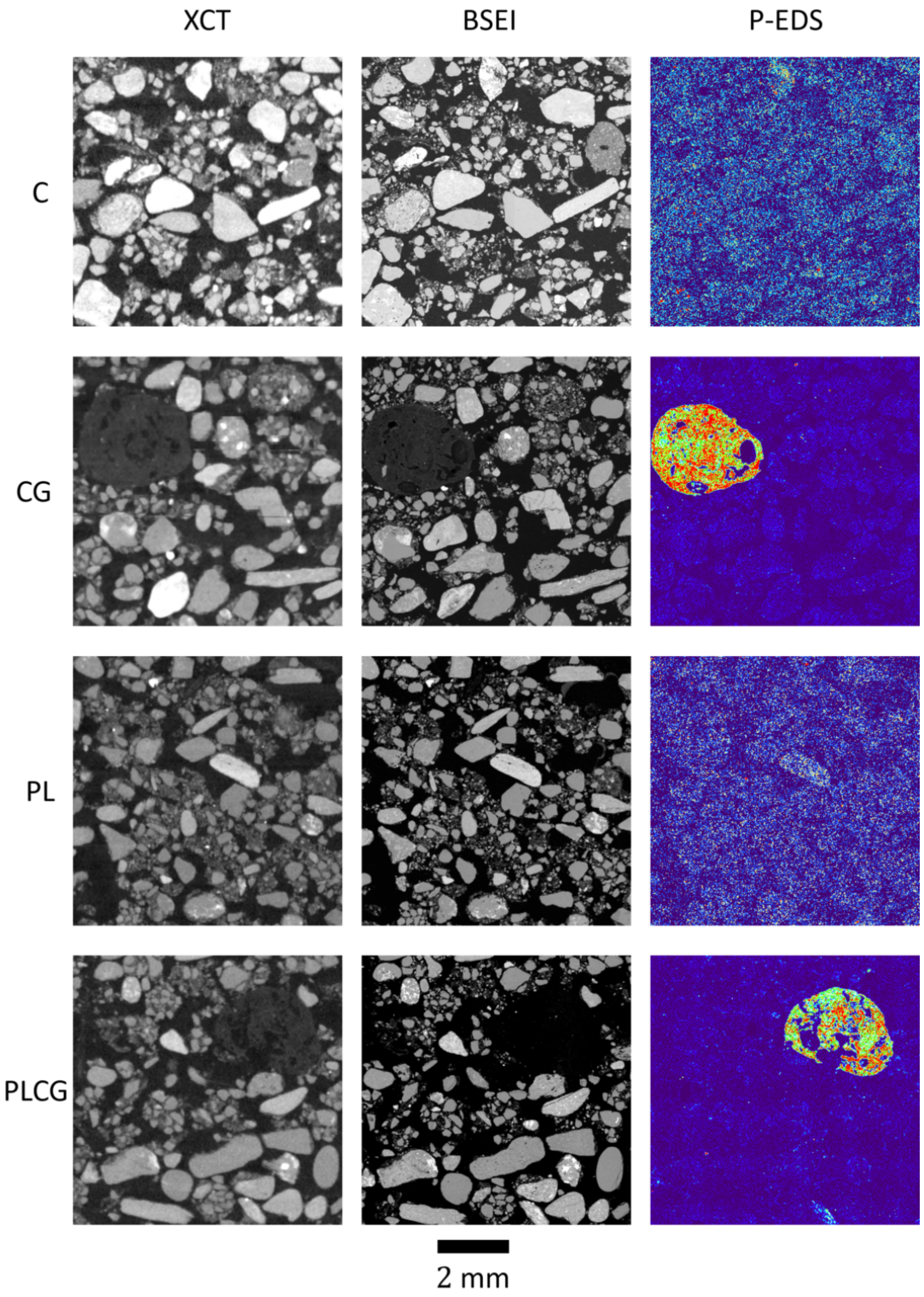


FIGURE 2.8: Visual comparison of sub-regions of the aligned XCT slice, BSEI and P EDS map for each thin-section. The P-EDS maps are shown as a heat map to highlight the contrast. Note, to capture the contrast within each image the brightness contrast is varied between images, thus the heat map scales are relative to each image.

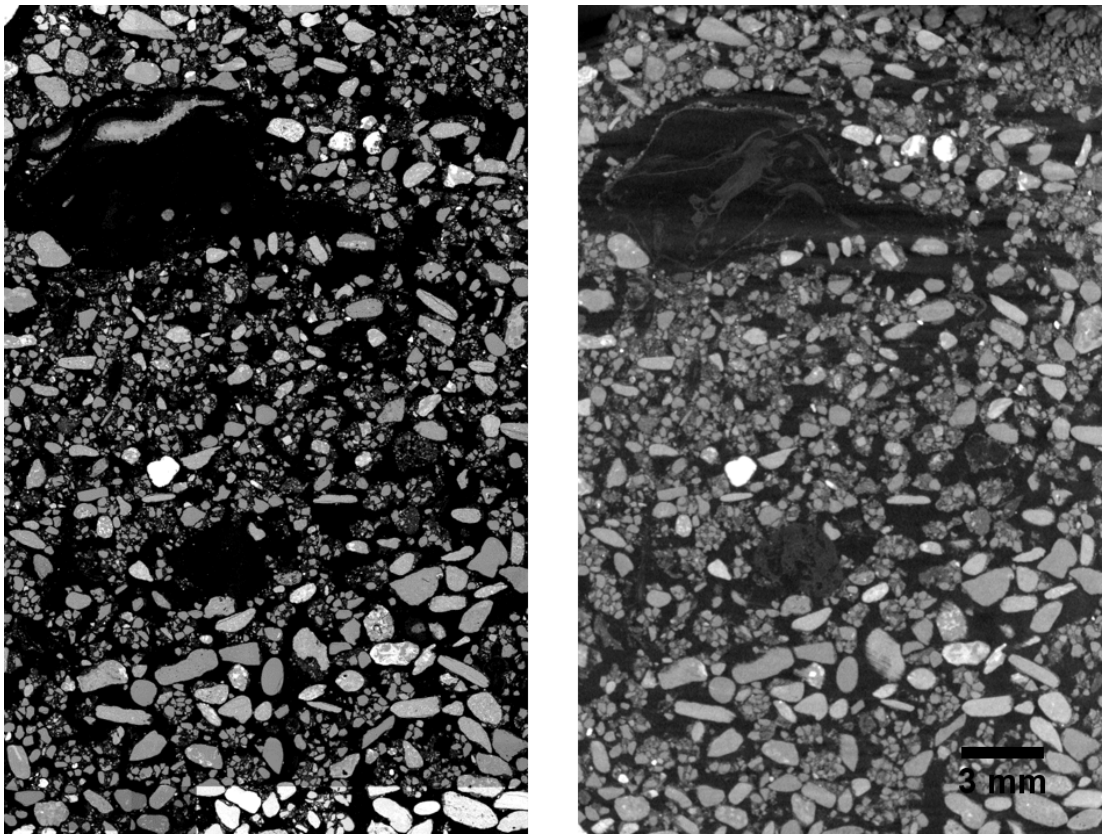


FIGURE 2.9: XCT data aligned with the BSEI of the thin-section of the plant-fertiliser treatment. Left shows the aligned pre-resin XCT slice, right shows the BSEI of the thin-section. The seed region can be seen in the top left of each image. This is the best match with a PCC of 0.485.

### 2.5.2 Modelling

#### 2.5.2.1 Equilibrium reaction diffusion model

By averaging P intensity in annuli of increasing distance from the fertiliser pellet high-resolution P gradients originating from the fertiliser pellet could be observed (Figure 2.12). Solving the minimisation described by Equation (2.5) yielded an effective diffusion coefficient of $D_{eff} = 1.64 \times 10^{-10}$ m$^2$ s$^{-1}$, the model fit to the data can be seen in Figure 2.12. This equates to the buffer power of P taking a value of approximately 4. The initial condition, $c_0$ was fit as 1.468 CGEDS units. The same analysis was applied to the PLCG treatment yielding approximately the same effective diffusion coefficient. However, the model did not account for the presence of roots.

There is a trade-off between noise/heterogeneity and resolution when choosing the thickness of annuli to average over. Thin annuli yield noisy data with higher spatial resolution while thick

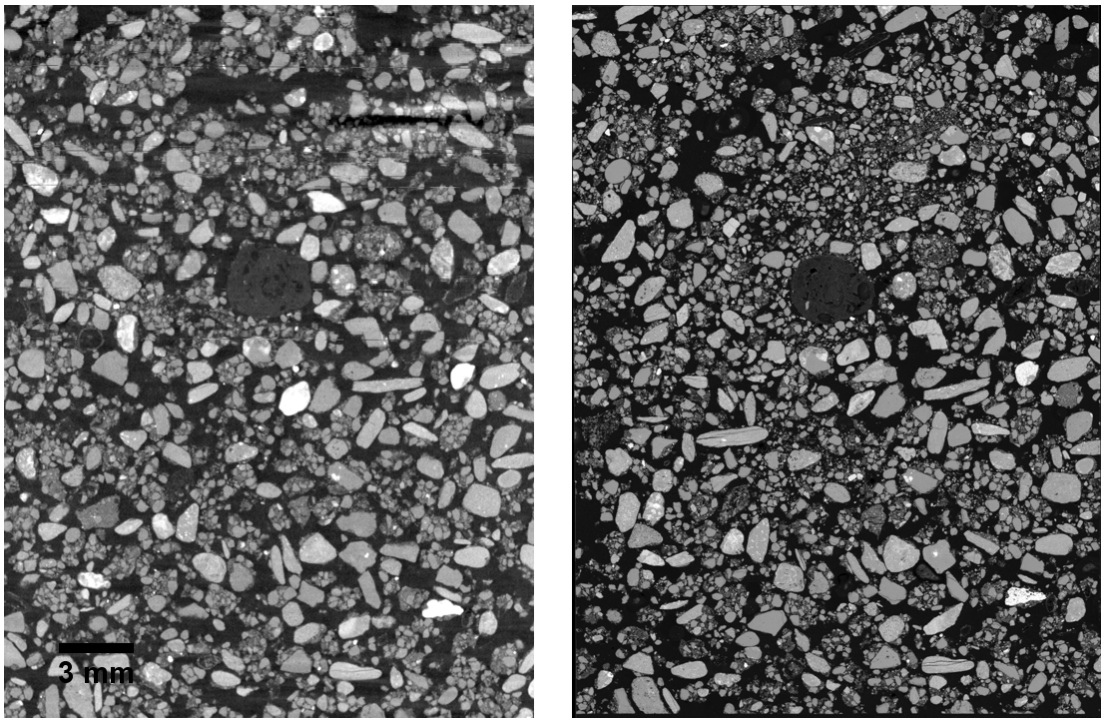


FIGURE 2.10: XCT data aligned with the BSEI of the thin-section of the fertiliser treatment. Left shows the aligned pre-resin XCT slice, right shows the BSEI of the thin-section. This was the worst match with a PCC of 0.091.

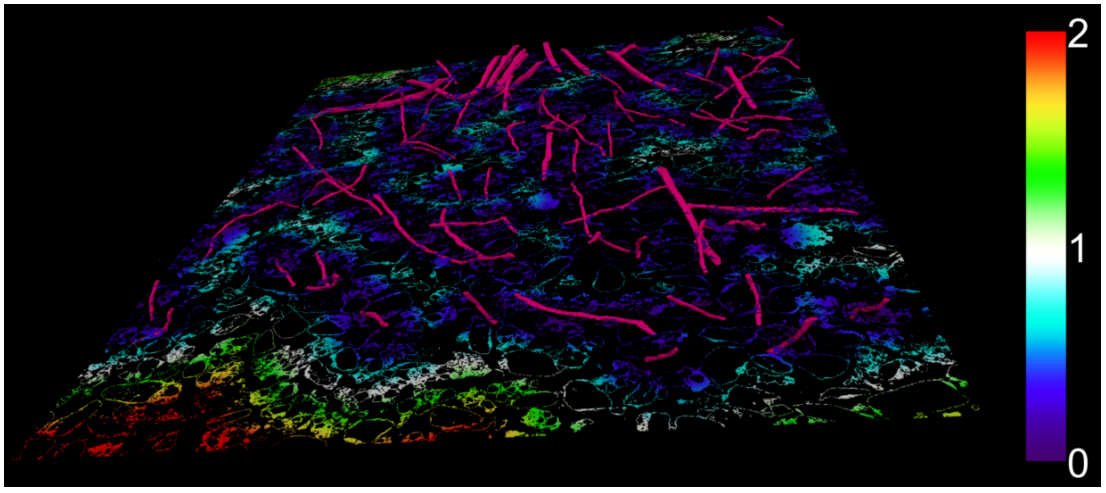


FIGURE 2.11: Nearest root distance on the thin-section. The heat map shows the 3D distance of each clay-water mixture pixel from its nearest root (in mm) for the thin-section of the PL treatment. The 3D segmented roots (rendered in magenta) were used to calculate this distance.

annuli produces smoother, lower spatial resolution data. Figure 2.13 shows that an annulus thickness between 0.53 and 3 mm yields stable results from the data fitting. It was assumed the image-based model minimisation problems have a similar stability for annulus size, these were fit with 1.194 mm thick annuli.

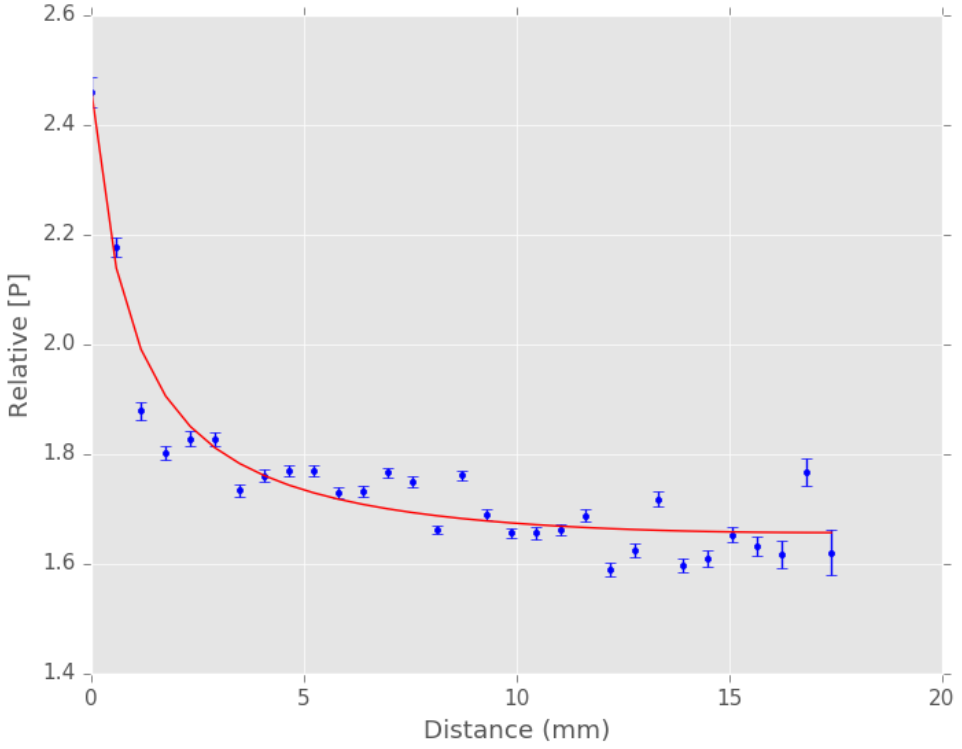


FIGURE 2.12: Preliminary spherical model compared to averaged fertiliser only SEM-EDS data. Blue points show average P SEM-EDS intensity (annulus thickness= 0.58 mm) with distance from the edge of the fertiliser granule in the CG treatment thin-section, the error bar shows the standard error in each annulus. The line shows a solution of the spherical-diffusion equation (described by Equations (2.1-2.4)) with $D_{eff} = 1.64 \times 10^{-10}$ m$^2$s$^{-1}$, fitting the data.

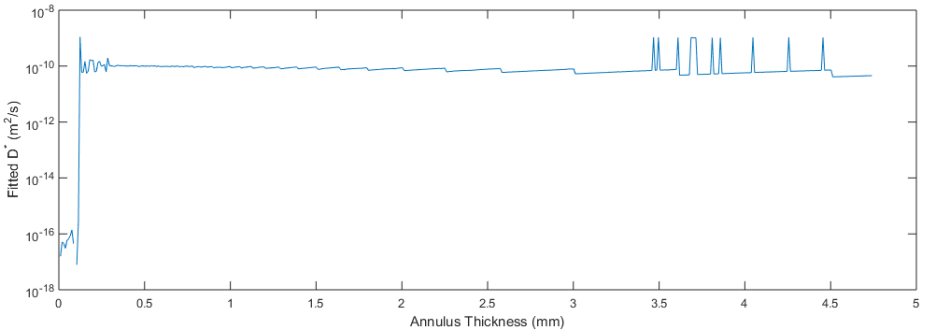


FIGURE 2.13: Fitted effective diffusion values (using the equilibrium reaction diffusion model, Equations (2.1-2.4)) against annulus thickness in soil-fertiliser treatment. Shows the value of $D_{eff}$ obtained by minimising Equation (2.5) when the size of the annuli used to average the SEM-EDS data varies in the soil-fertiliser treatment.

### 2.5.3 Parameterising the image-based model

Solving the minimisation problem described by Equation (2.11) results in $P_l^0 = 1.6985$ CGEDS units $= 1.231$ PLCGEDS units and $b = 418$ (implying $D_{eff} = 1.05 \times 10^{-12}$ m$^2$s$^{-1}$). Solving

the minimisation problem described by Equation (2.12) results in a root uptake rate of $\lambda = 4 \times 10^{-8}$ ms$^{-1}$. Figure 2.14a shows how the fitted image-based model solution on the plane representing the thin-section after 30 days compares to the averaged EDS data in the PLCG treatment. The root length density (a measurement from the entire 3D subvolume, from the centre of the fertiliser pellet) is also plotted to explain the region of low P concentration in the model between 11.5 and 14.5 mm from the edge of the fertiliser pellet. The seed location is contained within this region causing a high root length density (see the arrow in Figure 2.14a, the top region of Figure 2.9 shows the seed region on the thin-section). If data near the seed region is excluded when solving the minimisation problem described by equation (2.12), the resulting root uptake rate was found to be $\lambda = 1.67 \times 10^{-7}$ ms$^{-1}$, producing a better fit in this region, Figure 2.14b. This is attributed to a large air filled void around the seed. Hence, roots in this area cannot acquire P easily from the soil. The model does not take this into account as it assumes a homogeneous soil-pore distribution. This allows simulated roots to draw P from the void region. The following numerical experiments are solved in the entire domain, hence the root uptake rate fit in the entire domain was used.

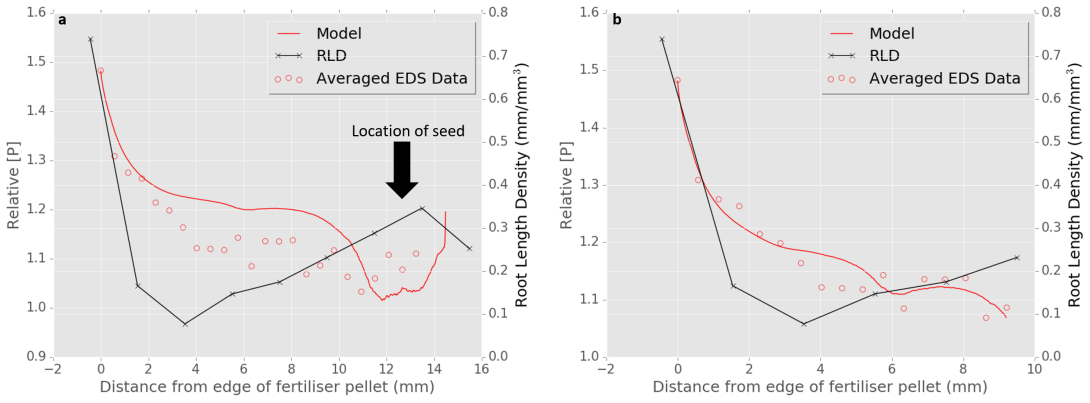


FIGURE 2.14: Image-based model compared to averaged plant-fertiliser averaged SEM-EDS data. Shown in black is the root length density (RLD) from the PLCG treatment to explain P-depletion in the model. The red circles show the averaged EDS data from the same sample. A P gradient is seen originating from the pellet. The red line shows the image-based model solution (using the fitted parameters and domain extracted from the XCT data of the same treatment) on the plane representing the thin-section after 30 days. a) Shows the fit when the entire EDS data is considered, including the region containing the seed (see arrow) resulting in $\lambda = 4 \times 10^{-8}$ m s$^{-1}$, b) Shows the fit when the region containing the seed is ignored, resulting in $\lambda = 1.67 \times 10^{-7}$ m s$^{-1}$.

### 2.5.4 Numerical experiments

The evolution of root uptake rate per root surface area with distance from the centre of the fertiliser pellet over 30 days is shown in Figure 2.15. Only roots within 2 mm of the centre of the fertiliser pellet have enhanced P uptake over the 30 day simulation in both cases. The roots further from the pellet use up the local P supply over time, decreasing their uptake rate. In the PLCG treatment, roots at 10 and 12 mm have a lower uptake rate as they are more densely packed in this region, increasing the rate at which P depletes from the soil. In the PLCG case, the rate for roots 4 mm away from the pellet initially decreases, then slowly increases as P from pellet diffuses from the pellet replenishing this soil region's P supply.

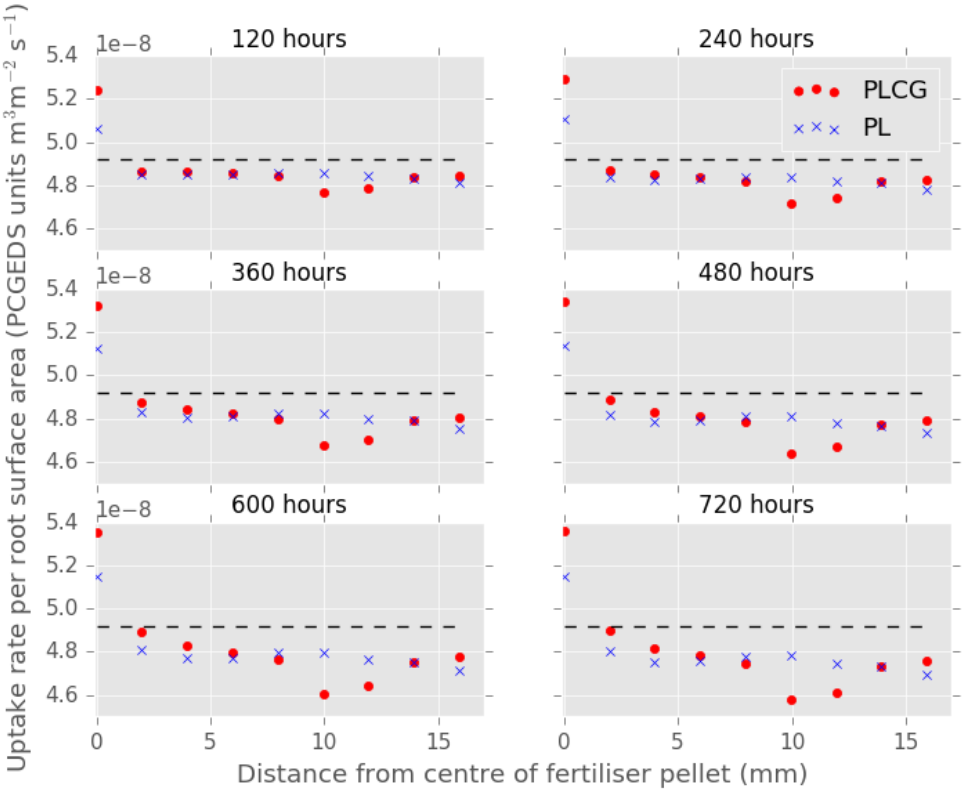


FIGURE 2.15: Root P uptake rate per root surface area with distance from the centre of the fertiliser pellet over 30 days in the entire subvolume. The red circles show the PLCG treatment, the blue crosses show the PL treatment and the black dashed line shows the rate at 0 hours. The uptake rate per root surface area are reported at 120, 240, 360, 480, 600 and 729 hours.

The total root surface area in the PLCG treatment is $1.32 \times 10^{-4}$ m$^2$ and $1.254 \times 10^{-4}$ m$^2$ in the PL treatment. Total P uptake over the 30 day period per total root surface area in the plant fertiliser treatment is 0.123 [PLCGEDS units m$^3$m$^{-2}$] and 0.124 [PLCGEDS units m$^3$m$^{-2}$] in

the plant treatment with an added fertiliser pellet. When only roots within 4 mm of the fertiliser pellet were considered, total P uptake over 30 days per root surface area in the plant fertiliser treatment is 0.13329 [PLCGEDS $m^3m^{-2}$] and 0.1262 [PLCGEDS units $m^3m^{-2}$] in the plant treatment with the added fertiliser pellet. At 30 days the total amount of P adsorbed to soil particles in both the plant fertiliser and plant treatment is $7.8 \times 10^{-4}$ [PLCGEDS units $m^3$].

## 2.6 Discussion

It has been suggested that struvite based fertiliser pellets can potentially reduce the need for crops to allocate carbon to root growth for soil P acquisition (Talboys et al. (2016)). The method of modelling P uptake from a fertiliser pellet described in this chapter offers a novel approach to answer these types of hypotheses. Whereas previous models can only estimate P uptake from a pellet per plant (Talboys et al. (2016)), image-based models show promise as a means for investigating plastic RSA changes on nutrient uptake from a fertiliser pellet in-situ. To our knowledge this was the first time image-based models were verified by elemental mapping, giving them both a geometrical and chemical grounding.

The spatial accuracy of elemental mapping was used to detect high resolution P gradients originating from a fertiliser pellet in soil. As the samples were dried and resin perfused before scanning, it is unclear if it was plant available P that was measured using this approach. It has been suggested that when P concentration in soil solution is high, such as near a fertiliser pellet, precipitation of P as calcium, iron or aluminium phosphates occurs (Barber (1995)). These forms of P are included in the measurements using this method. Precipitated P is typically unavailable to plants directly, however, it can be seen as a proxy for plant available P.

Segmentation of XCT data showed that root length density increased within 2 mm from the centre of the fertiliser pellet in two repeats (Figure 2.6 and 2.14). This result confirms findings from previous studies regarding root response to regions of high P concentration, but in a more local region and *in vivo* (Drew & Saker (1978)). Furthermore, in each of the PLCG treatments many lateral roots were found in the struvite pellet, suggesting roots can promote dissolution of the fertiliser.

As large averages are taken over the P SEM-EDS maps, improved resolution in the method is unlikely to affect the results. An improvement on the method could instead be made by identifying the clay-water mixture phase using mineralogy from the collection of EDS maps instead of density alone. Improving the resolution and contrast to noise in the XCT could allow an automated root segmentation method, vastly increasing the throughput of the method. There is scope to improve resolution as these preliminary studies suggest a smaller region around the fertiliser pellet could be imaged while still capturing the change in RSA away from the pellet.

The alignment demonstrates that the resin perfusion and thin-sectioning process does not disturb the samples spatially. The correlation coefficients between the aligned XCT slices and SEM-EDS BSEIs are similar to those reported from the alignment method of Hapca et al. (2011). However, in this study much larger images were considered and each alignment took approximately three hours. The best alignments in terms of PCC were the samples containing roots. It could be conceivably hypothesised that the roots bind the soil thus minimising the disturbance caused when transporting the samples from XCT scanning to thin-sectioning. The alignment allowed 3D distance from the roots to be calculated on the thin-section. Although P gradients were not detected around roots in this study, we suggest in further investigations to use the same method in a clay soil with added homogenised phosphate to detect P depletion zones.

Numerical experiments showed that the treatment with a plant and a fertiliser pellet was more efficient in P uptake near the pellet than the plant only treatment with an artificial pellet added to the computational mesh. Using an approximate carbon cost per root length value of 1.7 μmol $mm^{-1}$ (Nielsen et al. (1994)), we calculated that the plant in the plant-fertiliser treatment has to spend $1.94 \times 10^{-6}$ μmol ($2.3 \times 10^{-11}$ g) more carbon on its root system within 4 mm of the pellet than the plant in the plant only treatment to extract 12.5% more P from within 4 mm of the fertiliser pellet over the 30 day simulation. These numerical experiments were controlled for RSA changes caused by the pellet during the growth period, suggesting that root plasticity is important for efficient P uptake from a fertiliser pellet. Overall P efficiency was roughly equal when considering the entire subvolumes. This was caused by the plant-fertiliser subvolume containing the seed in the top region, creating a region of densely packed roots (Figure 2.9). These roots access P from the same region of soil depleting supplies rapidly, decreasing P uptake efficiency (see Figure 2.15 data points between 8 and 14 mm from the centre of pellet), while

the plant only treatment had more evenly distributed roots. The model predicts both the plant fertiliser and plant only treatment had approximately equal amounts of soil-adsorbed P after 30 days. However, the model assumed the P adsorption/desorption reactions were in equilibrium and it did not consider root exudates which are thought to be important for P solubilisation and P use efficiency (Oburger, Jones & Wenzel (2011)). To investigate the efficiency of fertiliser pellets in terms of immobilised P, a model which considers dynamic P-soil reactions as well as organic acids is required.

The fertiliser pellet only enhanced the P uptake rate per root surface area of roots within 2 mm of the pellet over a 30 day period; it seems the important mechanism for P uptake from a fertiliser pellet is root proliferation near the pellet, rather than the diffusion of P from the pellet to the roots. Furthermore, the roots were observed inside the pellets, this could be due to direct fertiliser solubilisation by root exudates, possibly another important mechanism for P uptake from a fertiliser pellet. On the other hand, regions of soil containing densely packed roots with no means for P replenishment were seen to rapidly deplete soil P supplies, reducing P uptake efficiency. Root P uptake rate did not reach an equilibrium over the 30 day simulation, Figure 2.15. Longer numerical simulations are required to predict P uptake over the full growing season and soil P profile for the next season. However, the 30 day simulation captured the early stage of P nutrition, known to be an indicator of crop yield (Talboys et al. (2016)).

This study invokes a simplified mathematical description of the physical system with parameters that can be fit accurately and uniquely to the data. While a more complex model could provide deeper insights into the underlying processes, it would introduce more system parameters, thus requiring extra experimental data not available in the current study. For example, this model considers a linear uptake on the root surface. While this assumption is consistent with literature, a more physically detailed description would be to impose Michaelis-Menten uptake on the root surfaces (Barber (1995)). However, this introduces an extra parameter that requires temporal resolution in the experimental data to fit accurately. Similarly, considering buffer power to describe adsorbed P is a simplification from the dynamics involved in the Langmuir isotherm model. However, as it reduces the complexity, this approximation lends itself to unique parameter estimations given the data used in this study.

The fitted model predicts the buffer power of P ($b$, the ratio of sorbed to solution P) for the sand-textured Eutric Cambisol under the P conditions induced by the fertiliser pellet as 418. Oburger, Jones & Wenzel (2011) calculated the buffer power of a similar soil to be 6. This is not inconsistent with the current result. The assumption that adsorbed P can be approximated by solution P using a constant buffer power is only accurate in a certain concentration range as soil sorption sites become saturated (Barber (1995)). The amount of solubilised P in the experiment of Oburger, Jones & Wenzel (2011) is likely much more than that provided by the 0.3 g fertiliser pellet which provides 84 mg of solid P to a local soil region. In the current experimental setup the soil contains a wide range of P concentrations, a nonlinear reaction such the Freundlich or Langmuir isotherm would be more suitable to capture the change in sorption (Barber (1995)). As mentioned above, this would introduce an extra parameter overfitting the experimental data.

Care has to be taken when translating the results to the field scale due to the unnatural growth conditions, the 50 ml tubes constrained the root system over the 30 day growth period. However, increased RLD near the pellet was seen in the plant fertiliser treatment and not the plant only treatment, suggesting increased RLD near the pellet was not caused by growing constraints.

The model assumes the roots were in the configuration of the 30 day time point over the entire simulation. It can be argued this approximation did not incur a large error: a barley root's typical elongation rate is between 20 and 35 mm day$^{-1}$ (Rajala et al. (2002)), therefore the root-growth time scale is over 100 times faster than the P effective diffusion time scale and the two processes can be time-separated as done in this chapter.

The method developed in this study shows great potential as a means for investigating plastic RSA changes on nutrient uptake. Preliminary studies suggest that a RSA reaction to nutrients from a fertiliser pellet is important for efficient P uptake in terms of root carbon cost. Due to the slow transport of P through soil, roots finding and reacting to the fertiliser pellet contributes more to P uptake from the pellet than P diffusing from the pellet to roots at greater proximity over a 30 day period. Results suggest that models which describe P uptake from fertiliser pellets should consider the plastic RSA as an important mechanism.

## 2.7 Acknowledgements

D.M.M.F., S.D.K., K.R.D., A.v.V., and T.R. are funded by ERC Consolidator grant 646809 (Data Intensive Modelling of the Rhizosphere Processes). T.R. is also funded by BBSRC SARISA BB/L025620/1, EPSRC EP/M020355/1, BBSRC SARIC BB/P004180/1 and NERC NE/L00237/1. The authors acknowledge the μ-VIS X-Ray Imaging Centre at the University of Southampton for provision of tomographic imaging facilities, supported by EPSRC grant EP-H01506X. The authors acknowledge the Scanning Electron Microscope Facility at the National Oceanography Centre Southampton.

# Chapter 3

# Quantifying citrate enhanced phosphate root uptake using microdialysis

**Daniel M. McKay Fletcher**[a], **R Shaw**[b], **A.R. Sánchez-Rodrìguez**[b,c], **Keith R. Daly**[a], **Arjen van Veelen**[a], **D.L. Jones**[b,d], **Tiina Roose**[a]

[a]Bioengineering Sciences Research Group, Department of Mechanical Engineering, School of Engineering Sciences, Faculty of Engineering and Physical Sciences, University of Southampton, Southampton, UK.

[b]Environment Centre Wales, Bangor University, Deiniol Road, Bangor, Gwynedd, LL57 2UW, UK.

[c]Agronomy Department, University of Còrdoba, Campus de Rabanales. Edificio C4 Celestino Mutis, 14071 Còrdoba, Spain.

[d]SoilsWest, UWA School of Agriculture and Environment, The University of Western Australia, Crawley, WA 6009, Australia.

## 3.1 Abstract

Organic acid exudation by plant roots is thought to promote phosphate (P) solubilisation and bioavailability in soils with poorly available nutrients (Chen & Liao (2016)). Here we describe a new combined experimental (microdialysis) and modelling approach to quantify citrate enhanced P desorption and its importance for root P uptake.

To mimic the rhizosphere, microdialysis probes were placed in soil and perfused with citrate solutions (0.1, 1.0 and 10 mM) and the amount of P recovered from the soil was used to quantify rhizosphere P availability (Demand et al. (2017)). Parameters in a mathematical model describing probe P uptake, citrate exudation, P movement and citrate enhanced desorption were fit to the experimental data. These parameters were used in a model of a root which exuded citrate and absorbed P. The importance of soil citrate-P mobilisation for root P uptake was then quantified using this model.

A plant needs to exude citrate at a rate of 0.73 μmol $cm^{-1}$ of root $h^{-1}$ to see a significant increase in P absorption. Microdialysis probes with citrate in the perfusate were shown to absorb similar quantities of P to an exuding root.

A single root exuding citrate at a typical rate ($4.3 \times 10^{-5}$ μmol $m^{-1}$ of root $h^{-1}$) did not contribute significantly to P uptake. This is in contrast with other modelling studies which have found that citrate exudation contributed significantly to P uptake (Gerke, Beißner & Römer (2000), Zygalakis & Roose (2012)). Microdialysis probes show promise for measuring rhizosphere processes when calibration experiments and mathematical modelling are used to decouple microdialysis and rhizosphere mechanisms.

**Keywords**: method, modelling, nutrient uptake, phosphorus mobilisation, soil solution

## 3.2 List of Symbols

| | |
|---|---|
| $\Omega \subset \mathbb{R}^3$ | model domain representing homogeneous soil in a microfuge tube |
| $\Gamma_p \subset \mathbb{R}^2$ | microdialysis probe membrane |

| | |
|---|---|
| $\Gamma_e \subset \mathbb{R}^2$ | microfuge tube boundary and tip of probe |
| $P_l$ | phosphorus concentration in soil solution [μmol $m^{-3}$] |
| $P_s$ | phosphorus concentration bound to soil particles [μmol $m^{-3}$] |
| $C_l$ | citrate concentration in soil solution [μmol $m^{-3}$] |
| $C_s$ | citrate concentration bound to soil particles [μmol $m^{-3}$] |
| $\phi_l$ | volumetric water content [$m^3$ of soil solution $m^{-3}$ of total soil] |
| $\phi_s$ | volumetric soil content [$m^3$ of soil $m^{-3}$ of total soil] |
| $\beta_1$ | the rate at which phosphorus adsorbs to soil particles [$s^{-1}$] |
| $\beta_1$ | the rate at which phosphorus desorbs to soil particles [$s^{-1}$] |
| $\beta_3$ | the rate of citrate enhanced phosphorus desorbtion [$m^3$ $s^{-1}$ μmol$^{-1}$] |
| $D_P$ | diffusion rate of phosphorus in soil solution [$m^2$ $s^{-1}$] |
| $D_C$ | diffusion rate of citrate in soil solution [$m^2$ $s^{-1}$] |
| $\gamma_1$ | the rate at which citrate adsorbs to soil particles [$s^{-1}$] |
| $\gamma_2$ | the rate at which citrate desorbs to soil particles [$s^{-1}$] |
| $\lambda$ | the rate of citrate bio-degredation [$s^{-1}$] |
| $\delta_C$ | microdialysis probe permeability for citrate [m $s^{-1}$] |
| $\mathbf{n_p}$ | unit normal to probe membrane |
| $\mathbf{n_e}$ | unit normal to $\Gamma_e$ |
| $C_0$ | concentration of citrate in the perfusate [mol $m^{-3}$] |
| $\delta_P^0$ | microdialysis probe permeability for phosphorus [m $s^{-1}$] |
| $\delta_P^1$ | citrate enhanced microdialysis probe permeability for phosphorus [$m^4$ $s^{-1}$ μmol$^{-1}$] |
| $b_P$ | buffer power of phosphorus [-] |
| $b_C$ | buffer power of citrate [-] |
| $P_{add}$ | concentration of phosphorus added to the soil [μmol $m^{-3}$] |

| | |
|---|---|
| $J_{M_i}$ | $i = 1,2,3,4,5$ model microdialysis probe flux of citrate/phosphorus for varying conditions |
| $J_{E_i}$ | $i = 1,2,3,4,5$ experimental microdialysis probe flux of citrate/phosphorus for varying conditions |
| $\sigma_i$ | $i = 1,2,3,4,5$ experimental standard deviation corresponding to the above fluxes |
| $obj_i$ | $i = 1,2,3,4,5$ objective function comparing experimental and model fluxes for varying conditions |
| $p = \{100, 1000, 10000\}$ | concentrations of phosphorus added to the soil [$\mu$M] |
| $c = \{100, 1000, 10000\}$ | concentrations of citrate in the perfusate [$\mu$M] |
| $T_1 = \{1,2,3,4,5,6,8,12\}$ | microdialysis probe sampling times in citrate exudation experiments [hours] |
| $T_2 = \{1,\ldots,12\}$ | microdialysis probe sampling times for phosphorus absorption experiments [hours] |
| $F_C$ | root citrate exudation rate [$\mu$mol m$^{-2}$ s$^{-1}$] |
| $F_P$ | maximum root phosphorus uptake rate [$\mu$mol m$^{-2}$ s$^{-1}$] |
| $K_P$ | phosphorus concentration when root uptake is half $F_P$ [$\mu$mol m$^{-3}$] |

## 3.3 Introduction

Low phosphate (P) availability in soil is often one of the most severe constraints to crop production worldwide (Barber (1995), Vitousek et al. (2010)). This is particularly pertinent in low income countries where farmers have insufficient capital to replenish their soil P supply with synthetic P fertilisers (Sanchez (2002)). Under-fertilisation is not the only reason for low P availability in soils. P strongly adsorbs to soil particle surfaces (e.g. Fe/Al oxides) and can become immobilised by microbes, both of which decreases the amount of P directly available to plants (Barber (1995), Oburger, Jones & Wenzel (2011)).

To overcome P limitation in soils, plants have evolved a range of strategies to manipulate the soil environment to increase P bioavailability. Of these, the exudation of organic acids (*e.g.*

citrate and oxalate) by roots of many species has been shown to promote P mobilisation (Chen & Liao (2016)). This has been shown to occur via four main mechanisms: 1) the co-excretion of $H^+$ and organic acid anions to lower the pH of the soil solution and promote ligand competition and desorption of inorganic P held on Fe and Al mineral surfaces, referred to as 'specific adsorption'; 2) release of organic acids leading to the protonation of mineral surfaces which decreases P binding strength; 3) the direct attack and removal of cations on mineral surfaces by organic acid anions leading to inorganic P release, referred to as 'ligand-promoted dissolution'; and 4) solubilisation of organic P (Oburger, Jones & Wenzel (2011)). These mechanisms are summarised in Figure 3.1. Note the inclusion of a negative effect of organic acids on P solubilisation, Figure 3.1g. For soils in which the sorption sites have low P saturation, it was found that ligand-promoted dissolution was the dominant mechanism, while specific adsorption is dominant when sorption sites in soil are saturated with P (Oburger, Jones & Wenzel (2011)). Typically, it is difficult to decouple these four effects from each other as they often occur simultaneously. However, specific adsorption and ligand-promoted dissolution can be decoupled from pH in experiments by counteracting pH changes caused by organic acids with the addition of strong acids or bases to achieve constant pH levels (Gerke, Beißner & Römer (2000), Oburger, Jones & Wenzel (2011)).

A number of models have been proposed to describe P solubilisation by organic acids. The simplest approach is to introduce a singular 'solubilisation parameter' per solubilised species (Nye (1983)) to increase solubility of one species based on the concentration of the competing species. Instances of models using this approach assume all solute-soil reactions are fast and hence the bound concentration is well approximated by solution concentration (Gerke, Beißner & Römer (2000), Zygalakis & Roose (2012)). Competitive Langmuir reaction equations assume there is a given number of binding sites per mass of soil, which two species compete for, each occupying a given number of binding sites per ion bound. This approach introduces three additional parameters along with the rate constants. Similar to the previous approach, this model is often considered in equilibrium (Schnepf et al. (2012)). Both approaches fail to capture the complex changes in soil reactions over long time periods (Barrow (1989)).

Experiments used for studying the adsorption and desorption of molecules such as organic acids and P in soil can be classified into 'equilibrium' and dynamic experiments. For the vast majority

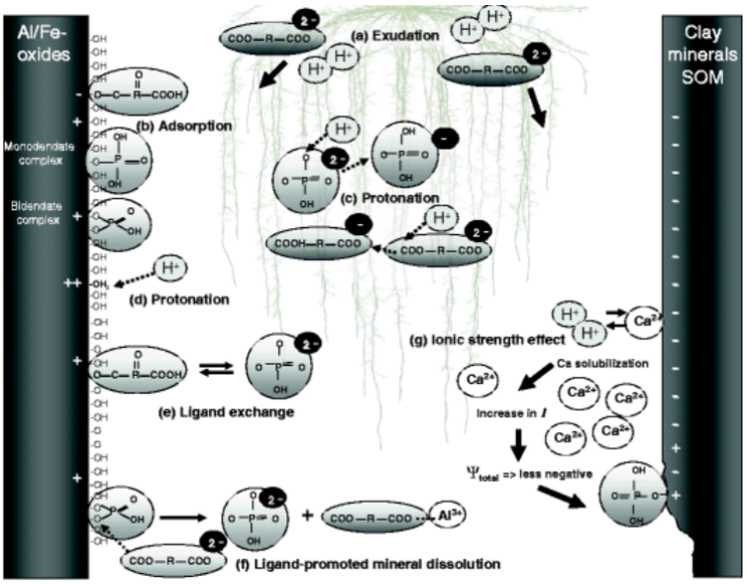


FIGURE 3.1: Summary of the mechanisms of inorganic phosphorus solubilisation by organic acids. a) Exudation of organic acids by plant roots into the soil solution. b) Adsorption of organic acids and phosphate onto soil surfaces. c) Protonation (oxidation) of phosphate molecules, decreasing binding strength of phosphate molecules. d) Protonation of soil surfaces, decreasing binding strength of the soil surfaces e) Ligand exchange ('specific adsorption') of organic acid for phosphate molecule on soil surfaces, increasing phosphate concentration in soil solution. f) Ligand-promoted dissolution, direct attack of mineral surfaces by organic acid anions, removing adsorbed phosphate. g) Ionic strength effects, increase in cation concentration from acidification, causing a less negative mineral surface charge, ultimately resulting in stronger binding of phosphate to the mineral surface. Figure taken from Oburger, Jones & Wenzel (2011).

of equilibrium experiments, a known amount of P or organic acid is added to soil, the sample is left to reach apparent equilibrium and then the amount of P and/or organic acid remaining in solution is measured (Barrow (1978), Geelhoed et al. (1998), Jones & Brassington (1998), Oburger, Leitner, Jones, Zygalakis, Schnepf & Roose (2011)). However, these methods only assess the equilibrium behaviour of molecules in bulk soil, failing to capture the dynamic rhizosphere processes which are thought to be highly influential in plant P capture from soil. Dynamic experiments are less common when estimating P and organic acid adsorption as soil reactions are often assumed to reach equilibrium state quickly (Gerke, Beißner & Römer (2000), Roose & Fowler (2004), Zygalakis & Roose (2012)). Furthermore, it is difficult to analyse the dynamic processes without disrupting the in situ soil sample during measurement. Pseudo-dynamic experiments to measure P and organic acid adsorption/desorption reaction rates have been undertaken whereby different replicates are destructively sampled after a range of equilibration times (Keyes et al. (2013), Oburger, Leitner, Jones, Zygalakis, Schnepf & Roose (2011)). These measurements may not be representative of rhizosphere processes due to variation across replicates.

Consequently, estimating the significance of organic acids for alleviating P deficiency remains extremely difficult.

Microdialysis probes offer a non-destructive method for assessing soil solution ion concentrations with high spatial and temporal resolution. Microdialysis has been used to estimate nitrogen (N) availability and diffusion in soils (Inselsbacher & Näsholm (2012), Inselsbacher et al. (2011), Shaw et al. (2014)); to sample Cu and Ni in soil solution (Mosetlha et al. (2007)); to sample organic acids exuded by roots in soil with high temporal and spatial resolution (Sulyok et al. (2005)); and P availability in soil (Demand et al. (2017)). It has been argued that microdialysis probes may offer a superior method of assessing soil nutrient availability for plant-uptake due to its diffusive-based method of sampling (Inselsbacher & Näsholm (2012), Shaw et al. (2014)). A further advantage of the microdialysis method is that it allows the simultaneous efflux of compounds from the dialysate and influx of solutes from the soil solution, creating a pseudo-rhizosphere (Demand et al. (2017)). Demand et al. (2017) found perfusing the probes with citrate (1 mM) increased the uptake of P by the probe in an Endostagnic Luvisol soil (high water-extractable P), while in a Dystric Cambisol (low water-extractable P) little difference was seen. They also showed that the pH of the external solution did not alter probe P uptake between the ranges of 3.5 and 6.5. However, factors such as ionic strength were shown to have a large effect on the uptake rate of P by microdialysis probes (Demand et al. (2017)). Furthermore, a diffusive based method may not give reliable results for nutrients which are transported primarily via advection. Thus, directly inferring plant-uptake or plant induced nutrient mobilisation using microdialysis probes may be a naïve approach; these measurements depend on a multitude of factors which can affect either the osmosis-driven mass flow movement of water in and out of the microdialysis probe or the diffusion of molecules into and out of the perfusate (Demand et al. (2017), Menacherry et al. (1992), Shaw et al. (2014)). Therefore, the technique lends itself to a combined experimental-modelling approach to decouple the effects of varying microdialysis osmosis rates and *in-situ* rhizosphere processes from the microdialysis measurements. This approach could provide a unique method for investigating how organic acids exuded by roots affect the availability of P and potentially increase plant uptake.

In this study, we aimed to quantify the effectiveness of citrate exuded by roots on improving

P mobilisation in a Eutric Cambisol soil using microdialysis probes in combination with modelling. After careful calibration of microdialysis probe influx and efflux rates, the microdialysis probes were perfused with citrate at a range of concentrations to simulate root efflux. The recovery of added isotopically labelled phosphate from the soil was used to quantify the effect of the citrate efflux on P influx. As discussed above, understanding the mechanisms of soil P mobilisation directly through experimentation is difficult and interpreting microdialysis-derived results is complex. Therefore, the experimental data was used to parameterise a kinetic model that describes the efflux of citrate from the microdialysis probe and the subsequent uptake of P. The model was then used to explore how citrate efflux affected P availability in the rhizosphere. The experimental and modelling results are discussed within both a mechanistic and an ecological context. The results offer a better understanding of small-scale *in-situ* rhizosphere processes.

## 3.4 Materials and Methods

### 3.4.1 Soil characterisation and sampling

The soil used in this study was sampled from the Ahp horizon of a *Lolium perenne* L. dominated agricultural grassland located at the Henfaes Research Station, Abergwyngregyn, Wales, UK (53°14'N, 4°01'W). The soil is classified as a Eutric Cambisol and has a sandy clay loam texture and a fine crumb structure (Wrb (2015)). Four independent soil samples ($n = 4$) were taken to a depth of 15 cm from $30 \times 30$ cm areas within the field. The soil was sieved to pass 2 mm and refrigerated at 4°C until required. The properties of the soil are summarised in table 3.2.

### 3.4.2 Microdialysis set up

To characterise citrate P mobilisation using microdialysis, calibration of the microdialysis probes with P and citrate was required. A description of microdialysis theory and nomenclature can be found in subsection 1.5.1. Two calibration experiments were designed to estimate the microdialysis probes efflux of citrate from the perfusate into the soil and the microdialysis probes influx of P into the probe at varying concentrations of citrate in the perfusate.

TABLE 3.2: General properties of the Eutric Cambisol soil used in the experiments. Measurements of crystalline and amorphous Fe and Al, and total Fe, Al and Ca taken from Oburger, Jones & Wenzel (2011) analysis on the same soil. CDB indicates citrate-dithionate-bicarbonate extractable (Jackson et al. (1986)), AAO indicates acid-ammonium-oxalate extractable (Loeppert & Inskeep (1996)). Available phosphate was extracted with 0.5 M acetic acid using a soil-to-solution ratio (SSR) of 1 : 10 (w/v) (Oburger et al. (2009)). Values represent means ± Standard Error of the Mean (SEM). Nutrient data expressed on a dry soil weight basis

| Property | Mean± SEM |
|---|---|
| pH($H_2O$) | $6.12 \pm 0.05$ |
| Electrical conductivity ($\mu S\ cm^{-1}$) | $26.5 \pm 0.1$ |
| Water holding capacity ($g\ kg^{-1}$) | $356 \pm 6$ |
| Total C ($g\ kg^{-1}$) | $25.35 \pm 1.47$ |
| Total N ($g\ kg^{-1}$) | $2.95 \pm 0.06$ |
| Clay (%) | 20 |
| Silt (%) | 37 |
| Sand (%) | 43 |
| Crystalline Fe/Al (CBD) | |
| Fe ($g\ kg^{-1}$) | $1.4 \pm 0.1$ |
| Al ($g\ kg^{-1}$) | $1.6 \pm 0.0$ |
| Amorphous Fe/Al (AAO) | |
| Fe ($g\ kg^{-1}$) | $5.0 \pm 0.1$ |
| Al ($g\ kg^{-1}$) | $1.6 \pm 0.0$ |
| Total (Aqua regia) | |
| Fe ($g\ kg^{-1}$) | $46 \pm 0.5$ |
| Al ($g\ kg^{-1}$) | $28 \pm 0.6$ |
| Ca ($g\ kg^{-1}$) | $1.9 \pm 0.1$ |
| Exchangeable Ca ($mg\ kg^{-1}$) | $501 \pm 122$ |
| Exchangeable K ($mg\ kg^{-1}$) | $46.1 \pm 12.6$ |
| Exchangeable Na ($mg\ kg^{-1}$) | $25.4 \pm 5.1$ |
| Available P ($mg\ kg^{-1}$) | $22.6 \pm 6.2$ |
| P sorption capacity ($mg\ kg^{-1}$) | 150 |

For all experiments described here, a WM-205u peristaltic pump (Watson-Marlow Ltd., Falmouth, UK) was used to pump citrate solutions through CMA 20 microdialysis probes (CMA Microdialysis AB, Kista, Sweeden). The probes had a 20 kDa molecular weight cut-off and polyethersulfone membrane (4 mm long, 500 µm external diameter). The pump flow rate was set to 3.3 $\mu l\ min^{-1}$ to maximise the relative recovery of solutes from the soil (Inselsbacher et al. (2011)). Dialysates were continuously collected in 1.5 ml microfuge tubes or 5 ml polypropylene vials, which were covered with Parafilm-M (Bemis Inc., Neenah, WI) to prevent evaporative losses. Prior to use, the microdialysis probes were placed in high purity water (18 MΩ resistance) and flushed with perfusate to remove any contaminants. Prior to dialysate collection, the

microdialysis probes were run for approximately 10 min, to ensure the dead volume in the microdialysis probe had been flushed. Throughout the microdialysis experiments the soil moisture was maintained at 80% field capacity.

#### 3.4.2.1 Quantifying citrate efflux rate into the soil using microdialysis probes

Sieved field-moist soil (1.3 g; 1 g DW equivalent) was placed in a 1.5 ml microfuge tube and packed to a density of 1 g $cm^{-3}$. A microdialysis probe was inserted into the soil using the needle and introducer supplied by the manufacturer so that the top of the probe membrane was located 5 mm below the soil surface. Sterile solutions of $^{14}$C-labelled citrate at concentrations 0.1, 1 and 10 mM; 1.7 kBq $ml^{-1}$ (with pH 5.6, 4.6 and 3.6 respectively) were pumped through the microdialysis probes and the dialysate collected after 1, 2, 3, 4, 5, 6, 8 and 12 h in 5 ml polypropylene vials ($n > 3$). The amount of $^{14}$C-citrate remaining in the dialysate (*i.e.* not passed into the soil) was determined using a Wallac 1404 liquid scintillation counter (PerkinElmer Inc., Waltham, MA) following the addition of 4 ml of HiSafe-3 scintillant (PerkinElmer Inc.). The amount of $^{14}$C-citrate lost to the soil was calculated as the difference between the amount of $^{14}$C in the influent versus that in the effluent (dialysate). The volume of dialysate recovered was also recorded to confirm that there was no significant mass flow of water either into or out of the probes.

#### 3.4.2.2 P recovery from standard solutions using microdialysis probes

To calibrate P recovery by the microdialysis probes and to evaluate the osmotic effects of the citrate perfusate, a simple experiment was performed. Briefly, microdialysis probes were placed in 1.5 ml microfuge tubes containing 1 ml of a $^{33}$P-labelled $KH_2PO_4$ standard solution (0, 0.1, 1 or 10 mM, $n = 4$; 1.7 kBq $ml^{-1}$). The microdialysis probes were perfused with solutions of citrate concentrations of 0, 0.1, 1 and 10 mM and the dialysate collected in 5 ml polypropylene vials over a 1 h period, the amount of $^{33}$P in the dialysate and the volume of dialysate was determined as described above.

#### 3.4.2.3 P recovery from soil using microdialysis probes

Soil (1.3 g) was placed in individual microfuge tubes ($n = 4$). Subsequently, 100 µl of a $^{33}$P-labelled solution (1 mM $KH4_2PO_4$; 370 kBq ml$^{-1}$) was injected into the soil. The soil was mixed and left to stand at 20°C for 24 h to approach equilibrium. A microdialysis probe was inserted into the soil as described above. Solutions of citrate (0, 0.1, 1 or 10 mM) were perfused through the microdialysis probe and the dialysate collected hourly over a 12 h period. The amount of $^{33}$P in the dialysate was determined using liquid scintillation counting as described earlier.

### 3.4.3 Modelling and Data Fitting

#### 3.4.3.1 Mathematical Model

The measurements obtained by the experiments are the result of pore scale reactions between citrate, P, soil and the microdialysis probe. Understanding these mechanisms directly through experiments is difficult. Thus, a model was constructed to aid the interpretation of the results. Linear approximations of the mechanisms were used to circumvent the danger of over-fitting the data by introducing excess parameters. In particular, the experiments do not measure P or citrate isotherms, thus we cannot accurately parameterise models including the full set of parameters. The adsorption/desorption part of the model is similar to Zygalakis & Roose (2012) with the soil reactions maintained in their dynamic form. The model used was a kinetic model that describes the efflux of citrate into the soil and the absorption of P by the microdialysis probe. The model considers the diffusion and buffering of citrate and P, and specific adsorption between P and citrate on soil sorption sites. It is hypothesised that citrate mobilises P held on the soil, but also influences P influx rate at the probe-soil interface (Demand et al. (2017)). The effect of acidity is not directly considered in the model because the effect of pH cannot be uncoupled from specific adsorption in the current experiments; instead, any additional P absorbed by the probe due acidity is attributed to the specific adsorption mechanism during the subsequent data fitting. This is a simplification of the complex relationship between pH and citrate mobilisation of phosphate, for example, at high pHs citrate can complex with calcium in the soil, reducing the effectiveness of specific adsorption (Barrow et al. (2018)).

The domain considered is a cylindrical region of soil with a diameter of 10 mm and height of 19.1 mm, centred about the cylindrical microdialysis probe with a diameter of 0.5 mm and height of 4 mm. These dimensions are chosen to match the experimental set up. The soil domain is denoted $\Omega \subset \mathbb{R}^3$, the microdialysis probe membrane is denoted $\Gamma_p$ and the remainder of the boundary is denoted $\Gamma_e$. The soil is assumed to be homogenous with approximate volumetric water content $\phi_l$ [$m^3$ of soil solution $m^{-3}$ of total soil] and volumetric soil solid content $\phi_s$ [$m^3$ of soil solid $m^{-3}$ of total soil]. Due to rotational symmetry of the problem, the domain can be simplified to a 2D axisymmetric representation as shown in Figure 3.2; for generality, the governing equations are stated in 3D Cartesian co-ordinates, but implemented numerically as 2D cylindrical co-ordinates.

P and citrate are assumed to exist in either bound or unbound (in solution) states. In particular, $P_l(t,x)$ [$\mu$mol $m^{-3}$ of soil solution] is the P concentration in solution, $C_l(t,x)$ [$\mu$mol $m^{-3}$ of soil solution] represents citrate concentration in solution, $P_s(t,x)$ [$\mu$mol $m^{-3}$ of soil solid] is the concentration of P bound to soil particles, and $C_s(t,x)$ [$\mu$mol $m^{-3}$ of soil solid] is the amount of citrate bound to soil particles.

P and citrate can adsorb to, and desorb from, soil particles. This was modelled using a reversible first-order chemical reaction. The process of specific adsorption promotes P desorption as more citrate is adsorbed to the soil. This was implemented by adding a cross term to the P desorption-adsorption reaction (Equations (3.1-3.2)). Citrate is known to be consumed by microbes in the rhizosphere. However, sorption of citrate to soil particles causes a significant reduction in biodegradation rate (up to 99%) (Jones & Edwards (1998), Van Hees et al. (2003)). Therefore, citrate in the model is allowed to biodegrade only in the soil solution. Hence, assuming conservation of mass and neglecting convective transport, the diffusion-sorption-reactions for P and citrate can be written as

$$\phi_l \frac{\partial P_l}{\partial t} = \nabla \cdot \phi_l D_P \nabla P_l - \phi_l \beta_1 P_l + \phi_s \beta_2 P_s + \phi_s \beta_3 C_s P_s, \tag{3.1}$$

$$\phi_s \frac{\partial P_s}{\partial t} = \phi_l \beta_1 P_l - \phi_s \beta_2 P_s - \phi_s \beta_3 C_s P_s, \tag{3.2}$$

$$\phi_l \frac{\partial C_l}{\partial t} = \nabla \cdot \phi_l D_C \nabla C_l - \phi_l \lambda C_l - \phi_l \gamma_1 C_l + \phi_s \gamma_2 C_s, \tag{3.3}$$

$$\phi_s \frac{\partial C_s}{\partial t} = \phi_l \gamma_1 C_l - \phi_s \gamma_2 C_s, \tag{3.4}$$

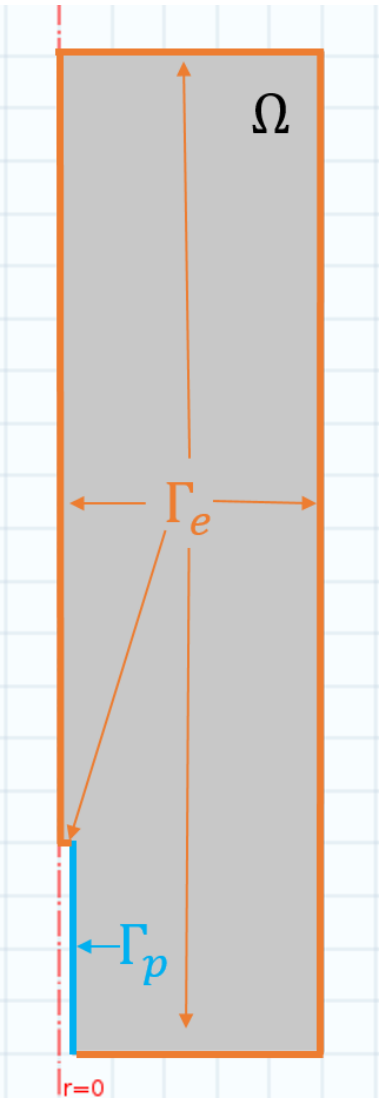


FIGURE 3.2: Axisymmetric representation of the domain for the model. The red-dashed line shows the axis of symmetry, $\Omega$ represents the homogenous soil within the 1.5 ml microfuge tube, $\Gamma_p$ represents the microdialysis probe membrane, shown in blue and $\Gamma_e$ represents the microfuge tube boundary and tip of the probe, shown in orange.

where $\beta_1$ [$s^{-1}$] is the rate at which P adsorbs to soil particles, $\beta_2$ [$s^{-1}$] is the rate at which P desorbs from soil particles, $\beta_3$ [$m^3$ of soil solid $s^{-1}$ $\mu mol^{-1}$] is the rate associated with specific adsorption between citrate and P on soil sorption sights, $\gamma_1$ [$s^{-1}$] is the rate at which citrate adsorbs to soil particles, $\gamma_2$ [$s^{-1}$] is the rate at which citrate desorbs from soil particles, $D_P$ and $D_C$ [$m^2$ of soil solution $s^{-1}$] are the diffusion coefficients of P and citrate in water respectively (when $\phi_s > 0$, these include a geometric impedance factor of 0.3), and $\lambda$ [$s^{-1}$] is the rate of citrate bio-degradation.

In Equations (3.1-3.4), adsorbed citrate and P are treated as separate chemical species from citrate and P in solution. The terms in Equations (3.1) and (3.2) with no spatial derivative

describe a reversible chemical reaction between adsorbed and solution P where adsorbed citrate acts as a catalyst for P desorption. As linear kinetics is used to describe soil adsorption and desorption instead of non-linear kinetics, such as the competitive Langmuir equation, the model is only valid for a limited concentration range near 0. Furthermore, it is assumed that citrate affects P adsorption but not vice-versa, contrary to some other modelling studies (Schnepf et al. (2012)). This simplified approach was taken to minimise the number of fitting parameters and avoid over-fitting. The impact of this simplification and valid concentration ranges is examined in the discussion section 3.6. The prefactors $\phi_l$ and $\phi_s$ are included to ensure that the model accounts for changes in soil saturation, *i.e.* when soil saturation or soil content approaches zero the reaction terms are altered accordingly.

To solve Equations (3.1-3.4), a set of boundary equations is required for the microdialysis probe. The pump rate of the microdialysis probe is assumed to be fast enough so that there is an infinite supply of citrate and when P is absorbed by the microdialysis probe it is instantly transported away. It is assumed that the microdialysis probe exudes citrate at a rate proportional to the difference in concentration of citrate in the perfusate and in solution,

$$\phi_l D_C \nabla C_l \cdot \mathbf{n}_p = \delta_C (C_0 - C_l), \quad \mathbf{x} \in \Gamma_p, \tag{3.5}$$

where $C_0$ [$\mu$mol m$^{-3}$ of perfusate] is the concentration of citrate in the perfusate, $\mathbf{n}_p(\mathbf{x})$ is the unit normal to $\Gamma_p$ pointing out of $\Omega$ for $\mathbf{x} \in \Gamma_p$, and $\delta_C$ [ms$^{-1}$] is the membrane permeability. In the absence of citrate, the microdialysis probe absorbs P at a rate proportional to the concentration of P in soil solution. Ionic strength of the external solution is known to alter microdialysis probe uptake rates, hence, in the model citrate can alter microdialysis probe P uptake (Demand et al. (2017)). This process is not fully understood so a general citrate dependent microdialysis probe P uptake rate is used,

$$\phi_l D_P \nabla P_l \cdot \mathbf{n}_p = -\delta_P(C_l) P_l, \quad \mathbf{x} \in \Gamma_p, \tag{3.6}$$

where $\delta_P$ [m of soil solution s$^{-1}$] is a function of citrate concentration that controls microdialysis probe P uptake. In general, $\delta_P$ is a function of microdialysis probe membrane thickness, porosity and surface chemistry etc. To fit the data, $\delta_P(C_l)$ needs to be specified, but we do not know its functional form. To overcome this, $\delta_P$ is approximated as its first order Taylor expansion about

$C_l = 0$,

$$\delta_P(C_l) = \delta_P^0 + \delta_P^1 C_l + \mathscr{O}(C_l^2). \tag{3.7}$$

Using this approximation, Equation (3.6) becomes,

$$\phi_l D_P \nabla P_l \cdot \mathbf{n}_p = -(\delta_P^0 + \delta_P^1 C_l + \mathscr{O}(C_l^2)) P_l, \quad \mathbf{x} \in \Gamma_p \tag{3.8}$$

where $\delta_P^0$ has units [m of soil solution $s^{-1}$] and $\delta_P^1$ has units [$m^4$ of soil solution $s^{-1}$ $\mu mol^{-1}$]. The parameters $\delta_P^i$ are constants and can be fit using standard methods explained in the following section. The remaining parts of the boundary are closed and are described using no flux conditions

$$D_P \nabla P_l \mathbf{n}_e = 0, \quad \mathbf{x} \in \Gamma_e, \tag{3.9}$$

$$D_C \nabla C_l \cdot \mathbf{n}_e = 0, \quad \mathbf{x} \in \Gamma_e, \tag{3.10}$$

where $\mathbf{n}_e(\mathbf{x})$ is the unit normal pointing out of $\Omega$ for $\mathbf{x} \in \Gamma_e$. Finally, the initial conditions are given by,

$$C_l(0,\mathbf{x}) = C_s(0,\mathbf{x}) = 0, \tag{3.11}$$

$$P_l(0,\mathbf{x}) = \frac{P_{add}}{\phi_l(1+b_P)}, \tag{3.12}$$

$$P_s(0,\mathbf{x}) = \frac{\phi_l}{\phi_s} b_P P_l(0,\mathbf{x}), \tag{3.13}$$

where $b_P = \frac{\beta_1}{\beta_2}$ [1] is the buffer power of P in soil and $P_{add}$ [$\mu mol\ m^{-3}$ of total soil] is the concentration of labelled P added to the soil. Notice, after time-equilibration $P_s = \frac{\phi_l}{\phi_s} b_P P_l$, thus we have $\phi_l P_l + \phi_s P_s = P_{add}$ and therefore mass is conserved in the initial conditions.

There are 9 unknown parameters introduced by the model, namely $\beta_1, \beta_2, \beta_3, \gamma_1, \gamma_2.\lambda, \delta_C, \delta_P^0$ and $\delta_P^1$ which are summarised in Table 3.3. In the past, the soil reaction parameters have been estimated based purely on physical intuition (Zygalakis & Roose (2012) or have been simplified to equilibrium reaction models (*i.e.* they approximate sorbed P by solution P using the buffer power) by assuming the reaction rates are fast and parameterised using bulk equilibrium experiments (Gerke, Römer & Beißner (2000)). In order to resolve soil soprtion, the reaction rate parameters must be carefully fit to experimental data. The value of $\beta_3$ is of particular interest

for understanding P mobilisation by citrate. However, to calculate $\beta_3$ the other parameters must also be known.

TABLE 3.3: Parameters used in the model

| Parameter | Description | Unit | Value |
|---|---|---|---|
| $\phi_l$ | $m^3$ of soil solution per $m^3$ of total soil | $m^3$ of soil solution $m^{-3}$ of total soil | 0.3 or 1 |
| $\phi_s$ | $m^3$ of solid soil per $m^3$ of total soil | $m^3$ of soil solid $m^{-3}$ of total soil | 0.6 or 0 |
| $b_P = \frac{\beta_1}{\beta_2}$ | Buffer power of P in soil | 1 | Fit |
| $b_C = \frac{\gamma_1}{\gamma_2}$ | Buffer power of citrate in soil (Oburger, Jones & Wenzel (2011)) | 1 | 4.78 |
| $\beta_1$ | P adsorption rate to solid soil | $s^{-1}$ | Fit |
| $\beta_2$ | P desorption rate from solid soil | $s^{-1}$ | Fit |
| $\beta_3$ | P enhanced desorption from soil solid due to adsorbed citrate | $m^3$ of soil solid $s^{-1}$ $\mu mol^{-1}$ | Fit |
| $\gamma_1$ | Citrate adsorption rate to solid soil | $s^{-1}$ | $b_C \times \gamma_2$ |
| $\gamma_2$ | Citrate desorption rate to solid soil | $s^{-1}$ | Fit |
| $\lambda$ | Rate of citrate biodegradation | $s^{-1}$ | Fit |
| $\delta_C$ | Efflux of citrate from perfusate into the system | $m^4$ of soil solution $m^{-3}$ of total soil $s^{-1}$ | Fit |
| $\delta_P^0$ | Absorption rate of P by microdialysis probe when no citrate is present | m of soil solution $s^{-1}$ | Fit |
| $\delta_P^1$ | Absorption rate of P by microdialysis probe affected by citrate | $m^4$ of soil solution $s^{-1}$ $\mu mol^{-1}$ | Fit |
| $D_{P/C}$ | Diffusion rate of P or citrate in soil/water | $m^5$ of soil solution $m^{-3}$ of total soil $s^{-1}$ | $7 \times 10^{-10}$ or $2.1 \times 10^{-11}$ |
| $t_{max}$ | Time scale of experiment | hours | 1 or 12 |
| $\lvert\gamma_P\rvert$ | Surface area of the semi-permeable membrane | $m^2$ | $5.0265 \times 10^{-6}$ |
| $\lvert\Omega\rvert$ | Eppendorf tube volume | $m^3$ | $1.5 \times 10^{-6}$ |

#### 3.4.3.2 Data fitting

To calculate the parameters controlling P mobilization by citrate, model parameters were varied and numerical solutions were compared to experimental results to achieve the best fit. First, the parameters controlling citrate efflux and soil reactions were fit to the results from the microdialysis organic acid calibration experiments as these parameters are independent of the P parameters. Next, the P efflux rates were fit to the results of the microdialysis P calibration results for the standard solutions as these are independent of soil reactions. Following this process, the only unknown parameters are those controlling P adsorption/desorption to soil; these were

then fit to the results of the microdialysis P recovery experiments performed in soil. In each phase of the data fitting, the least-squares distance between the experimental and model values normalised by the standard deviation of the experimental data was used as an objective function. A schematic explaining the data fitting procedures is presented in Figure 3.3.

Instances of the model were solved numerically on the 2D-axisymmetric domain displayed in Figure 3.2, using a finite element method implemented in Comsol Multiphysics 5.3 (Comsol Ltd., Cambridge, UK). Minimisations were calculated using MATLAB 2016 (MathWorks Inc., Natick, MA) fmincon implementation of an interior-point algorithm.

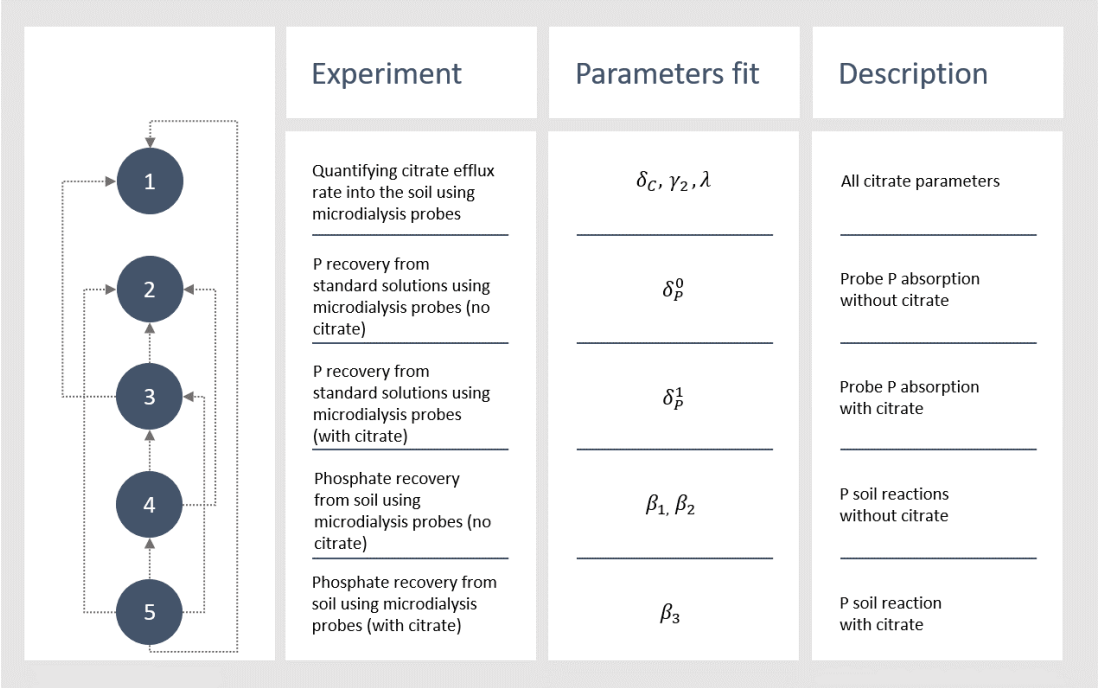


FIGURE 3.3: Schematic of all the data fitting procedures. The numbers dictate the order of the data fitting and the arrows represent the data fitting's dependencies.

**Calculating microdialysis probe citrate efflux and citrate soil reactions in this specific soil, $\delta_C$, $\gamma_2$ and $\lambda$.**

The model was compared to the results of the experiment described in the 'Quantifying citrate efflux rate into the soil using microdialysis probes experiment *i.e.* step 1 shown on Figure 3.3. As $\gamma_1 = b_C\gamma_2$ where $b_C$ is the known buffer power of citrate in the soil (Oburger, Jones & Wenzel (2011)), only one of the soil reaction parameters needed to be fit, in this case $\gamma_2$. There was no P in this case, so the experiment is modelled by Equations (3.1-3.13) with P initial conditions,

Equations (3.12) and (3.13), exchanged with,

$$P_l(0,\mathbf{x}) = 0, \tag{3.14}$$

$$P_s(0,\mathbf{x}) = 0, \tag{3.15}$$

so that there is no P in the model. If $C_l^{\delta_C,\gamma_2,\lambda,C_0}$ is the solution to Equations (3.1-3.11)+(3.14,3.15) with $\phi_l = 0.3$ and $\phi_s = 0.6$ for a given $\delta_C$, $\gamma_2$, $\lambda$ and $C_0$ then the model total citrate exudation at time $t$ is given by,

$$J_{M_1}(C_0,t;\delta_C,\gamma_2,\lambda) = \int_0^t \int_{\Gamma_p} D_C \nabla C_l^{\delta_C,\gamma_2,\lambda,C_0} \cdot \mathbf{n}_p d\mathbf{x} d\tau \tag{3.16}$$

The average experimental flux at time $t$ for a given concentration of citrate in the perfusate, $C_0$, is denoted $J_{E_1}(C_0,t)$ (Figure 3.4, orange lines), with corresponding standard deviation $\sigma_1(C_0,t)$. Then $\gamma_C$ and $\gamma_2$ were found by minimising the absolute difference between $J_{M_1}$ and $J_{E_1}$. As the data is spread over a large range, it was normalised by its standard deviation. Thus, to approximate $\delta_C$, $\gamma_2$ and $\lambda$ the following objective function was minimised

$$obj_1(\delta_C,\gamma_2,\lambda) = \sum_{t\in T_1}\sum_{C_0\in c} \frac{|J_{M_1}(C_0,t;\delta_C,\gamma_2,\lambda) - J_{E_1}(C_0,t)|^2}{\sigma_1(C_0,t)^2} \tag{3.17}$$

where $T_1 = \{1,2,3,4,5,6,8,12\}$ hours and $c = \{100,1000,10000\}$ μM.

**Calculating microdialysis probe P influx with no citrate, $\delta_P^0$**

In order to calculate $\delta_P^0$ the model was compared to the results of the 'P recovery from standard solutions using microdialysis probes' experiment without citrate *i.e.* step 2 shown on Figure 3.3. The model that describes the experimental setup is given by Equations (3.1-3.13) with $C_0 = 0$, $\phi_l = 1$, $\phi_s = 0$ and solution P initial conditions given by $P_l(t=0,\mathbf{x}) = P_0$ instead of Equation (3.12) where $P_0$ is the concentration of P solution in the standard solutions. These conditions produce a model with no soil or citrate. If $P_l^{\delta_P^0,P_0}$ is the solution, for a given $\delta_P^0$ and $P_0$ then the model total influx of P into microdialysis probe at time $t$ is given by

$$J_{M_2}(P_0,t;\delta_P^0) = \int_0^t \int_{\Gamma_P} D_P \nabla P_l^{\delta_P^0,P_0} \cdot \mathbf{n}_p d\mathbf{x} d\tau, \tag{3.18}$$

The experimental average total influx at time $t$ for a given concentration of P in the soil, $P_0$, is denoted $J_{E_2}(P_0)$ (Figure 3.5, orange lines), with corresponding standard deviation $\sigma_2(P_0)$. To approximate $\delta_P^0$ the following objective function was minimised

$$obj_2(\delta_P^0) = \sum_{P_0 \in p} \frac{|J_{M_2}(P_0, t^*; \delta_P^0) - J_{E_2}(P_0)|^2}{\sigma_2(P_0)^2} \tag{3.19}$$

where $p = \{100, 1000, 10000\}$ μM and $t^* = 1$ hour.

**Calculating microdialysis probe P influx with citrate, $\delta_P^1$**

In order to calculate $\delta_P^1$ the model is compared to the results of the experiment described in 'P recovery from standard solutions using microdialysis probes' experiment with citrate *i.e.*, step 3 shown on Figure 3.3. The model that describes the experiment is given by Equations (3.1-3.2) with $\phi_l = 1$ and $\phi_s = 0$ and solution P initial conditions given by $P_l(t = 0, \mathbf{x}) = P_0$ instead of Equation (3.12) where $P_0$ is the concentration of P in the standard solution. These conditions produce a model with no soil. If $P_l^{\delta_P^1, P_0, C_0}$ is the solution for a given $P_0$, $C_0$ and $\delta_P^1$ then the total model influx at time $t$ is given by

$$J_{M_3}(P_0, C_0, t; \delta_P^1) = \int_0^t \int_{\Gamma_p} D_P \nabla P_l^{\delta_P^1, P_0, C_0} \cdot \mathbf{n}_p d\mathbf{x} d\tau. \tag{3.20}$$

The average total experimental influx at time $t$ for a given concentration of P in the soil, $P_0$, is denoted $J_{E_3}(P_0, C_0)$ (Figure 3.6, orange lines), with corresponding standard deviation $\sigma_3(P_0, C_0)$. To approximate $\delta_P^1$ the following objective function was minimised

$$obj_3(\delta_P^1) = \sum_{P_0 \in p} \sum_{C_0 \in c} \frac{|J_{M_3}(P_0, C_0, t^*; \delta_P^1) - J_{E_3}(P_0, C_0)|^2}{\sigma_3(P_0, C_0)^2}. \tag{3.21}$$

**Calculating P-soil reaction parameters without citrate, $\beta_1$, $\beta_2$**

In order to calculate the P-soil reaction parameters without the effect of citrate the model was compared to the results of the experiment described in 'P recovery from soil using microdialysis probes' experiment with no citrate *i.e.* step 4 shown on Figure 3.3. The ratio of $\beta_1$ and $\beta_2$ determines the buffer power, $b_P$, of P in this soil. The equations which describe this experiment are Equations (3.1-3.13) with $C_0 = 0$, $\phi_l = 0.3$, $\phi_s = 0.6$ and $P_{add} = 66731$ μmol m$^{-3}$ (calculated as the 0.1 μmol of P added to 1.5 ml of soil as described in the 'P recovery from soil using

microdialysis probes' experiment). If $P_l^{\beta_1,\beta_2}$ is the solution for a given $\beta_1$ and $\beta_2$ then the model total P influx at time $t$ is given by

$$J_{M_4}(t;\beta_1,\beta_2) = \int_0^t \int_{\Gamma_p} D_P \nabla P_l^{\beta_1,\beta_2} \cdot \mathbf{n}_p d\mathbf{x} d\tau. \tag{3.22}$$

The average total experimental influx at time $t$ is denoted $J_{E_4}(t)$ (Figure 3.7, orange lines), with corresponding standard deviation $\sigma_4(t)$. To approximate and $\beta_1$ and $\beta_2$ the following objective function was minimised

$$obj_4(\beta_1,\beta_2) = \sum_{t\in T_2} \frac{|J_{M_4}(t;\beta_1,\beta_1) - J_{E_4}(t)|^2}{\sigma_4(t)^2}, \tag{3.23}$$

where $T_2 = \{1,2,3,4,5,6,7,8,9,10,11,12\}$ hours.

**Calculating the P-soil reaction parameter with citrate, $\beta_3$**

Finally, $\beta_3$ was fit by comparing the model to the results of the 'P recovery from soil using microdialysis probes' experiment with citrate *i.e.*, step 5 shown on Figure 3.3. If $P_l^{\beta_3,C_0}$ is the solution to Equations (3.1-3.13) with $\phi_l = 0.3$ and $\phi_s = 0.6$ for a given $\beta_3$, and $C_0$ then the model total P influx at time $t$ is given by

$$J_{M_5}(C_0,t;\beta_3) = \int_0^t \int_{\Gamma_p} D_P \nabla P_l^{\beta_3,C_0} \cdot \mathbf{n}_p d\mathbf{x} d\tau. \tag{3.24}$$

The average total experimental influx at time $t$ for a given concentration of P in the soil and citrate concentration in the perfusate is denoted $J_{E_5}(C_0,t)$ (Figure 3.7, orange lines), with corresponding standard deviation $\sigma_5(t)$. To approximate $\beta_3$ the following objective function was minimised,

$$obj_5(\beta_3) = \sum_{t\in T_2} \sum_{C_0\in c} \frac{|J_{M_5}(C_0,t;\beta_3) - J_{E_5}(C_0,t)|^2}{\sigma_5(C_0,t)^2}. \tag{3.25}$$

As a measure of relative error of the fits, the percentage difference in cumulative exuded/absorbed citrate/P between the experiment and the model for each initial condition was reported. For example, after fitting $\delta_C$, $\gamma_2$ and $\lambda$ the percentage error for 100 μM of citrate in the perfusate ($C_0 = 100$) case is

$$\frac{J_{M_1}(C_0 = 100, t = 12h;\delta_C,\gamma_2,\lambda) - J_{E_1}(100,12h)}{J_{E_1}(100,12h)} \times 100. \tag{3.26}$$

When the percentage error is positive, the model over predicts exudation/absorption.

#### 3.4.3.3 Numerical Experiments

Once the model was calibrated to the microdialysis data, simulations were carried out to answer specific scientific questions: 1) Does the microdialysis probe behave well as a model root in terms of P uptake and citrate exudation? 2) How does citrate-P solubilisation contribute to root (and microdialysis probe) P uptake? 3) Under what soil buffering and citrate biodegradation conditions is typical root citrate exudation efficient for P absorption. The following simulations were deigned to answer these questions.

**Are microdialysis probes good root analogues?**

To compare microdialysis probe and root behaviour, a suitable model for a root is proposed. This was achieved by changing the boundary conditions for the microdialysis probe in the model described above to suitable equations which describe root citrate exudation and P uptake. In particular, the P boundary condition is changed from an osmosis uptake to Michaelis–Menten kinetics, as root P uptake is active and enzyme mediated (Barber (1995)). The citrate boundary condition is changed to a constant rate of exudation (Geelhoed et al. (1999), Zygalakis & Roose (2012)). More precisely, Equation (3.5) is replaced by

$$\phi_l D_C \nabla C_l \cdot \mathbf{n}_p = F_c, \quad \mathbf{x} \in \Gamma_p, \tag{3.27}$$

where $F_C$ [μmol m$^{-2}$ s$^{-1}$] is the root citrate exudation rate; and Equation (3.8) is replaced by

$$\phi_l D_P \nabla P_l \cdot \mathbf{n}_p = \frac{-F_P P_l}{K_P + P_l}, \quad \mathbf{x} \in \Gamma_p, \tag{3.28}$$

where $F_P$ [μmol m$^{-2}$ s$^{-1}$] is the maximum P uptake rate achieved by the root and $K_P$ [μmol m$^{-3}$] is the P concentration where the uptake rate is half $F_P$. Typical exudation rates of citrate for P-starved rape roots grown in nutrient solution at 27°C is $1.2037 \times 10^{-5}$ μmol s$^{-1}$ m$^{-1}$ of root (Hoffland (1992)). These roots typically have a root radius of approximately $4 \times 10^{-4}$ m (Kjellström & Kirchmann (1994)), meaning an approximate citrate exudation rate per root surface area (assuming the root is a cylinder) of $F_C = 4.7894 \times 10^{-3}$ μmol m$^{-2}$ s$^{-1}$. Typically, $F_P = 3.26 \times 10^{-2}$ μmol m$^{-2}$ s$^{-1}$ and $K_P = 1.5 \times 10^{2}$ μmol m$^{-3}$ (Barber (1995)). The model with Equations (3.5) and (3.8) will be referred to as the microdialysis probe model; when these equations are replaced by Equations (3.27) and (3.28) the collection of equations will be referred to as the root model. To make the models comparable, the root is assumed to have the same dimensions as the microdialysis probe.

To test whether the microdialysis probe behaves like a synthetic root in terms of citrate exudation and P uptake, the concentration of citrate in the perfusate, $C_0$, which produces the most similar exudation rates as the model root was found using data fitting. The P uptake rates between the root model and microdialysis probe model (using the optimal $C_0$) were then compared to determine how well the microdialysis probe behaves like a root.

**Citrate contribution to P uptake**

To investigate how citrate contributes to both microdialysis probe and root P absorption, both models are solved numerically with a range of citrate exudation rates and P flux rate per surface area is plotted in time.

**Under what soil conditions and and biodegradation rates is citrate important?**

To determine which soil conditions citrate exudation is important for root P uptake, the root model is solved with a range of buffer powers with and without citrate exudation. The buffer power is varied by keeping desorption ($\beta_2$) as the fitted value from the experiments and changing adsorption $\beta_1$. Similarly, citrate biodegradation rates were also varied. The percentage difference of P uptake between exuding and non-exuding roots over a 12 hour period was plotted against buffer power.

## 3.5 Results

### 3.5.1 Experimental

The experiments which measured the efflux of citrate from the microdialysis probes into the soil showed that the exudation rate decays in time to reach a steady efflux rate (Figure 3.4). Furthermore, when the concentration of citrate in the perfusate increased, the total quantity of citrate exuded in the soil increased linearly.

Measurements of P recovery from standard solutions using the microdialysis probes showed that when citrate was absent in the perfusate, the quantity of P absorbed by the microdialysis probe increased linearly with the concentration of P in the standard solutions (Figure 3.5). When the concentration of citrate in the perfusate increased, the amount of P absorbed by the microdialysis probe increased, except in the experiment where there was 100 μM of P in the standard solution (Figure 3.6).

#### 3.5.1.1 Data Fitting

The value of each parameter as found by the minimisation problems described in the Data fitting section can be found in Table 3.4. Furthermore, the goodness of fits for minimisations described by Equations (3.17,3.19,3.21,3.23,3.25) as described in Figure 3.3 can be seen in Figure 3.4, 3.5, 3.6 ($C_0 = 0$ μM) and 3.7 ($C_0 = 1000, 10000$ μM), respectively. The data fitting only concerns mass transfer across the membrane of the dialysis probe. Figure 3.8 demonstrates the predicted distribution of P and citrate in the external soil with $P_{add} = 6.67$ μM and $C_0 = 10.48$ μM when the fitted parameters were used. The fitted parameters found in this section were used for the rest of the microdialysis probe simulations.

TABLE 3.4: Results of minimisations described in the data fitting section. The heading Objective function refers to functions which were minimised, argmin refers to the parameter values which achieve the minimum as found by the interior-point algorithm, Objective value shows the value of the objective function at the parameter values which achieve the minimum; and Percentage error shows percentage difference in cumulative exuded/absorbed citrate/phosphate between the experiment and the model for each initial condition, a positive value means the model over predicts the exudation/absorption.

| Objective function | argmin | Objective value | Percentage error |
|---|---|---|---|
| $obj_1(\delta_C, \gamma_2, \lambda)$ | $\delta_C = 4.348 \times 10^{-4}$ m s$^{-1}$, $\gamma_2 = 1.2 \times 10^{-2}$ s$^{-1}$, $\lambda - 1.1 \times 10^{-3}$ s$^{-1}$ | 30.26 | $C_0 = 100:\ -21.4\%$<br>$C_0 = 1000:\ -13.6\%$<br>$C_0 = 10000:\ 16.3\%$ |
| $obj_2(\delta_P^0)$ | $\delta_P^0 = 2.936 \times 10^{-7}$ m s$^{-1}$ | 349.9 | $P_0 = 100:\ -0.02\%$<br>$P_0 = 1000:\ -31.2\%$<br>$P_0 = 10000:\ -34.5\%$ |
| $obj_3(\delta_P^1)$ | $\delta_P^1 = 1.7031 \times 10^{-12}$ m$^4$ s$^{-1}$ μmol$^{-1}$ | 110.7 | $P_0 = 100, C_0 = 100:\ -14\%$<br>$P_0 = 100, C_0 = 1000:\ 60\%$<br>$P_0 = 100, C_0 = 10000:\ 49\%$<br>$P_0 = 1000, C_0 = 100:\ -63\%$<br>$P_0 = 1000, C_0 = 1000:\ 22\%$<br>$P_0 = 1000, C_0 = 10000:\ 95\%$<br>$P_0 = 10000, C_0 = 100:\ -30\%$<br>$P_0 = 10000, C_0 = 1000:\ -29\%$<br>$P_0 = 100, C_0 = 10000:\ -13\%$ |
| $obj_4(\beta_1, \beta_2)$ | $\beta_1 = 7.899 \times 10^{-6}$ s$^{-1}$, $\beta_2 = 1.993 \times 10^{-7}$ s$^{-1}$ | 1.2 | $C_0 = 0:\ -1.7\%$ |
| $obj_5(\beta_3)$ | $\beta_3 = 3.41 \times 10^{-13}$ m$^3$ of soil solid s$^{-1}$ μmol$^{-1}$ | 100.8 | $C_0 = 1000:\ 1.6\%$<br>$C_0 = 10000:\ -8.7\%$ |

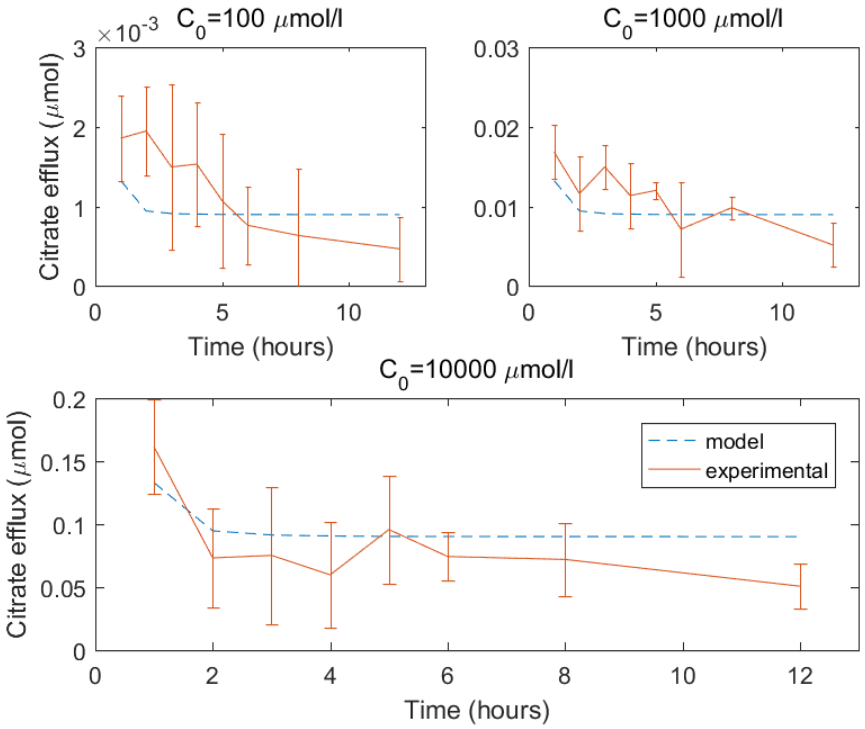


FIGURE 3.4: Comparison of experimental and model microdialysis probe citrate efflux using the fitted parameters $\delta_C = 4.348 \times 10^{-4}$ ms$^{-1}$, $\gamma_2 = 1.2 \times 10^{-2}$ s$^{-1}$ and $\lambda = 1.1 \times 10^{-3}$ s$^{-1}$. The error bars on the experimental data shows standard deviation, $n = 4$ for $C_0 = 1000$ μM, while $n = 3$ for $C_0 = 100$ and 1000 μM.

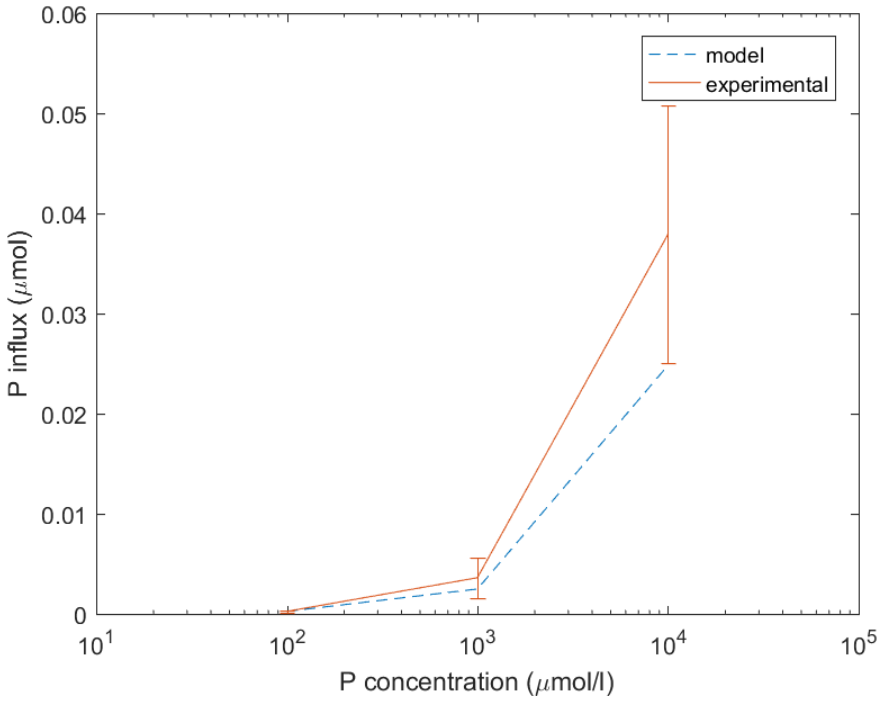


FIGURE 3.5: Comparison of experimental and model microdialysis probe P influx using the fitted parameter $\delta_P^0 = 2.9357 \times 10^{-7}$ m s$^{-1}$. The error bars on the experimental data shows standard deviation, $n = 4$, $\log_{10}$ scale on the x-axis.

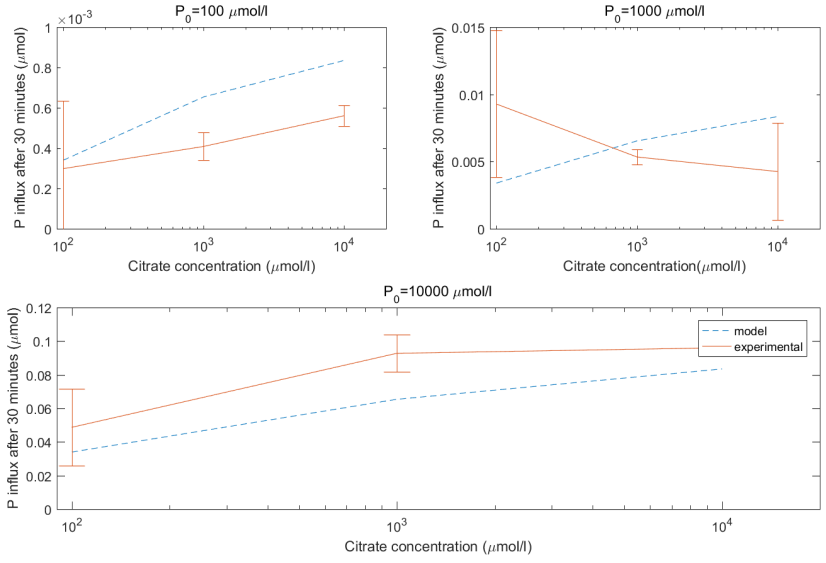


FIGURE 3.6: Comparison of experimental and model microdialysis probe P influx with citrate in the perfusate using the fitted parameter $\delta_P^1 = 1.7031 \times 10^{-12}$ m$^4$ s$^{-1}$ µmol$^{-1}$ . Error bars shows standard deviation, $n = 4$.

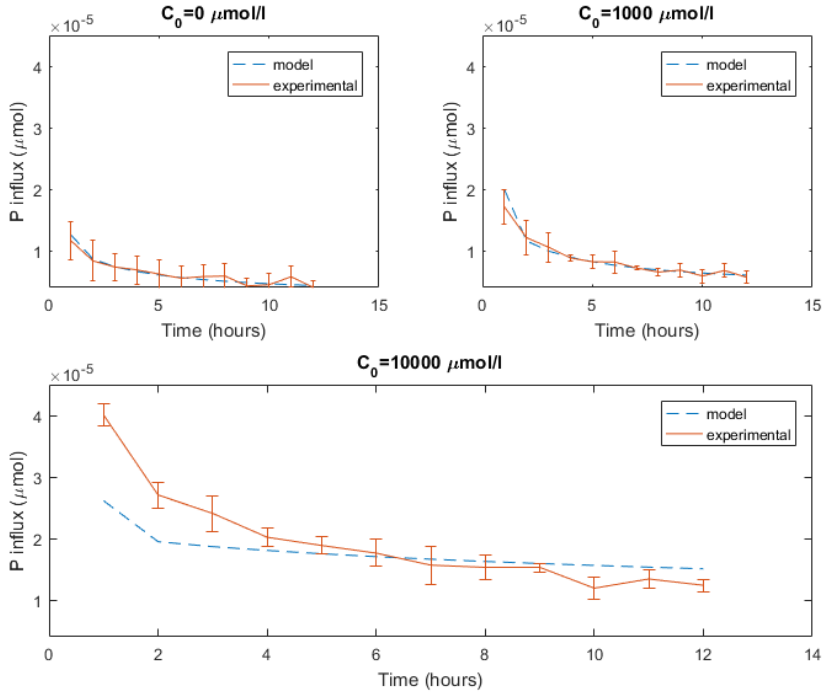


FIGURE 3.7: Comparison of experimental and model microdialysis probe P influx in soil with and without citrate in the perfusate. Using the parameters $\beta_1 = 7.899 \times 10^{-6}$ s$^{-1}$ and $\beta_2 = 1.993 \times 10^{-7}$ s$^{-1}$ produces the best fit to the experimental data when there is no citrate ($C_0 = 0$ μM). Using the parameter $\beta_3 = 3.41 \times 10^{-13}$ produces the best fit to the experimental data when there is citrate in the perfusate ($C_0 = 1000, 10000$ μM). Error bars shows standard deviation, $n = 4$.

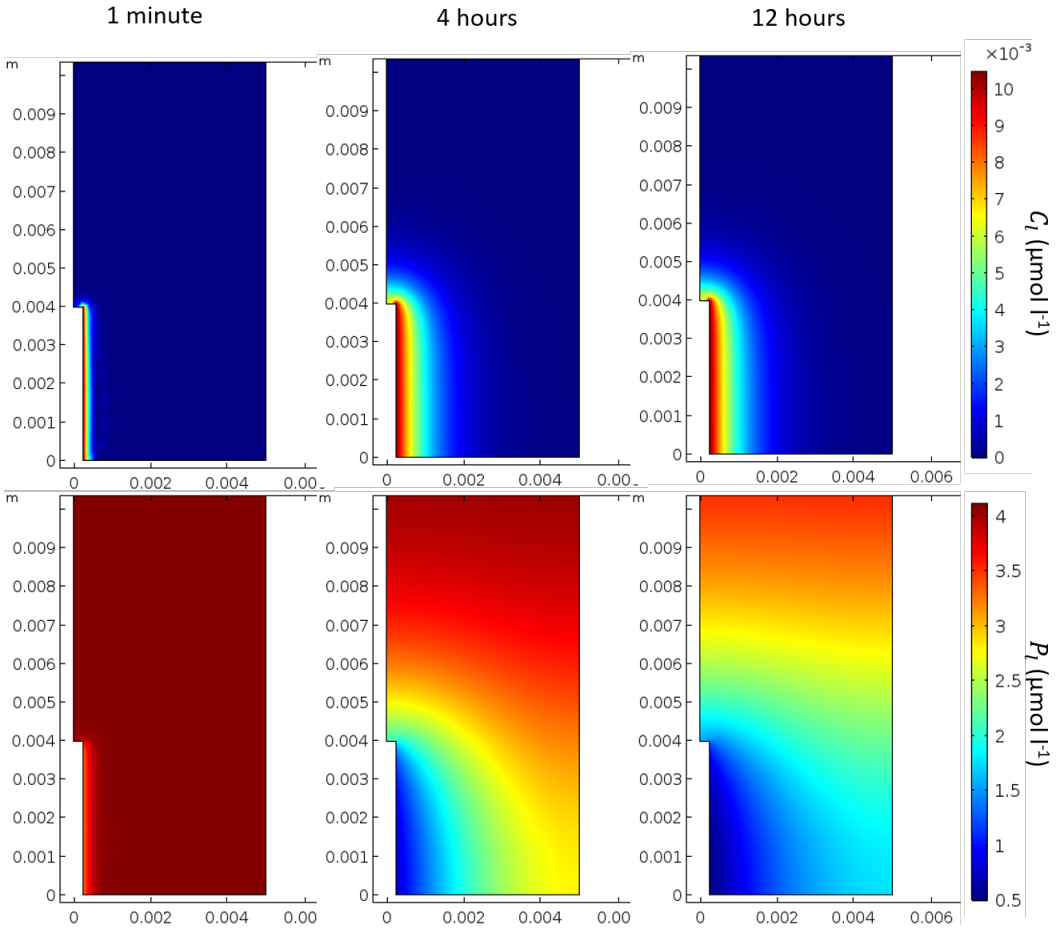


FIGURE 3.8: Solutions of the microdialysis probe model after 1 minute, 4 hours and 12 hours using the fitted parameters described above with $P_{add}$=6.67 µmol $l^{-1}$ of soil and $C_0 = 10.48$ µM. The top row shows the solution for citrate ($C_l$) and the bottom row for phosphate ($P_l$)

### 3.5.2 Numerical Experiments

#### Microdialysis probes as model roots

It was found that a citrate concentration of 10.48 µM in the perfusate produced the most similar citrate exudation pattern to a model rape root (Figure 3.9a). The P absorption for microdialysis probe and root model was also compared using the same initial P additions as the $\beta_1$, $\beta_2$ and $\beta_3$ data fitting ($P_{add} = 66731$ µmol $m^{-3}$ of total soil) Figure 3.9b. It was found that at this initial concentration of P in the soil and citrate in the perfusate, the microdialysis probe under predicts root P absorption.

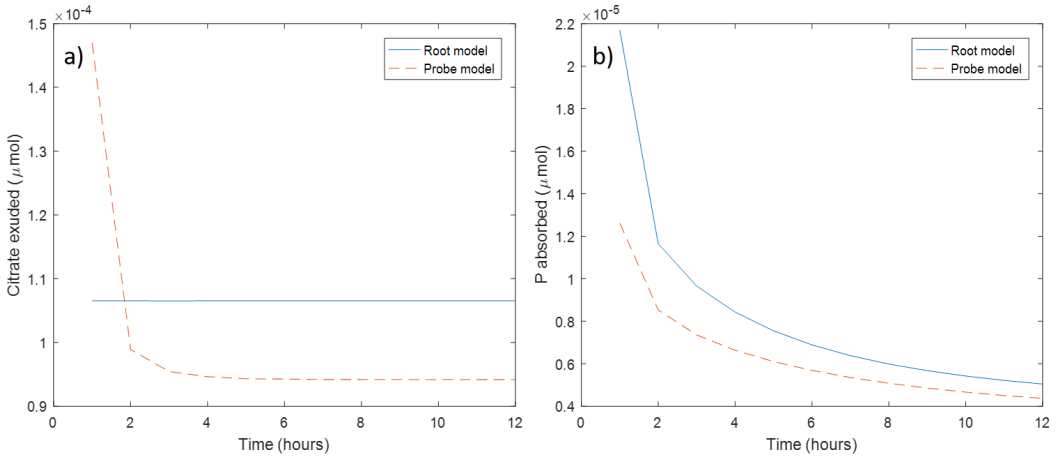


FIGURE 3.9: Comparison of the model root and model microdialysis probe in terms of citrate exuded and P absorbed using the concentration of citrate in the perfusate which produces the most similar citrate exudation to a typical root ($C_0 = 10.48$ μM). **a)** Root and microdialysis probe model citrate exudation measured every hour; **b)** Root and microdialysis probe model P absorption measured every hour

### Citrate's contribution to P uptake

The P uptake rate per surface area of both a model microdialysis probe and root exuding citrate ($C_0 = 10.48$ μM, $F_C = 4.7894 \times 10^{-3}$ μmol m$^{-2}$ s$^{-1}$) was compared to those with no citrate (Figure 3.10a). Similarly, Figure 3.10b shows the effect on P uptake when citrate exudation is dramatically increased (with $C_0 = 50000$ μM, and $F_C = 21.25$ μmol m$^{-2}$ s$^{-1}$ to produce similar root and microdialysis probe citrate exudation). Little difference in P absorption between a model exuding microdialysis probe/root (exuding at a typical rate for plants) and non-exuding microdialysis probe/root could be seen ($< 1\%$). Figure 3.11 shows P influx versus time for a range of citrate exudation rates. Microdialysis probe and root P uptake dynamics remained similar for a range of citrate exudation quantities. Furthermore, uptake dynamics changed drastically as more citrate was exuded into the soil. When enough citrate was exuded into the soil, large increases in P influx can be obtained for both a root and microdialysis probe.

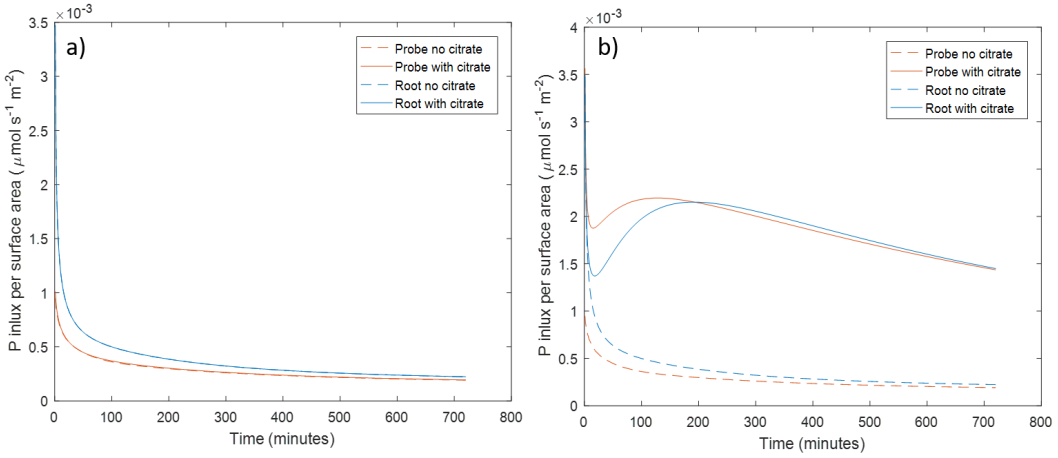


FIGURE 3.10: P influx per surface area in a model root and microdialysis probe with and without citrate exudation. **a)** In the microdialysis probe model the concentration of citrate in the perfusate is $C_0 = 10.48$ µM, which produces similar citrate exudation to the root model with exudation rate $F_C = 4.7894 \times 10^{-3}$ µmol m$^{-2}$ s$^{-1}$, typical for a rape root. The no exudation cases overlap the exudation cases. **b)** In the microdialysis probe model the concentration of citrate in the perfusate is $C_0 = 50000$ µM, which produces similar exudation to the root model with exudation rate $F_C = 21.25$ µmol.

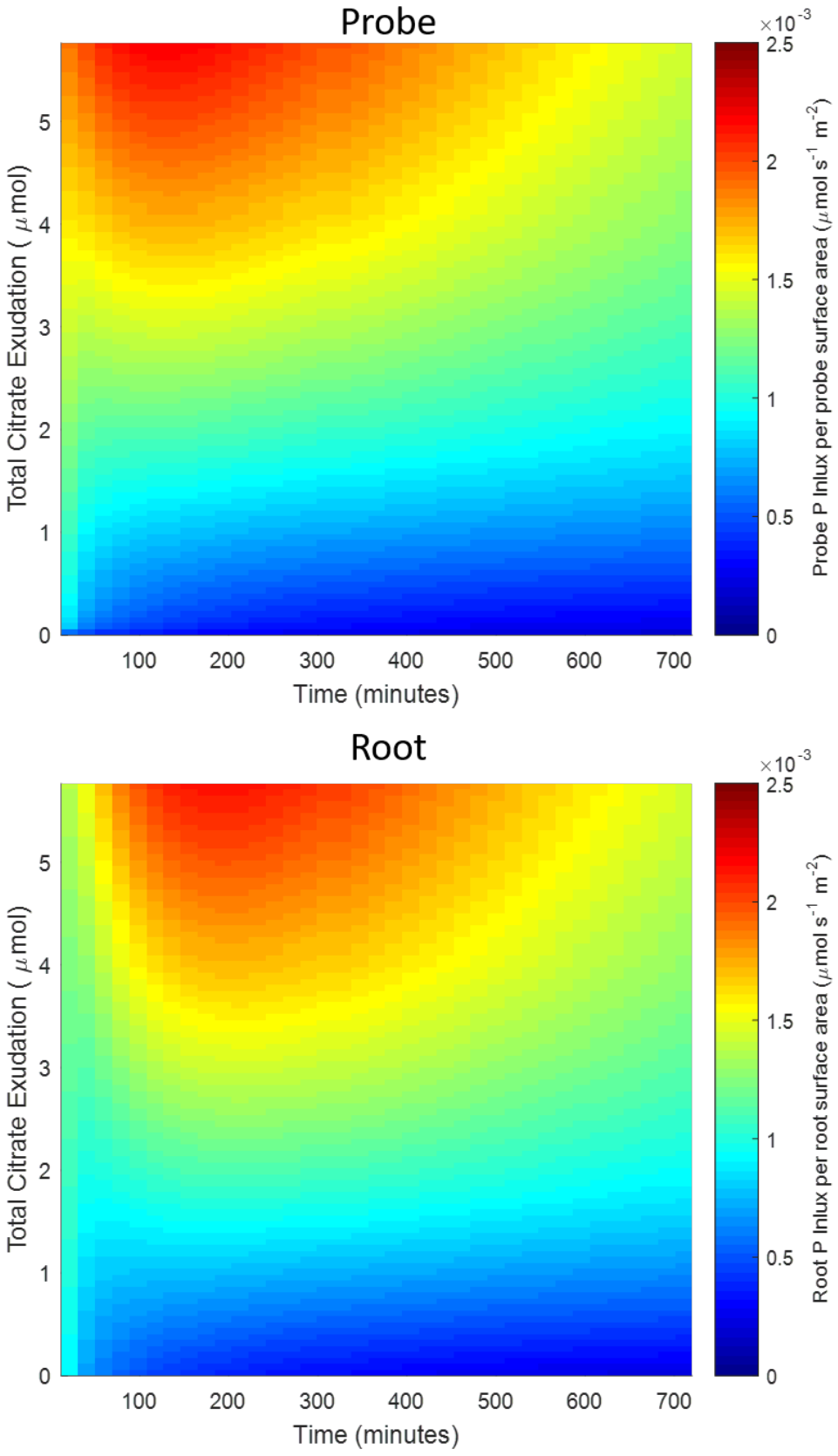


FIGURE 3.11: Heat map showing P influx per surface area against time and total amount of citrate exuded into the soil over 12 hours for both a model root and microdialysis probe. The increasing exudation total are evaluated by solving the Probe and Root models with increasing values of $C_0$ and $F_C$ respectively.

**Under what soil conditions is citrate important?**

The buffer power and biodegradation rate were varied to determine which soil conditions citrate exudation is important for P absorption. Figure 3.12a shows the percentage difference in P absorbed when comparing an exuding root to a non-exuding root when the citrate biodegradation rate is varied. Figure 3.12b shows the same when buffer power is varied. Percentage additional P absorbed decreases exponentially in citrate biodegradation and increases linearly in buffer power (notice the $y$ axis in Figure 3.12 are logarithmic). Error from the numerical scheme is evident due to the small relative changes (relative error of the method is at most 0.01%).

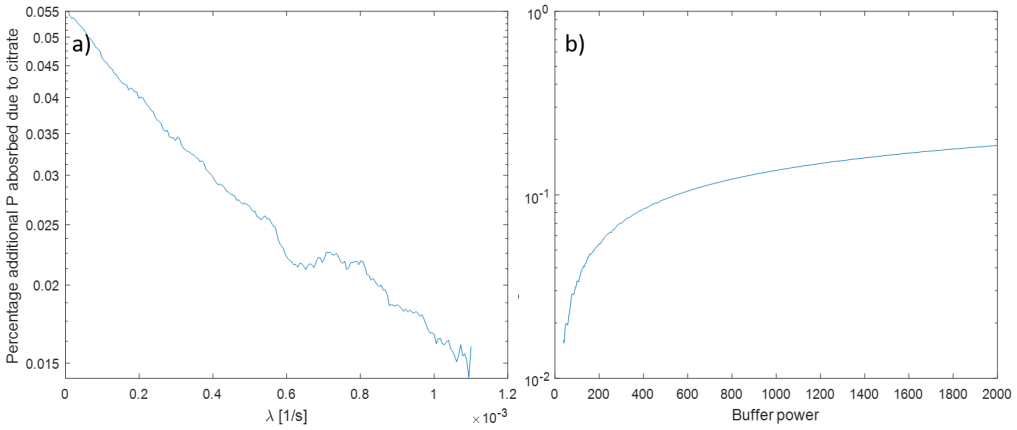


FIGURE 3.12: Plots of percentage additional P absorbed due to citrate when compared to a non-exuding root, **a)** when citrate biodegradation, $\lambda$ was increased from 0, **b)** when P buffer power, $b$ was increased from 39.

## 3.6 Discussion

**Modelling P mobilisation by citrate in soil**

The model proposed here introduces a parameter ($\beta_3$) which controls the rate of mobilisation of soil phosphate by citrate. This was similar to parameters found in many other soil P mobilisation models (Gerke, Beißner & Römer (2000), Zygalakis & Roose (2012)). Of critical importance, however, was that we were able to experimentally derive this key parameter which had only previously been estimated from intuition. Our model fitted well to the dynamic data from the 'P recovery from soil using microdialysis probes' experiment when the concentration of the citrate in the perfusate was 0 or 1000 μM, and it fitted well to the cumulative behaviour of the probe

when the concentration was 10000 μM. Thus, we conclude that the mechanism of citrate enhanced P-desorption assumed in the model is consistent with experiments and could account for the enhanced P influx by the microdialysis probe for a limited range of citrate and P concentrations. In particular, as the model uses first order kinetics to model sorption, it is not suitable for long-term modelling where P concentrations vary (Dari et al. (2015)). To improve the suitability of the model for a wide range concentrations, the first order kinetics should be expanded upon, when more data emerges, to include the non-linear relationship between citrate and P concentration with sorption and citrate enhanced P desorption. Oburger et al. (2009) calculated the bio-degradation rate of citrate in a similar soil to be $\lambda = 6.87 \times 10^{-5}$ $s^{-1}$ by measuring $CO_2$ respiration, while our calculation was $\lambda = 1.1 \times 10^{-3}$ $s^{-1}$. However, Oburger et al. (2009) used a double first order exponential decay model to fit the data, while we used a single first order decay model and considered soil adsorption. We also ascribe this difference to the significant temporal decoupling which can occur between substrate uptake and mineralization which leads to an underestimation of $\lambda$ using the $CO_2$-based approach (Gunina et al. (2017)). However, our approach measured biodegradation and sorption together while the $CO_2$ respiration approach targets microbial activity. Furthermore, Figure 3.12a suggests such changes in biodegradation only makes small changes to the amount of P absorbed and hence would not be detectable by microdialysis.

**Data fitting**

In total, 8 parameters were fit to 72 data points with varying citrate and P conditions and time resolution. The data fitting approach was to determine the dependency of the parameters, as seen in Figure 3.3, then design experiments suitable for determining the parameters which had the least dependencies. The parameters dependent on multiple processes could then be fit to experiments. This approach allowed us to decouple parameters' effects from one another. For example, if all parameters were fit together, P desorption ($\beta_2$) could increase at the expense of citrate enhanced solubilisation ($\beta_3$) and citrate enhanced desorption would be underestimated (or vice versa). Although the cumulative exudation of citrate over the 12 hour period in the model was within 21% of the experimental values for each citrate concentration (Table 3.4), there were mechanisms regarding probe citrate exudation that the model was not capturing (see Figure 3.4). Notably, the experiments showed that probe citrate exudation slows gradually,

while the microdialysis probe model rapidly decreased to reach a steady state efflux rate. Time-dependent probe permeability could explain this. There are also many citrate processes in the soil that are not included in the model, such as microbial mineralisation and immobilization of citrate and microbial population dynamics that could account for the poor temporal fit to the data (Glanville et al. (2016)). These processes were not included in the current model as they were not measured in the experiments. Additional microdialysis probe experiments, such as citrate flux in water and citrate recovery from soil are required to determine which mechanism to include and to fit the parameters reliably. However, as the cumulative error is relatively small, the effect on the subsequent data fitting procedures will be minimal.

Poor fits were achieved when fitting citrate enhanced probe P uptake ($\delta_P^1$, Table 3.4, Figure 3.6), this was assigned to two possible causes: 1) Inconsistent and variable experimental data; 2) Linearizing $\delta_P(C)$ about $C_l = 0$ (Equation 3.8) incurred a larger error. Linearizing about $C_l = C_0$ may be more suitable in the future when only one concentration of citrate in the perfusate is used. However, in our model, including this mechanism was important for the subsequent fitting of citrate enhanced solubilisation ($\beta_3$). If citrate enhanced probe P uptake was not included then the additional absorbed P due to citrate altering probe osmosis rates would be attributed to citrate solubilising P, and $\beta_3$ would have been overestimated. Although the correction has errors, the following results are more precise rather than having not included the correction.

**Microdialysis probes as root analogues**

After the soil P parameters were derived, a root model was proposed to determine if the microdialysis probes can be used to mimic root behaviour under the soil conditions detailed in Table 3.2, and the P additions stated in the experimental section. The microdialysis probe was found to underestimate root P uptake, with the difference narrowing as time progressed. We attribute this to the P supply rapidly depleting adjacent to the root, putting the Michaelis–Menten kinetics into the linear range of P concentrations. The probe under predicts root uptake as the linearized root uptake rate constant is $F_P/K_P = 2.17 \times 10^{-4}$ m s$^{-1}$ while probe permeability is $\delta_P^0 = 2.9 \times 10^{-7}$ m s$^{-1}$. Using a linearized Michaelis–Menten expression is only valid for a small range of P concentrations near 0. It was shown experimentally that microdialysis probe exudation rate decayed over time while we assumed the root exuded citrate at a constant rate, as evidenced by other authors (Geelhoed et al. (1999), Schnepf et al. (2012), Zygalakis & Roose

(2012)). Constant root exudation could be realistic as a large electrochemical potential gradient exists between the root and soil which can drive citrate exudation even against a large external concentration (Jones (1998)). This contrasts with the microdialysis probe where citrate exudation is solely driven by the strength of the diffusion gradient and associated ion sieving effects at the microdialysis probe-soil interface (Galach & Waniewski (2012)). Our findings, however, suggest that a suitable concentration of citrate can be used in the perfusate so that the microdialysis probe exudes the same quantity of citrate as a model root in total, but fails to mimic the dynamic behaviour.

**Modelling the impact of organic acid exudation on root P uptake**

When we used a citrate exudation rate similar to an oilseed rape plant (Hoffland (1992)) and added 0.1 μmol of P to the model soil, it was found that little additional P was absorbed compared to a non-citrate exuding root ($< 1\%$ enhancement of P acquisition). In comparison, other models report significant gains from citrate exudation. After 16 days of model time, Schnepf et al. (2012) found an entire root system could gain between 4 and 19% extra P depending on exudation patterns. Schnepf et al. (2012) used the kinetic competitive Langmuir reaction equation (Van de Weerd et al. (1999)) and they assumed desorption was fast to send citrate enhanced P solubilisation into equilibrium (the parameters were not experimentally verified) and considered multiple roots which interacted. Zygalakis & Roose (2012) used a similar model of citrate enhanced P solubilisation to that used in the current work, with the reactions sent into equilibrium. They used a $\beta_3/\beta_1$ ratio two orders of magnitude larger than the current (with no experimental support) and predicted cluster roots can absorb up to 35% more P due to citrate exudation. However, assuming the soil reactions are fast relative to diffusion to send the soil reactions into equilibrium can incur an error. Using a similar non-dimensionalisation to Zygalakis & Roose (2012) (non-dimensionalise P concentration with $K$, sorbed citrate concentration with the maximum achieved when using the realistic root exudation rate ($C_s^{max}$) and length, $l$, with the height of the Eppendorf tube) we find that adsorption happens at rates on the order of $10^0$ ($\frac{\beta_1 l^2}{D}$) desorption at $10^{-1}$ ($\frac{\beta_2 l^2}{D}$) citrate enhanced desorption $10^{-5}$ ($\frac{\beta_3 l^2 C_s^{max}}{D}$) and diffusion $10^0$ ($\frac{D}{D}$) when in regions of high citrate concentrations and using the fitted parameters. Thus, assuming reactions are fast relative to diffusion in the current geometry would not be valid. However, as the size

of the geometry, $l$, increases, assuming the reactions are in equilibrium becomes more appropriate. In contrast, previous experiments are in agreement with the current finding, both Güsewell & Schroth (2017) and Ryan et al. (2014) could not detect P uptake gains in high carboxylate exuding plants in comparison to low carboxylate exuding subgenus/near-isogenic species.

When citrate exudation was increased incrementally, P uptake dramatically increased (Figure 3.10 and 3.11) and P uptake reached a distinct maximum at approximately 250 minutes when citrate exudation reached appropriate levels (Figure 3.11). The latter effect is attributed to a solubilisation peak caused by P mobilisation. This mimics experiments performed in this same soil where high soil citrate concentrations (10 mM) were needed to promote plant $^{33}$P uptake (Khademi et al. (2010), Palomo et al. (2006)).

The reader should be aware that the model may not be as accurate for very high concentrations of citrate as suggested by the relatively poor fit to the temporal experimental data in Figure 3.7, $C_0 = 10000$ μM. In contrast, the fit for $C_0 = 1000$ μM case was good. This is a manifestation of the error from the linear approximations of P/citrate soil reactions (the error is $\mathscr{O}(C_l^2)$ or $\mathscr{O}(P_l^2)$ *i.e.* the error increases as concentration increases). Citrate enhanced solubilisation of P speeds up with increased citrate concentration and a Langmuir-like isotherm for citrate/P adsorption and citrate enhanced solubilsation may be needed to capture the temporal behaviour for both citrate concentrations simultaneously. The error from the linearized kinetics may also become apparent when the P and citrate concentrations vary due to the probe absorbing and exuding. However, we cannot justifiably include the non-linear terms as the current experiments do not measure these concentration dependent effects. In future work additional experiments with varying P concentration in the soil could be used to fit the additional parameters which control these mechanisms. This would require a series of further microdialysis experiments designed to investigate citrate/P adsorption and desorption for varying concentrations.

Although citrate concentrations in the bulk soil are typically $< 50$ μM, concentrations up to 10 mM have been reported in the rhizosphere for certain plants under P deficiency (Dessureault-Rompré et al. (2006)), the current parameterisation of the model may not be accurate for such high concentrations. In addition, the model only considers 4 mm of a single root exuding, while cluster roots, or roots in close proximity may act together to exude larger quantities of citrate. From Figure 3.11, we estimate that a plant would need to exude citrate at a rate of 0.73 μmol

$cm^{-1}$ of root $h^{-1}$ to see a significant increase in P absorption. Alfalfa (*Medicago sativa* L.) can exude 1.3 μmol of citrate $g^{-1}$ of dry root $d^{-1}$ when under P stress (Lipton et al. (1987)), which equates to approximately $1.4 \times 10^{-5}$ $cm^{-1}$ of root $h^{-1}$ (Solaiman et al. (2007)), orders of magnitude lower than the required rate. Hence, P gains could only be achieved if the roots were densely packed. This concurs with the modelling findings of Zygalakis & Roose (2012) and Gerke, Römer & Beißner (2000) who both found that large clusters of roots benefit most from citrate exudation. The rates calculated in this work could be used to parametrise image-based models to assess different root system architectures, such as cluster roots, and the utilization of solubilized P. Gerke, Beißner & Römer (2000) found that more than 10 μmol of citrate $g^{-1}$ soil was needed for a significant increase in P solubilisation using bulk-equilibrium experiments. Gerke, Beißner & Römer (2000) did not see P solubilisation with lower citrate concentrations, however, this does not necessarily imply that plants would fail to see enhanced P uptake as seen in this work (Figure 3.11) for a number of reasons. Firstly, the calculation of $\beta_3$ in this work suggests that the rate citrate solubilises phosphate is in fact slow and should be considered dynamically; fast-equilibration arguments to approximate adsorbed P by P in solution would not stand, nor would equilibrium experiments be representative of a root absorbing P. Furthermore, citrate is exuded from a root creating a local region of high concentration, allowing the dramatic citrate-phosphate solubilisation as seen in Gerke, Beißner & Römer (2000) near the root surface.

Unsurprisingly, when citrate biodegradation decreases, the percentage additional P absorbed by the root due to citrate increases, however, the importance of this was less than some other factors in the model. For example, when the value of the buffer power was increased and P becomes held more strongly on the solid phase, citrate exudation had more benefit at solubilising P. This agrees with both the experimental work of Zhang et al. (1997), who suggest that low-molecular weight organic acids help radish (*Raphanus sativus* L.) and rape (*Brassica napus* L.) utilize sparingly soluble P; and the modelling work of Schnepf et al. (2012) who found citrate solubilised more P in strongly sorbing soils.

The $\beta_1$ and $\beta_2$ parameters calculated in this study results in a buffer power of 39.6 for phosphate in this soil. Although this was not unreasonable for such a soil and P additions (Barber (1995)), some caution is required when interpreting this result. Firstly, the microdialysis probe was only calibrated for P influx in standard solutions, however, when the microdialysis probe was placed

in soil, the ionic strength of the soil may have altered the uptake rate of the microdialysis probe. During the data fitting, this effect was included in the $\beta_1$ and $\beta_2$ parameters and may not be representative of the actual buffer power. This could be overcome by calibrating the probes at a similar ionic strength and compositions as exists in the soil. Furthermore, large quantities of P added to the soil can lower the buffer power (Barber (1995)) and the scintillation counting used in this chapter only measured the isotopically labelled P added to the soil, not the P originally present in the soil. However, these artefacts were accounted for during the $\beta_1$ and $\beta_2$ data fitting as ionic strength affects were measured implicitly during the corresponding experiment, thus will not affect the $\beta_3$ data fitting. Similarly, any gains in P uptake by the probe due to acidification by the un-buffered citrate was attributed to $\beta_3$, the parameter controlling specific adsorption, during the data fitting.

**Conclusions**

Here we demonstrated that microdialysis can be used to provide an effective measure of the diffusive flux of solutes both into and out of soil. The microdialysis probes can be easily used to mimic root exudation. Their small size and rapid response time makes them ideal to detect the spatial and temporal dynamics of solutes at the soil-root interface. We also demonstrated that assumptions about mechanisms of citrate and P in bulk soil can be used to create a model which describes the recovery of P by the probes. Parameters in this model were then varied so that the model fluxes across the microdialysis probe membrane were consistent with microdialysis experiments, allowing accurate measurements (up to the validity of the assumptions made) of soil properties. Critically, we showed the importance of calibrating the microdialysis probe influx and efflux rates in separate specially designed experiments to correct for the sensitivity of the microdialysis probes to external factors. This approach proved effective in calculating citrate enhanced P desorption and may be useful in calculating other important dynamic plant-soil interactions.

## 3.7 Acknowledgments

D.M.M.F., K.R.D. A.v.V., and T.R. are funded by ERC Consolidator grant 646809 (Data Intensive Modelling of the Rhizosphere Processes). T.R. is also funded by BBSRC SARISA

BB/L025620/1, EPSRC EP/M020355/1, BBSRC SARIC BB/P004180/1 and NERC NE/L00237/1. D.L.J.is supported by NE/K01093X/1.

# Chapter 4

# Linking root structure to functionality: The impact of root system architecture on citrate enhanced phosphate uptake

**Daniel M. McKay Fletcher**[a], **Siul Ruiz**[a], **Tiago Dias**[a], **Chiara Petroselli**[a], **Tiina Roose**[a]

[a]Bioengineering Sciences Research Group, Department of Mechanical Engineering, School of Engineering Sciences, Faculty of Engineering and Physical Sciences, University of Southampton, Southampton, UK.

## 4.1 Abstract

Root citrate exudation is thought to be important for phosphate solubilisation (Oburger, Jones & Wenzel (2011)). Previous research has concluded that cluster-like roots benefit most from this exudation in terms of increased phosphate uptake, suggesting root structure plays an important role in citrate enhanced uptake (additional phosphate uptake due to citrate exudation) (Lambers et al. (2006)).

Time resolved computed tomography images of wheat root systems were used as the geometry for 3D citrate-phosphate solubilisation models. Citrate enhanced uptake was compared with

morphological measures of the root systems to determine which were important for citrate enhanced uptake.

A large variation of citrate enhanced uptake over 11 root structures was observed. Root surface area dominated absolute phosphate uptake, but did not explain citrate enhanced uptake. Number of exuding root tips correlated well with citrate enhanced uptake. Root tips in close proximity to each other could collectively exude high amounts of citrate, resulting in a delayed spike in citrate enhanced uptake.

Root system architecture plays an important role in citrate enhanced uptake. Singular morphological measurements of the root systems cannot entirely explain variations in citrate enhanced uptake. Root systems with many tips would benefit greatly from citrate exudation. Quantifying citrate enhanced uptake experimentally is difficult as variations in root surface area would overwhelm citrate benefits. This is consistent with previous experimental results which have failed to consistently verify the phosphorus uptake benefit of citrate exudation (Ryan et al. (2014)).

**Key Words:** Root system architecture, citrate, exudation, phosphorus, a-biotic stress, modelling.

## 4.2 List of Symbols

| | |
|---|---|
| $\Omega \subset \mathbb{R}^3$ | image-based model domain representing homogeneous soil containg roots |
| $\Gamma \subset \mathbb{R}^2$ | boundary of $\Omega$ |
| $\Gamma_r(t) \subset \Gamma$ | active absorbing portion of the root surface |
| $\Gamma_o n(t) \subset \Gamma$ | active exuding portion of the root surface |
| $\Gamma_e(t) \subset \Gamma$ | non-active portion of the root surface and pot boundary |
| $P_l$ | phosphorus concentration in soil solution [$\mu$mol m$^{-3}$] |
| $P_s$ | phosphorus concentration bound to soil particles [$\mu$mol m$^{-3}$] |
| $C_l$ | citrate concentration in soil solution [$\mu$mol m$^{-3}$] |
| $C_s$ | citrate concentration bound to soil particles [$\mu$mol m$^{-3}$] |

| | |
|---|---|
| $\phi_l$ | volumetric water content [$m^3$ of soil solution $m^{-3}$ of total soil] |
| $\phi_s$ | volumetric soil content [$m^3$ of soil $m^{-3}$ of total soil] |
| $\beta_1$ | the rate at which phosphorus adsorbs to soil particles [$s^{-1}$] |
| $\beta_1$ | the rate at which phosphorus desorbs to soil particles [$s^{-1}$] |
| $\beta_3$ | the rate of citrate enhanced phosphorus desorbtion [$m^3$ $s^{-1}$ $\mu mol^{-1}$] |
| $D_P$ | diffusion rate of phosphorus in soil solution [$m^2$ $s^{-1}$] |
| $D_C$ | diffusion rate of citrate in soil solution [$m^2$ $s^{-1}$] |
| $\gamma_1$ | the rate at which citrate adsorbs to soil particles [$s^{-1}$] |
| $\gamma_2$ | the rate at which citrate desorbs to soil particles [$s^{-1}$] |
| $\lambda$ | the rate of citrate bio-degredation [$s^{-1}$] |
| $\mathbf{n_{on}}$ | unit normal to $\Gamma_{on}(t)$ |
| $\mathbf{n_r}$ | unit normal to $\Gamma_r(t)$ |
| $b_P$ | buffer power of phosphorus [-] |
| $b_C$ | buffer power of citrate [-] |
| $P_{tot}$ | total concentration of phosphorus in the soil [$\mu mol$ $m^{-3}$] |
| $F_C$ | root citrate exudation rate [$\mu mol$ $m^{-2}$ $s^{-1}$] |
| $F_P$ | maximum root phosphorus uptake rate [$\mu mol$ $m^{-2}$ $s^{-1}$] |
| $K_P$ | phosphorus concentration when root uptake is half $F_P$ [$\mu mol$ $m^{-3}$] |
| $G(t)$ | root growth rate function [m $s^{-1}$] |
| $g_i$ | $i = 0,2,4,6,8$ days, root growth rate from day $i$ to $i+1$ [m $s^{-1}$] |
| $dep_t(z)$ | indicator function returning 1 if the root has reached depth $z$ by time $t$ |
| $tip_t(z)$ | indicator function returning 1 if the root tip is at depth $z$ at time $t$ |
| $\rho(x,y)$ | Pearson Correlation Coefficient (PCC) of $x$ and $y$ |

$S_i(t)$ Surface area of root system $i$ at time $t$ [$m^2$]

## 4.3 Introduction

Phosphorus (P) is considered one of the key macro-nutrients required by plants (Barber (1995)). A characteristic feature of P in soil is that it strongly binds to soil particle surfaces and undergoes mineralisation. Both processes decrease the quantity of P available to plants (Barber (1995), Oburger, Jones & Wenzel (2011)). Therefore, it is difficult for crops to acquire the necessary amount of P for higher yields without large amounts of fertilisation. Typically, an annual crop producing 10 tons $ha^{-1}$ of biomass needs 30 kg $ha^{-1}$ of P during the growing season (Sylvester-Bradley et al. (2017)).

Typically, crops are bred to produce large yields in optimal nutrient and water conditions (Koevoets et al. (2016), Wissuwa et al. (2009)); this is usually guided by aboveground performance which can negatively impact belowground traits (Den Herder et al. (2010)). For example, studies have suggested that plants bred for high fertility soils have lost the ability to develop symbiotic relationships with mycorrhiza fungi, which are beneficial for acquiring P in poor conditions (Wissuwa et al. (2009)). Belowground traits are known to be vital in nutrient/water scarce conditions (Den Herder et al. (2010)). With climate change causing more extreme droughts and floods, breeders need to produce high yielding varieties in sub-optimal conditions (Den Herder et al. (2010), Koevoets et al. (2016)). Only a small number of genes have been identified that control root traits, one of which enhances early root growth and increases yield in P-deficient soils (Gamuyao et al. (2012), Uga et al. (2013)). This gene is notably absent in modern "phosphorous-starvation-intolerant" rice varieties (Gamuyao et al. (2012)). Although this is an example of one gene, there is still a vast pool of bio-diversity from which root traits can be found to increase crop yield in poor agricultural settings. Thus, understanding the functionality of root system architecture (RSA) traits will provide important insight as to how we might improve crop breeding to withstand soil changes posed by climate change (Topp et al. (2016)). However, unlike above ground traits (e.g. grain mass), it is difficult to assign and measure functionality of root traits due to the complexity of root/soil structure, chemistry, biology, as well as the difficulty of visualising roots in soil.

Under natural conditions, plants have evolved traits to mitigate deficient labile-P supplies. Organic acids, such as citrate or oxalate, exuded by roots can lower the soil pH promoting solubilisation of previously inaccessible soil-P supplies (Oburger, Jones & Wenzel (2011). Furthermore, organic acids exuded by roots can mobilise P adsorbed to soil particles, thereby enhancing plant P uptake (Gerke, Beißner & Römer (2000)). The benefits of exuding citrate may not only be limited to P deficient soils; locally increased solubilisation makes sorbed P available to plants, allowing farmers to decrease the quantity of fertilizer applied, therefore reducing run-off and P fertilisation (Manschadi et al. (2014)).

The contribution of P mobilisation by organic acids in phosphate absorption is in question. Duputel et al. (2013) found that the addition of citrate can both increase and decrease available P depending on the soil type. Gerke, Beißner & Römer (2000) found that more than 10 μmol of citrate $g^{-1}$ soil was needed for a significant increase in phosphate solubilisation; while typical exudation rates of citrate for P-starved rape roots grown in nutrient solution is $1.2 \times 10^{-6}$ μmol $s^{-1}$ $m^{-1}$ of root (Hoffland (1992)). At this rate it would take 1 cm of root length almost ten days to exude the 10 μmol required to see significant phosphate solubilisation, not accounting for bio-degradation of the exuded compounds. Furthermore, previous microdialysis work found a single model root exuding citrate into 1 g dry weight of soil did not increase root phosphate uptake significantly (see chapter 3).

Plants can form cluster-root architectures that collectively exude large quantities of citrate into a small region of soil in a short burst to intensively solubilise phosphate and other immobile nutrients (Lambers et al. (2006), Neumann & Martinoia (2002). This is consistent with the modelling findings of Zygalakis & Roose (2012) and Gerke, Römer & Beißner (2000) who both found that cluster roots dominate the phosphate benefits gained by citrate exudation. However, neither of these studies considered the explicit root system geometry in their models. On the other hand, dauciform root forming species (described as roots similar to cluster roots (Lambers et al. (2015))) were found to exude less organic acids and absorbed similar quantities of P to a subgenus that did not form dauciform roots (Güsewell & Schroth (2017)). Furthermore, Ryan et al. (2014) found that citrate enhanced relative biomass in only 2 out of 6 trials by using a low and high exuding wheat (*Triticum aestivum*).

Densely packed root systems are known to have low P uptake efficiency in terms of root carbon cost as roots in close proximity to one another compete for the same P supply (Fletcher, Keyes, Daly, Van Veelen & Roose (2019)). It could be hypothesised that the cumulative organic acid exudation from densely packed roots can mitigate the decreased P uptake efficiency. Oburger, Jones & Wenzel (2011) argued that unlike cluster root forming species, most crop species can only exude small to medium amounts of organic acids, bringing the importance of citrate-phosphate solubilisation in agriculture into question. Lambers et al. (2006) proposed that cluster-root forming species are so successful in highly weathered soil due to their specialized morphology and physiology. Clearly, RSA is linked to organic acid exudation and it may play a role in resulting phosphate gains.

Modelling techniques that consider the RSA (or other structures) can be a useful approach for linking geometry to functionality. Tron et al. (2015) used a root-growth model coupled to a soil-water model to determine which root traits are important for drought tolerance. They found that different RSAs were better in certain drought hydrological scenarios, highlighting the importance of RSA when discussing functionality (although the root systems in this case were simulated). Landl et al. (2019) used a coupled root growth model and water uptake model to determine the role of biopores on RSA and water uptake. Schnepf et al. (2012) modelled the impact of RSA on citrate-enhanced phosphate absorption using a root growth model, as their modelling work has a similar scope to the current, we highlight the differences and similarities in the discussion section.

Image-based modelling, a technique which uses images as modelling domains, is a powerful modelling approach for considering real geometries and their function. Koebernick et al. (2017) used image-based modelling to determine whether effective diffusion of nutrients and hydraulic connectivity of rhizosphere soil was altered by root hairs. They found no differences between rhizosphere soil of wild type barley and a root-hairless mutant. Considering the geometry explicitly is not always necessary; Daly et al. (2018) found that a simple averaged water-uptake model, which represented different RSAs using root length density parameters, predicted water uptake within 2% of an image-based model which used real 3D RSAs extracted from X-ray Computed Tomography (XCT) data. However, the simplified model did not capture the heterogeneous water distribution seen in the image-based model. It is important to note that the root

surface area parameter in the simplified model of Daly et al. (2018) was calculated directly from the XCT data to make the averaged model comparable to the image-based model. Image-based models are not limited to plant-soil research and have given insight when linking function to structure (as opposed to structure to function). Two dimensional image-based modelling was used to determine that the morphogenesis of regulatory networks in kidneys had the same genetic mechanism as lung networks (Menshykau et al. (2019)).

Currently, it is difficult to address the impact of the RSA on citrate-enhanced phosphate uptake due to the difficulties in quantifying roots, root exudation (Oburger & Jones (2018)) and measuring phosphate uptake simultaneously. This work aims to link RSA morphology to phosphate gains from citrate exudation and disentangle many of the conflicting results regarding P-uptake gains associated with citrate exudation. Specifically, we quantify the impact of the RSA on citrate-enhanced phosphate uptake using mathematical models solved directly on RSAs extracted from XCT images using experimentally verified parameters. RSAs from 11 time-resolved XCT scans were used as geometries for image-based modelling. The growing RSA both exuded citrate and absorbed P; in the soil, citrate is assumed to enhance P desorption. P uptake for exuding and non-exuding roots is compared under two soil P conditions: High P low buffering (denoted High P) and low P high buffering (denoted Low P) to determine the effect of citrate exudation in highly fertilised soils and low P soils, respectively. Geometrical measures of RSAs were compared to increases in P uptake associated with citrate exudation in order to identify root traits that are important for P benefits from citrate exudation. Furthermore, for the densest RSA, the model is solved with High P conditions and increasing exudation rates to investigate the effect of high citrate concentrations on the P uptake dynamics.

## 4.4 Materials and Methods

### 4.4.1 Root system architect and image based domain

This study used imaged wheat (*cv*. Zebedee) root systems grown in two soils: Eutric Cambisol (loamy sand, denoted LS) and Argillic Pelosol (clay loam, denoted CL) at 2,4,6,8 and 12 days after germination with 6 replicates (Daly et al. (2018)). The RSAs from the 12 day scans were used as the geometry for a model describing a citrate-exuding root absorbing phosphate. The 12

day state of each RSA can be seen in Figure 4.1. In the current work, root growth in the model was simulated by 'activating' the roots at the appropriate root growth rate as calculated from the previous XCT scans, details of which are given in the following sections. The root systems were segmented in the top 60 mm of the pots to avoid capturing effects of the pot on the RSA (Daly et al. (2018)). Often, the seminal roots reach this depth before 12 days. The scan resolution (30 μm voxel edge length) was not sufficient to observe and segment fine lateral roots, hence these roots are not included in the segmented RSA. The impact on their exclusion is examined in the discussion.

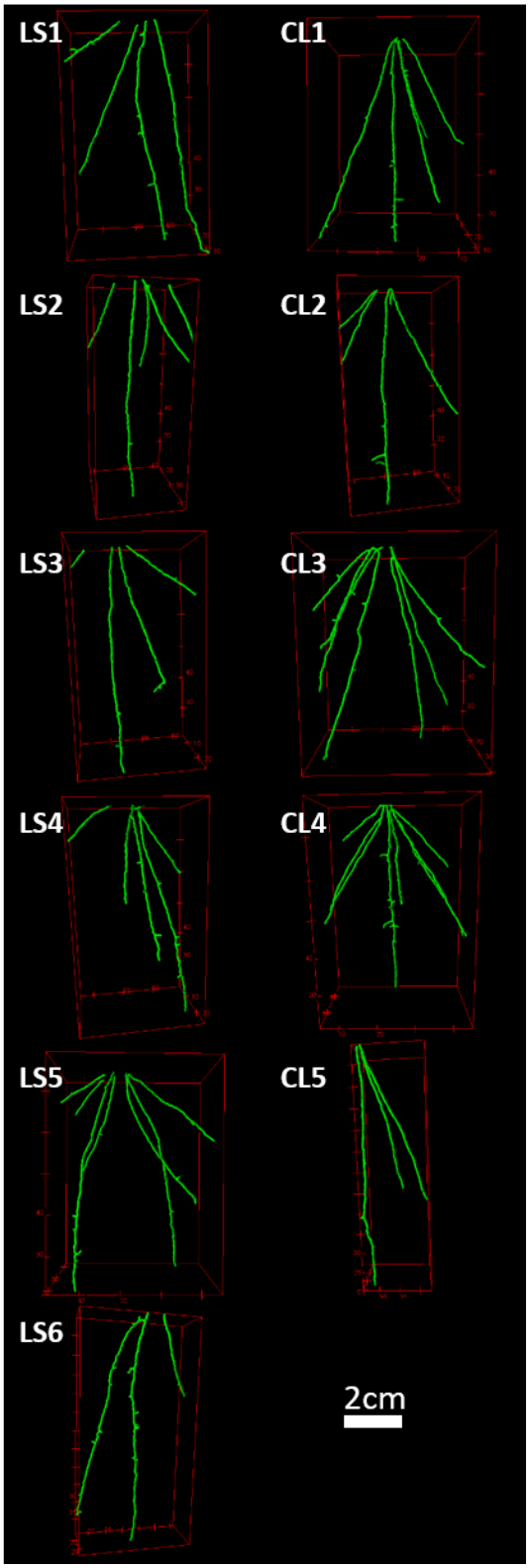


FIGURE 4.1: Each root system architecture in its 12 day state. The left column shows the roots grown in loamy sand (LS) and the right column shows those grown in clay loam (CL).

### 4.4.2 Citrate phosphate mathematical model

In chapter 3 we developed a model describing citrate root exudation, P absorption, diffusion in soil and P reactions to the soil with enhanced desorption due to citrate. Here we apply the same model to a cylindrical pot of soil with a diameter 50 mm and 80 mm high containing growing roots. The 12 day RSAs, as extracted from the XCT scans, were used as the root surfaces in the model. The root surfaces associated with the RSAs from the XCT scans were activated along the depth in accordance to the individual plant growth rates. We first describe the citrate and phosphate governing equations, then describe the implementation of the growing RSA.

The soil domain is denoted $\Omega \subset \mathbb{R}^3$ (Figure 4.2). The whole root surface, as extracted from the 12 day XCT scan is denoted $\Gamma$ (Figure 4.2). The active absorbing surface at time $t$ is denoted, $\Gamma_r(t)$, while the portion of the root exuding citrate at time $t$ is denoted $\Gamma_{on}(t)$ (Figure 4.2). Notice $\Gamma_{on}(t)$ is contained within $\Gamma_r(t)$, which is itself contained within $\Gamma$ as a citrate exuding region of the root can also absorb phosphate and the root grows into the 12 day RSA as illustrated in Figure 4.2. The remainder of the boundary *i.e.* the inside of the pot and the non-functioning part of the root is denoted $\Gamma_e(t)$. Figure 4.2 shows a schematic of the domain and its boundaries. The soil is assumed to be homogenous with approximate volumetric water content $\phi_l$ [$m^3$ of soil solution $m^{-3}$ of domain] and volumetric soil solid volume fraction $\phi_s$ [$m^3$ of soil solid $m^{-3}$ of domain].

We assume P and citrate to exist either bound to soil surfaces or unbound in solution in soil. In particular, $P_l(t,\mathbf{x})$ [$\mu$mol $m^{-3}$ of soil solution] is the P concentration in solution, $C_l(t,\mathbf{x})$ [$\mu$mol $m^{-3}$ of soil solution] represents citrate concentration in solution, $P_s(t,\mathbf{x})$ [$\mu$mol $m^{-3}$ of soil solid] is the concentration of P bound to soil particles, and $C_s(t,\mathbf{x})$ [$\mu$mol $m^{-3}$ of soil solid] is the amount of citrate bound to soil particles.

P and citrate can adsorb to and desorb from soil surfaces and this is modelled using a reversible first order chemical reaction (Barber (1995)). The process of citrate-enhanced phosphate desorption is assumed to be dominated by ligand-exchange. That is, citrate competes with phosphate for binding spots on soil mineral surfaces, increasing the amount of available P (Oburger, Jones & Wenzel (2011)). This is modelled by adding a cross term to the P desorption-adsorption reaction (Equations (4.1-4.2)). Citrate is known to be consumed by microbes in the rhizosphere.

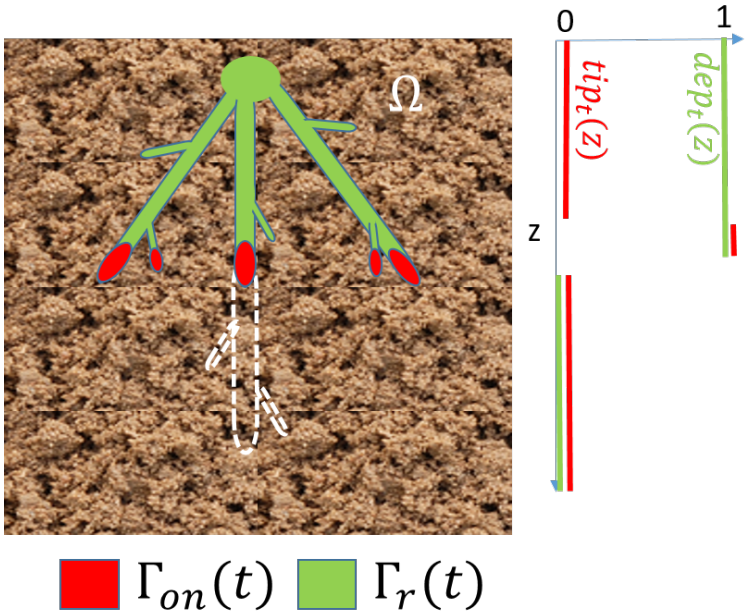


FIGURE 4.2: A schematic of the domain for simulations. The absorbing parts of the RSA, $\Gamma_r(t)$, and the exuding part, $\Gamma_{on}(t)$, are shown for a given time point within $\Omega$. As time progresses, the roots will grow in to the 12 day state, highlighted in the white-dashed lines. The indicator functions $dep_t(z)$, described by Equation (4.13), and $tip_t(z)$, described by Equation (4.14) are also plotted. These functions are used to activate the roots system at the appropriate times.

However, sorption of citrate to soil particles causes a significant reduction in biodegradation rate (up to 99%) (Van Hees et al. (2003)). Therefore, citrate in the model is allowed to biodegrade only in the soil solution. Hence, assuming conservation of mass and neglecting convective transport, the diffusion-sorption-reactions for P and citrate, the model can be written as (see also chapter 4)

$$\phi_l \frac{\partial P_l}{\partial t} = \nabla \cdot \phi_l D_P \nabla P_l - \phi_l \beta_1 P_l + \phi_s \beta_2 P_s + \phi_s \beta_3 C_s P_s, \quad \mathbf{x} \in \Omega \tag{4.1}$$

$$\phi_s \frac{\partial P_s}{\partial t} = \phi_l \beta_1 P_l - \phi_s \beta_2 P_s - \phi_s \beta_3 C_s P_s, \quad \mathbf{x} \in \Omega, \tag{4.2}$$

$$\phi_l \frac{\partial C_l}{\partial t} = \nabla \cdot \phi_l D_C \nabla C_l - \phi_l \lambda C_l - \phi_l \gamma_1 C_l + \phi_s \gamma_2 C_s, \quad \mathbf{x} \in \Omega, \tag{4.3}$$

$$\phi_s \frac{\partial C_s}{\partial t} = \phi_l \gamma_1 C_l - \phi_s \gamma_2 C_s, \quad \mathbf{x} \in \Omega \tag{4.4}$$

where $\beta_1$ [$s^{-1}$] is the rate at which P adsorbs to soil particles, $\beta_2$ [$s^{-1}$] is the rate at which P desorbs from soil particles, $\beta_3$ [$m^3$ of soil solid $s^{-1}$ $\mu mol^{-1}$] is the rate associated with ligand exchange between citrate and P on soil sorption sites, $\gamma_1$ [$s^{-1}$] is the rate at which citrate adsorbs to soil particles, $\gamma_2$ [$s^{-1}$] is the rate at which citrate desorbs from soil particles, $D_P$ [$m^2$ of soil

solution $s^{-1}$] is the diffusion rate of P in soil solution, $D_C$ [$m^2$ of soil solution $s^{-1}$] is the diffusion rate of citrate in soil solution (diffusion coefficients include geometric impedance) and $\lambda$ [$s^{-1}$] is the rate of citrate bio-degradation.

Boundary conditions are imposed on the root surface and the edge of the pot. In particular, the root is assumed to take up P using Michaelis–Menten kinetics (Barber (1995)) and exude citrate at a steady rate (Geelhoed et al. (1999), Zygalakis & Roose (2012)). More precisely, the citrate root boundary condition is

$$\phi_l D_C \nabla C_l \cdot \mathbf{n}_{on} = F_C, \quad \mathbf{x} \in \Gamma_{on}(t), \tag{4.5}$$

where $F_C$ [$\mu$mol $m^{-2}$ $s^{-1}$] is the root citrate exudation rate and $\mathbf{n}_{on}$ is the unit normal to the exuding part of the root. The P root boundary condition is

$$\phi_l D_P \nabla P_l \cdot \mathbf{n}_r = \frac{-F_P P_l}{K_P + P_l}, \quad \mathbf{x} \in \Gamma_r(t), \tag{4.6}$$

where $F_P$ [$\mu$mol $m^{-2}$ $s^{-1}$] is the maximum P uptake rate achieved by the root, $K_P$ [$\mu$mol $m^{-3}$] is the P concentration where the uptake rate is half of maximum possible and $\mathbf{n}_r$ is the unit normal to the active part of the root. Typical exudation rates of citrate for P-starved rape roots grown in nutrient solution at 27°C is $1.2 \times 10^{-5}$ $\mu$mol $s^{-1}$ $m^{-1}$ of root (Hoffland (1992)). These roots typically have a root radius of approximately $4 \times 10^{-4}$ m (Kjellström & Kirchmann (1994)), meaning an approximate citrate exudation rate per root surface area (assuming the root is a cylinder) of $F_C = 4.79 \times 10^{-3}$ $\mu$mol $m^{-2}$ $s^{-1}$. Typically $F_P = 3.26 \times 10^{-2}$ $\mu$mol $m^{-2}$ $s^{-1}$ and $K_P = 5.8 \times 10^3$ $\mu$mol $m^{-3}$ (Barber (1995)). On the pot boundary and non-active part of the root a no flux condition is imposed for both phosphate and citrate,

$$D_P \nabla P_l \cdot \mathbf{n}_e = 0, \quad \mathbf{x} \in \Gamma_e(t), \tag{4.7}$$

$$D_C \nabla C_l \cdot \mathbf{n}_e = 0, \quad \mathbf{x} \in \Gamma_e(t), \tag{4.8}$$

where $\mathbf{n}_e$ is the unit normal to the inactive part of the root and the edge of the pot. Initially, there is no citrate in the soil,

$$C_l(0,\mathbf{x}) = C_s(0,\mathbf{x}) = 0, \quad \mathbf{x} \in \Omega \tag{4.9}$$

Furthermore, there is a known initial concentration of total phosphate in the soil, $P_{tot}$ [$\mu$mol m$^{-3}$ of total soil] which exists in equilibrium between adsorbed and solution phosphate,

$$P_l(0,\mathbf{x}) = \frac{P_{tot}}{\phi_l(1+b_P)}, \quad \mathbf{x} \in \Omega, \tag{4.10}$$

$$P_s(0,\mathbf{x}) = \frac{\phi_l}{\phi_s} b_P P_l(0,\mathbf{x}), \quad \mathbf{x} \in \Omega, \tag{4.11}$$

where $b_P = \frac{\beta_1}{\beta_2}$ is the buffer power of phosphate in the soil. Two soil P conditions are used in the numerical experiments, high P low buffering (denoted High P) and low P high buffering (denoted Low P). All parameters used in the model are summarised in Table 4.2.

TABLE 4.2: Parameters used in the model

| Parameter | Description | Unit | Value |
|---|---|---|---|
| $\phi_l$ | m$^3$ of soil solution per m$^3$ of total soil | m$^3$ of soil solution m$^{-3}$ of total soil | 0.3 or 1 |
| $\phi_s$ | m$^3$ of solid soil per m$^3$ of total soil | m$^3$ of soil solid m$^{-3}$ of total soil | 0.6 or 0 |
| $b_P = \frac{\beta_1}{\beta_2}$ | Buffer power of P in soil | 1 | 39.6 High P, 1072 Low P |
| $b_C = \frac{\gamma_1}{\gamma_2}$ | Buffer power of citrate in soil (Oburger, Jones & Wenzel (2011)) | 1 | 4.78 |
| $\beta_1$ | P adsorption rate to solid soil | s$^{-1}$ | $7.899 \times 10^{-6}$ |
| $\beta_2$ | P desorption rate from solid soil | s$^{-1}$ | $2 \times 10^{-7}$ High P, $7.4 \times 10^{-9}$ Low P |
| $\beta_3$ | P enhanced desorption from soil solid due to adsorbed citrate | m$^3$ of soil solid s$^{-1}$ $\mu$mol$^{-1}$ | $3.4 \times 10^{-13}$ chapter 3 |
| $\gamma_1$ | Citrate adsorption rate to solid soil | s$^{-1}$ | $b_C \times \gamma_2$ |
| $\gamma_2$ | Citrate desorption rate to solid soil | s$^{-1}$ | $1.2 \times 10^{-2}$ |
| $\lambda$ | Rate of citrate biodegradation | s$^{-1}$ | $6.87 \times 10^{-5}$ |
| $D_{P/C}$ | Effective diffusion rate of P or citrate in soil | m$^5$ of soil solution m$^{-3}$ of total soil s$^{-1}$ | $7 \times 10^{-10}$ |
| $P_{tot}$ | Total amount of P | $\mu$mol m$^{-3}$ of total soil | $2.26 \times 10^4$ for High P 941.7 for low P |
| $F_C$ | Root citrate exudation rate | $\mu$mol m$^{-2}$ s$^{-1}$ | $4.789 \times 10^{-3}$ |
| $F_P$ | Maximum P uptake rate achieved by the root | $\mu$mol m$^{-2}$ s$^{-1}$ | $3.26 \times 10^{-2}$ |
| $K_P$ | The P concentration where the uptake rate is half $F_P$ | $\mu$mol m$^{-3}$ | $5.8 \times 10^3$ |

### 4.4.3 Root growth model

In the citrate phosphate model the root boundary is time dependent, therefore, a suitable model describing the evolution of the root absorbing surfaces, $\Gamma_r(t)$, and exuding surfaces, $\Gamma_{on}(t)$, in

time was required. Numerically, this was implemented by "activating the roots" in the RSA extracted from the 12 day scans using the growth rates calculated from the previous scans. More precisely, growth rates were calculated for each time point by finding the deepest root in each scan, subtracting the depth of the deepest root in the previous scan and dividing by the time difference. As a reference, wheat seminal root elongation rate is typically between 0.0926 and 0.277 μm $s^{-1}$ depending on soil compaction (Ruiz et al. (2017), Watt et al. (2003)). Citrate exudation is typically limited to the apical zone of the root (Hoffland et al. (1989)), this was implemented in the model by allowing only the portion of the root within 3 mm of the tip to exude. Mathematically, for each pot the following piecewise function is defined to implement the growing RSA,

$$G(t) = \begin{cases} g_0, & 0 \text{ day} \leq t \leq 2 \text{ day} \\ g_2, & 2 \text{ day} < t \leq 4 \text{ day} \\ g_4, & 4 \text{ day} < t \leq 6 \text{ day} \\ g_6, & 6 \text{ day} < t \leq 8 \text{ day} \\ g_8, & 8 \text{ day} < t \leq 12 \text{ day} \end{cases} \tag{4.12}$$

where $g_i$ [m $s^{-1}$]$\in \mathbb{R}_{\geq 0)}$, $i = 0,2,4,6,8$ are the growth rates as calculated from the XCT scans. A root depth indicator function is defined for each $t$,

$$dep_t(z) = \begin{cases} 1, & 0 \leq z \leq \int_0^t G(\tau)d\tau, \\ 0, & \text{else}, \end{cases} \tag{4.13}$$

where $z$ is the space variable representing the vertical direction. Similarly, a root tip indicator function is defined

$$tip_t(z) = \begin{cases} 1, & \int_0^t G(\tau) - 0.003d\tau \leq z \leq \int_0^t G(\tau)d\tau, \\ 0, & \text{else}, \end{cases} \tag{4.14}$$

to determine the location of the exuding section of the root. The growing root and root tip are then defined as $\Gamma_r(t) = \{(x,y,z) \in \Gamma \text{ such that } dep_t(z) = 1\}$ and $\Gamma_{on}(t) = \{(x,y,z) \in \Gamma \text{ such that } tip_t(z) = 1\}$. A schematic of the relationship between $dep_t(z)$ and $\Gamma_r(t)$; and $tip_z(t)$ and $\Gamma_{on}$ can be seen in Figure 4.2. For the purposes of numerical simulations, $tip_t(z)$ and $dep_t(z)$ are smoothed.

## 4.5 Numerical Experiments

In order to assess the impact of RSA on citrate enhanced phosphate uptake, the model is solved on each of the RSAs with and without citrate exudation. Two P soil conditions are simulated: High P, representative of a UK arable field with $P_{tot} = 2.26 \times 10^4$ μmol m$^{-3}$ (corresponding to 24 kg per hectare (DEFRA soil nutrient balances UK provisional)) with P adsorption rate $\beta_1 = 7.899 \times 10^{-6}$ s$^{-1}$ and desorption rate $\beta_2 = 1.993 \times 10^{-7}$ s$^{-1}$ equating to a buffer power of 40 (Barber (1995)). Low P, representative of a poor P soil with $P_{tot}$=941.7 μmol m$^{-3}$ (corresponding to 1 kg per hectare (DEFRA soil nutrient balances UK provisional)) with P adsorption rate $\beta_1 = 7.899 \times 10^{-6}$ s$^{-1}$ and desorption rate $\beta_2 = 7.3684 \times 10^{-9}$ s$^{-1}$ equating to a buffer power of 1072 (Barber (1995)).

To determine which morphological root system measures were important for increased P uptake from citrate exudation, percentage increase due to citrate was compared to root surface area, number of exuding tips, average inter tip distance, solidity (defined as the ratio of root volume to RSA convex hull volume), and total number of exuding tips. Some of these measurements require an image analysis protocol that will be described in the following section. Additionally, using the densest RSA geometry, the model was solved with an increasing range of citrate exudation rates in the High P soil, and P influx is plotted to investigate the gain in P absorption for higher citrate exudations.

A finite element method was used to solve the image-based models using Comsol Multiphysics 5.3. Typically, the meshes had approximately $1.5 \times 10^6$ volume elements and $2.4 \times 10^5$ surface elements. Lagrange polynomials of order two were used to approximate the solution in each element. Backwards differentiation formulas between orders 1 were 5 were used in the time discretization. To reduce memory requirements a segregated approach was taken. As citrate dynamics are independent of P, at each time step $C_l$ and $C_s$ were solved for first and then $P_l$ and $P_s$. Any non-linarites were linearized using one Newton-Raphson iteration. All resulting systems of linear equations were solved using the MUMPS algorithm. Numerical solutions were saved every 3 hours of solution time.

The Pearson Correlation Coefficient (PCC) was used to measure linear correlation between P uptake and root measures (such as number of exuding tips or root surface area etc) over all time

points and RSAs. For example, if $P_l^i$ is the solution to Equations (4.1-4.11) solved on the i$^{\text{th}}$ RSA with citrate exudation and let $S_i(t)$ be the root surface area at time $t$ of the $i^{\text{th}}$ RSA. The total root uptake rate for the $i^{\text{th}}$ RSA at time $t$ is then the active root integrated flux of P:

$$F_i(t) = \int_{\Gamma_r(t)} \phi_l D_P \nabla P_l^i(t) \cdot \mathbf{n}_r d\Gamma_r(t). \tag{4.15}$$

The PCC of P uptake rates, $F_i(t)$, with root surface area over all 11 RSAs and saved model times, $T = \{k \times 3 \text{ hours, for } k = 1,2,\ldots,96\}$, is calculated as

$$\rho(F_i(t), S_i(t)) = \frac{\sum_{\substack{i\in 1,\ldots,11 \\ t\in T}} F_i(t)\cdot S_i(t) - n\bar{F}\bar{S}}{(\sum_{\substack{i\in 1,\ldots,11 \\ t\in T}} (F_i(t)^2 - n\bar{F}^2))^{\frac{1}{2}} (\sum_{\substack{i\in 1,\ldots,11 \\ t\in T}} (S_i(t)^2 - n\bar{S}^2))^{\frac{1}{2}}}, \tag{4.16}$$

where $n = 11$ reps $\times 96$ time points and bar denotes average over all RSAs and model times.

The term "citrate enhanced uptake" is used to describe both percentage additional root P flux due to citrate at a given time point, and percentage additional P absorbed by the roots.

### 4.5.1 Image Analysis

#### Average inter-tip distance

An image analysis protocol to calculate number of exuding tips and average inter-tip distance was developed to compare with increased P absorption. The 12-day segmented RSA was skeletonized using BoneJ (Doube et al. (2010)). The slice in the skeletonized stack representing the deepest root at the given time point was selected using the growth rates as described by Equation (4.12). The number of connected components on this slice determined the number of exuding tips at the given time . The mean coordinate of each component was calculated, and the average distance between these means was used to determine average inter tip distance at a given time point. This approach means the measurements are in line with the model RSA as opposed

**Solidity**

Solidity of an RSA is defined as the ratio of the root volume and RSA convex hull volume (Zurek et al. (2015)). Solidity was hypothesised to positively correlate with citrate enhanced uptake, as root systems with high solidity would be contained in a small region of soil and hence collectively create regions of high citrate concentration. Solidity was calculated using the convex hull function in Scipy (Jones et al. (2001)) for the 12 day RSAs.

## 4.6 Results

### 4.6.1 Root growth rates

Figure 4.3 shows the growth rates for each of the replicates as calculated from the time-resolved XCT data. Each root system has grown past the area of segmentation by day 8.

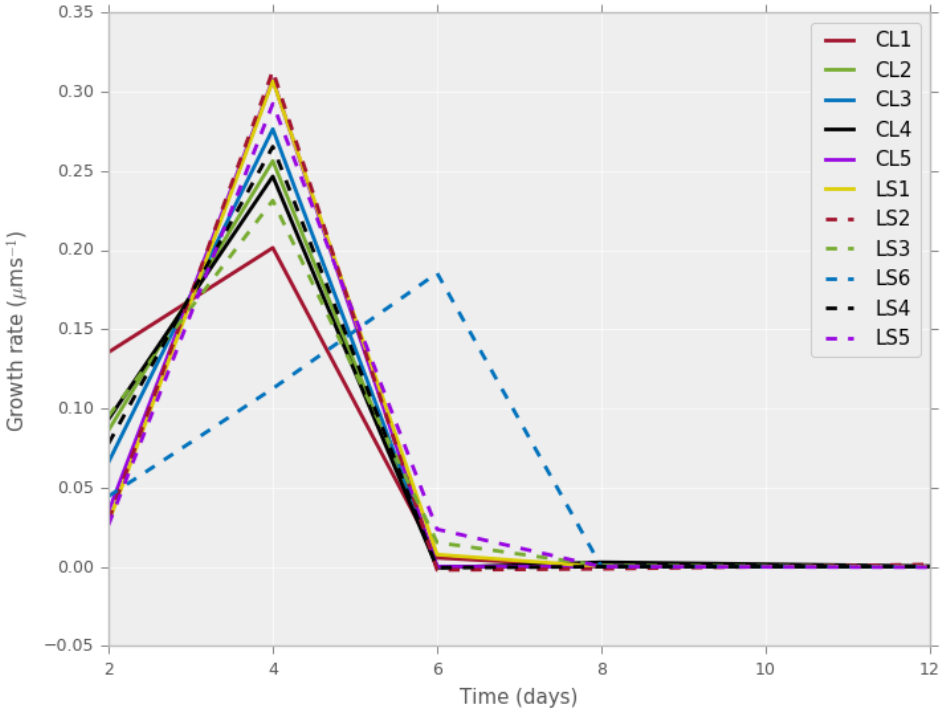


FIGURE 4.3: Growth rates of each RSA and time point. Growth rates are calculated by finding the deepest root in each scan, subtracting the deepest root in the previous scan and dividing by the time difference.

### 4.6.2 Numerical Experiments

First, P uptake rates in the exuding and non-exuding case in the High P soil are compared; citrate enhanced uptake rate is compared with root measures in the Low P soil; citrate concentrations are displayed on planes within the soil; cumulative citrate enhanced uptake is compared amongst the RSAs and compared with total number of root tips and solidity; finally the evolution of citrate enhanced uptake is examined for increasing exudation rates.

Figure 4.4 shows a comparison of P uptake rate in time for the exuding and non-exuding model roots for each of the root systems in the High P case. Increased root surface area strongly correlates with P absorption rate (Figure 4.4), with a PCC of 0.955 over all RSAs and times in High P conditions.

Although P uptake rate still strongly correlates with root surface area in Low P conditions (PCC of 0.9583 over all RSAs and times) citrates contribution to P uptake rate is more noticeable. Figure 4.5 shows a comparison of percentage increased uptake between the two soil conditions for three RSAs. In the High P scenario, the difference in total absorbed P between the exuding and non-exuding case never exceeded 0.2% across the 11 RSAs (such variations are within the numerical error of the method). Figure 4.4 shows there is little difference between the exuding (line) and non-exuding (stars) case. In contrast, results suggest that there can be $> 5\%$ increase in uptake for early time points and RSAs in the Low P conditions. There is a large variation in percentage increase due to citrate across the RSAs as well as the growth states in the Low P case, Figure 4.5 and 4.6. For example, in Figure 4.6 citrate enhanced uptake reaches a maximum of 10% in CL3 while LS1, CL1 and LS3 never achieve more than 5%. Furthermore, citrate enhanced uptake has two local maxima in LS5, CL5 and LS6 while the others have only one local maxima. This all suggests RSA is an important factor in P gains due to citrate exudation.

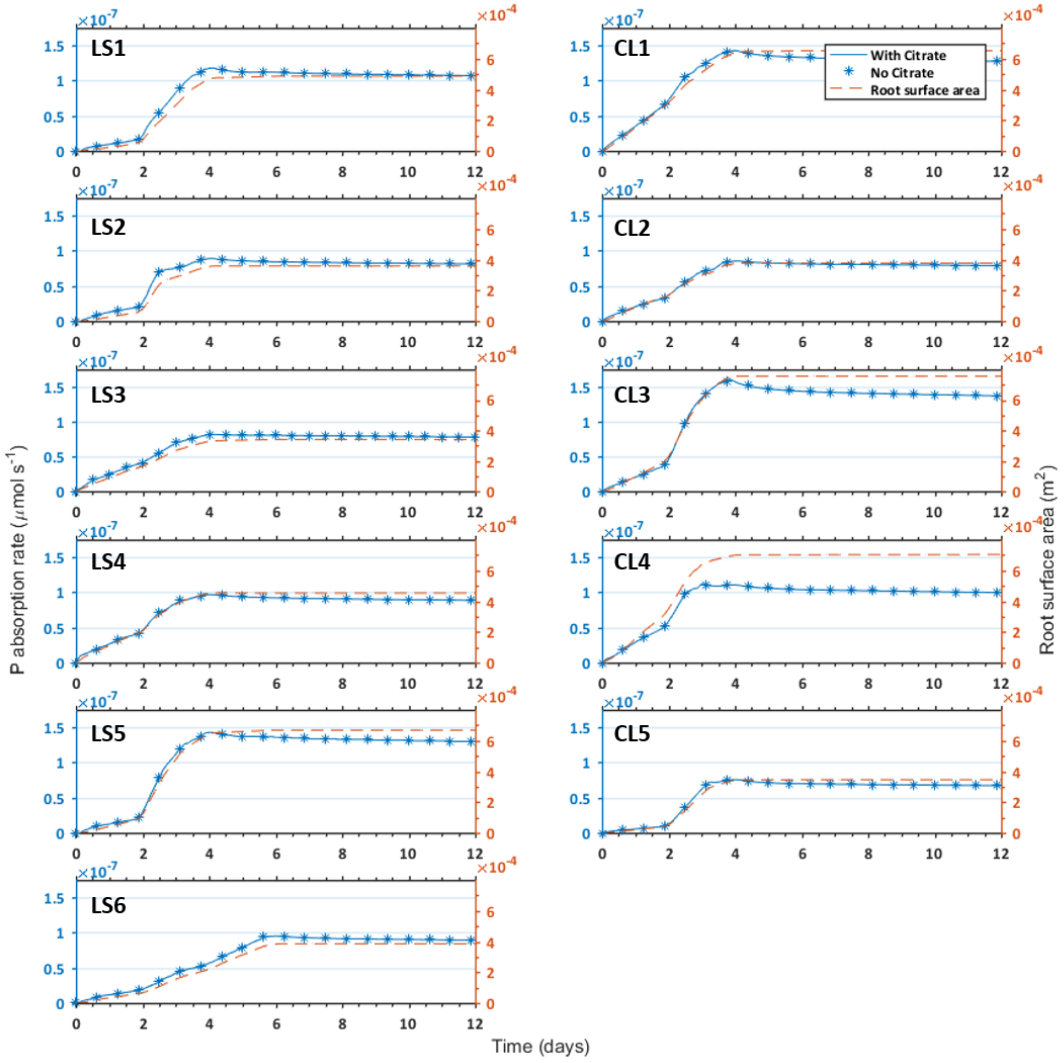


FIGURE 4.4: Effect of citrate exudation on P absorption rates in High P soil. P absorption rates of the root system architecture throughout the 12 day simulation period in the exudation (blue line) and no exudation (blue stars) cases. Root surface area throughout the simulation is also plotted in orange dashed lines. The left and right columns show plants grown in the loamy sand and clay loam respectively.

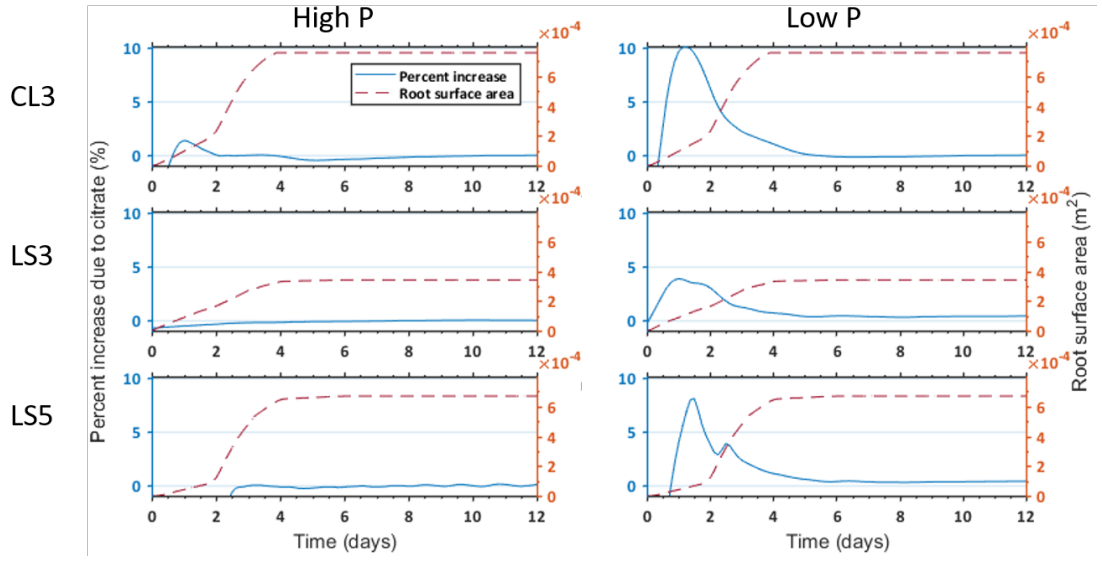


FIGURE 4.5: Comparison of citrate enhanced uptake in the High P (left column) and Low P high buffering soil (right column) conditions. Percentage increase of P absorption rate due to citrate exudation is shown in the blue line for the CL3, LS3 and LS5 treatments. Root surface area is also plotted in orange dashed lines.

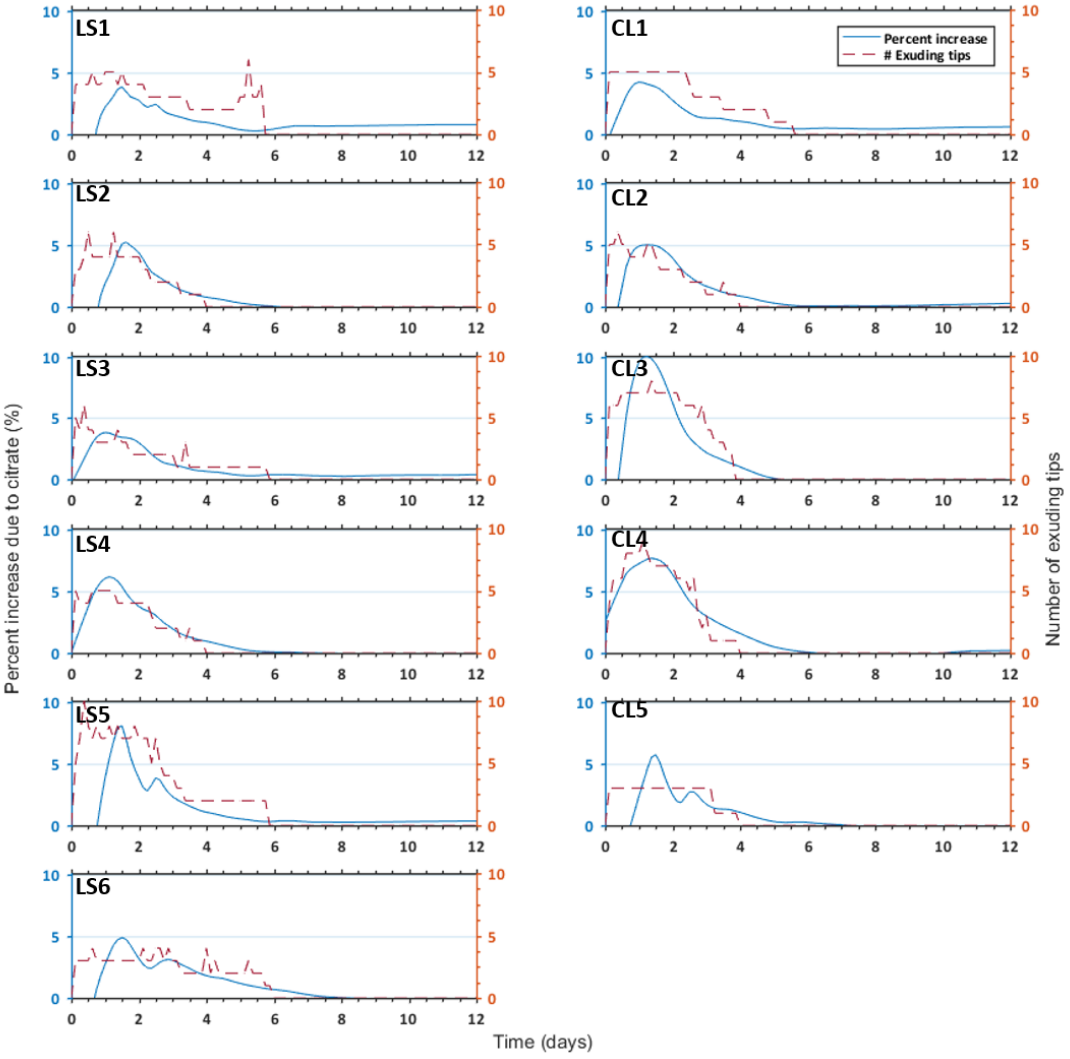


FIGURE 4.6: Benefit of citrate exudation on P absorption in Low P soil with number of exuding root tips. Percentage increase of P absorption rate due to citrate exudation is shown in the blue line. Number of exuding tips throughout the simulation is also plotted in orange dashed lines. The left and right columns show plants grown in the loamy sand and clay loam respectively.

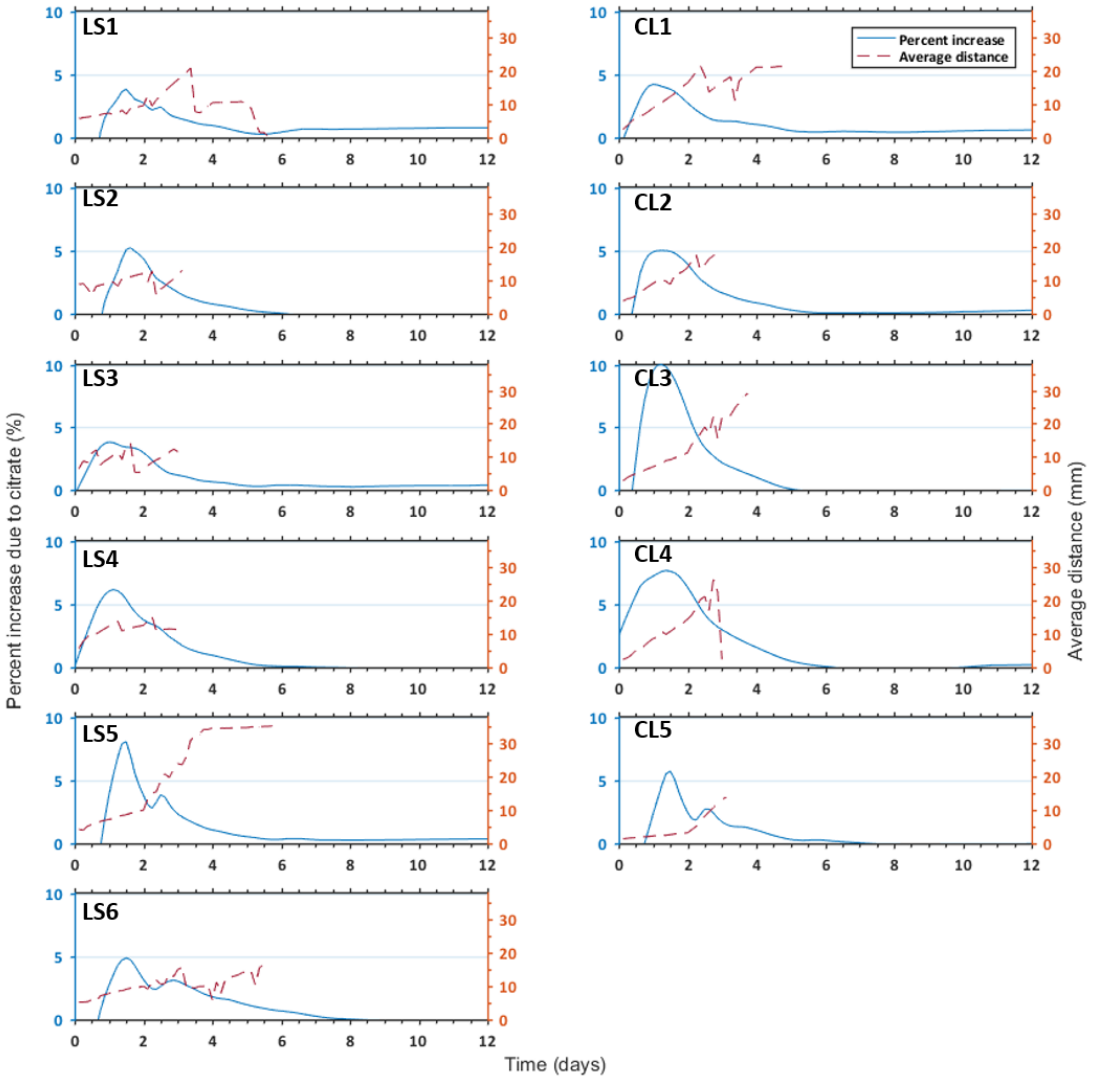


FIGURE 4.7: Benefit of citrate exudation on P absorption in Low P soil with average inter-tip distance. Percentage increase of P absorption rate due to citrate exudation is shown in the blue line. Average inter-tip distance throughout the simulation is also plotted in orange dashed lines. The left and right columns show plants grown in the loamy sand and clay loam respectively.

Root surface area does not explain citrate enhanced uptake, the correlation between citrate enhanced P-uptake rates and root surface area had a PCC of $-0.07$ (Figure 4.5). Number of exuding root tips (Figure 4.6) and average inter tip distance (Figure 4.7) were plotted with percentage increase in P uptake rate due to citrate to see if they can explain the variation amongst RSAs. Number of exuding tips had a PCC of 0.39 with percentage increase in P uptake rate due to citrate, while average inter tip distance had a PCC of 0.09. The PCC does not capture the

relationship between citrate enhanced uptake and average inter tip distance. A period of high citrate enhanced uptake is often preceded by low average inter tip distance (Figure 4.7). This can be explained by a positive interference of citrate concentrations when root tips are in close proximity. Figure 4.8 shows the concentration of citrate in solution on 2D planes located at the depth of the roots at 12, 24 and 48 hours after germination for the CL4 RSA. The state of the root system at the given times is also displayed. At 12 hours, Figure 4.8a, the root tips are in close proximity, between them there is a region of high citrate concentration (greater than 6 $\mu$mol $l^{-1}$ of soil solution). The plant benefit of the solubilised P in this region is not seen until later (Figure 4.7 CL4 plot at 1.5 days) as the movement of P in the soil is slow. At 24 hours, Figure 4.8b, the root tips have grown farther apart and less positive interference can be seen. By 48 hours, Figure 4.8c, only regions of soil immediately adjacent to the root have high citrate concentrations, explaining the reduced citrate enhanced uptake after 2 days, seen in Figure 4.7 CL4 plot.

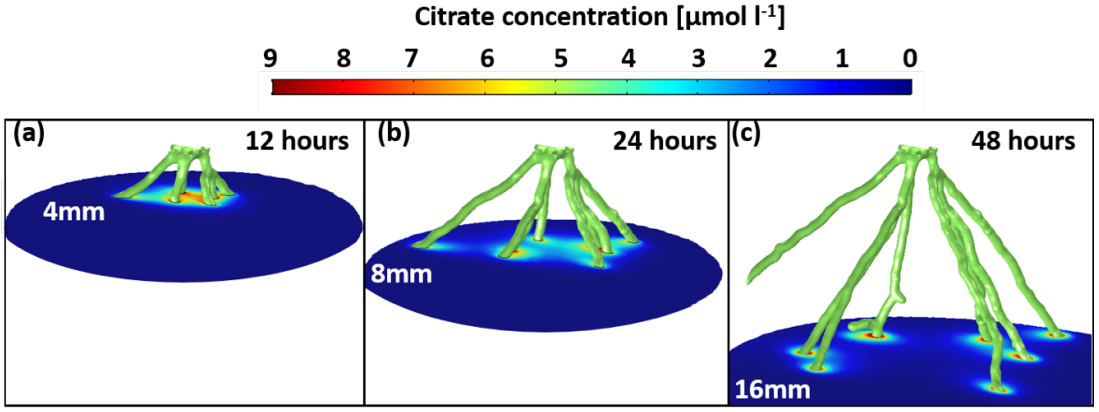


FIGURE 4.8: Citrate concentrations on 2D planes for the CL4 root system. Citrate solution concentration at **a)** 12 hours shown on the $x-y$ plane at 4 mm depth, **b)** 24 hours shown on the $x-y$ plane at 8 mm depth, and **c)** 48 hours shown on the $x-y$ plane at 16 mm depth. The depths of planes were chosen to be the location of the root tips at the given time.

Cumulative additional P absorbed due to citrate (normalised by citrate exudation) for each of the root system architectures in the Low P soil is plotted in Figure 4.9. A wide variation amongst the RSA can be observed, which is attributed to the variations in RSA morphology. Furthermore,

plants maintain high additional P absorbed per citrate exuded from 2 days through to 6 days, similarly low values are maintained in time, Figure 4.9.

To determine if analysis of the whole root system could predict citrate enhanced uptake, two measurements of the 12 day root systems were plotted against percentage additional P absorbed by plants cumulatively due to citrate after 8 days in the Low P conditions; namely solidity, Figure 4.10a, and number of root tips at 12 days, Figure 4.10b. Additional P absorbed by plants cumulatively due to citrate had a PCC with solidity of $-0.5$ (Figure 4.10a). Number of root tips at 12 days, however, had a PCC with additional P absorbed by plants cumulatively due to citrate of 0.84, Figure 4.10b.

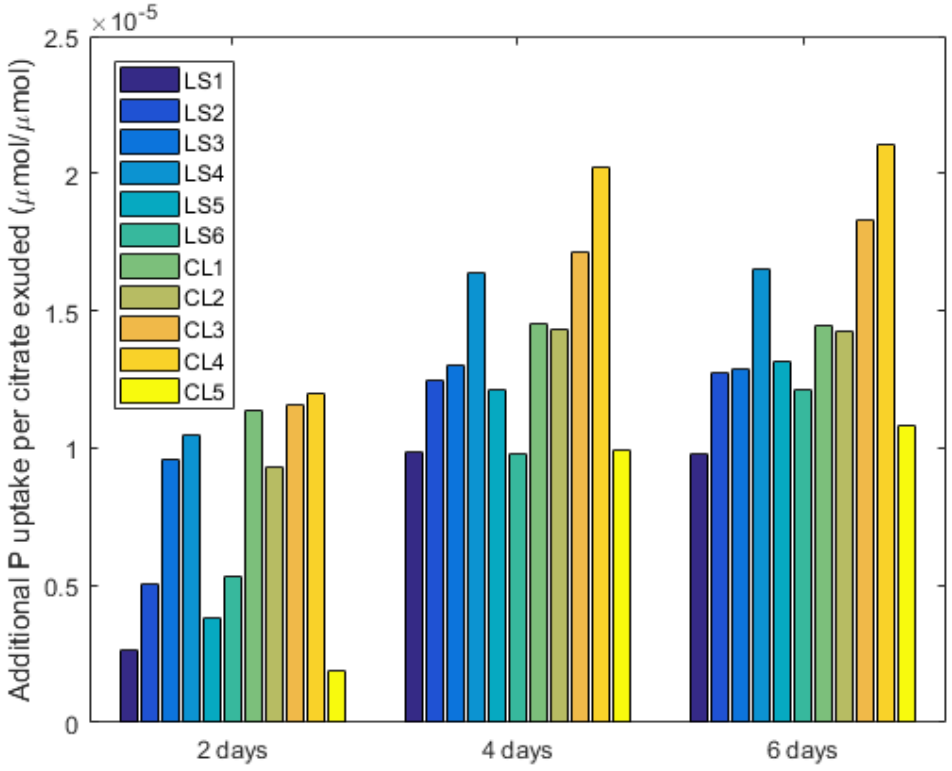


FIGURE 4.9: Cumulative additional P absorbed by plants due to citrate at 2, 4 and 6 days in the Low P soil normalised by cumulative citrate exudation at the given times.

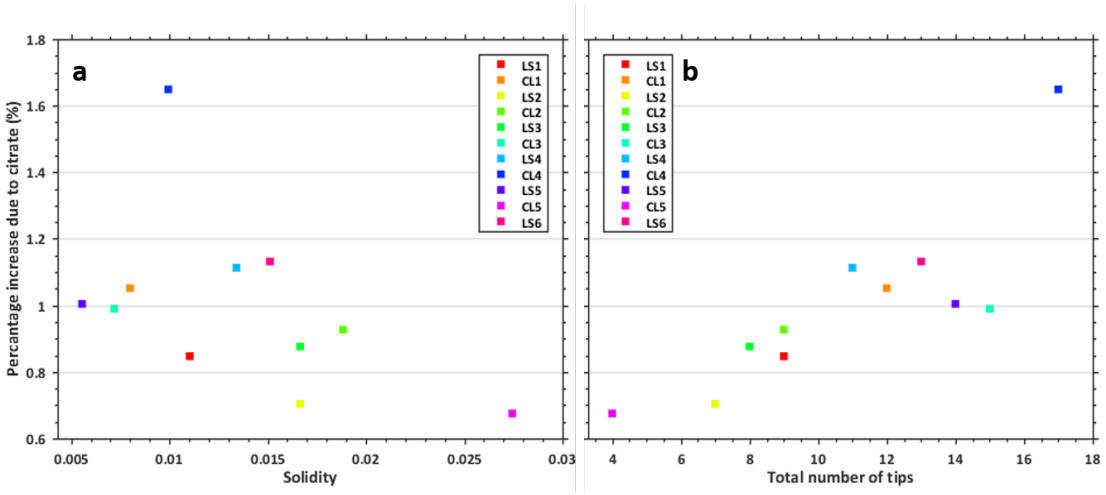


FIGURE 4.10: The effect of solidity and total number of tips on citrated enhanced uptake. Percentage additional P absorbed by plants cumulatively due to citrate after 8 days in the Low P soil against **a)** solidity of the root system (solidity is defined as the total volume of the roots over the volume of the convex hull of the RSA) and **b)** total number of root tips.

In the no citrate exudation case seen in Figure 4.4, initially, the plant rapidly grows into the soil increasing the P absorption rate. Once the RSA stops growing P supplies in the soil are used up with no means for replenishment except for diffusion from regions of higher P concentration, hence P absorption rate slowly decreases. In the cases with higher citrate exudation there is a contrasting evolution of P uptake rates, Figure 4.11. P uptake increases to a distinct maximal value then as root growth slows, P uptake rapidly decreases due to reduced citrate exudation and citrate biodegradation. In the highest citrate exudation case (yellow line, Figure 4.11) the root system has absorbed enough citrate during the initial growth period that the uptake rate drops below the no citrate exudation case at 150 hours due to low P supplies in the soil. As citrate exudation rate increases from 0 to 21.2 $\mu$mol m$^{-2}$ s$^{-1}$ the PCC of P uptake rate with root surface area decreases from 0.98 to $-0.15$ while the PCC of P uptake rate with citrate exudation rate increases from $-0.1$ to 0.44; exudation rather than root growth becomes the dominant mechanism for P uptake.

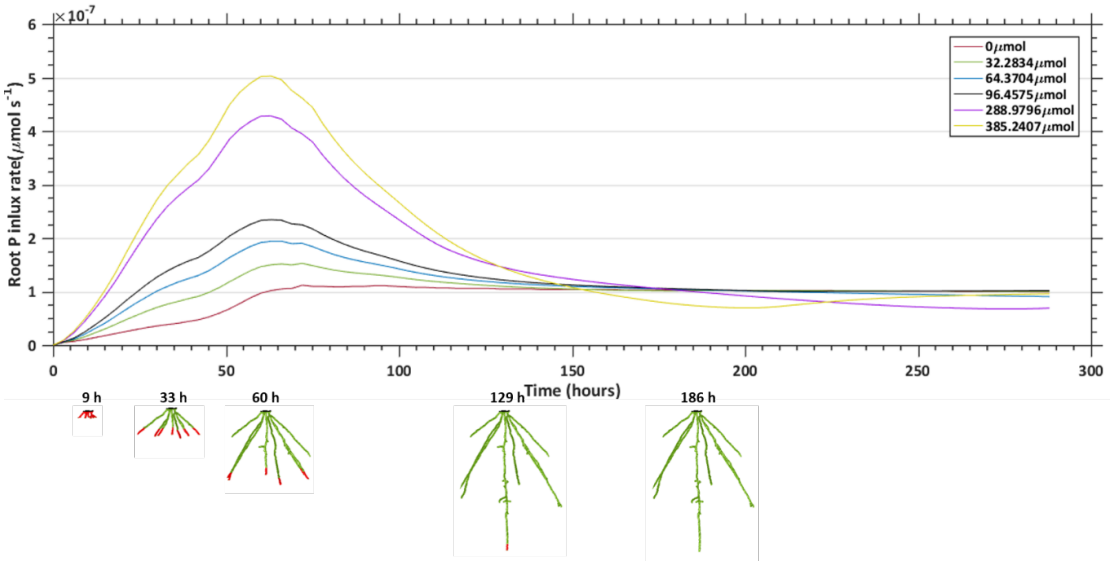


FIGURE 4.11: Effect of increased citrate exudation on root P influx rate. Exudation rates are increased from 0 to 21.2 µmol $m^{-2}$ $s^{-1}$ and the P influx rates are plotted in time for the CL4 RSA with High P soil conditions. Plots are labelled by the total amount of citrate exuded by the RSA over the simulation period. A selection of RSA states throughout the simulation are shown along the bottom. Red parts of the roots are exuding citrate ($\Gamma_{on}(t)$) and green and red parts of the root are absorbing P ($\Gamma_r(t)$).

## 4.7 Discussion

### The role of root system architecture on citrate enhanced uptake

Although extensive research has been carried out on the role of citrate in phosphate solubilisation and uptake, little research has been focused directly on the role of RSA. In the current study, time resolved XCT-extracted RSA were used as the geometries for image-based models, in which roots grew, exuded citrate from their tips and absorbed phosphate. The model simulated scenarios with and without citrate exudation to determine the benefit of P uptake from exuding citrate in different soil P conditions. Our approach allowed us to carefully control for citrate exudation which is otherwise hard to achieve in experimental designs. Even with the control that we had in our simulations, our results demonstrated that there were still large variations in the amount of extra P that plants absorb due to citrate exudation amongst the 11 RSAs. When citrate enhanced uptake was normalised by citrate exudation, the largest gain in P due to citrate

was almost 1.5 times the smallest (Figure 4.9); suggesting that RSA plays a key role in the phosphate benefit from citrate exudation.

Morphological measurements of the root system were used to determine if a plant's citrate enhanced uptake can be estimated by solely measuring its RSA, elevating some of the need for time consuming mathematical modelling. While root surface area correlated well with absolute root P uptake (Figure 4.4), it correlated poorly with citrate enhanced uptake (Figure 4.5). The number of exuding tips was a good indicator for citrate enhanced uptake (Figure 4.6). As a rule of thumb for the Low P conditions, one extra exuding root tip increases P uptake rate by one percent (Figure 4.6). The relationship with average inter-tip distance was more subtle. Periods of low average inter-tip distance were followed by high citrate enhanced uptake (Figure 4.7). Root tips in close proximity to each other can cumulatively create regions of high citrate concentrations which can explain this increased citrate enhanced uptake, Figure 4.8. This effect is noticeable in early root system development, where primary roots are inherently close together due to a single origination point. This proximity provides a boost of P uptake due to citrate exudation at approximately one and a half days after germination (Figure 4.7). This feature of citrate exudation may be important as P nutrition at the very early stages of development is critical for crop yield (Grant et al. (2001), Nadeem et al. (2011)). Furthermore, citrate exudation may justify the reduced P uptake efficiency (in terms of RSA carbon cost) of densely packed roots (Fletcher, Keyes, Daly, Van Veelen & Roose (2019)).

A more holistic measurement of the root system is solidity, which was hypothesised to correlate positively with citrate enhanced uptake. Instead, we found solidity negatively correlated with citrate enhanced uptake (Figure 4.10a), while total number of root tips correlated positively with citrate enhanced uptake (Figure 4.10b). A possible explanation is that a roots system with many root tips have many lateral roots which grow horizontally, increasing the convex hull volume of the root system and thus lowering solidity.

**The role of soil buffering and P content on citrate enhanced uptake**

With High P soil conditions (similar to British agricultural soil, 24 kg $ha^{-1}$ of P in the soil) little benefit could be observed from citrate exudation ($< 0.1\%$ extra P absorbed over the 12 day simulation, this is within the numerical error of the method). However, in the Low P soil (1 kg $ha^{-1}$) a more noticeable effect of citrate was observed (Figure 4.5), which is consistent with

previous research stating that citrate solubilises strongly sorbed phosphates and is effective in low P conditions (Oburger, Jones & Wenzel (2011), Ryan et al. (2014)).

**Comparison to experimental results**

The experimental analogue of this modelling study would measure plant P mass in both a high-exuding mutant and low-exuding mutant (similar to Güsewell & Schroth (2017) or Ryan et al. (2014)). It would be difficult to detect P gains due to citrate in the experimental setup as even slight variations in root surface area would overwhelm the P gains from citrate, making it difficult to separate and quantify morphological (RSA) and physiological (organic acid exudation) phosphate gains experimentally. For example, although Ryan et al. (2014) found citrate exudation could not explain increased biomass between high exuding and low exuding near-isogenic wheat lines, this may have been due to their experimental design. The normalisation of the results presented in the work of Ryan et al. (2014) did not take into account variations in RSA, thus, any gains due to citrate exudation would not be detected due to variations in root surface areas.

Experimental literature suggests that organic acid concentrations greater than 1 mM in the soil solution are required to solubilise significant amounts of P (Gerke, Beißner & Römer (2000), Jones & Darrah (1994), Khademi et al. (2010), Mench & Martin (1991)). Typically, concentrations of organic acids in soil are between 1 μM and 50 μM (Khademi et al. (2010)). Across all the simulations and time points, the citrate concentrations in soil solution never exceeded 48 μM. Although citrate concentrations did not reach the experimentally-required concentration to significantly solubilise P, increased uptake in the Low P conditions was observed in the simulations (Figure 4.5). Three possible reasons are proposed to explain this discrepancy. Firstly, singular time point bulk scale solubilisation experiments, such as those cited above, may not be able to simultaneously capture diffusion, uptake, adsorption, and desorption, which occur at different timescales. Using a similar non-dimensionalisation to Zygalakis & Roose (2012) (non-dimensionalise P concentration with $K$, and citrate concentration with the maximum achieved in the simulations) we find that adsorption happens at rates on the order of $10^1$, desorption at $10^{-3}$, citrate enhanced desorption $10^{-1}$ and diffusion $10^0$ when we are in regions of high citrate concentrations . Secondly, bulk scale measurements (even when analysing rhizosphere soil) do not

measure local pore scale concentrations. It is likely there are local regions of higher concentrations near the root surface despite bulk scale measurements being low (Jones (1998), Khademi et al. (2010)). Finally, differences in soil labile P between the exudation and no-exudation cases are small. There was at most a 0.25% difference when average P concentration in soil solution over the whole domain is compared between the no exudation and exudation cases in the Low P soil. Such a small difference in bulk solubilized P would be difficult to detect experimentally. We conclude lack of bulk scale measured P solubilisation does not imply lack of citrate enhanced uptake.

**Comparison to other root-system modelling approaches**

The model presented and aims of this chapter are comparable to the work of Schnepf et al. (2012), as such it is worth discussing the similarities and differences. The modelling approach of Schnepf et al. (2012) used a local 1D-cylindrical-diffusion model of competitive adsorption between phosphate and citrate for a single root in order to calculate root volumetric fluxes of phosphate and citrate in a global finite difference model. Within the domain of a global finite difference model, a root growth model is solved (Leitner et al. (2010*b*)). This is used to determine the surface area of roots in each discretised volume. For each time step and each discretised volume, the local uptake model, based on local root surface area at that time point, is solved to determine root exudation and uptake to be applied as a volume flux in the global model. Although the aims of the model of Schnepf et al. (2012) are similar to this work, the modelling approach is fundamentally different. Mathematically, our model explicitly considers the roots as surfaces within soil, while Schnepf et al. (2012) considers them as parameters such as root-surface-area density. The approach of Schnepf et al. (2012) has an advantage over the current approach in terms of computational complexity. When using our approach, if the root system became larger and more detailed, the number of elements in the mesh would increase to capture the root surface complexity and computation time would scale at least linearly with the the number of elements (Farmaga et al. (n.d.)). While in Schnepf et al. (2012) the same grid could be used for arbitrary RSAs. This advantage may come at the expense of accuracy. Average root length measurements do not capture the geometry within each discretized volume —- each root can access all the P within its discretized volume in the approach of (Schnepf et al. (2012)). This error may be larger for slow moving nutrients like P.

Mechanistically, there are key differences between the two models. Schnepf et al. (2012) uses the kinetic competitive Langmuir reaction equations to model competitive adsorption between citrate and phosphate, while our model uses a cross exchange. However, Schnepf et al. (2012) assume the reactions between adsorbed and solution species happen instantly, thus adsorbed phosphate and citrate can be approximated by their solution concentrations, while in our model these are maintained as time-dynamic reactions. Furthermore, Schnepf et al. (2012) use a model of a growing root system in a small thin rhizotron, which are not necessarily representative of roots and growth conditions, in particular, roots are forced closer together. The scientific contrasts in Schnepf et al. (2012) are varying root exudation zones, as opposed to varying RSA as in the current work. Schnepf et al. (2012) conclude that citrate enhanced P uptake is dependent on the age distribution of the root system and cumulative P influx is 11% higher for RSAs exuding citrate from their tips. Indeed, as the root systems in the current chapter age, citrate enhanced uptake decreases, corroborating the result of Schnepf et al. (2012), although care needs to be taken when comparing the results.

It is difficult to compare the results in the current work to the work of Schnepf et al. (2012) due to the lack of comparisons between the modelling methods. The comparisons between the modelling differences need to be addressed before the differences in physical mechanisms can be discussed. We propose that both numerical schemes are used to solve the same governing equations on the same RSAs to determine differences and similarities in the output of the approaches. This will not only be useful for comparing the results of the current work and Schnepf et al. (2012) but also literature that has similar contrasting modelling approaches (Daly et al. (2018), Landl et al. (2019)).

**Auxiliary factors influencing citrate enhanced uptake**

Rates of plant organic anion exudation is thought to be controlled by a number of properties including soil nutrient status and the plant diurnal rhythm (Shane & Lambers (2005), Dessureault-Rompré et al. (2007)). In the model a constant rate of citrate exudation was used, parameterised by a hydroponic experiment over 30 minutes (Hoffland (1992)). This is a common assumption made in models of citrate exudation (Gerke, Beißner & Römer (2000), Schnepf et al. (2012), Zygalakis & Roose (2012), De Parseval et al. (2017)). Even when models considered the effect of a diurnal rhythm on deoxymugineic acid (DMA) enhanced zinc uptake with roots distributed

0.9 mm apart (Ptashnyk et al. (2011)), DMA exudation had little effect on enhanced zinc uptake provided the total quantity exuded on DMA was the same. As such, the temporal variability of citrate exudation was not included in the model. However, we note that other factors may be important when considering a growing root system. For example, if the exudation rates were reduced during periods of low inter-tip distance, the peaks in citrate enhanced uptake would be less pronounced. Currently there is not enough experimental data on the temporal variations of exudation to include an accurate time-dependent exudation function in the model without introducing further approximations. Including such a function would detract from the aim of this study by introducing uncertainty to whether the findings were a result of RSA or the chosen diurnal rhythm. Future studies could consider the impacts of time varying root exudation rates and decouple these dynamics from the aforementioned factors.

Fine lateral roots were not included in the model geometry as they were not detected in the XCT scans. This was due to the trade-off between field-of-view and resolution when using XCT; to capture the full RSA using XCT, the resulting voxel size was not sufficient to resolve the finer lateral roots. The omission of fine lateral roots will potentially affect P and citrate enhanced uptake. However, we believe the qualitative findings regarding the role of root-system architecture in citrate enhanced uptake will persist with the inclusion of fine lateral roots. The inclusion of fine lateral roots will likely amplify citrate enhanced uptake due to the increased number of exuding tips in close proximity.

Additionally, it was assumed the full root surface area absorbed P independent of age, this is a common approximation for modelling. However, effects of root age on P uptake rates are minimal within 28 days after germination (Jungk & Barber (1975)). As the simulation time is over 12 days we assume this to have minor influences on the results. The current modelling approach is not suitable for including more detailed or larger RSA due to computational limitations. The largest simulation required up to 250GB of memory and 8 days of computation time, including fine lateral roots would increase both these to impractical levels. The modelling approach of Schnepf et al. (2012) would be more suitable for larger RSA after comparison with the current approach for smaller RSA.

The 12 day old plants used in this study still rely on P from their seed supply. However, plants older than 5 days absorb P from the soils (Nadeem et al. (2011)). Early P nutrition is known to

be important for yields (Grant et al. (2001)), hence, the extra P acquired by the young plants due to citrate exudation during the 12 day simulation is agriculturally significant.

**Conclusions**

Measurements of the functionality of root traits could be important for plant breeders to develop crops that can perform well under sub-optimal conditions. However, measuring root functionality experimentally can prove difficult. Our approach allowed careful control of citrate exudation in order to assess the impact of RSA on citrate enhanced uptake. Our study found that root structure plays an important role in P uptake gains from citrate exudation. The number of exuding tips correlated with citrate enhanced uptake and periods where root tips were in close proximity were followed by periods of increased citrate enhanced uptake. Inductively, cluster-like roots would benefit greatly from citrate exudation. We found that lack of bulk-scale measured P solubilisation by citrate does not imply lack of citrate enhanced P uptake. This is an important consideration for future experimental design.

## 4.8 Acknowledgments

D.M.M.F. and C.P. are funded by ERC Consolidator grant 646809 (Data Intensive Modelling of the Rhizosphere Processes). S.R. and T.R are funded by BBSRC SARISA BB/L025620/1, BBSRC SARIC BB/P004180/1 and NERC NE/L00237/1, T.R. is also funded by EPSRC EP/M020355/1.

We would like to thank Dr. Chris Topp (Danforth Center,USA) for discussions on plant phenotyping and function which contributed to this chapter.

# Chapter 5

# Conclusions and Further Work

This project aimed to quantify the changes in P uptake associated with root plasticity and organic acid exudation using experimentally calibrated mathematical models. We proposed two novel approaches for parameterising image-based models that described plant P uptake. Chapter 2 used elemental mapping and XCT to determine the P uptake benefit associated with a root system responding plastically to the presence of a fertiliser pellet. Chapter 3 used a combination of mathematical modelling and microdialysis probe experiments to determine the rate at which citrate solubilised soil sorbed P. Chapter 4 extended the model in chapter 3 to image-based root architectures. This model was used to examine the impact of root system architecture on citrate-enhanced P uptake. Before summarising the conclusions of the thesis, we remind the reader of the research questions arising from the introduction:

1. How does root plasticity affect P uptake efficiency from the fertiliser pellet?
2. Can microdialysis probes be used to determine the P uptake benefit due to organic acid exudation?
3. Can microdialysis probes be used as model roots in experiments?
4. Does root system architecture affect the P uptake benefit of citrate exudation? If so, is there any measures of the root system architecture that can predict the P uptake benefit?

## 5.1 Review of Main Findings and Limitations

### 5.1.1 A multi image-based approach for modelling plant-fertiliser interaction

In chapter 2, an elemental mapping technique, SEM-EDS, in combination with XCT was proposed as an approach for determining elemental and structural information in models of P uptake. To demonstrate the utility of our model model, the P uptake efficiency (P uptake per root surface area) from a fertiliser pellet was compared between different root system architectures.

Analysing the XCT data revealed that the plant in the presence of a fertiliser pellet proliferated roots within 2 mm from the centre of the pellet. Additionally, many roots were found within the fertiliser pellet. This imaging and image-processing approach for measuring spatial variations in root length density extended the work of Flavel et al. (2012) who compared root length density in plants grown in soil with banded and uniformly distributed P using XCT. They found no difference in total root length density between the two treatments, however, they did not investigate root length density changes with distance from the P bands, as was done for the fertiliser pellet in chapter 2. We believe such an approach utilises the richness of XCT data and is suitable for further investigation of root length density variations within soil. We concluded that barley plants can detect P from the pellet and proliferate locally in that region. However, analysis was only carried out on two fertiliser treatments and two controls; more replicates are required to confirm this result. Furthermore, the plants were constrained to falcon tubes for the purposes of imaging which may not be representative of field conditions.

Averaging the elemental images revealed narrow P gradients originating from the fertiliser pellet. To our knowledge this is the first time such gradients have been detected from a fertiliser pellet in soil. These gradients served as data to parameterise the image-based P uptake model. Using the parameterised model, we found the plant that had reacted plastically to the source of P from the pellet absorbed more P. Furthermore, the responding plant spent marginally more carbon on developing the roots near the fertiliser pellet to obtain this uptake benefit. The fertiliser pellet only enhanced P uptake per root surface area of roots within 2 mm of pellet over the 30 day simulation. With this in mind, we argued that an important mechanism for P uptake from a fertiliser pellet is the plant finding and promoting root growth near the pellet as opposed to P slowly diffusing from the pellet to roots further afield. Hence, when modelling P uptake from a fertiliser

pellet, root plasticity should be considered. Furthermore, we found that densely packed roots in regions of soil which were not replenished by the fertiliser pellet, had low uptake efficiency due to multiple roots competing for the same soil P supply. We concluded that this approach serves as a means to determine the benefit of plastic root responses to a fertiliser pellet, however there are limitations. SEM-EDS was used on soil samples that were dried, resin-perfused then thin-sectioned. As such, the P that was measured was not in soil solution and hence not directly available to plants. Even though the P measurements were limited to the clay water mixture phase to limit the inclusion of P minerals, it is unclear how much measured P was available to plants. However, we argued that P in the clay water mixture phase is a proxy for plant available P. Furthermore, as the SEM-EDS sample preparation method is destructive, it cannot be used for time-resolved mapping. Therefore, this method is not suitable for parameterising models that include more complex mechanisms such as dynamic and/or non-linear P-soil reactions, which require more detailed data to fit accurately. There was a limited number of root systems used as the geometry in the models. This was due to the time-consuming nature of manual segmentation and elemental mapping. Further replicates are required to confirm the modelling results. Currently, semi-automated segmentation is underway on the root system images from Ahmed et al. (2016). In these experiments, wheat plants were grown from seed to seed with either MAP, struvite or no fertiliser with three replicates each. The plants were scanned weekly using XCT. We plan to use these images to further analyse root length density changes near fertiliser pellets and use a similar modelling approach to chapter 1 to investigate how these changes can affect P uptake efficiency.

A method borrowed from medical imaging was used to align the 2D SEM-EDS data with the 3D XCT data (Chicherova et al. (2014)). The approach produced fast and accurate registrations between the two imaging modes. Furthermore, the algorithm scales well with image sizes and miss-matches in image-dimensions and is an improvement on other 2D-3D alignment methods used in soil science (Hapca et al. (2015)). We believe this approach will be a useful tool in 2D-3D multi-model imaging of soil.

### 5.1.2 Quantifying citrate enhanced phosphate root uptake using microdialysis

In chapter 3, microdialysis probes in combination with modelling was proposed as a means to determine the rate at which citrate solubilises soil-sorbed P. Microdialysis probes perfused with citrate were placed in soil to determine how citrate altered probe P uptake. P uptake/citrate exudation of a model microdialysis probe in soil was compared to actual microdialysis probe uptake/exudation and parameters were varied to determine which best fitted the experimental data. Dependencies of parameters were first calculated (Figure 3.3) and calibration experiments were designed to isolate the parameters with the least dependencies. The model was then adjusted to match the calibration experiments to fit these parameters. The dependent parameters were then calculated until the rate at which citrate solubilises soil-sorbed P could be determined. This parameter was then used in a model of a single root to determine the uptake benefit of citrate exudation.

Using this approach, we approximated the rate at which citrate solubilises P (under the assumptions made in the model) which had only been estimated in previous modelling papers. Dynamic first order kinetics were used to model citrate and soil adsorption. The model fit the temporal P uptake data well when 1000 μM of citrate was in the perfusate but not for 10000 μM (although the total P uptake fit well in this case). We concluded that first order kinetics were not suitable to capture the mechanisms over a large range of citrate concentrations and non-linear sorption isotherms would be more suitable. However, additional microdilaysis experiments were required to determine the parameters in dynamic sorption isotherm models. When using microdialysis probes to fit soil parameters, it is important to first calibrate the probe parameters, such as membrane permeability, in order to decouple probe and soil mechanisms. Furthermore, it is important to consider that the probe is removing solute from the system.

A model of a single root exuding citrate at a typical rate predicted that the root would absorb little additional P due to exudation. This result was in contrast with previous modelling work which found that citrate contributed with significant gains to P uptake. Many previous modelling studies assumed soil reactions were fast relative to diffusion to put reactions into equilibrium. However, non-dimensionalization on the model determined that P sorption/desorption rates were *not* fast relative to diffusion, hence assumptions used to put soil reactions into equilibrium were not valid. Although, the non-dimensionalised reaction rates were dependent on the length scale

squared. Therefore, as the size of the geometry increased, equilibrium reaction arguments become more valid. Microdialysis probes could behave similarly to model roots provided the correct amount of citrate was added to the perfusate, the Michaelis-Menten kinetics was in the linear range of P concentrations (low concentrations) and the experimental time-scale was short. However, the probes would underestimate P uptake.

### 5.1.3 Linking root structure to functionality: The impact of root system architecture on citrate enhanced phosphate uptake

In chapter 4, the parameterised model of chapter 3 was solved on time-resolved image-based growing root systems to determine the role of root system architecture on citrate enhanced P uptake. Citrate enhanced uptake was compared amongst 11 root system architectures. Additionally, morphological measures of the root systems were compared with citrate enhanced uptake to determine if they can be used as a proxies for the P benefit from citrate exudation. Two soil conditions were considered, optimal P conditions, denoted High P and poor P conditions, denoted Low P.

In both soil conditions, root surface area dominated absolute P uptake. In the High P conditions, little additional P was absorbed due to citrate across all 11 root systems. However, in the Low P conditions, up to 1.6% additional P was absorbed due to citrate exudation over the 12 day simulation and up to 10% additional root P flux could be observed. A peak in citrate enhanced P flux was observed within the first two days in each of the 11 root system architectures. We argued that this early P boost could be important because P nutrition at early stages of plant development is important for yield. Furthermore, the early P boost could provide the nutrients needed to develop roots to acquire more P later in development (as proposed in subsection 1.3.2).

Citrate enhanced P uptake per unit of citrate exuded varied across the 11 root system architectures. This suggested that root system architecture plays an important role in citrate enhanced uptake. The number of exuding tips correlated well with both total enhanced uptake and enhanced P flux. Periods of low average inter-tip distance were followed by peaks in enhanced P flux. Furthermore, regions of facilitation from adjacent roots could be observed near the root tips. Solidity (total volume per convex hull volume) was hypothesised to positively correlate

with citrate enhanced uptake, however, this was not the case. To explain this counter intuitive result, we argued that systems with many root tips will have more roots growing horizontally, ultimately increasing convex hull volume.

We argued that experiments using high/low exuding mutants would not be able to detect P gains due to citrate exudation unless root length/surface area was well measured and used to normalise the results. The maximum citrate concentration in soil solution was much less than the required amount to see significant P solubilisation based on the literature. Furthermore, there was at most a 0.25% difference in bulk solution P between the exudation and no-exudation simulations. Nonetheless, citrate-enhanced uptake was observed in the model. This led to an important consideration when designing future experiments regarding citrate enhanced P uptake: lack of bulk scale measured P solubilisation in an experiment does not imply lack of citrate enhanced uptake. The model used in this chapter was compared with a similar one from the literature (Schnepf et al. (2012)). We argued it was difficult to compare the mechanisms and results due to differences in modelling approaches. We proposed bench marking the models by using them to solve the same system of equations on the same RSA.

The approach used for assessing the functionality of root system architectures used in this chapter could be a useful tool for plant breeding and phenotyping. The functionality of a phenotype could be assessed to determine the serviceability of a variety. Additionally, phenotypic differences between genotypes may become more obvious after assessing their functionality using modelling.

## 5.2 The Contribution as a Whole and Further Work

Considering citrate exudation and root system architecture as entirely separate P acquisition strategies may miss important co-action. From chapter 4, it is clear that root system architecture plays an important role in citrate enhanced P uptake. Furthermore, the reduced P uptake efficiency of densely packed roots seen in chapter 2, could be mitigated by the resulting accumulation of citrate by adjacent roots. In the future, this could be investigated by using modelling to determine the P uptake per carbon spent (both on root growth and citrate exudation) of root system architectures with varying root length densities. Additionally, organic acids are known

to promote fertiliser pellet (struvite) dissolution (Talboys et al. (2016)). Future models could include this mechanism of pellet dissolution to further understand P uptake efficiency from a fertiliser pellet. We hypothesise that considering organic acid exudation and root plasticity in unison will increase P uptake efficiency, in terms of carbon spent on both exudation and root growth, from a fertiliser pellet more than the sum its parts.

The rate at which citrate solubilised soil-sorbed P, $\beta_3$, calculated in chapter 3 was used in 4. In chapter 3, we used linear adsorption kinetics for P soil reactions, which meant that the parameterisation was only valid for a small range of concentrations. In chapter 4, we went on to vary the concentration of P in the soil, bringing its validity into question. However, the error would only affect the absolute values and not the trends. To ensure accuracy for a wide range of concentrations, we propose that the dynamic competitive Langmuir equation is used for P and citrate soil reactions (as seen in Schnepf et al. (2012)), parameterised by microdialysis probe experiments using a range of P concentrations. Notice, using the competitive Langmuir equation fully couples citrate and P dynamics, which will dramatically increase computation time, this is particularly pertinent for image-based models.

In this thesis, two approaches were used to parameterise models of P uptake. In chapter 2, we used elemental mapping to directly parameterise an image-based model, while in chapter 3 we used microdialysis probes to parameterise a cylindrical model, the parameters were then used in an image-based model in chapter 4. We argue that the microdilaysis probe approach is the most suitable for parameterising image-based models for a number of reasons. Firstly, elemental mapping is a destructive method, thus only one measurement can be taken. The resulting data is then not suitable for fitting dynamic mechanisms. Furthermore, as discussed previously, SEM-EDS measures a number of P pools, hence, when using it to parameterise models it is unclear what P pool is being modelled. Although SEM-EDS has high resolution, the images were eventually averaged to denoise the data, thus the spatial accuracy was not fully utilised. On the other hand, microdialysis probes directly sample soil solution continuously, producing time-resolved data of P in soil solution. Additionally, as shown in this thesis, they can be used to simultaneously exude solutes while sampling soil solution. When using microdialysis probes however, care has to be taken to decouple probe and soil mechanisms using calibration

experiments. In future work, we propose using SEM-EDS images as initial data in 2D pore-scale finite difference schemes. Each pixel in the image could represent a node in the numerical scheme, while the segmented back scattered electron image could be used as the boundaries of soil constituents. Such an approach would make use of the spatial accuracy of SEM-EDS.

In future work, the approach used in chapter 4 to link root system measurements to citrate enhanced uptake could be used to assess the functionality between plant species or genotypes. It would be of interest to measure the citrate enhanced uptake of cluster roots for example. Furthermore, it could be extended to assess other root processes, including the uptake of water and other nutrients. However, there are two main challenges to overcome when extending this approach. Firstly, the time consuming and expensive nature of segmenting roots from time resolved XCT scans is a bottle neck in the process. Second, the scalability of the numerical solver to larger root systems or more complex mechanics poses a computational difficulty. For example, solving the exudation cases of chapter 4 took approximately 5 days per root system. Due to the increased use of XCT imaging for belowground phenotyping, collaborations with phenotyping research groups could provide access to these data sets. Furthermore, phenotyping research groups likely have crop varieties whose functionality would be of interest to plant breeders. To address the scalability of the numerical scheme, we propose comparing the approach of Schnepf et al. (2012) described in section 4.7 (known as the finite difference approach from here on in) to the image-based models of chapter 4 by solving models with the same (small) root system architectures and governing equations. The same grid can be used for arbitrary root systems in the finite difference approach, offering a large computational advantage over image-based modelling for large root systems. Once solutions of the finite difference approach are accurate relative to the experimentally verified image-based models, the finite difference approach can then be used to assess the functionality for older and larger plants. This type of benchmarking has already been done for water uptake; there was little difference in water uptake between volumetric uptake models and image-based models (Daly et al. (2018), Schnepf et al. (2019)). However, the author believes this would be less certain for slow moving nutrients like P due to the approximation in the finite difference approach that allows each root to absorb P from the entire discretized sub-volume equally. However, this could be amended by decreasing the size of the volumes. This P-uptake modelling frame work would provide a robust tool for plant

breeding and phenotyping, ultimately contributing to narrowing the yield growth gap (Furbank & Tester (2011)).

# Bibliography


Abdu, N. (2006), 'Soil-phosphorus extraction methodologies: A review', *African Journal of Agricultural Research* **1**(5), 159–161.

Adeleke, R., Nwangburuka, C. & Oboirien, B. (2017), 'Origins, roles and fate of organic acids in soils: a review', *South African Journal of Botany* **108**, 393–406.

Ahmed, S., Klassen, T. N., Keyes, S., Daly, M., Jones, D. L., Mavrogordato, M., Sinclair, I. & Roose, T. (2016), 'Imaging the interaction of roots and phosphate fertiliser granules using 4D X-ray tomography', *Plant and soil* **401**(1-2), 125–134.

Arahou, M. & Diem, H. (1997), 'Iron deficiency induces cluster (proteoid) root formation in Casuarina glauca', *Plant and Soil* **196**(1), 71–79.

Barber, S. A. (1995), *Soil nutrient bioavailability: a mechanistic approach*, John Wiley & Sons.

Barrow, N. (1978), 'The description of phosphate adsorption curves', *Journal of Soil Science* **29**(4), 447–462.

Barrow, N. (1989), 'Testing a mechanistic model. IX. competition between anions for sorption by soil', *Journal of soil science* **40**(2), 415–425.

Barrow, N., Debnath, A. & Sen, A. (2018), 'Mechanisms by which citric acid increases phosphate availability', *Plant and soil* **423**(1-2), 193–204.

Baulcombe, D., Crute, I., Davies, B., Dunwell, J., Gale, M., Jones, J., Pretty, J., Sutherland, W. & Toulmin, C. (2009), *Reaping the benefits: science and the sustainable intensification of global agriculture*, The Royal Society.

Bhat, K. & Nye, P. (1973), 'Diffusion of phosphate to plant roots in soil', *Plant and Soil* **38**(1), 161–175.

Bhat, K. & Nye, P. (1974), 'Diffusion of phosphate to plant roots in soil: III. Depletion around onion roots without root hairs', *Plant and Soil* pp. 383–394.

Bhuiyan, M., Mavinic, D. & Beckie, R. (2007), 'A solubility and thermodynamic study of struvite', *Environmental technology* **28**(9), 1015–1026.

Breeuwsma, A. & Silva, S. (1992), *Phosphorus fertilisation and environmental effects in the Netherlands and the Po region (Italy)*, DLO The Winand Staring Centre Wageningen,, Netherlands.

Brodowski, S., Amelung, W., Haumaier, L., Abetz, C. & Zech, W. (2005), 'Morphological and chemical properties of black carbon in physical soil fractions as revealed by scanning electron microscopy and energy-dispersive X-ray spectroscopy', *Geoderma* **128**(1-2), 116–129.

Cengiz, S., Karaca, A. C., Çakır, İ., Üner, H. B. & Sevindik, A. (2004), 'SEM-EDS analysis and discrimination of forensic soil', *Forensic science international* **141**(1), 33–37.

Chang, K. & Roberts, J. K. (1991), 'Cytoplasmic malate levels in maize root tips during K+ ion uptake determined by 13C-NMR spectroscopy', *Biochimica et Biophysica Acta (BBA)-Molecular Cell Research* **1092**(1), 29–34.

Chen, Z. C. & Liao, H. (2016), 'Organic acid anions: an effective defensive weapon for plants against aluminum toxicity and phosphorus deficiency in acidic soils', *Journal of genetics and genomics* **43**(11), 631–638.

Chicherova, N., Fundana, K., Müller, B. & Cattin, P. C. (2014), *Histology to μCT Data Matching Using Landmarks and a Density Biased RANSAC*, Springer, pp. 243–250.

Cooper, L., Daly, K., Hallett, P., Naveed, M., Koebernick, N., Bengough, A. G., George, T. & Roose, T. (2017), Fluid flow in porous media using image-based modelling to parametrize Richards' equation, *in* 'Proc. R. Soc. A', Vol. 473, The Royal Society, p. 20170178.

Cordell, D., Drangert, J.-O. & White, S. (2009), 'The story of phosphorus: global food security and food for thought', *Global environmental change* **19**(2), 292–305.

Cornish, P. S. (2009), 'Research directions: Improving plant uptake of soil phosphorus, and reducing dependency on input of phosphorus fertiliser', *Crop and Pasture Science* **60**(2), 190–196.

Daly, K. R., Keyes, S. D., Masum, S. & Roose, T. (2016), 'Image-based modelling of nutrient movement in and around the rhizosphere', *Journal of experimental botany* **67**(4), 1059–1070.

Daly, K. R., Tracy, S. R., Crout, N. M., Mairhofer, S., Pridmore, T. P., Mooney, S. J. & Roose, T. (2018), 'Quantification of root water uptake in soil using X-ray computed tomography and image-based modelling', *Plant, cell & environment* **41**(1), 121–133.

Dari, B., Nair, V. D., Colee, J., Harris, W. G. & Mylavarapu, R. (2015), 'Estimation of phosphorus isotherm parameters: a simple and cost-effective procedure', *Frontiers in Environmental Science* **3**, 70.

De Boever, W., Derluyn, H., Van Loo, D., Van Hoorebeke, L. & Cnudde, V. (2015), 'Data-fusion of high resolution X-ray CT, SEM and EDS for 3D and pseudo-3D chemical and structural characterization of sandstone', *Micron* **74**, 15–21.

De Parseval, H., Barot, S., Gignoux, J., Lata, J.-C. & Raynaud, X. (2017), 'Modelling facilitation or competition within a root system: importance of the overlap of root depletion and accumulation zones', *Plant and Soil* **419**(1-2), 97–111.

Delhaize, E., Hebb, D. M. & Ryan, P. R. (2001), 'Expression of a Pseudomonas aeruginosa citrate synthase gene in tobacco is not associated with either enhanced citrate accumulation or efflux', *Plant Physiology* **125**(4), 2059–2067.

Demand, D., Schack-Kirchner, H. & Lang, F. (2017), 'Assessment of diffusive phosphate supply in soils by microdialysis', *Journal of Plant Nutrition and Soil Science* **180**(2), 220–230.

Den Herder, G., Van Isterdael, G., Beeckman, T. & De Smet, I. (2010), 'The roots of a new green revolution', *Trends in plant science* **15**(11), 600–607.

Dessureault-Rompré, J., Nowack, B., Schulin, R. & Luster, J. (2007), 'Spatial and temporal variation in organic acid anion exudation and nutrient anion uptake in the rhizosphere of lupinus albus l.', *Plant and Soil* **301**(1-2), 123–134.

Dessureault-Rompré, J., Nowack, B., Schulin, R. & Luster, J. (2006), 'Modified micro suction cup/rhizobox approach for the in-situ detection of organic acids in rhizosphere soil solution', *Plant and Soil* **286**(1-2), 99–107.

Ding, S., Wang, Y., Xu, D., Zhu, C. & Zhang, C. (2013), 'Gel-based coloration technique for the submillimeter-scale imaging of labile phosphorus in sediments and soils with diffusive gradients in thin films', *Environmental science & technology* **47**(14), 7821–7829.

Doube, M., Klosowski, M. M., Arganda-Carreras, I., Cordelières, F. P., Dougherty, R. P., Jackson, J. S., Schmid, B., Hutchinson, J. R. & Shefelbine, S. J. (2010), 'BoneJ: Free and extensible bone image analysis in ImageJ', *Bone* **47**(6), 1076–1079.

Drew, M. (1975), 'Comparison of the effects of a localised supply of phosphate, nitrate, ammonium and potassium on the growth of the seminal root system, and the shoot, in barley', *New Phytologist* **75**(3), 479–490.

Drew, M. & Saker, L. (1978), 'Nutrient supply and the growth of the seminal root system in barley: III. Compensatory increases in growth of lateral roots, and in rates of phosphate uptake, in response to a localized supply of phosphate', *Journal of Experimental Botany* **29**(2), 435–451.

Duncan, S. J., Daly, K. R., Fletcher, D. M. M., Ruiz, S., Sweeney, P. & Roose, T. (2019), 'Multiple Scale Homogenisation of Nutrient Movement and Crop Growth in Partially Saturated Soil', *Bulletin of mathematical biology* **81**(10), 3778–3802.

Duputel, M., Devau, N., Brossard, M., Jaillard, B., Jones, D. L., Hinsinger, P. & Gérard, F. (2013), 'Citrate adsorption can decrease soluble phosphate concentration in soils: Results of theoretical modeling', *Applied geochemistry* **35**, 120–131.

Everaert, M., Degryse, F., McLaughlin, M. J., De Vos, D. & Smolders, E. (2017), 'Agronomic effectiveness of granulated and powdered P-exchanged Mg–Al LDH relative to struvite and MAP', *Journal of agricultural and food chemistry* **65**(32), 6736–6744.

Farmaga, I., Shmigelskyi, P., Spiewak, P. & Ciupinski, L. (n.d.), Evaluation of computational complexity of finite element analysis, *in* '2011 11th International Conference The Experience of Designing and Application of CAD Systems in Microelectronics (CADSM)', IEEE, pp. 213–214.

Fedoroff, N. V., Battisti, D. S., Beachy, R. N., Cooper, P. J., Fischhoff, D. A., Hodges, C., Knauf, V. C., Lobell, D., Mazur, B. J., Molden, D. et al. (2010), 'Radically rethinking agriculture for the 21st century', *Science* **327**(5967), 833–834.

Fitter, A., Williamson, L., Linkohr, B. & Leyser, O. (2002), 'Root system architecture determines fitness in an Arabidopsis mutant in competition for immobile phosphate ions but not for nitrate ions', *Proceedings of the Royal Society of London B: Biological Sciences* **269**(1504), 2017–2022.

Flavel, R. J., Guppy, C. N., Tighe, M., Watt, M., McNeill, A. & Young, I. M. (2012), 'Non-destructive quantification of cereal roots in soil using high-resolution X-ray tomography', *Journal of Experimental Botany* **63**(7), 2503–2511.

Fletcher, D. M. M., Keyes, S. D., Daly, K. R., Van Veelen, A. & Roose, T. (2019), 'A multi image-based approach for modelling plant-fertiliser interaction', *Rhizosphere* p. 100152.

Fletcher, D. M. M., Shaw, R., Sánchez-Rodríguez, A. R., Daly, K. R., van Veelen, A., Jones, D. L. & Roose, T. (2019), 'Quantifying citrate-enhanced phosphate root uptake using microdialysis', *Plant and Soil* .
**URL:** *https://doi.org/10.1007/s11104-019-04376-4*

Fletcher, D., Ruiz, S., Dias, T., Petroselli, C. & Roose, T. (2020), 'Linking root structure to functionality: The impact of root system architecture on citrate enhanced phosphate uptake', *New Phytologist* **-**(-), –.

Fogel, R. (1985), 'Roots as primary producers in below-ground ecosystems', *Special publications series of the British Ecological Society* .

Furbank, R. T. & Tester, M. (2011), 'Phenomics–technologies to relieve the phenotyping bottleneck', *Trends in plant science* **16**(12), 635–644.

Gahoonia, T. S. & Nielsen, N. E. (1992), 'The effects of root-induced pH changes on the depletion of inorganic and organic phosphorus in the rhizosphere', *Plant and soil* **143**(2), 185–191.

Galach, M. & Waniewski, J. (2012), 'Membrane transport of several ions during peritoneal dialysis: mathematical modelling', *Artificial organs* **36**(9), E163–E178.

Gamuyao, R., Chin, J. H., Pariasca-Tanaka, J., Pesaresi, P., Catausan, S., Dalid, C., Slamet-Loedin, I., Tecson-Mendoza, E. M., Wissuwa, M. & Heuer, S. (2012), 'The protein kinase Pstol1 from traditional rice confers tolerance of phosphorus deficiency', *Nature* **488**(7412), 535.

Geelhoed, J. S., Hiemstra, T. & Van Riemsdijk, W. H. (1998), 'Competitive interaction between phosphate and citrate on goethite', *Environmental Science & Technology* **32**(14), 2119–2123.

Geelhoed, J., Van Riemsdijk, W. & Findenegg, G. (1999), 'Simulation of the effect of citrate exudation from roots on the plant availability of phosphate adsorbed on goethite', *European Journal of Soil Science* **50**(3), 379–390.

Gerke, J., Beißner, L. & Römer, W. (2000), 'The quantitative effect of chemical phosphate mobilization by carboxylate anions on P uptake by a single root. I. The basic concept and determination of soil parameters', *Journal of Plant Nutrition and Soil Science* **163**(2), 207–212.

Gerke, J., Römer, W. & Beißner, L. (2000), 'The quantitative effect of chemical phosphate mobilization by carboxylate anions on P uptake by a single root. II. The importance of soil and plant parameters for uptake of mobilized P', *Journal of Plant Nutrition and Soil Science* **163**(2), 213–219.

Glanville, H., Hill, P., Schnepf, A., Oburger, E. & Jones, D. (2016), 'Combined use of empirical data and mathematical modelling to better estimate the microbial turnover of isotopically labelled carbon substrates in soil', *Soil Biology and Biochemistry* **94**, 154–168.

Goldstein, J. I., Newbury, D. E., Michael, J. R., Ritchie, N. W., Scott, J. H. J. & Joy, D. C. (2017), *Scanning electron microscopy and X-ray microanalysis*, Springer.

Grant, C., Flaten, D., Tomasiewicz, D. & Sheppard, S. (2001), 'The importance of early season phosphorus nutrition', *Canadian Journal of Plant Science* **81**(2), 211–224.

Gross, K. L., Peters, A. & Pregitzer, K. S. (1993), 'Fine root growth and demographic responses to nutrient patches in four old-field plant species', *Oecologia* **95**(1), 61–64.

Grossman, J. D. & Rice, K. J. (2012), 'Evolution of root plasticity responses to variation in soil nutrient distribution and concentration', *Evolutionary Applications* **5**(8), 850–857.

Gunina, A., Smith, A. R., Kuzyakov, Y. & Jones, D. L. (2017), 'Microbial uptake and utilization of low molecular weight organic substrates in soil depend on carbon oxidation state', *Biogeochemistry* **133**(1), 89–100.

Gérard, F., Blitz-Frayret, C., Hinsinger, P. & Pagès, L. (2017), 'Modelling the interactions between root system architecture, root functions and reactive transport processes in soil', *Plant and Soil* **413**(1-2), 161–180.

Güsewell, S. & Schroth, M. H. (2017), 'How functional is a trait? phosphorus mobilization through root exudates differs little between Carex species with and without specialized dauciform roots', *New Phytologist* **215**(4), 1438–1450.

Hammer, G. L., Dong, Z., McLean, G., Doherty, A., Messina, C., Schussler, J., Zinselmeier, C., Paszkiewicz, S. & Cooper, M. (2009), 'Can changes in canopy and/or root system architecture explain historical maize yield trends in the us corn belt?', *Crop Science* **49**(1), 299–312.

Hapca, S., Baveye, P. C., Wilson, C., Lark, R. M. & Otten, W. (2015), 'Three-dimensional mapping of soil chemical characteristics at micrometric scale by combining 2D SEM-EDX data and 3D X-Ray CT images', *PloS one* **10**(9), e0137205.

Hapca, S. M., Wang, Z. X., Otten, W., Wilson, C. & Baveye, P. C. (2011), 'Automated statistical method to align 2D chemical maps with 3D X-ray computed micro-tomographic images of soils', *Geoderma* **164**(3), 146–154.

Hattingh, M., Gray, L. & Gerdemann, J. (1973), 'Uptake and translocation of 32P-labeled phosphate to onion roots by endomycorrhizal fungi', *Soil Science* **116**(5), 383–387.

Heppell, J., Talboys, P., Payvandi, S., Zygalakis, K., Fliege, J., Withers, P., Jones, D. & Roose, T. (2015*a*), 'How changing root system architecture can help tackle a reduction in soil phosphate (P) levels for better plant P acquisition', *Plant, cell & environment* **38**(1), 118–128.

Heppell, J., Talboys, P., Payvandi, S., Zygalakis, K., Fliege, J., Withers, P., Jones, D. & Roose, T. (2015*b*), 'How changing root system architecture can help tackle a reduction in soil phosphate (P) levels for better plant P acquisition', *Plant, cell & environment* **38**(1), 118–128.

Hermans, C., Hammond, J. P., White, P. J. & Verbruggen, N. (2006), 'How do plants respond to nutrient shortage by biomass allocation?', *Trends in Plant Science* **11**(12), 610–617.

Hoffland, E. (1992), 'Quantitative evaluation of the role of organic acid exudation in the mobilization of rock phosphate by rape', *Plant and Soil* **140**(2), 279–289.

Hoffland, E., Findenegg, G. R. & Nelemans, J. A. (1989), 'Solubilization of rock phosphate by rape', *Plant and soil* **113**(2), 155–160.

Hübel, F. & Beck, E. (1993), 'In-situ determination of the P-relations around the primary root of maize with respect to inorganic and phytate-P', *Plant and Soil* **157**(1), 1–9.

Inselsbacher, E. & Näsholm, T. (2012), 'A novel method to measure the effect of temperature on diffusion of plant-available nitrogen in soil', *Plant and Soil* **354**(1-2), 251–257.

Inselsbacher, E., Öhlund, J., Jämtgård, S., Huss-Danell, K. & Näsholm, T. (2011), 'The potential of microdialysis to monitor organic and inorganic nitrogen compounds in soil', *Soil Biology and Biochemistry* **43**(6), 1321–1332.

Iserles, A. (2007), 'Lecture notes in numerical solution of differential equations. part iii'.

Itoh, S. & Barber, S. (1983), 'A numerical solution of whole plant nutrient uptake for soil-root systems with root hairs', *Plant and Soil* **70**(3), 403–413.

Jackson, M. L., Lim, C. H. & Zelazny, L. W. (1986), 'Oxides, hydroxides, and aluminosilicates 1', *Methods of Soil Analysis: Part 1—Physical and Mineralogical Methods* (methodsofsoilan1), 101–150.

Jackson, R. & Caldwell, M. (1989), 'The timing and degree of root proliferation in fertile-soil microsites for three cold-desert perennials', *Oecologia* **81**(2), 149–153.

Jackson, R. & Caldwell, M. (1991), 'Kinetic responses of Pseudoroegneria roots to localized soil enrichment', *Plant and Soil* **138**(2), 231–238.

Jackson, R. & Caldwell, M. (1996), 'Integrating resource heterogeneity and plant plasticity: modelling nitrate and phosphate uptake in a patchy soil environment', *Journal of Ecology* pp. 891–903.

Johnson, J. F., Vance, C. P. & Allan, D. L. (1996), 'Phosphorus deficiency in Lupinus albus (altered lateral root development and enhanced expression of phosphoenolpyruvate carboxylase)', *Plant physiology* **112**(1), 31–41.

Jones, D. & Brassington, D. (1998), 'Sorption of organic acids in acid soils and its implications in the rhizosphere', *European Journal of Soil Science* **49**(3), 447–455.

Jones, D. & Edwards, A. (1998), 'Influence of sorption on the biological utilization of two simple carbon substrates', *Soil Biology and Biochemistry* **30**(14), 1895–1902.

Jones, D. L. (1998), 'Organic acids in the rhizosphere–a critical review', *Plant and soil* **205**(1), 25–44.

Jones, D. L. & Darrah, P. R. (1994), 'Role of root derived organic acids in the mobilization of nutrients from the rhizosphere', *Plant and soil* **166**(2), 247–257.

Jones, E., Oliphant, T. & Peterson, P. (2001), 'SciPy: Open source scientific tools for Python'.

Jungk, A. & Barber, S. (1975), 'Plant age and the phosphorus uptake characteristics of trimmed and untrimmed corn root systems', *Plant and Soil* **42**(1), 227–239.

Jungk, A. & Claassen, N. (1989), 'Availability in soil and acquisition by plants as the basis for phosphorus and potassium supply to plants', *Zeitschrift für Pflanzenernährung und Bodenkunde* **152**(2), 151–157.

Jungk, A. & Claassen, N. (1997), 'Ion diffusion in the soil-root system', *Advances in agronomy (USA)* .

Keyes, S., Cooper, L., Duncan, S., Koebernick, N., Mckay Fletcher, D., Scotson, C., Van Veelen, A., Sinclair, I. & Roose, T. (2017), 'Measurement of micro-scale soil deformation around roots using four-dimensional synchrotron tomography and image correlation', *Journal of The Royal Society Interface* **14**(136), 20170560.

Keyes, S. D., Daly, K. R., Gostling, N. J., Jones, D. L., Talboys, P., Pinzer, B. R., Boardman, R., Sinclair, I., Marchant, A. & Roose, T. (2013), 'High resolution synchrotron imaging of wheat root hairs growing in soil and image based modelling of phosphate uptake', *New Phytologist* **198**(4), 1023–1029.

Khademi, Z., Jones, D., Malakouti, M. & Asadi, F. (2010), 'Organic acids differ in enhancing phosphorus uptake by Triticum aestivum L.—effects of rhizosphere concentration and counterion', *Plant and soil* **334**(1-2), 151–159.

Kinniburgh, D. G. (1986), 'General purpose adsorption isotherms', *Environmental Science & Technology* **20**(9), 895–904.

Kjellström, C. & Kirchmann, H. (1994), 'Dry matter production of oilseed rape (Brassica napus) with special reference to the root system', *The Journal of Agricultural Science* **123**(3), 327–332.

Koebernick, N., Daly, K. R., Keyes, S. D., George, T. S., Brown, L. K., Raffan, A., Cooper, L. J., Naveed, M., Bengough, A. G. & Sinclair, I. (2017), 'High-resolution synchrotron imaging shows that root hairs influence rhizosphere soil structure formation', *New Phytologist* **216**(1), 124–135.

Koevoets, I. T., Venema, J. H., Elzenga, J. T. & Testerink, C. (2016), 'Roots withstanding their environment: exploiting root system architecture responses to abiotic stress to improve crop tolerance', *Frontiers in Plant Science* **7**, 1335.

Koyama, H., Kawamura, A., Kihara, T., Hara, T., Takita, E. & Shibata, D. (2000), 'Overexpression of mitochondrial citrate synthase in Arabidopsis thaliana improved growth on a phosphorus-limited soil', *Plant and Cell Physiology* **41**(9), 1030–1037.

Kubias, A., Deinzer, F., Feldmann, T., Paulus, D., Schreiber, B. & Brunner, T. (2008), '2D/3D image registration on the GPU', *Pattern Recognition and Image Analysis* **18**(3), 381–389.

Kuchenbuch, R. & Jungk, A. (1982), 'A method for determining concentration profiles at the soil-root interface by thin slicing rhizospheric soil', *Plant and Soil* **68**(3), 391–394.

Kume, T., Sekiya, N. & Yano, K. (2006), 'Heterogeneity in spatial P-distribution and foraging capability by Zea mays: effects of patch size and barriers to restrict root proliferation within a patch', *Annals of botany* **98**(6), 1271–1277.

Lambers, H., Martinoia, E. & Renton, M. (2015), 'Plant adaptations to severely phosphorus-impoverished soils', *Current opinion in plant biology* **25**, 23–31.

Lambers, H., Shane, M. W., Cramer, M. D., Pearse, S. J. & Veneklaas, E. J. (2006), 'Root structure and functioning for efficient acquisition of phosphorus: matching morphological and physiological traits', *Annals of botany* **98**(4), 693–713.

Landl, M., Schnepf, A., Uteau, D., Peth, S., Athmann, M., Kautz, T., Perkons, U., Vereecken, H. & Vanderborght, J. (2019), 'Modeling the Impact of Biopores on Root Growth and Root Water Uptake', *Vadose Zone Journal* **18**(1).

Laperche, V., Logan, T. J., Gaddam, P. & Traina, S. J. (1997), 'Effect of apatite amendments on plant uptake of lead from contaminated soil', *Environmental Science & Technology* **31**(10), 2745–2753.

Leitner, D., Klepsch, S., Bodner, G. & Schnepf, A. (2010*a*), 'A dynamic root system growth model based on L-systems', *Plant and Soil* **332**(1-2), 177–192.

Leitner, D., Klepsch, S., Bodner, G. & Schnepf, A. (2010*b*), 'A dynamic root system growth model based on L-systems', *Plant and Soil* **332**(1-2), 177–192.

Liang, R. & Li, C. (2003), 'Differences in cluster-root formation and carboxylate exudation in Lupinus albus L. under different nutrient deficiencies', *Plant and soil* **248**(1-2), 221–227.

Lipton, D. S., Blanchar, R. W. & Blevins, D. G. (1987), 'Citrate, malate, and succinate concentration in exudates from P-sufficient and P-stressed medicago sativa l. seedlings', *Plant Physiology* **85**(2), 315–317.

Loeppert, R. & Inskeep, W. (1996), 'Iron. p. 639–664. DL Sparks (ed.) Methods of soil analysis. Part 3. SSSA Book Ser. 5. SSSA, Madison, WI', *Iron. p. 639–664. In DL Sparks (ed.) Methods of soil analysis. Part 3. SSSA Book Ser. 5. SSSA, Madison, WI.* pp. –.

Lopez-Bucio, J., de la Vega, O. M., Guevara-Garcia, A. & Herrera-Estrella, L. (2000), 'Enhanced phosphorus uptake in transgenic tobacco plants that overproduce citrate', *Nature biotechnology* **18**(4), 450.

Lowe, D. G. (1999), Object recognition from local scale-invariant features, *in* 'Computer vision, 1999. The proceedings of the seventh IEEE international conference on', Vol. 2, IEEE, pp. 1150–1157.

Lü, J., Gao, X., Dong, Z., Yi, J. & An, L. (2012), 'Improved phosphorus acquisition by tobacco through transgenic expression of mitochondrial malate dehydrogenase from Penicillium oxalicum', *Plant cell reports* **31**(1), 49–56.

Lynch, J. (1995), 'Root architecture and plant productivity.', *Plant physiology* **109**(1), 7.

Manschadi, A. M., Kaul, H.-P., Vollmann, J., Eitzinger, J. & Wenzel, W. (2014), 'Developing phosphorus-efficient crop varieties—an interdisciplinary research framework', *Field Crops Research* **162**, 87–98.

Marschner, H. (1995), 'Mineral nutrition of higher plants. 2nd', *Edn. Academic Pres* .

Menacherry, S., Hubert, W. & Justice, J. B. (1992), 'In vivo calibration of microdialysis probes for exogenous compounds', *Analytical chemistry* **64**(6), 577–583.

Mench, M. & Martin, E. (1991), 'Mobilization of cadmium and other metals from two soils by root exudates of Zea mays L., Nicotiana tabacum L. and Nicotiana rustica L', *Plant and soil* **132**(2), 187–196.

Menshykau, D., Michos, O., Lang, C., Conrad, L., McMahon, A. P. & Iber, D. (2019), 'Image-based modeling of kidney branching morphogenesis reveals GDNF-RET based Turing-type mechanism and pattern-modulating WNT11 feedback', *Nature communications* **10**(1), 239.

Mooney, S. J., Pridmore, T. P., Helliwell, J. & Bennett, M. J. (2012), 'Developing X-ray computed tomography to non-invasively image 3-D root systems architecture in soil', *Plant and soil* **352**(1-2), 1–22.

Mosetlha, K., Torto, N. & Wibetoe, G. (2007), 'Determination of Cu and Ni in plants by microdialysis sampling: Comparison of dialyzable metal fractions with total metal content', *Talanta* **71**(2), 766–770.

Nadeem, M., Mollier, A., Morel, C., Vives, A., Prud'homme, L. & Pellerin, S. (2011), 'Relative contribution of seed phosphorus reserves and exogenous phosphorus uptake to maize (Zea mays L.) nutrition during early growth stages', *Plant and Soil* **346**(1-2), 231–244.

Neumann, G. & Martinoia, E. (2002), 'Cluster roots–an underground adaptation for survival in extreme environments', *Trends in plant science* **7**(4), 162–167.

Nielsen, K. L., Lynch, J. P., Jablokow, A. G. & Curtis, P. S. (1994), 'Carbon cost of root systems: an architectural approach', *Plant and Soil* **165**(1), 161–169.

Niu, Y. F., Chai, R. S., Jin, G. L., Wang, H., Tang, C. X. & Zhang, Y. S. (2012), 'Responses of root architecture development to low phosphorus availability: a review', *Annals of botany* **112**(2), 391–408.

Nye, P. (1983), 'The diffusion of two interacting solutes in soil', *Journal of Soil Science* **34**(4), 677–691.

Oburger, E. & Jones, D. L. (2018), 'Sampling root exudates–mission impossible?', *Rhizosphere* **6**, 116–133.

Oburger, E., Jones, D. L. & Wenzel, W. W. (2011), 'Phosphorus saturation and pH differentially regulate the efficiency of organic acid anion-mediated P solubilization mechanisms in soil', *Plant and Soil* **341**(1-2), 363–382.

Oburger, E., Kirk, G. J., Wenzel, W. W., Puschenreiter, M. & Jones, D. L. (2009), 'Interactive effects of organic acids in the rhizosphere', *Soil Biology and Biochemistry* **41**(3), 449–457.

Oburger, E., Leitner, D., Jones, D., Zygalakis, K., Schnepf, A. & Roose, T. (2011), 'Adsorption and desorption dynamics of citric acid anions in soil', *European Journal of Soil Science* **62**(5), 733–742.

Osorio Vega, N. W. (2007), 'A review on beneficial effects of rhizosphere bacteria on soil nutrient availability and plant nutrient uptake', *Revista Facultad Nacional de Agronomía Medellín* **60**(1), 3621–3643.

Palomo, L., Claassen, N. & Jones, D. L. (2006), 'Differential mobilization of P in the maize rhizosphere by citric acid and potassium citrate', *Soil Biology and Biochemistry* **38**(4), 683–692.

Pellet, D. M., Grunes, D. L. & Kochian, L. V. (1995), 'Organic acid exudation as an aluminum-tolerance mechanism in maize (Zea mays L.)', *Planta* **196**(4), 788–795.

Peth, S., Horn, R., Beckmann, F., Donath, T., Fischer, J. & Smucker, A. (2008), 'Three-dimensional quantification of intra-aggregate pore-space features using synchrotron-radiation-based microtomography', *Soil Science Society of America Journal* **72**(4), 897–907.

Peyton, R., Haeffner, B., Anderson, S. & Gantzer, C. (1992), 'Applying X-ray CT to measure macropore diameters in undisturbed soil cores', *Geoderma* **53**(3-4), 329–340.

Ptashnyk, M., Roose, T., Jones, D. L. & Kirk, G. J. (2011), 'Enhanced zinc uptake by rice through phytosiderophore secretion: a modelling study', *Plant, cell & environment* **34**(12), 2038–2046.

Radon, J. (1917), 'On the determination of functions from their integrals along certain manifolds', *Ber. Verh, Sachs Akad Wiss.* **69**, 262–277.

Raghothama, K. & Karthikeyan, A. (2005), 'Phosphate acquisition', *Plant and Soil* **274**(1-2), 37.

Rajala, A., Peltonen-Sainio, P., Onnela, M. & Jackson, M. (2002), 'Effects of applying stem-shortening plant growth regulators to leaves on root elongation by seedlings of wheat, oat and barley: mediation by ethylene', *Plant Growth Regulation* **38**(1), 51–59.

Rajaniemi, T. K. (2007), 'Root foraging traits and competitive ability in heterogeneous soils', *Oecologia* **153**(1), 145–152.

Rennenberg, H. (1984), 'The fate of excess sulfur in higher plants', *Annual Review of Plant Physiology* **35**(1), 121–153.

Rich, S. M. & Watt, M. (2013), 'Soil conditions and cereal root system architecture: review and considerations for linking darwin and weaver', *Journal of experimental botany* **64**(5), 1193–1208.

Rogers, E. D. & Benfey, P. N. (2015), 'Regulation of plant root system architecture: implications for crop advancement', *Current Opinion in Biotechnology* **32**, 93–98.

Roose, T. & Fowler, A. (2004), 'A mathematical model for water and nutrient uptake by plant root systems', *Journal of theoretical biology* **228**(2), 173–184.

Roose, T., Fowler, A. & Darrah, P. (2001), 'A mathematical model of plant nutrient uptake', *Journal of mathematical biology* **42**(4), 347–360.

Roose, T., Keyes, S., Daly, K., Carminati, A., Otten, W., Vetterlein, D. & Peth, S. (2016), 'Challenges in imaging and predictive modeling of rhizosphere processes', *Plant and Soil* **407**(1-2), 9–38.

Ruiz, S. A., Koebernick, N., Duncan, S., McKay Fletcher, D., Scotson, C., Boghi, A., Marin, M., Bengough, A. G., George, T., Brown, L. et al. (2019), 'Significance of root hairs at the field scale–modelling root water and phosphorus uptake under different field conditions', *Plant and Soil* .

Ruiz, S., Fletcher, D. M., Boghi, A., Williams, K., Duncan, S., Scotson, C., Petroselli, C., Dias, T., Chadwick, D., Jones, D. et al. (2020), 'Image-based quantification of soil microbial dead zones induced by nitrogen fertilization', *Science of The Total Environment* p. 138197.

Ruiz, S., Schymanski, S. J. & Or, D. (2017), 'Mechanics and energetics of soil penetration by earthworms and plant roots: higher rates cost more', *Vadose Zone Journal* **16**(8).

Ryan, P. R., James, R. A., Weligama, C., Delhaize, E., Rattey, A., Lewis, D. C., Bovill, W. D., McDonald, G., Rathjen, T. M. & Wang, E. (2014), 'Can citrate efflux from roots improve phosphorus uptake by plants? Testing the hypothesis with near-isogenic lines of wheat', *Physiologia Plantarum* **151**(3), 230–242.

Sanchez, P. A. (2002), 'Soil fertility and hunger in Africa', *Science* **295**(5562), 2019–2020.

Sanchez, P. A. & Uehara, G. (1980), 'Management considerations for acid soils with high phosphorus fixation capacity', *The role of phosphorus in agriculture* pp. 471–514.

Santner, J., Zhang, H., Leitner, D., Schnepf, A., Prohaska, T., Puschenreiter, M. & Wenzel, W. W. (2012), 'High-resolution chemical imaging of labile phosphorus in the rhizosphere of Brassica napus L. cultivars', *Environmental and Experimental Botany* **77**, 219–226.

Sattari, S., Bouwman, A., Rodriguez, R. M., Beusen, A. & Van Ittersum, M. (2016), 'Negative global phosphorus budgets challenge sustainable intensification of grasslands', *Nature Communications* **7**, 10696.

Sayen, S., Mallet, J. & Guillon, E. (2009), 'Aging effect on the copper sorption on a vineyard soil: Column studies and sem–eds analysis', *Journal of colloid and interface science* **331**(1), 47–54.

Schnepf, A., Black, C. K., Couvreur, V., Delory, B. M., Doussan, C., Koch, A., Koch, T., Javaux, M., Landl, M., Leitner, D. et al. (2019), 'Call for participation: Collaborative benchmarking of functional-structural root architecture models. the case of root water uptake', *BioRxiv* p. 808972.

Schnepf, A., Leitner, D. & Klepsch, S. (2012), 'Modeling phosphorus uptake by a growing and exuding root system', *Vadose Zone Journal* **11**(3).

Schubert, S. (2005), 'Structure and Functioning of Cluster Roots and Plant Responses to Phosphate Deficiency, H. Lambers, P. Poot (Eds.), Kluwer Academic Publishers, Dordrecht (2003),(376pp., price EURO 96.30), ISBN: 1-4020-0434-6'.

Shane, M. W. & Lambers, H. (2005), Cluster roots: a curiosity in context, *in* 'Root physiology: from gene to function', Springer, pp. 101–125.

Shaw, R., Williams, A. & Jones, D. (2014), 'Assessing soil nitrogen availability using microdialysis-derived diffusive flux measurements', *Soil Science Society of America Journal* **78**(5), 1797–1803.

Silberbush, M. & Barber, S. (1983), 'Sensitivity of simulated phosphorus uptake to parameters used by a mechanistic-mathematical model', *Plant and soil* **74**(1), 93–100.

Singh, S., Kalra, M. K., Hsieh, J., Licato, P. E., Do, S., Pien, H. H. & Blake, M. A. (2010), 'Abdominal CT: comparison of adaptive statistical iterative and filtered back projection reconstruction techniques', *Radiology* **257**(2), 373–383.

Solaiman, Z., Marschner, P., Wang, D. & Rengel, Z. (2007), 'Growth, P uptake and rhizosphere properties of wheat and canola genotypes in an alkaline soil with low P availability', *Biology and Fertility of Soils* **44**(1), 143.

Stutter, M. I., Shand, C. A., George, T. S., Blackwell, M. S., Bol, R., MacKay, R. L., Richardson, A. E., Condron, L. M., Turner, B. L. & Haygarth, P. M. (2012), 'Recovering phosphorus from soil: a root solution?'.

Sulyok, M., Miró, M., Stingeder, G. & Koellensperger, G. (2005), 'The potential of flow-through microdialysis for probing low-molecular weight organic anions in rhizosphere soil solution', *Analytica chimica acta* **546**(1), 1–10.

Sylvester-Bradley, R., Withers, P. J., Rollett, A., Talboys, P., Walker, R., Edwards, T., Payvandi, S., Heppel, J. P., Roose, T. & Jones, D. (2017), 'Improving the sustainability of phosphorus use in arable farming–'Targeted P'', *AHDB Research Report* .

Talboys, P. J., Heppell, J., Roose, T., Healey, J. R., Jones, D. L. & Withers, P. J. (2016), 'Struvite: a slow-release fertiliser for sustainable phosphorus management?', *Plant and Soil* **401**(1-2), 109–123.

Tinker, P. B. & Nye, P. H. (2000), *Solute movement in the rhizosphere*, Oxford University Press.

Topp, C. N., Bray, A. L., Ellis, N. A. & Liu, Z. (2016), 'How can we harness quantitative genetic variation in crop root systems for agricultural improvement?', *Journal of integrative plant biology* **58**(3), 213–225.

Topp, C. N., Iyer-Pascuzzi, A. S., Anderson, J. T., Lee, C.-R., Zurek, P. R., Symonova, O., Zheng, Y., Bucksch, A., Mileyko, Y., Galkovskyi, T. et al. (2013), '3D phenotyping and quantitative trait locus mapping identify core regions of the rice genome controlling root architecture', *Proceedings of the National Academy of Sciences* **110**(18), E1695–E1704.

Tracy, S. R., Roberts, J. A., Black, C. R., McNeill, A., Davidson, R. & Mooney, S. J. (2010), 'The X-factor: visualizing undisturbed root architecture in soils using X-ray computed tomography', *Journal of experimental botany* **61**(2), 311–313.

Tron, S., Bodner, G., Laio, F., Ridolfi, L. & Leitner, D. (2015), 'Can diversity in root architecture explain plant water use efficiency? A modeling study', *Ecological modelling* **312**, 200–210.

Tsubota, K.-i. & Adachi, T. (2004), 'Changes in the fabric and compliance tensors of cancellous bone due to trabecular surface remodeling, predicted by a digital image-based model', *Computer methods in biomechanics and biomedical engineering* **7**(4), 187–192.

Uga, Y., Sugimoto, K., Ogawa, S., Rane, J., Ishitani, M., Hara, N., Kitomi, Y., Inukai, Y., Ono, K. & Kanno, N. (2013), 'Control of root system architecture by DEEPER ROOTING 1 increases rice yield under drought conditions', *Nature genetics* **45**(9), 1097.

Van de Weerd, H., Van Riemsdijk, W. & Leijnse, A. (1999), 'Modeling the dynamic adsorption/desorption of a NOM mixture: Effects of physical and chemical heterogeneity', *Environmental science & technology* **33**(10), 1675–1681.

Van Hees, P., Vinogradoff, S., Edwards, A., Godbold, D. & Jones, D. (2003), 'Low molecular weight organic acid adsorption in forest soils: effects on soil solution concentrations and biodegradation rates', *Soil Biology and Biochemistry* **35**(8), 1015–1026.

Van Veelen, A., Koebernick, N., Scotson, C. S., McKay-Fletcher, D., Huthwelker, T., Borca, C. N., Mosselmans, J. F. W. & Roose, T. (2019), 'Root induced soil deformation influences Fe, S and P: rhizosphere chemistry investigated using synchrotron XRF and XAS', *New Phytologist* .

Vaz, M. R., Edwards, A., Shand, C. & Cresser, M. (1993), 'Phosphorus fractions in soil solution: influence of soil acidity and fertiliser additions', *Plant and Soil* **148**(2), 175–183.

Vereecken, H., Schnepf, A., Hopmans, J. W., Javaux, M., Or, D., Roose, T., Vanderborght, J., Young, M., Amelung, W. & Aitkenhead, M. (2016), 'Modeling soil processes: Review, key challenges, and new perspectives', *Vadose Zone Journal* **15**(5).

Vitousek, P. M., Porder, S., Houlton, B. Z. & Chadwick, O. A. (2010), 'Terrestrial phosphorus limitation: mechanisms, implications, and nitrogen–phosphorus interactions', *Ecological applications* **20**(1), 5–15.

Voegelin, A., Weber, F.-A. & Kretzschmar, R. (2007), 'Distribution and speciation of arsenic around roots in a contaminated riparian floodplain soil: Micro-XRF element mapping and EXAFS spectroscopy', *Geochimica et Cosmochimica Acta* **71**(23), 5804–5820.

Wan, J., Tyliszczak, T. & Tokunaga, T. K. (2007), 'Organic carbon distribution, speciation, and elemental correlations within soil microaggregates: applications of STXM and NEXAFS spectroscopy', *Geochimica et Cosmochimica Acta* **71**(22), 5439–5449.

Wang, E., Ridoutt, B. G., Luo, Z. & Probert, M. E. (2013), 'Using systems modelling to explore the potential for root exudates to increase phosphorus use efficiency in cereal crops', *Environmental modelling & software* **46**, 50–60.

Wang, S., Jin, X., Pang, Y., Zhao, H., Zhou, X. & Wu, F. (2005), 'Phosphorus fractions and phosphate sorption characteristics in relation to the sediment compositions of shallow lakes in the middle and lower reaches of Yangtze River region, China', *Journal of colloid and interface science* **289**(2), 339–346.

Wang, Y., Xu, H., Kou, J., Shi, L., Zhang, C. & Xu, F. (2013), 'Dual effects of transgenic Brassica napus overexpressing CS gene on tolerances to aluminum toxicity and phosphorus deficiency', *Plant and Soil* **362**(1-2), 231–246.

Watt, M., McCully, M. E. & Kirkegaard, J. A. (2003), 'Soil strength and rate of root elongation alter the accumulation of Pseudomonas spp. and other bacteria in the rhizosphere of wheat', *Functional Plant Biology* **30**(5), 483–491.

Wissuwa, M., Mazzola, M. & Picard, C. (2009), 'Novel approaches in plant breeding for rhizosphere-related traits', *Plant and Soil* **321**(1-2), 409.

Wrb, I. W. G. (2015), 'World Reference Base for Soil Resources 2014, update 2015 International soil classification system for naming soils and creating legends for soil maps', *World Soil Resources Reports No. 106* p. 192.

Yano, K. & Kume, T. (2005), 'Root morphological plasticity for heterogeneous phosphorus supply in Zea mays L.', *Plant production science* **8**(4), 427–432.

Yarlagadda, P. S., Matsumoto, M. R., VanBenschoten, J. E. & Kathuria, A. (1995), 'Characteristics of heavy metals in contaminated soils', *Journal of environmental engineering* **121**(4), 276–286.

Zeller-Plumhoff, B., Roose, T., Katsamenis, O., Mavrogordato, M., Torrens, C., Schneider, P. & Clough, G. (2017), 'Phase contrast synchrotron radiation computed tomography of muscle spindles in the mouse soleus muscle', *Journal of anatomy* **230**(6), 859–865.

Zhang, B., Fang, F., Guo, J., Chen, Y., Li, Z. & Guo, S. (2012), 'Phosphorus fractions and phosphate sorption-release characteristics relevant to the soil composition of water-level-fluctuating zone of Three Gorges Reservoir', *Ecological Engineering* **40**, 153–159.

Zhang, F., Ma, J. & Cao, Y. (1997), 'Phosphorus deficiency enhances root exudation of low-molecular weight organic acids and utilization of sparingly soluble inorganic phosphates by radish (Raghanus satiuvs L.) and rape (Brassica napus L.) plants', *Plant and Soil* **196**(2), 261–264.

Zhang, H. & Forde, B. G. (1998), 'An Arabidopsis MADS box gene that controls nutrient-induced changes in root architecture', *Science* **279**(5349), 407–409.

Zhao, J., Butters, T. D., Zhang, H., LeGrice, I. J., Sands, G. B. & Smaill, B. H. (2013), 'Image-based model of atrial anatomy and electrical activation: a computational platform for investigating atrial arrhythmia', *IEEE transactions on medical imaging* **32**(1), 18–27.

Zurek, P. R., Topp, C. N. & Benfey, P. N. (2015), 'Quantitative trait locus mapping reveals regions of the maize genome controlling root system architecture', *Plant Physiology* **167**(4), 1487–1496.

Zygalakis, K. & Roose, T. (2012), 'A mathematical model for investigating the effect of cluster roots on plant nutrient uptake', *The European Physical Journal Special Topics* **204**(1), 103–118.